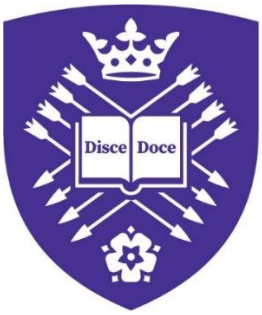

University of Sheffield

Investigating the Application of Bioinspired Materials for the Immobilisation of Carbonic Anhydrase.

Author: Jennifer Anne Hancock

A thesis submitted in partial fulfilment of the requirements for the degree of Doctor of Engineering (EngD).

Supervisors: Siddharth Patwardhan, Mohamed Pourkashanian, Derek Ingham.

The University of Sheffield

Faculty of Engineering

School of Chemical, Materials and Biological Engineering & Energy Institute

April 2025

Table of Contents

i. Acknowledgments

I am deeply grateful to many people for helping me through the course of this PhD, firstly I would like to thank my supervisor Prof. Siddharth Patwardhan for his patience and guidance in steering me through this project. Secondly, I would like to thank everyone in the Green Nanomaterials Research Group, for their help, encouragement and good humour. Particularly Gwen. I would also like to thank my industry mentor Dr. Tom Lowes, who has been an amazing help to me in making contacts in industry and guiding me through technical problems as part of my CDT. I would also like to thank my Energy 2050 Supervisors Prof. Derek Ingham and Prof. Mohamed Pourkashanian and the IFRF for being my industrial sponsors and PMT technologies who have helped me financially through my unfunded period. Finally, I would like to thank my partner Derek, from the bottom of my heart for his constant support and faith in me and our dog Ed, who kept my feet warm while I wrote this thesis.

ii. Specific scientific contributions

In addition to my supervisors, I would like to thank Charles Oseghale for running my N_2 Gas Adsorption samples and Gwen Chimonides for help and scientific advice though my lab work.

iii. Abbreviations

ATR-FTIR – Attenuated total reflectance Fourier transform infrared spectroscopy
BECCS – Bioenergy with carbon capture and storage
BET – Brunauer, Emmett and Teller
BIS – Bio-inspired silica
BJH – Barrett, Joyner and Halenda
Bn – Billion
BSA – Bovine serum albumin
CA – Carbonic anhydrase
$CaCO_3$ – Calcium carbonate
CCC – Carbon capture and conversion
CCS – Carbon capture and storage
CCU – Carbon capture and utilisation
CCUS – Carbon capture, utilisation and storage
CDR – Carbon dioxide removal
CH_3OH – Methanol
CLEA – Cross-linked enzyme aggregates
CLEC – Cross-linked enzyme crystals
CO_2 – Carbon dioxide
°C – Celsius
DACCS – Direct air carbon capture and storage
DIW – Deionized water
ERW – Enhanced rock weathering
FTIR – Fourier transform infrared spectroscopy
Gt – Gigatonnes
H_2 – Hydrogen
ha – Hectare
HCl – Hydrochloric acid
HCO_3^- – Bicarbonate
HTC – Hydrothermal char
IPCC – Intergovernmental panel for climate change
km – Kilometre
MCM – Mobile Crystalline Material
MEA – Monoethanolamine
MIP – Mercury intrusion porosimetry
MOF – Metal–organic framework
MPTES – (4-Methoxyphenyl)methanamine
Mt – Megatonnes
NAD^+/NADH – Nicotinamide adenine dinucleotide
OAPS – Octa(aminophenyl)silsesquioxane
p-NPA – *p*-Nitrophenyl acetate
PD – Pore diameter
PEHA – Pentaethylenehexamine
ppm – Parts per million
PV – Pore volume
RT – Room temperature

SA – Surface area
SBA – Santa Barbara
SFG – Surface functional groups
SiO_2 – Silicon dioxide
T – Tonne
TERC – Translational Energy Research Centre
WT – Woodtek

iv. Declaration

I, Jennifer Hancock, confirm that the contents of this thesis are my own work. I acknowledge the universities rules on the Use of Unfair Means (Unfair means, cheating and plagiarism | Support for new students | The University of Sheffield). None of the presented works have been used for any other academic accreditation or industrial purposes, other than the presentation of some of the data at conferences.

Plans to publish the results of Chapters 3 and 4 are in progress.

I also declare the use of ChatGPT as a writing and grammar tool.

v. Summary

The capture and conversion of CO_2 into valuable chemicals such as methanol (CH_3OH) represents a promising strategy for mitigating industrial carbon emissions, particularly in hard-to-decarbonise sectors. The most well-developed systems for CO_2 upgrading to CH_3OH, while effective, face challenges relating to cost and sustainability. Enzyme-based catalysis, with the addition of carbonic anhydrase (CA) to enhance CO_2 sequestration, offers a greener alternative due to its ability to enhance CO_2 hydration rates. For industrial application, enzyme recovery and reusability are crucial, and immobilisation is a common solution for this issue. Porous frameworks are particularly popular, since they offer higher surface area (SA) for enzyme loading. This study investigates two potential porous frameworks, biochar and bioinspired silica (BIS), for their suitability in CA immobilisation.

A meta-analysis of biochar synthesis parameters (pyrolysis temperature, feedstock, and activation treatment) revealed significant variability in porosity characteristics. No biochar candidates met the minimum requirements for pore diameter (PD), pore volume (PV), and SA necessary for effective enzyme immobilisation and activity. Subsequently, a recently developed BIS synthesis method was used to [redacted] frameworks, engineered to meet ideal porosity conditions.

Porosity analyses confirmed that [redacted] samples exhibited suitable PV (>0.3 $cm^3\ g^{-1}$) and SA (50 – 500 $m^2\ g^{-1}$), with [redacted] showing enhanced SA at higher reactant concentrations. CA was immobilised via entrapment and adsorption methods. While adsorption resulted in limited enzyme loading and activity, some [redacted] entrapped CA samples exhibited comparable activity to the free enzyme, indicating some potential as an industrial application but further rigorous development would be required.

Overall, this study highlights BIS as a promising, tunable platform for enzyme immobilisation, although further optimisation is needed to improve consistency and performance for industrial CO_2 capture and conversion applications.

Chapter 1: Introduction

1.1 Overview

This chapter focuses on introducing the problem of carbon dioxide (CO_2) emissions, their impact on the atmosphere, the resulting harm to natural systems, and the serious threats they pose to human health and society. It will begin with the sources of these CO_2 emissions and the technological, financial, and legislative challenges which make them difficult to address. The issue of unavoidable CO_2 emissions will then be covered, followed by an overview of the range of technology options under development for mitigating them. Focus will be paid to CO_2 upgrading into useful fuels and chemicals, followed by the barriers to rolling out these technologies at scale. This thesis then focuses on the important prospective role of methanol (CH_3OH) in a net-zero CO_2 emissions system and the status and challenges around its synthesis using waste CO_2 as a feedstock. It will then focus on immobilised enzyme catalysis systems as a highly novel means of hydrating CO_2 to form CH_3OH, and the developments required to progress research in this technology. One of the principal areas of research is enzyme immobilisation and the addition of the enzyme carbonic anhydrase (CA) to aid CO_2 hydration into the aqueous reaction system. The extensive literature relating to the immobilisation of CA will then be discussed along with and identification of the key features of the most successful immobilised CA systems to date. The technical details regarding the formation of silica frameworks will then be described in detail along with recent improvements in the sustainable manufacture of bioinspired silica (BIS) and how the selection of biological molecules can enable the tailoring of porosity to suit the needs of an enzyme system. Briefly, the attributes of biochar as a framework for immobilised enzymes will then be discussed prior to a far deeper discussion in Chapters 3 and 4. The introduction will conclude with aims and hypotheses to explore the feasibility of the application of BIS and biochar as a framework for CA and the dehydrogenase enzyme alcohol dehydrogenase.

1.2 The Climate Crisis

The burning of fossil fuels in the form of coal, natural gas and oil has facilitated prodigious improvements, in the health, well-being, education and social development of a large proportion of humankind[1,2]. Unfortunately, it is now abundantly clear that this leap in progress has come at great cost to the earth's atmosphere, environment, and its natural systems. The combustion of fossil fuels has increased CO_2 in the earths atmosphere[2,3]. As of March 2025, its concentration reached 428.01 parts per million (ppm) globally, the highest amount in the last 800,000 years[4]. This increase in CO_2 concentrations, along with other human industrial activities such as agriculture, deforestation and manufacturing are creating a global heating imbalance[5,6] with around 30 - 40% of the human population experiencing an average warming

of 1.5 Celsius (°C)[7]. This has already had profound effects on our planet's natural systems, with trends showing an intensity of weather extremes such as heatwaves, tropical cyclones, heavy rain events and drought[5]. Unless drastic action is taken to reduce CO_2 emissions and enhance sinks the world will have warmed by 4°C by the end of the century[7]. If this happens, major cities will be submerged due to rising sea levels; mass extinctions will occur and large parts of the world will degrade into uninhabitable desert, leaving holes in the planet's web of life and the global food supply chain[7]. Action is required to conserve our planet's climate to an average 1.5°C rise in temperature[7], which would "reduce the probability of extreme drought, precipitation deficits and risks associated with water availability"[7].

Global commitments and actions are growing, with nations investing in radical plans to decarbonise their national energy systems[8]. In addition to decarbonising current energy systems, future requirements and demands must also be considered including: the rising global population, estimated to be between 9 to 10 billion people by 2050, and the projected increases in global standards of living, which could push energy demand up by 60% compared to the current needs[2]. The IPCC has outlined that, if demand rises as anticipated, global electricity supply will need to come from 70 - 85% renewable electricity by 2050 if temperatures are to be kept below a 1.5°C increase from pre-industrial levels. To meet this target, the rate of energy-system decarbonisation and carbon dioxide removal (CDR) must be increased four-fold compared with current efforts[2]. These measures include:

- Lowering the carbon content of electricity.
- Reducing the share of coal-fired power generation and its subsidies.
- Incentivising consumers to switch from hydrocarbon to electric-powered vehicles.
- Improving efficiency in energy consumption
- Investing in carbon capture and storage (CCS) and CDR strategies[9].

1.3 Challenges Associated with Addressing CO_2 Emissions

Despite efforts to enact the measures required to tackle climate change, several key challenges remain. Beginning with strong lobbying and financial incentives to maintain current policies[10]. Another issue is that many sectors have CO_2 emissions which are challenging to abate. Transport, comprising aviation, shipping and road freight, currently accounts for 6% of global CO_2 emissions and currently presents another major hurdle in achieving decarbonisation[11]. Whilst light transport vehicles can be changed to hydrogen (H_2) or electricity with comparatively fewer technical challenges, heavier forms of transport such as trucks, ships and air freight require a larger cargo carrying capacity to justify the economic costs of operation[11].

Heavy materials manufacture is another sector facing challenges with decarbonisation. The iron and steel industry and the cement industry as examples. The iron and steel industry accounts for 7 - 9% of global CO_2 emissions The cement industry accounts for a further 7% of global CO_2 emissions and is the second most in-demand resource in the world after fresh water[12].

Both cement and steel face difficulties with decarbonisation due to the inherent nature of their manufacturing processes. In the case of steel and iron, coking coal is used to reduce iron oxide in iron ore to create crude steel, resulting in the emission of 1.6 to 3.1 tons of CO_2 per ton of steel[11]. In the case of cement, 60% of CO_2 emissions per ton of clinker arises because of the burning of calcium carbonate at high temperatures to create lime [13,11].

One solution for these industries with hard to prevent emissions is CO_2 removal (CDR). The IPCC has estimated that in >50% of global models to limit warming to less than 1.5 °C there will be a need to perform CDR at scale[14]. They also indicate that the longer the delay in peak global CO_2 emissions, the greater the need will be for atmospheric CDR strategies for achieving climate goals[15].

1.4 CDR for Assisting Emissions Reduction

The most prominent CDR strategies include afforestation and reforestation (AR), biomass derived biochar manufacture, soil carbon sequestration (SCS), enhanced rock weathering (ERW), ocean fertilization (OF), bioenergy with carbon capture and storage (BECCS), ocean alkalinity enhancement and direct air carbon capture and storage (DACCS)[16]. Recent estimates calculated that to limit global temperature rise to 1.5°C above pre-industrial records, there needed to be approximately 7 - 9 gigatonnes (Gt) of atmospheric CO_2 removed between 2024 and 2025[16]. Current CDR strategies are estimated to remove around 2 Gt CO_2 per year, with most of the removal occurring because of AR, habitat restoration, and SCS, not surprisingly as these are the most well-researched and established practices[16]. The other, more novel CDR methods such as OF, DACCS, BECCS, biochar, ERW currently remove an estimated 1.3 Megatonnes (Mt) CO_2[16].

Increasing annual CDR from 2 up to 9 $GtCO_2$ per year is achievable, but challenging[16]. One of the overarching difficulties in increasing uptake of novel CDR methods is the large gap in innovation between technologies[40]. Whilst AF is already a cost-effective and established practice, huge costs and technological uncertainty are associated with other novel technologies; DACCS for example has focused almost entirely on research and development, with comparatively little work being done in determining total demand, cost/benefit ratios, and public attitudes towards implementation[17]. To put this into perspective, a current 1 $MtCO_2$ / year DACCS plant would cover an area equivalent to 28 football fields (0.2 km^2) and

the water use alone could range between 7-13 Mt per year[18]. Such demands on land and freshwater resources could leave DACCS vulnerable to prohibitive costs and social acceptance[18]. Progress of CDR deployment is also hindered by a distinct lack of interdisciplinary cooperation to track deployment of CDR projects and determine whether these deployments are enough to satisfy a nations CO_2 reduction commitment[19].

Finally, there is also a notable lack of CDR technologies in existence at the Gt scale, resulting in a lack of data to indicate their true environmental impact; as such, their projected contribution to climate goals is considered to be uncertain by some researchers[20]. Therefore, in addition to progressing CDR technology development and impact assessments, a greater focus should be given to technologies which prevent or reduce CO_2 emissions at the source.

1.5 Preventing CO_2 Emissions via Capture and Storage

Despite these issues with CDR another technology that can be deployed for industries which have built in non-preventable emissions is carbon capture, utilization and/or storage (CCUS)[11]. CCUS takes two forms, the first and most mature of these being carbon capture and storage (CCS), which captures CO_2 and transfers it to a storage site. The second and more novel is carbon capture and utilisation (CCU), which captures CO_2 and uses it commercially[21]. These technologies are receiving rapid investment and, in some cases, have already been successfully deployed. Such as in the case of a cement manufacturer in Brevik Norway where they have successfully deployed a viable commercial scale amine CO_2 capture plant. However, whilst there is some adoption of alternative technologies for both CO_2 emission prevention, progress is still not on track in 2025 for cement, and iron and steel production[22,23], but it is hoped that, like CDR, CCUS will compliment international efforts to reach decarbonisation targets[24].

1.5.1 CO_2 Capture

Three of the most mature technologies under development for CO_2 capture are post-conversion, pre-conversion and oxy-fuel combustion capture[25]. For each process, several materials and chemicals have been explored as possible adsorbents and absorbents for CO_2[21]. In the case of post and pre-conversion capture, the most favourable method already being applied at industrial scale is solvent absorption using monoethanolamine (MEA), which releases high-purity CO_2 via a temperature swing process[26,27]. Unfortunately, a high heat consumption is incurred because of MEA regeneration, resulting in increased energy costs[26]. Another key challenge with the use of MEA is degradation, due to the solvent's tendency to react with oxygen, SOx and NOx[28]. This produces a toxic waste stream which must then be safely disposed of and continuously replaced[28]. High levels of corrosion are also associated with MEA plants[28].

Another chemical absorbent-process is calcium-looping, this process has been found to produce high-purity CO_2 at low capacity and reasonable cost at pilot scale, following temperature swing[29]. A limitation of this method however is that temperatures of 850 – 950 °C are required to decompose the $CaCO_3$ to release the pure CO_2 stream[29]. Porous solid adsorbents such as solid amine, carbon, zeolite, metal organic frameworks (MOFs) and alkali-carbonates have also been explored[30–32]. Unfortunately, these physical adsorbents are limited by poor adsorption selectivity, owing to the relatively low partial pressure of CO_2 in the flue gas stream as well as the large amounts of flue gas that needs to be treated[31]. Physical solvents such as Rectisol^{tm} and Selexol^{tm} have also been applied to pre-conversion capture processes where high-heat recovery is not needed, such as coal gasification; however, studies have found that a high purity stream of CO_2 is required to achieve competitive process efficiency[33–35].

Oxy-fuel combustion avoids the use of chemicals by instead burning fuel in pure oxygen; the result is a high-purity CO_2 stream devoid of nuisance NOx molecules[36]. Unfortunately, oxyfuel is both energy intensive and expensive, due to the need for the air-separation processes required to create a pure stream of oxygen[37]. As a means of overcoming these limitations, two newer technologies in the form of chemical looping and combustion and chemical looping and reforming have been developed. In the case of chemical looping and reforming this has produced positive improvements, such as “lower steam demand, higher fuel conversion efficiencies and better sulfur tolerance”[38] and can handle more dilute CO_2 streams[25,39]. Unfortunately, these breakthroughs have been mired by new issues, such as the high-pressure required of the system for it to be competitive with oxyfuel and post-combustion capture. In the case of chemical looping and combustion, further issues surround the technologies’ application to burning solid fuel and handling the ash. These issues mean that both chemical looping and combustion or reforming will not be expected to be ready for industry adoption until 2030[40].

1.5.2 Transportation

Further limitations to CCS deployment are the costs associated with CO_2 separation, enrichment and transportation. The cost for capturing a ton of CO_2 can vary significantly from \$15 - 25 / tonne (t) CO_2 for a dilute stream up to \$40 - 130 / tCO_2 for a concentrated stream suitable for repurposing for chemical production[41]. Once captured CO_2 must then be transported either by pipeline, ship, train or road to the storage or utilisation site. Pipelines are considered the most cost-effective means of transporting CO_2, with the cost varying depending on transportation distance[41]. Transport by pipeline costs can range from \$4 - 45 / tCO_2[41]. To put this into perspective, when considering the annual CO_2 emissions from a medium-sized cement plant and an 85% capture rate (~1 MtCO_2 / y), this gives a combined minimum

projected sunk cost for capture and transport of $15 m and $4 m respectively[41]. It is hoped that one of the driving factors for lowering the cost of CCS will be economies of scale - as increased numbers of industries capture CO_2 and 'plug - in' to the network, the associated cost will decrease[42]. However, industries with CO_2 emissions large enough to influence this economy of scale will be larger scale operations[47]. These are comparatively few in comparison to smaller facilities such as "pulp and paper plants, wastewater treatment centres and smaller gas-fired power stations" which might not emit enough to justify the expenditure[42].

1.5.3 Storage

Owing to the extensive experience of the fossil fuel industry in drilling and injection to access fossil fuel reserves, several deep geological storage options have been developed for compressed or liquified CO_2 to be injected into exhausted oil and gas fields, saline aquifers and coal seams[43–45]. It has also been suggested that CCS be combined with crude oil extraction as a means of enhancing recovery[30,46,47]. Whilst this form of storage appears to have the best potential for large-scale sequestration, particularly in saline aquifers and beneath the ocean, it has been met with significant trepidation[48,49]. Principally because although the theoretical capacity for CO_2 storage far exceeds the amount needed to achieve net-zero status, little is known about the true capacity of these reserves as well as their relative safety with regards to leaks[49–52]. Negative impacts have also been reported with regards to the natural ecology around injection sites[53–61].

1.6 Carbon Capture and Utilisation or Conversion

Considering the limitations posed by CCS, governments, industry and researchers have for some time been developing smaller CO_2 reduction routes in the form of CCU and carbon capture and conversion (CCC) where CO_2 is captured and changed to a product that can be useful in industry or stored[1]. CCU and CCC comparatively are not projected to reduce CO_2 as much as CCS, however they are still considered to be vital CO_2 mitigation strategies as they reduce the need for intentional CO_2 production from fossil fuels, while also providing another option to CCS where CO_2 storage options are limited[1]. CCU entails the direct commercial use of CO_2 in industries such as chemical and steel manufacture, fire extinguishers, food processing, and metal fabrication[62]. Unfortunately, the market for CO_2 in these industries is limited[63]. CCC seeks to further increase the market potential for CO_2 by converting CO_2 into other commercial products. This study will focus on this branch of CO_2 conversion hereafter.

1.6.1 CO_2 Capture and Conversion to Useful Fuels and Chemicals

The inert nature and stability of CO_2 presents a challenge to its efficient conversion. Large amounts of energy are required to break the highly stable bonds between the atoms

(Δ_r G^o = 0.84 kcal / mol)[64]. This would equate to 79.9 kJ per kg of CO_2. However, once this barrier has been overcome, CO_2 can serve as a highly flexible feedstock capable of producing over 150 different chemicals (Figure 1)[65–69]. Many of these are fine chemicals with a limited market; however, fuels such as CH_3OH, carbon monoxide, urea, syngas and di-methyl ether and other branch feedstock chemicals can also be produced (Figure 1)[30,63,66,70–75].

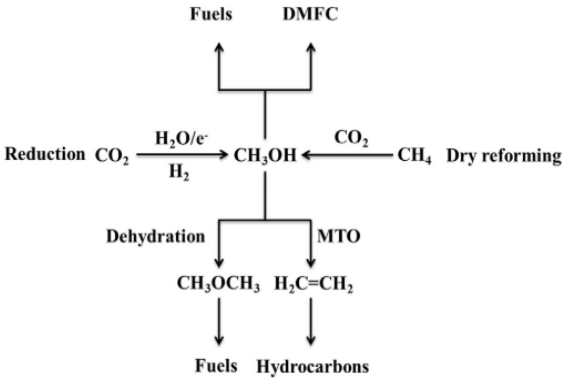

Figure 1. Conversion pathways of CO_2 to fuels and chemicals. MTO refers to the 'methanol to olefins' pathway, and DMFC refers to 'di-methyl ether and feedstock chemicals'. Taken from [76].

In this way CCC could help towards decarbonising awkward sectors such as transport, heavy industry and smaller industries unable to qualify for CCS by capturing CO_2 exhaust gases and transforming it back into high-value fuels or chemicals[1]. The 'fuels and feedstock chemicals' branch of CCC has attracted a lot of attention in recent years and has already been demonstrated in numerous studies and large-scale commercialised projects. These have in turn been summarised in several comprehensive critical reviews [32,74,77–82].

1.6.1.1 Carbon Capture and Conversion to CH_3OH

CH_3OH is a versatile and useful chemical for transportation fuels and as a foundation feedstock for thousands of other specialised chemicals[1,50,83]. It is also the second most effective chemical, after urea, for sequestering anthropogenic CO_2 emissions; with a capture capacity range between 1 - 10% of total annual emissions[25,84]. Although the market demand and price for urea is far higher, an established method of urea production which utilises CO_2 already exists[84]. Whereas the global production of CH_3OH, currently around 98 Mt per year, is predominantly facilitated using coal (35%) and gas (65%) feedstocks with only 0.2 Mt produced renewably[85,86]. As a result of the increasing global demand this industry's CO_2 emissions have also increased by 15% (28 Mt CO_2) between 2015 and 2018[87].

The simplicity of CH_3OH as a hydrocarbon and its chemical energy has allowed it to become an established and valued chemical within the global fossil-fuel-centric system (Figure 2). As of 2017, 19.6% of the global petrochemical market used CH_3OH as a feedstock[83]. CH_3OH is also favoured due to the ease with which it can be transported and stored[88]. Increasing use of

CH_3OH for both established and emerging applications, such as a source of H_2 for flex-fuel and fuel-cell vehicles and for the creation of dimethyl ether, has meant that demand is expected to rise by over 50% by 2030 and double by the end of 2050[85,89–91]. Its anticipated usefulness is such that a conceptual economy 'the methanol economy' was created around its use by the Nobel laureate George Olah[92]. If CH_3OH could be manufactured using waste CO_2 from industries struggling to decarbonise and from smaller industrial units that do not qualify for CCS, the economic return of a valuable product might incentivise the substantial investment required for CCUS technologies. It may also prevent emissions of >211 $MtCO_2$ per year arising from the use of coal and gas as the feedstock for its manufacture[87].

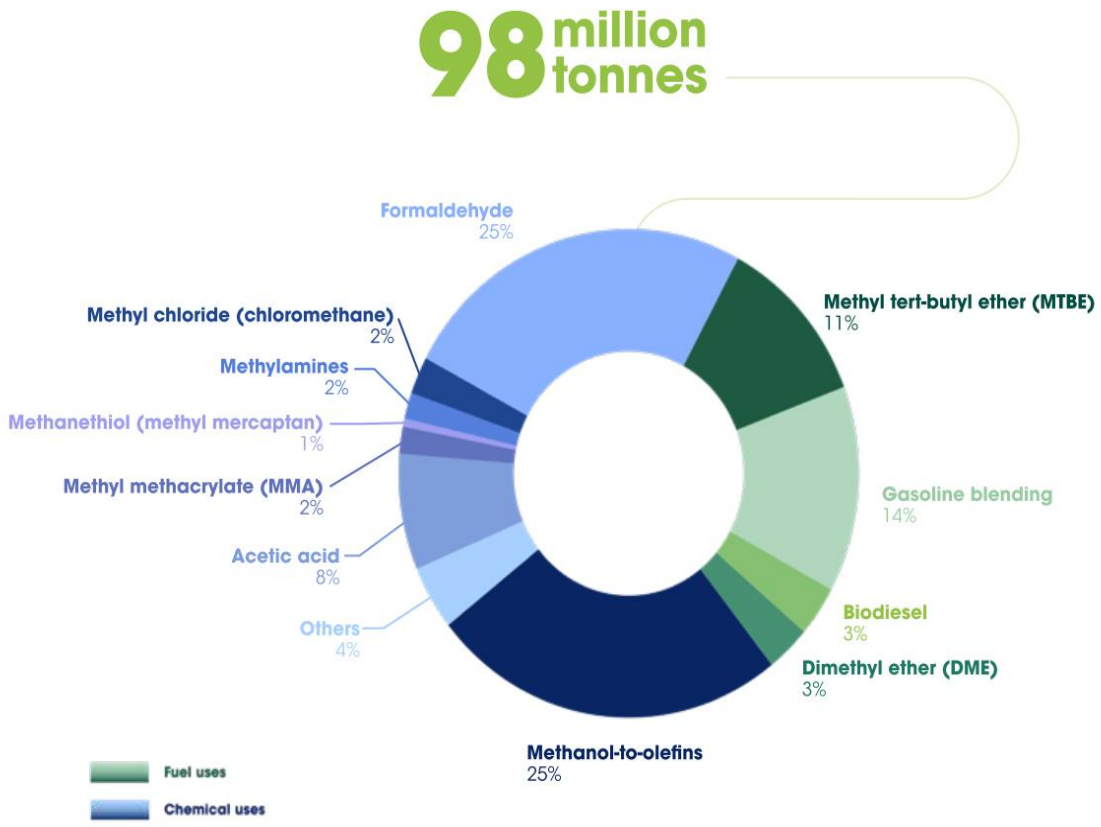

Figure 2. Global uses of CH_3OH, taken from [85].

As outlined in recent reviews[76,77,84], many novel approaches have been proposed for CO_2 to CH_3OH conversion. These include CO_2 conversion methods using renewable energy such as: wind, solar and biomass[85,93], photoreduction using metal catalysts[94–101], and bio-fixation using microalgae[102,103]. Integrated CH_3OH production systems have also been proposed alongside enhanced gas recovery and dimethyl ether generation[104,105]. Unfortunately, each of these methods has been met with challenges. In the case of photoreduction, rare-metal catalysts are often employed to drive the reaction in the desired direction, which have sustainability concerns[106]. Bio-fixation has encountered issues with scaling production: large, outdoor,

reactors have been found to not be as efficient for algal metabolic activity as those used in a laboratory setting and significant energy and environmental costs have been associated with algal biomass extraction and processing[76,102,103,107,108]. Whilst integrated CH_3OH, enhanced gas recovery and dimethyl ether generation have potential, the former is constrained by geography and costs and the latter is energy intensive as it requires high temperatures (250 – 300 °C)[104,105].

One of the most deeply explored and developed routes for methanol synthesis is CO_2 hydrogenation via Fischer-Tropsch synthesis[63]:

$$\text{(1.1)} \quad \mathrm{CO_2 + 3H_2 \rightleftarrows CH_3OH + H_2O\ \Delta H_{298K} = -40.9\ kJ/mol}$$

To further enhance the hydrogenation process, CO_2 can also be fed into a reverse water gas shift reaction to generate CO[63]:

$$\text{(1.2)} \quad \mathrm{CO_2 + H_2 \rightleftarrows CO + H_2O\ \Delta H_{298K} = 49.8\ kJ/mol}$$

This can then also be fed into the Fischer-Tropsch process[63]:

$$\text{(1.3)} \quad \mathrm{CO + 2H_2 \rightleftarrows CH_3OH\ \Delta H_{298K} = -90.7\ kJ/mol}$$

To overcome CO_2 stability, reach the activation energy for C-H bond formation and improve the yield and conversion rates, a copper (Cu)-based catalyst is often used in combination with one or multiple additives such as gold, indium oxide, nickel, gallium, manganese, cobalt, zirconium, zinc, titanium, aluminium, silicon, chromium, gallium again, palladium and cerium[63,74,109–121] to improve the process selectivity towards CH_3OH and limit unwanted by-product formation. Unfortunately, these methods have encountered significant issues, such as a tendency for the catalysts to rapidly disintegrate and dissociate. This issue has been somewhat mitigated with the introduction of aluminium oxide, zirconium dioxide, titanium dioxide, and silicon dioxide reaction frameworks, which have been reported to exhibit good performance and increase stability, manage reaction pH and promote successful substrate-product interactions[63,115–119,122,123]. Despite these breakthroughs, later studies reported that these catalysts and their additives still suffer from rapid disintegration and dissociation, while further reiterating their concerns surrounding their expense and sustainability[124–133]. Additional issues have also been cited regarding the often-intensive preparation required to create catalysts that will perform effectively[122,134,135]. In the case of copper-based catalysts, methods such as co-precipitation[116,136–139], sol-gel[140,141] and impregnation[142] have been developed to mitigate these negative effects, though unfortunately they are all still mired by limitations such as expense, time and pH sensitivity[120,134,143,144].

Despite these issues the use of metal-based catalysts for CH_3OH production via hydrogenation has been trialled in several pilot-scale facilities (Figure 3). Each have used varying combinations of reaction catalysts and promotors to produce CH_3OH with successively larger yields[63] (Figure 3). The most recent endeavour in Iceland, the George Oleh Plant operated by Carbon Recycling International, achieves commercial-level operational outputs of 4000 tons of methanol annually, which can be blended up to 3% with gasoline and fulfils "2.5% of Iceland's gasoline market"[76]. Despite these breakthroughs, significant challenges remain; principally the low reaction efficiency observed at pilot scale facilities, attributable to inefficient catalysts which results in low CO_2 conversion and poor CH_3OH selectivity[145–148].

Figure 3. Technology progress of metal-catalyst mediated CO_2 hydrogenation to CH_3OH, adapted from [63].

1.7 Enzymatic Conversion of CO_2 to CH_3OH

In recent years, enzymes have become increasingly recognised as a powerful and sustainable alternative to inorganic catalysis for the conversion of CO_2 to CH_3OH. This is due to their ability to reduce the activation energy required for CO_2 reduction as well as their high substrate specificity, resulting in a faster reaction[149,150]. Whilst enzymatic reduction of CO_2 to CH_3OH does not ordinarily occur in nature, it is made possible by assembling enzymes from different biological origins into a multi-enzymatic cascade system and optimising reaction conditions to drive the reaction in the desired direction. The first attempt was conducted by Obert and Dave in 1999 and utilised formate dehydrogenase, formaldehyde dehydrogenase and alcohol dehydrogenase[64,151]. Each works in reverse of the naturally occurring reaction, to reduce CO_2 to formate via formate dehydrogenase, followed by reduction to formaldehyde via formaldehyde dehydrogenase and then finally to CH_3OH via alcohol dehydrogenase, as described in E. 1.4 to 1.6[151,152]. This conversion is facilitated by an electron donor in the form of nicotinamide adenine dinucleotide (NADH), which is oxidised at each stage of the reaction

to become oxidised nicotinamide adenine dinucleotide (NAD^+). Overall, three moles of NADH are required to produce one mole of CH_3OH and four moles of H_2 are consumed[151].

$$(1.4) \quad CO_2 + NADH + H^+ \rightarrow HCOOH + NAD^+$$

$$(1.5) \quad HCOOH + NADH + H^+ \rightarrow CH_2O + NAD^+ + H_2O$$

$$(1.6) \quad CH_2O + NADH + H^+ \rightarrow CH_3OH + NAD^+$$

For research into enzyme-mediated conversion of CO_2 to CH_3OH to progress as a technology, it must have high rates of conversion for each substrate. In addition, enzymes must have high stability during practical applications against fluctuations outside of their optimal activity temperature and pH range[64,149,153]. The use of free enzymes in solution also creates unfeasibly high operational costs, due to low recovery rates[154]. These issues are not isolated to the field of enzyme-mediated CH_3OH production and efforts towards overcoming these challenges are underway within many other fields researching industrial enzymatic solutions[153]. These efforts fall into two main themes. The first is protein engineering[155], in which enzymes are altered through techniques “such as site-directed mutagenesis and direct evolution”[153]. The second is through immobilisation, with or without chemical modification[153,156]. This study will henceforth focus on immobilisation for improving the performance of enzyme-mediated CH_3OH production, since it presents a means of both stabilising and enhancing enzyme activity, whilst also having the potential to lower process costs through re-use and recovery[157].

1.7.1 Immobilisation methods

Enzyme immobilisation, with the help of advances in protein engineering, has expanded the range of molecules which are now able to be utilised in industrial biocatalysis[158]. In doing so, it has transformed many otherwise wasteful, toxic and intensive chemical synthesis processes into processes aligned with the principles of green chemistry[158,159].

Notable success stories of enzyme immobilisation include acrylate and 1,3-triglyceride synthesis. In the case of acrylate, the engineered enzyme mutant lipase B from *Candida antarctica* was immobilised onto polypropylene via adsorption[158]. The new system avoided high temperatures and acid catalysts associated with conventional acrylate manufacture, produced good yields of acrylate and has been expanded to include the manufacture of polymers and oleamides[158]. Precedent manufacturing methods of 1,3-triglycerides struggled to achieve the melting temperature required for oils and fats for margarine without processes such as “fractionation, hydrogenation, and chemical interestifcation”[158]. The application of immobilised lipases on diatomaceous earth and later silica particles enabled the interesterification of these oils without such intensive methods[158]. In both instances, enzyme immobilisation was a fundamental driver for this switch by industry to green chemistry practices.

A wide variety of different immobilisation frameworks have been explored in academia. However, their application at industrial scale often narrows down the range of frameworks to those which are straightforward to generate and economical[158]. They also must ensure that enzyme activity is also not detrimentally impacted. This is achieved by maximising cofactor, product and substrate diffusion access to the framework[158] and by avoiding compromising the enzyme structure by immobilisation[160] or through spatial constraints[161]. The two main methods for immobilising enzymes are defined as the chemical method and the physical method[162].

The chemical method is currently favoured by industry and entails crosslinking of the enzyme or covalent bonding to the support material[162]. Cross linking occurs by linking enzyme to other enzymes, proteins or supports to from aggregates or crystals and covalent bonding occurs via binding of the enzyme to the support using covalent bonds[162]. In both cases, these methods have been met with challenges[162]. Cross linking has been cited as difficult to reproduce and difficulties have also been cited with unfavourable interactions between enzymes and cross linkers[162]. Covalent bonding requires modification of the enzymes structure to form covalent bonds, this can lead to interference with the enzymes tertiary structure leading to misalignment of key residues required for the enzymes functional operation or structural stabilisation[163].

The second form of enzyme adherence to a framework is physical immobilisation, in which enzymes are entrapped within the material or adsorbed onto the framework via interactions of van der Waals forces, hydrogen bonds and ionic bonds between the surface charges of the enzyme and surface functional groups on the framework[160,164]. These types of associations between the enzyme and the support have generally been associated with a reduced risk of alterations to the enzymes structure and thus benefits its activity[165]. However, enzymes are required to directly interact with the support material and therefore must complement each other. If they do not denaturation can still occur[162]. For example, interactions with a hydrophobic surface have been found to interfere with enzyme structure by destabilising hydrophobic residues buried within the core of the proteins structure[166]. However, the affinity of an enzyme to the carrier can be improved via the application of modifying agents such as silanes, amines and carboxylic acids[165]. Another drawback with adsorption techniques is a potential for leaching of the enzyme from the framework[164167]. This is particularly problematic in industrial applications where multiple reaction cycles are needed[167].

Entrapment is another physical immobilisation technique, designed to immobilise the enzyme without altering its structure whilst simultaneously reducing leaching of the enzyme from the framework[167]. Entrapment of enzymes is achieved by synthesising a polymer framework in a reaction solution in the presence of an enzyme[167]. Common examples of entrapment frameworks and methods are polyacrylamide, hydrogels and sol-gel[167].

As the polymer matrix assembles, the enzyme becomes entrapped inside the support rather than on it, as is the case with adsorption[167]. Entrapment using hydrogels and sol-gels was originally designed for whole-cell immobilisation[167]. Since enzymes are far smaller, leaching from the framework remains a pervasive issue[167]. A suggested solution for this issue is to increase the size of the enzyme bulk using cross-linking molecules[167]. However, an alternative solution might be to select a framework with porosity suitable for accommodating enzymes and their activity but prevents enzyme dissociation[168].

The second form is chemical immobilisation, in which enzymes are covalently bound or cross-linked to the framework[169]. Compared with adsorption or entrapment, covalent bonding is a far stronger form of attachment which has been found to produce a more stable enzyme - associated matrix. An example of a common commercial covalent bonding substance is Eupergit® C[167]. Covalent bonding is often facilitated by cross-linking molecules, which serve as a bridge between enzyme and the framework. Common crosslinking agents include glutaraldehyde and tetramethyl ammonium hydroxide[169]. The advantage of crosslinking molecules is they can provide additional space between the enzyme and the framework, which can reduce the potential for steric hindrance and better expose the enzymes active site for interactions with the substrate[170,169]. A notable drawback to covalent bonding is irreversible denaturation of the enzyme and the active site, which can lead to potentially costly loss of enzyme[167].

1.7.2 Performance Criteria for Immobilisation and Activity.

In addition to the chemical influence on interactions between the enzyme and framework, the physical nature of the support material can also strongly influence the success of a biocatalytic system. Principally, a support material should be able to withstand the conditions (chemical, thermal, mechanical, solubility) imposed upon it in an industrial setting[167]. Then the impact of surface area (SA) must be considered. A SA between 25 - 500 $m^2 g^{-1}$ is considered acceptable an immobilisation framework, however higher protein loading and thus greater system efficiency is linked to SAs towards the greater end of this range[167,168]. Extensive SAs can be achieved using very small particle sizes, but has been found to lead to challenges during recovery of enzymes[167]. High SAs can also be obtained by utilising porous materials[164]. However, care should be given that the PD within a framework is large enough to allow enzyme access into the inner SA of a porous particle[168]. Once inside, the pore volumes (PVs) must also be large enough to allow efficient enzyme-substrate interactions[168]. In addition to accommodating enzymes, PDs and PVs should allow easy diffusion of products, substrates and cofactors. It has been observed that mesoporous materials with highly ordered pore structure are effective catalytic frameworks, owing to more even molecular diffusion and mass transfer[171]. A metanalysis by Bayne *et al.* was able to identify the porosity features (SA, PD

and PV) required for a successful enzyme immobilisation framework[168], these values were extracted from that study and are presented in Figure 4.

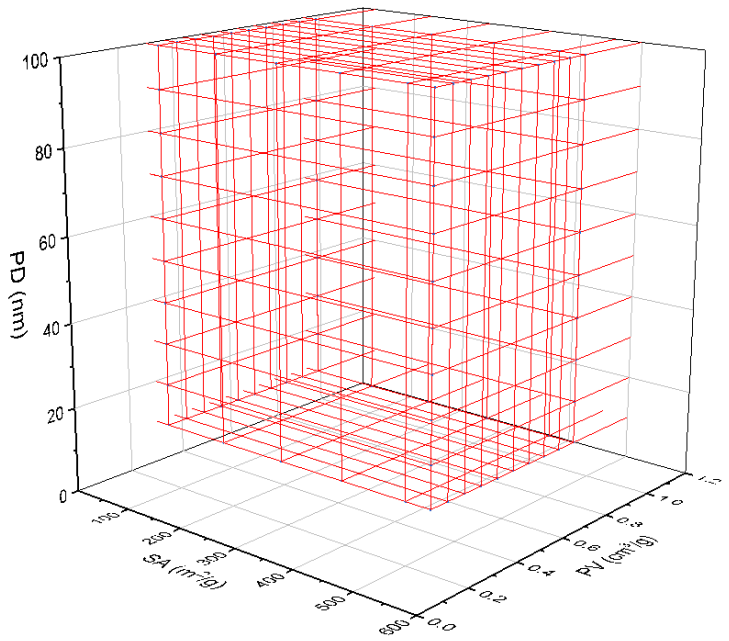

Figure 4. The 'ideal porosity zone' portrayed in red illustrates the ideal PD, PV and SA parameters required for enzyme immobilisation, substantiated by [168].

1.8 Immobilised Enzyme Systems for Conversion of CO_2 to CH_3OH

Following the initial experiment by Obert and Dave, many studies have since investigated the conversion of CO_2 to CH_3OH using other immobilization materials[151]. Later studies also incorporated modifications such as co-factor regeneration systems using glutamate dehydrogenase as part of their design[165]. Early studies in 1999 and 2003 employed sol-gel frameworks[172,173]. In later years, framework compositions diversified into beads made from tetramethoxysilane and alginate[174], protamine-silica beads coated a phospholipid microcapsule within a scaffold system[175], protamine-coated titania particles[176], phospholipid-silica nanoparticles[177] and, catechol and gelatine microcapsules[178]. In all these cases, biocatalytic productivity, defined as $\mu molCH_3OH$ / $mg_{enzyme} \cdot h$, was above or close to that of the free enzyme, suggesting a degree of success for these systems. However, when results from studies which included NADH regeneration systems are considered there are two instances in which free enzyme activity becomes markedly higher in comparison to the immobilised system[179,180]. This suggests that in earlier studies free enzyme activity may have been stunted by a limitation of NADH, giving a false impression that immobilised systems were as effective as the free ones.

Regarding immobilised systems, studies that included an NADH regeneration system in the form of glutamate dehydrogenase are characterised by increased biocatalytic productivity compared to those that did not. In the case of Cazelles *et al*., the initial amount of NADH was reduced by 80% compared with the non-regeneration system, and biocatalytic productivity rose by 393.1% (from 0.29 to 1.43 $\mu molCH_3OH$ / $mg_{enzyme} \cdot h$)[177]. This improvement is further illustrated by a significant increase in the system efficiency factor, defined here as $\mu molCH_3OH$ / $mg_{enzyme} \cdot h \cdot \mu mol_{NADH}$ - that is, the micromoles of CH_3OH produced per milligram of enzyme, per hour, per micromole of NADH used. In this system, the efficiency factor rose by 389.2% (from 9.77 to 47.8), suggesting that the far lower amounts of NADH present were being regenerated effectively[177]. In another study by Ji *et al.*, inclusion of an NADH regeneration system led to an increase in biocatalytic productivity of 33.3% (0.87 to 1.16 $\mu molCH_3OH$ / $mg_{enzyme} \cdot h$) with 98% lower initial NADH addition[179]. This increase in NADH efficiency and biocatalytic productivity activity despite far lower initial NADH levels highlights the effectiveness of including an NADH regeneration system.

Notable studies which did not include NADH regeneration and exceeded the biocatalytic activity of these aforementioned studies was Xu *et al.* in 2006 and Wang *et al.* in 2014[174,178]. In these cases respective biocatalytic productivity was 341% and 168% and 44.8% and 78.4% greater compared with the NADH regeneration systems of Cazelles *et al*. and Ji *et al*.[177–179]. This may be attributed to the far higher amounts of NADH initially added at the beginning of the reaction. These outcomes suggest that in the absence of an NADH regeneration system, good activity can instead be achieved by the introducing a large initial amount of NADH.

Setting the influence of NADH regeneration aside, another notable observation is that some of best outcomes in biocatalytic productivity appear to be associated with studies which have favourable framework spatial properties (SA, PD, PV). Unfortunately, no SA, PV or PV values could be discerned for the study by Xu *et al.*, which exhibited the best biocatalytic productivity[174]. However, other studies which generated alginate beads reported SAs between 76 - 165 $m^2 g^{-1}$, which is considered to be a good SA for effective enzyme loading (Figure 4)[181]. Additionally, the same study reported PDs of 450 nm[181]. This is far beyond the maximum for enzyme immobilisation (10 - 100 nm), however one observation is that PDs this large should have enabled full access to all of the available SA, resulting in high immobilisation[168] (Figure 4).

Whilst no study directly considers all three porosity factors (SA, PV and PD), certain studies reported some porosity factors which are above the minimum ranges defined in Figure 4. For example, the next best system for biocatalytic productivity was created by Wang *et al.* and reported PVs of 2.5 $cm^3 g^{-1}$, which is considered more than ample room for enzyme interaction

with substrates as well as the diffusion of associated products and co-factors[168,178]. Whilst PDs of 3.5 nm were reported, which are considered too small for enzymes to enter the PV, this may not have an impacted loading and activity in this case since the enzyme is trapped during aggregation of the colloidal particles, within the textual porosity of the framework[178]. Since the diameters of the enzymes are estimated to be between 7 - 10 nm, PDs of 3.5 nm should therefore trap the enzymes within the framework and prevent them from leaching out[178].

The next most successful study was Ji *et al*., who immobilised enzymes using coaxial, electro-spun polyurethane nanofibers with an estimated inner diameter between 700 – 1200 nm[179]. Considering the density and molar mass of polyurethane and assuming a cylindrical shape, this equates to an estimated PV and SA of 0.8 $cm^3\,g^{-1}$ and 6.2 $m^2\,g^{-1}$ respectively. This inner volume is well-within the required threshold for enzyme activity; however, the SA is well below what is adequate for good enzyme loading to create an efficient catalytic surface. This may be due to the high inner tube diameter, which would reduce overall SA in accordance with its size.

1.8.1 Impact of CA Addition

During their review of CO_2 to CH_3OH enzyme cascade systems, Marpani *et al.* suggested that the addition of the metalloenzyme CA might be an effective way of increasing the rate of CO_2 hydration and therefore its availability in solution for conversion[149,182]. Dissolution of CO_2 into an aqueous medium without CA can lead to the formation of several different molecules, depending on the pH of the solution (E. 1.7):

$$(1.7) \quad \underset{pH\,2\text{ - }6}{CO_2 + H_2O} \leftrightarrow \underset{pH\,6\text{ -}10}{H_2CO_3} \leftrightarrow \underset{pH\,10\text{ -}12}{HCO_3^- + H^+} \leftrightarrow CO_3^{2-} + 2H^+$$

At pH 6 – 10, with the aid of a zinc ion in its active site CA is able to catalyse the interconversion of CO_2 and bicarbonate (HCO_3^-)[177,182] (E. 1.8)

$$(1.8) \quad CO_2 + H_2O \xleftrightarrow{CA} H^+ + HCO_3^-$$

Depending on the species of CA, the hydration of CO_2 occurs at a rate of 104 - 106 reactions per second and is one of the fastest known enzymatic reactions[182–184]. The catalysis of CO_2 to HCO_3^- is able to occur due to a divalent zinc ion within the active site of CA[182] (Figure 5).

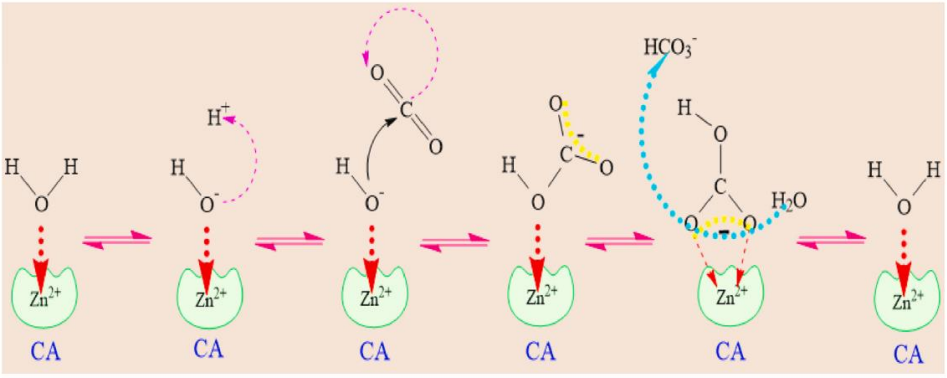

Figure 5. The reversible reaction pathway for the catalysed hydration of CO_2 via CA. Taken from [185].

In its hydrated form (HCO_3^-) reduction reaction kinetics are enhanced for subsequent reactions, such as conversion into formate via formate dehydrogenase (E. 1.9)[186], due to the reaction free energy being much lower ($\Delta_r G^o$ = - 165.39 kcal / mol at 25°C) compared to gaseous CO_2[64].

$$\text{(1.9)} \quad HCO_3^- + NADH + H^+ \overset{FDH}{\leftrightarrow} HCO_2^- + NAD^+ + H_2O$$

Therefore, the addition of CA could have important implications for improving the system efficiency of CO_2 to CH_3OH conversion as part of future scaling of this technology for an industrial application (Figure 6).

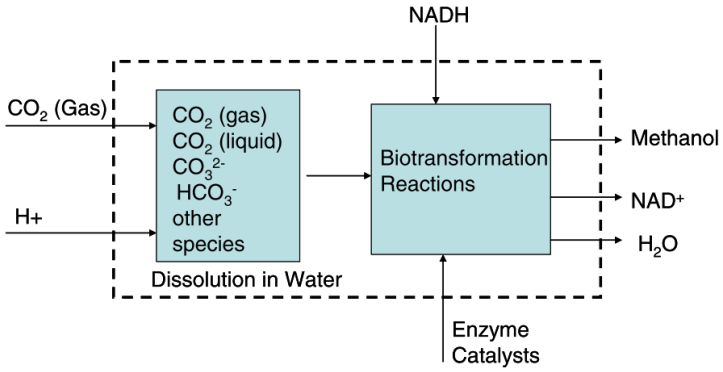

Figure 6. The role of CA in increasing the rate of conversion of gaseous CO_2 into hydrated forms (left box) to enhance CO_2 biotransformation into CH_3OH (right box). Taken from [64].

The addition of CA had been reported by several studies to be an effective means of increasing the reduction of CO_2 to useful fuels and products[187]. CA has been successfully applied as part of a free dehydrogenase system for converting CO_2 to formic acid, which led to a 4.2x increase in reaction rate[186]. In another study employing immobilised enzymes, CA addition improved the reaction rate by 1.3x and 4.7x compared to systems without CA[188,189]. In their 2015 study, Ji *et al.* included CA at the beginning of their reaction cascade and reported a 7.76%

improvement in biocatalytic productivity[179]. As of 2024, the market price of CH_3OH was approximately $353 per metric ton[190]. An ~8% increase in production efficiency could therefore translate to an additional $28 in revenue per ton of CH_3OH sold, which may have significant economic implications if the process is scaled commercially. Furthermore, if this productivity enhancement is coupled with continued development of framework materials to optimize enzyme loading and catalytic activity, it could substantially advance efforts to improve the economic viability of enzymatic CH_3OH production. A visualisation of this industrial reactor, with the inclusion of CA is depicted in Figure 7.

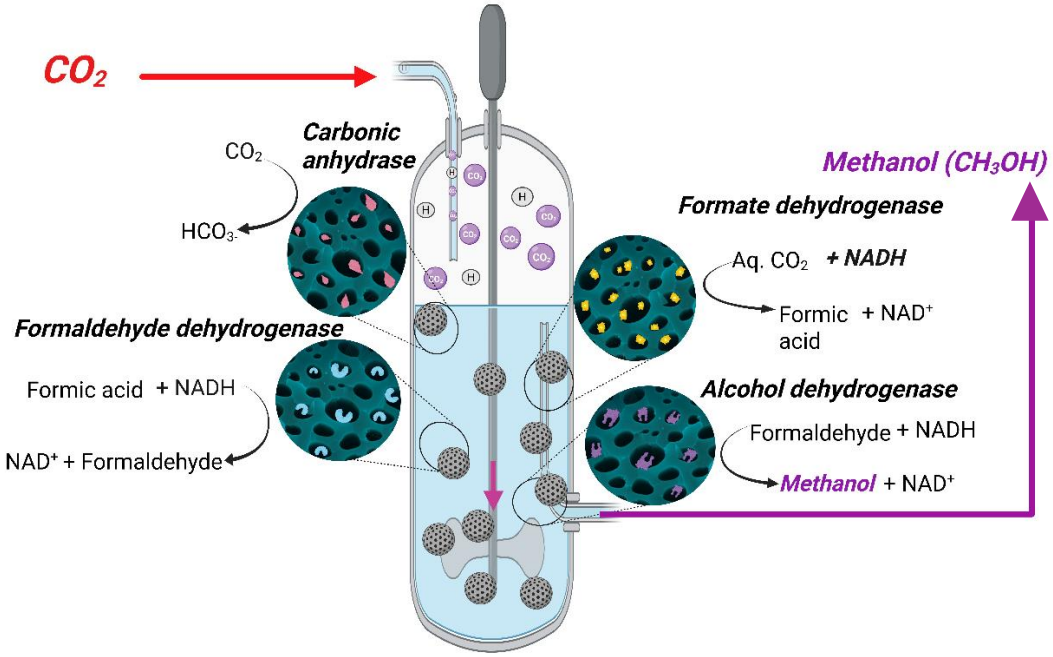

Figure 7. Visualisation of the enzymatic reaction pathway in an industrial bioreactor for the conversion of CO_2 to CH_3OH. CA is the first molecule in the cascade, followed by the dehydrogenase enzymes formate dehydrogenase, formaldehyde dehydrogenase and alcohol dehydrogenase[149]. Created using Biorender.

1.9 A Brief Literature Review of CA Immobilisation

As with the other enzymes used for industrial applications, researchers investigating CAs have experienced similar issues with enzyme recovery as well as limited reusability[185] often due to the high temperatures, high levels of organic amines, and trace pollutants commonly encountered in industrial applications of CA[182]. Numerous studies have sought to address these challenges by expanding the range of CA species explored for CO_2 hydration, focusing on variants capable of maintaining activity under extreme conditions[160,191–195]. Another field of research has been dedicated to investigating immobilisation, with conventional or more specialised CAs[160,185,193–218]. Immobilisation techniques have taken on a myriad of different forms (Figure 8) and have been reviewed extensively[185,219,220].

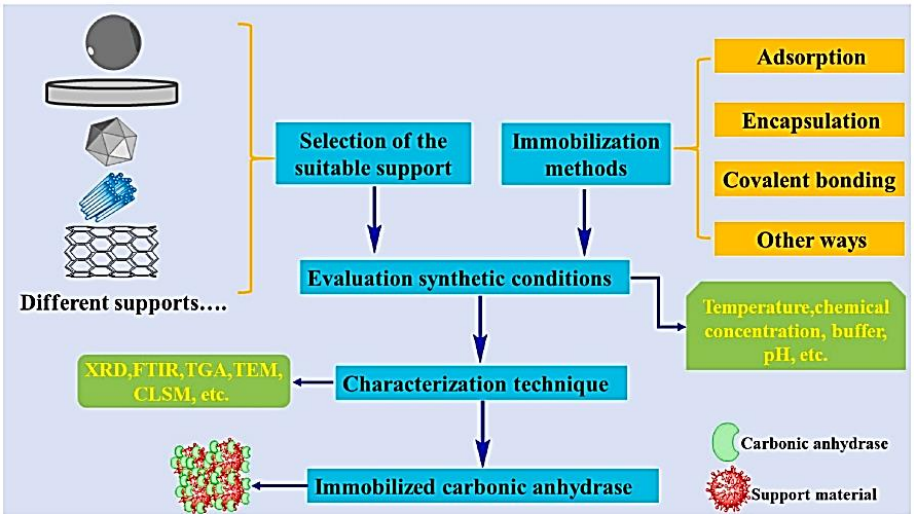

Figure 8. Immobilisation supports for CA[185].

Owing to its comparative affordability and applicability as a lone agent for CO_2 sequestration, CA has undergone many more years of intensive research by academia and industry compared with dehydrogenase enzymes. According to a recent review in 2021, CA has been "tested in a variety of configurations including packed columns, gas-liquid membrane contactors, dynamic devices and selective membranes"[219]. This has given rise to an extensive array of academic reports, which have been summarised in various comprehensive critical reviews[152,185,219,221–223]. These studies have used a variety of different species of CA and methods for measuring CA activity, such as hydrolysis of *p*-nitrophenyl acetate (p-NPA), CO_2 uptake by volume or pressure (manometric), precipitation of $CaCO_3$ and CO_2 hydrolysis via pH measurement. Within these methods, studies have also taken different approaches towards reporting CA activity, such as K_{cat}/K_m, V_{max}/K_m, V0, product removal efficiency and enzyme activity efficiency. This makes accurately identifying a single or a handful of studies based on the same metrics extremely difficult.

To identify promising immobilisation candidates, this study used a table created by Molina-Fernandez and Luis which summarised CA activity from 54 published reports[219]. This review included nanoflowers and metal-organic frameworks. Metal organic frameworks are created by assembling metal cations or clusters and organic ligands, this results in a material with adaptable pore structures such as cages or channels and pore sizes ranging from a few angstroms up to 10 nm[224]. Similarly to other frameworks, enzymes are then attached to metal organic frameworks via any of the immobilisation techniques previously described[224]. Nanoflowers are organic and inorganic structures arranged in layers or 'nano petals', which provide a large SA for enzyme binding and mass transfer of reactant molecules[225]. Despite their promise as an immobilisation framework, metal-organic frameworks and nanoflowers

were omitted from consideration for this study due to their fragility and low mechanical stability[219]. A low rate of enzyme replacement (kg CA / ton CO_2) has been cited to be essential for decreasing the operational costs of CA sequestration technologies. Since the focus of this study is identifying a sustainable enzyme framework for application within industrial carbon capture, these factors therefore make them unsuitable for their application at scale at present as they may be difficult to recycle or may deteriorate during rigorous industrial applications[219].

A huge diversity of different reporting methods across studies still existed within the 54 studies reported[219]. Which still made identification of "the best" frameworks challenging. This study therefore based much of its identification of studies for discussion on 'efficiency'. This was the most common factor and thus allowed the greatest comparisons between the most studies, however, there is some confusion in the literature regarding how to calculate this. Molina-Fernandez and Luis defined it as[167]:

$$(1.10)\quad immobilisation\ efficiency\ (\%) = \left(\frac{observed\ immobilised\ activity}{observed\ free\ enzyme\ activity}\right) \times 100$$

Whereas Sheldon and Van Pelt defined it as[167]:

$$(1.11)\quad immobilisation\ efficiency\ (\%) = \left(\frac{observed\ immobilised\ activity}{predicted\ immobilised\ activity}\right) \times 100$$

The efficiency measure was considered to be important because whilst a good immobilisation yield can be beneficial, it is meaningless if most of the immobilised enzymes are not active[167]. The results of the best-performing supports in terms of efficiency (>90%) are displayed in Figure 9.

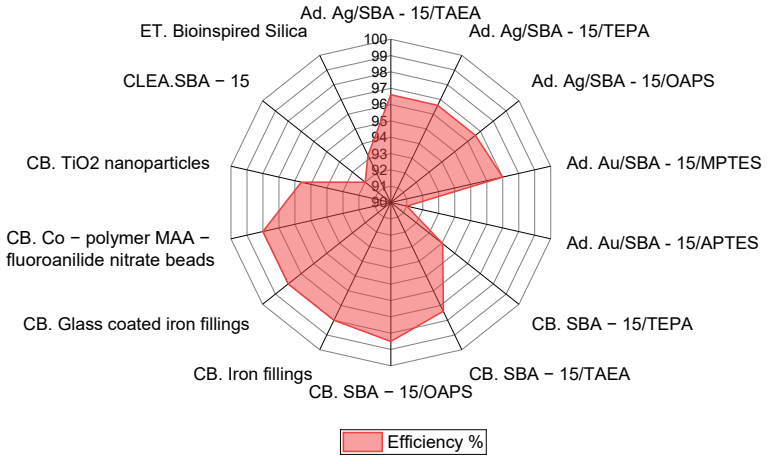

Figure 9. The activity efficiencies of the best-performing materials identified by [219]. ET refers to entrapment. AD refers to adsorption and CB refers to covalent bonding.

The supports which used covalent bonding performed best, with efficiencies between 98 – 98.6% (Figure 9). Studies which used covalent bonding to attach CA to iron filings, glass-coated iron filings, co-polymer methacrylic beads and SBA-15 as supports all reported efficiencies ~98% compared to the free enzyme (Figure 9)[198,199]. CA bound to iron filings, glass-coated iron filings, co-polymer methacrylic beads also displayed good stability against increased pH and temperature, with activity efficiency remaining above optimum levels up to pH 9.5 and just slightly below optimum (~90 - 95%) at 60°C[199].

However, when using the Molina-Fernandez and Luis immobilisation efficiency calculation this value does not consider how much of the enzyme is immobilised on the support. For example whilst it could have a high efficiency, if there is only a small amount of enzyme per weight of material, large amounts of support may be required to reach viable economies of scale[226]. Therefore, in addition to the Molina-Fernandez and Luis immobilisation efficiency the weight / weight loading (mg CA/mg support) was also considered (Figure 10).

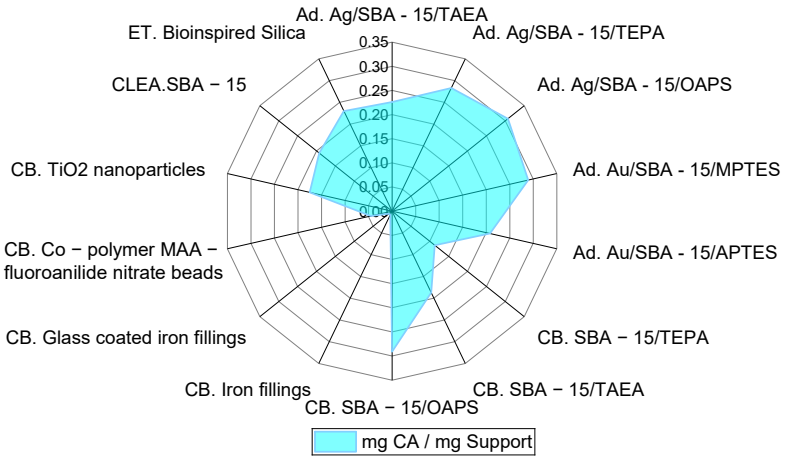

Figure 10. The w/w loading in terms of mg CA/mg support of the best-performing materials identified by [219]. ET refers to entrapment. AD refers to adsorption and CB refers to covalent bonding.

When loading is taken into consideration, this study had low amounts of loading in terms of mg CA/mg support. Typically, 0.02 mg enzyme / mg carrier is considered insufficient for industrial applications[226]. Iron filings, glass-coated iron filings, co-polymer methacrylic beads all had CA loadings 0.008 – 0.04[199] and leached between 10 - 18% from all these frameworks when in solution reducing this loading ratio further still[199]. Given this, further research into increasing CA immobilisation and preventing CA leaching may be worthwhile before this material could be used in industry[199].

Covalently bonded SBA-15, functionalised with octa(aminophenyl)silsesquioxane (OAPS) had both high activity and high CA loading of 0.3 mg/mg support[227] (Figures 9 and 10). This suggests it may be closer to the requirements of industrial applications; however, a leaching analysis would be required to ensure enzymes would not be lost from the framework which is an important criteria for immobilised enzyme systems[167,227]. Additionally, despite showing some tolerance to elevated pH the CA enzyme displayed low thermal tolerance, losing activity even before its optimum temperature of 37°C[198]. Such features would need to be improved it if could be considered as a candidate for industry[226].

Other supports with high efficiencies 96 – 97% were all derived from SBA -15, functionalised with various forms of amines with associated silver (Ag) or gold (Au) nanoparticles[217,228]. CA was then adsorbed via electrostatic interactions with these particles. In the case of Au nanoparticles, low leaching of CA was also reported for all of the materials assessed[218], which is a desirable trait for industrial applications. Another key observation is that whilst adsorption was intended to occur between CA and the Ag or Au particles on the surface of the SBA, it appears that the loading of CA was also influenced by the type of amine functionalisation molecule. For example, SBA-15 functionalised with tris(2-aminoethyl) amine and treated with Ag particles had a lower mg CA/mg support (~0.225 mg/mg support) compared with SBA-15 (0.3 mg/mg support) which also contained Ag particles but was functionalised with octa(aminophenyl)silsesquioxane (OAPS)[217] (Figure 10). In another example SBA-15 functionalised with (3-aminopropyl)triethoxysilane (APTES) and treated with Au particles displayed lower w/w loading (0.10 mg/mg support) and lower efficiency (90%), whilst the same material functionalised with (4-methoxyphenyl)methanamine (MPTES) displayed higher efficiency (97%) and higher w/w CA loading (~0.24 mg/mg)[228] (Figures 9 and 10). SBA-15 particles containing Ag and functionalised with OAPS or containing Au and functionalised with MPTES both achieved good activity and acceptable w/w loading and therefore show promise for industry[217,228] (Figures 9 and 10). However, a future direction in terms of progressing these materials would be to determine thermal and pH stability in the case of Au-MPTES-SBA-15 and leaching and thermal and pH stability for Ag-OAPS-SBA-15. Both of which are important metrics for progressing the assessment of their feasibility for industrial applications[226]. Despite some need for future investigations for these materials, when evaluating the studies depicted in Figures 9 and 10 for common themes between good efficiency % and higher w/w loading, CA immobilised to SBA-15 via covalent bonding and adsorption techniques appeared to achieve both criteria.

The observations from Figure 9 therefore strengthen the notion that porous supports may be some of the most effective for enzyme immobilisation and activity[229]. When available porosity data from these studies was collated and compared against the ideal porosity parameters

outlined by Bayne *et al*., it was found that SBA-15 silicas had SA which were beyond the upper limits of the ideal porosity zone[168]. However, the upper limit of SA was defined by Bayne *et al.* due to their findings that increasing SA concomitantly led to a reduction in PDs[168] but in the case of SBA-15, PDs and PVs remained suitable for optimal enzyme immobilisation and activity. Therefore in this case increased SA may have provided further SA for CA loading[168] (Figure 11).

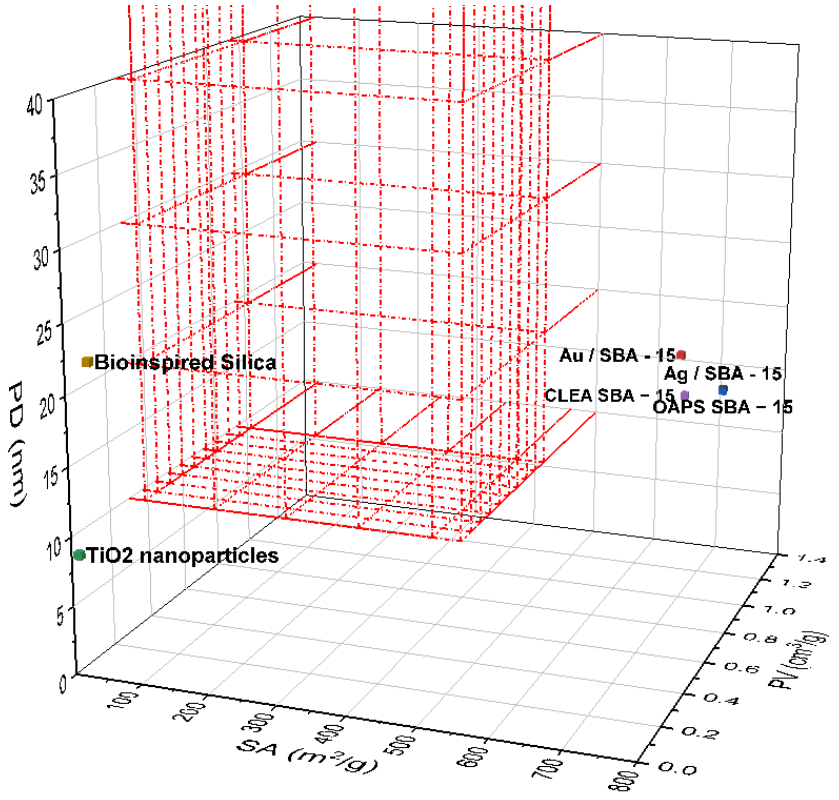

Figure 11. The 'ideal porosity zone' portrayed in red illustrates the ideal PD, PV and SA parameters required for enzyme immobilisation substantiated by [166], supplemented with the porosity features from the most successful CA activity studies identified from [219].

1.10 The Application of Silica Porous Frameworks for Enzyme Immobilisation

Silica, or more accurately silicon dioxide (SiO_2) is one of the most abundant minerals on earth and comprises >10% of the mass of the earth's crust. The ability of silica to form a highly ordered, chemically inert and porous substrate has made it the subject of intense interest for researchers, who have harnessed its potential for a number of practical applications within the modern world[230]. This has been achieved by the ability for scientists to exert great control over silicas formation by adjusting its chemical composition, resulting in bespoke specific sizes and structures[231].

1.10.1 Silica Formation

Silica begins its formation in basic or neutral aqueous media as a mono-silicic acid $(SiOH)_4$ or silicate anions $(SiO(OH)_3^-$ and $SiO_2(OH)_2^{-2}$ at pH >10)[230]. When the concentration of $Si(OH)_4$ monomers surpasses 100 – 200 ppm and forms SiO_2, polymerisation then occurs through the formation of dimeric and higher molecular weight forms of silicic acid (Figure 11)[230,232]. The process of polymerisation occurs via a condensation reaction, in which a molecule of H_2O is lost as a to create a siloxane bond (Si-O-Si) (Figure 11)[230](E. 1.12).

(1.12) $Si(OH)_4 + HO\text{-}Si(OH)_3 \rightarrow (OH)_3\ Si\text{-}O\text{-}Si(OH)_3 + H_2O$

Polymerisation of the dimer species into trimer, tetramer and oligomer molecules also occurs via E 1.12[230] (Figure 11).

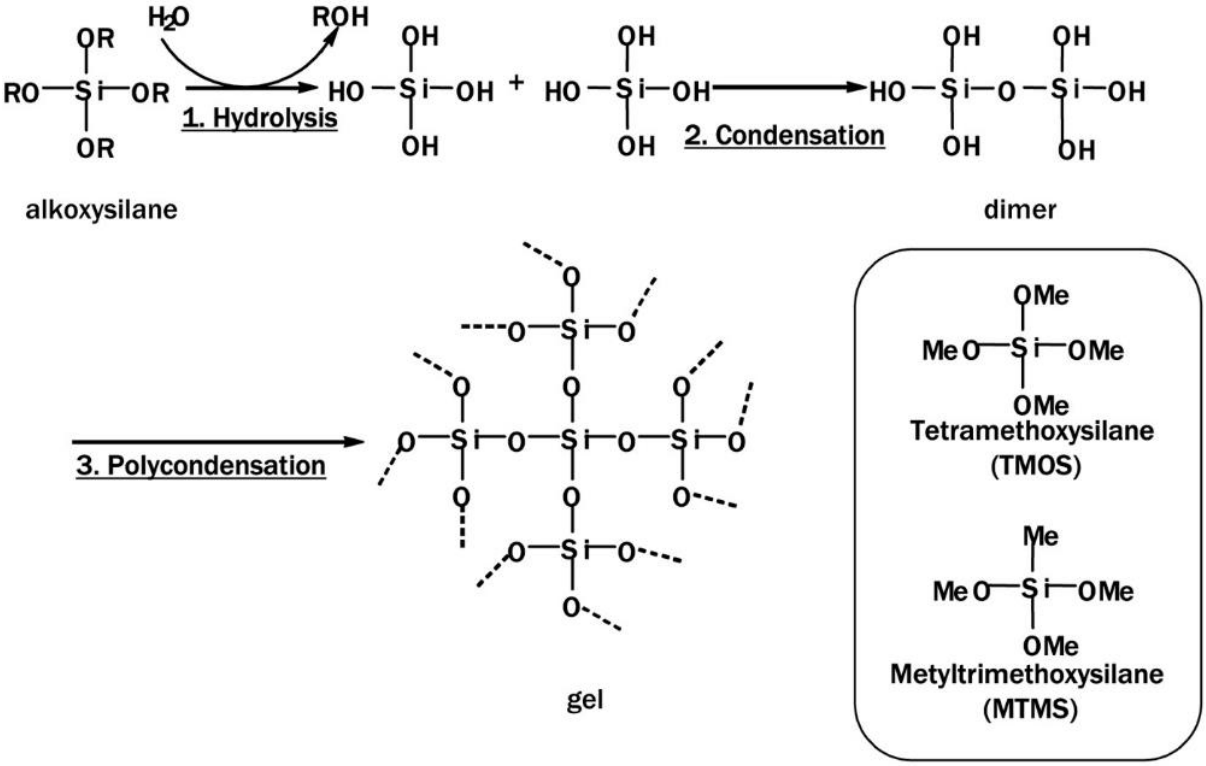

Figure 11: The behaviour of alkoxysilane monomers during the initial stages of sol-gel formation, taken from [233].

The nature in which these silicated extensions assemble into larger, visible crystals is largely governed by pH (Figure 12). If the pH is <7, there is low surface charge and repulsion, leading to the connection of particles as opposed to their growth leading to the formation of a 3D network[230,232]. When the pH is >7, higher surface charges means particles cannot aggregate and instead continue to grow as colloids; this eventually results in a homogeneous sol solution of particles which can have sizes ranging between 10 - 100 nm (Figure 12)[230].

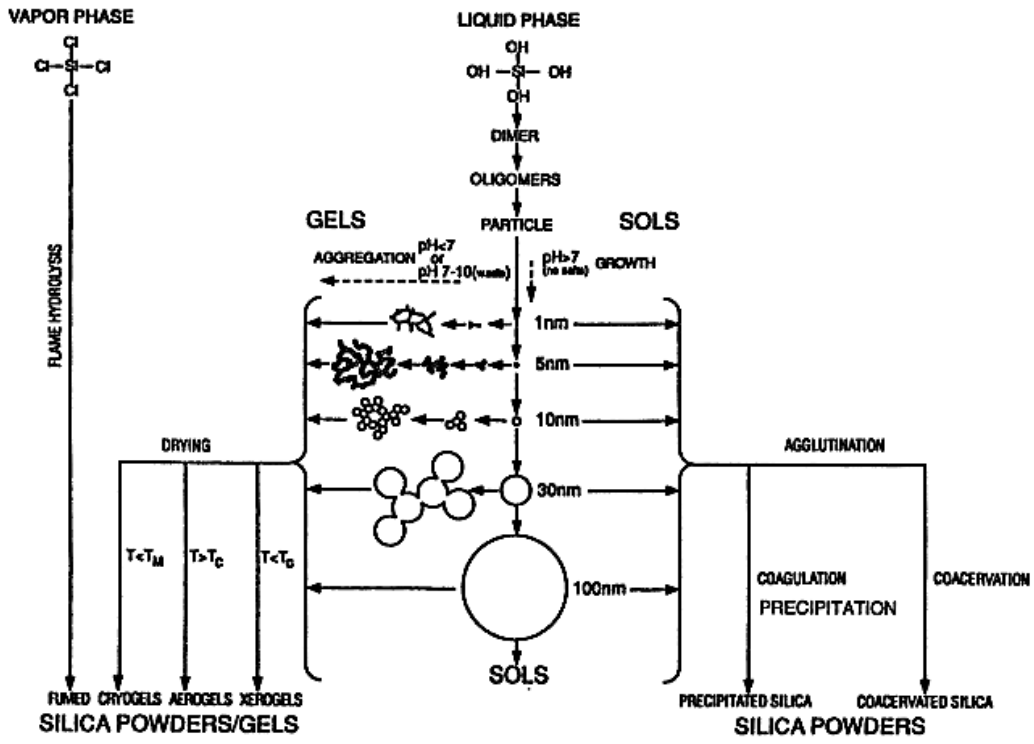

Figure 12. The pH-dependent pathways for different silica products, taken from [234].

The occurrence of free space within the matrix has enabled the entrapment of different biomolecules, including enzymes[235] (Figure 13). The success of entrapment and biomolecule functionality has been directly attributed to how well the engineered properties of the matrix suit the physiochemical needs of the biomolecule. This has given rise to several applications for sol-gel matrices as separation columns and bioreactors[233]. Attempts have been made to apply this mechanism to CA and dehydrogenase enzyme immobilisation[172]. In 1999, Badjic and Kostic used the gel formation pathway to encapsulate CA within the space between the gelled particles. They found that overall conformation of CA was better retained upon encapsulation[213]. CA was able to retain 77% of its structure when heated to 74 °C[213]. Unfortunately, this came at the cost of the specific activity of CA, which only retained 1 - 2% activity compared to the free CA in solution[213]. Researchers concluded that encapsulation had a deleterious effect on overall CA activity. An explanation for this might be because the formation of sol-gel in this way does not allow for the formation of a controlled pore structure, with pores and channels of a determined size[236]. Further, sol-gel formation uses the precursor molecule tetrahedral orthosilicate, which could affect the functionality of CA during *in-situ* encapsulation. In addition, a by-product of tetrahedral orthosilicate is methanol, which could also have impacted CA functionality[236].

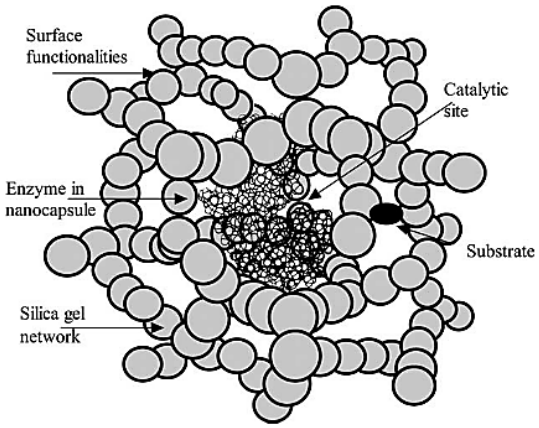

Figure 13. The result of in-situ encapsulation of a biomolecule in sol-gel. Taken from [235].

1.10.2 Immobilisation of Enzymes onto Supramolecular Templated Silicas

A way that sol-gel formation can be adapted to create materials with different physical properties is through the application of chemical templates to guide silica assembly[236]. These templates are called supramolecular surfactants and work by forming micelles which serve as the framework around which silicic acids then condense and establish a framework of silica[237]. Templates can take the form of lipids, amino groups and biological or synthetic polymers[238]. Once the template has performed its role, porosity is achieved by removing the template using either extraction or calcination[236] (Figure 14). The result is a highly ordered porous framework with consistent pore size. The wide-ranging availability of different templates has given rise to a plethora of different forms of silica, the most prolific being mesoporous Mobile Crystalline Material (MCM) and Santa Barbara (SBA)[237].

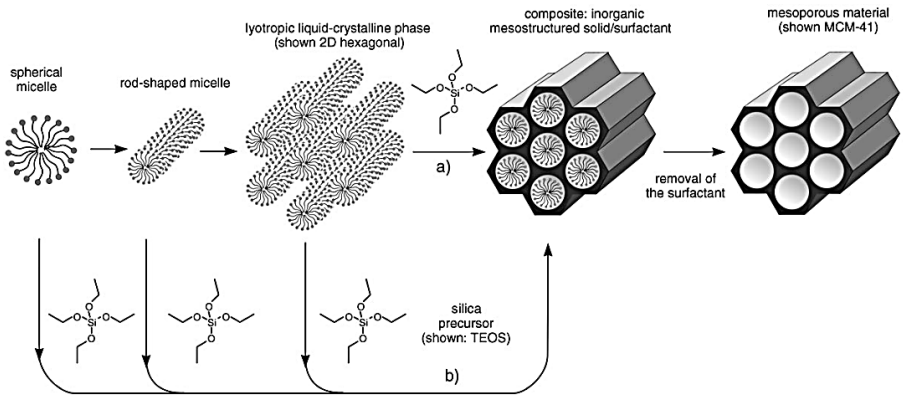

Figure 14. The application of template molecules for ordered assembly of silica and the types of products which can be produced, taken from [236].

Common variants in MCM silica structures are MCM-41, MCM-48 and MCM-50, which have hexagonal, cubic and laminar structures respectively and PDs of ~2 - 3 nm[214,236,237]. According

to the optimal porosity principles illustrated in Figure 4, pore sizes of this range are not good enough for enzyme immobilisation. Silica species with larger pore sizes can instead be created using tri-block co-polymer templates under acidic conditions[236]. These are known as SBA silicas. As discussed in Section 1.8, SBA - 15 has garnered significant success as an immobilisation framework for CA, which is an “ordered, two-dimensional carrier with PDs ranging between 5 - 15 nm”[214].

Manufacture of conventional ordered mesoporous silicas are currently characterised by energy-intensive and wasteful methods. Synthesis requires “high temperatures or ultrahigh vacuum leading to additional cost and energy”[239]. Post-synthesis treatment then utilises high amounts of water and energy, all of which results in a low final product yield[239]. To summate, conventional silica manufacture is therefore considered to not be in line with green chemistry principles.

1.10.3 Bioinspired Silica as a Green, Tuneable Enzyme Immobilisation Framework

Bioinspired silica (BIS) has emerged in recent years as a more sustainable method to produce high-value silicas. It has been developed based on revelations regarding how silica structures are formed in natural aqueous environments, using soluble silicic acid and additives in the form of proteins, poly-saccharides and small-amines[240]. The use of cheaper and more diverse analogues of these biomolecules has enabled researchers to create cost-effective, highly-tailored BIS possessing specific properties relating to particle size, surface chemistry, porosity and shape[240,241]. Further, this process avoids the use of toxic chemicals, wasteful synthesis processes and high energy input through its chemically and thermally mild synthesis route (pH 6 - 7; <40°C)[239,240,242]. This is achieved whilst maintaining a high degree of control over the synthesis process[240]. In brief, the reaction uses a silicate or an alkoxysilane precursor, which upon hydrolysis condenses to silica in the presence of a selected additive (Figure 15).

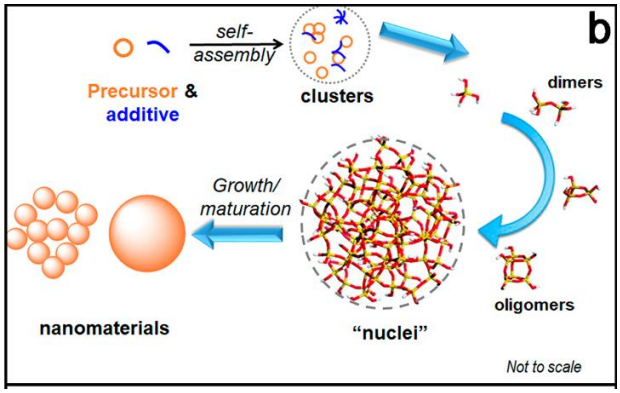

Figure 15. The formation of BIS from precursor to primary particles. Taken from [231].

The initial particles form at sizes of 5 to 10 nm and subsequently aggregate into secondary particles measuring approximately 200 to 400 nm, with additive molecules acting as interlinking agents between particles. Finally, tertiary particles form via further agglomeration of these 200 - 400 nm particles[231] (Figure 16). Porosity is characterised as the spaces between these polydisperse particles[231]. This is known as Generation 1 BIS. It is anticipated that BIS will result in lower cost-production of silica and significantly better sustainability through the reduction of energy, feedstock chemical input and waste avoidance while also achieving many of the principles of green chemistry[239].

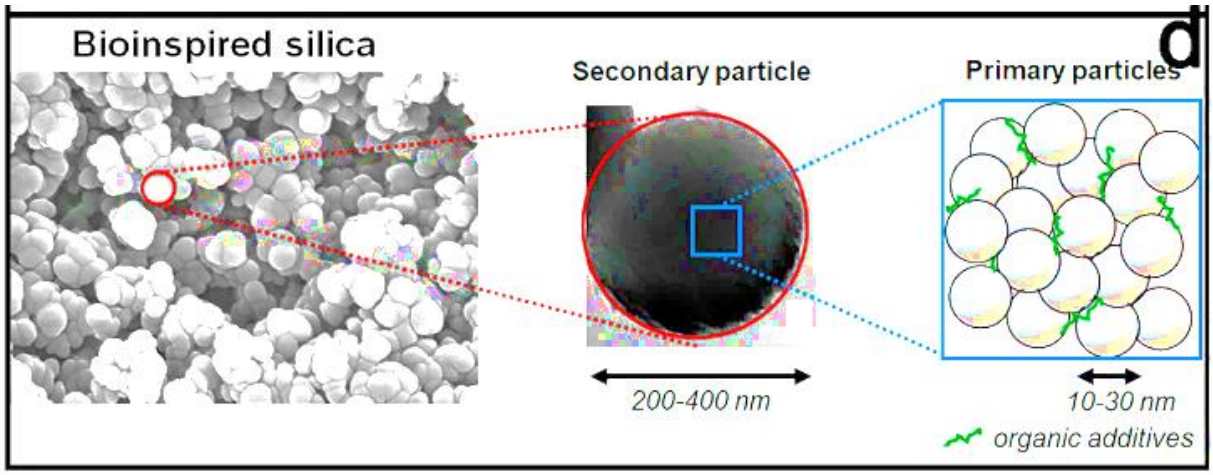

Figure 16. The stages of primary (right), secondary (middle) and tertiary particles (left) in BIS. Taken from [231].

1.10.3.1 Bioinspired Silica Formation and Enzyme Immobilisation

Additives can impact BIS properties by influencing its rate of formation and porosity (SA, PD, PV) characteristics through catalysing, scaffolding and templating and, aiding self-assembly and aggregation patterns[243]. Additives influence the aggregation during silica polymerisation by altering the interactions between oligomers, which are ordinarily negatively charged at pH 7[243]. The positively charged additives attract negatively charged silica species leading to additive-directed aggregation[243]. This leads to the formation of a disordered material, consisting of polydisperse particles.

In addition to other reaction parameters such as pH and reactant concentration, studies have discovered that adjusting the length of the additive or the number of amine groups within a molecule can influence the porosity of BIS, leading to an increase in the SA of BIS to 300 m^2 g^{-1}[244,245]. For instance, the use of the small amine additive pentaethylenehexamine (PEHA) has generally been found to result in a microporous BIS material with a low SA, functionalised with PEHA between its primary particles[231]. Polyethylenimine is a much larger molecule, and when used as an additive for BIS synthesis results in a mesoporous material

with greater SA[231]. In the case of PEHA additive removal via post-synthesis treatment with hydrochloric acid (HCl) has been found to increase porosity further, leading to non-functionalised PEHA with greater microporosity and SA[231].

The use of additives along with some modification to the BIS synthesis process has led to several studies exploring the entrapment of different species of enzyme within BIS pore spaces[212,246–251]. Further, several others have been immobilised via adsorption[252–254]. This is as a mild, green, low-cost route for immobilising enzymes using methods which are the least-likely to impact their activity. Studies have reported positive outcomes with regards to increased pH stability[246,247], thermal stability[212,246–249,252,253] and recycling stability[212,246–248,250,251]. In studies which reported porosity data, materials were generally of low PV <0.01 $cm^3\ g^{-1}$ and SA (<50 $m^2\ g^{-1}$) but mostly had PDs >10 nm (Figure 17). What is notable from Figure 17 is that no studies created a framework which fell within the ideal porosity zone outlined by Bayne *et al.*[168]. If studies were to use encapsulation, PD <10 nm may not be such an issue, since the enzyme should already be trapped inside the silica framework. However, the majority of Gen - 1 BIS still did not have PVs or SAs large enough to meet Bayne *et al.* porosity requirements[168]. This presents a problem in using Gen - 1 material for enzyme immobilisation and there is a need to produce mesoporous silica in a green way.

To this end, recent investigations within the Green Nanomaterials Research Group within the Department of Chemical and Biological Engineering at Sheffield University in the United Kingdom have uncovered a new [redacted] synthesis method for functionalised BIS with suitable porosity for enzyme immobilisation. [redacted]

[redacted] This second generation of BIS is termed Gen 2 and is mesoporous, with higher SA and PVs within the ideal range for enzyme immobilisation (Figure 11). Further to this, [redacted] can further increase framework porosity by removing the additves[255], creating a third generation of BIS (termed Gen 3). The application of these materials for immobilising CA creates an opportunity for progressing the field of enzyme-based reduction of CO_2 to valuable fuels and chemicals using a sustainable framework.

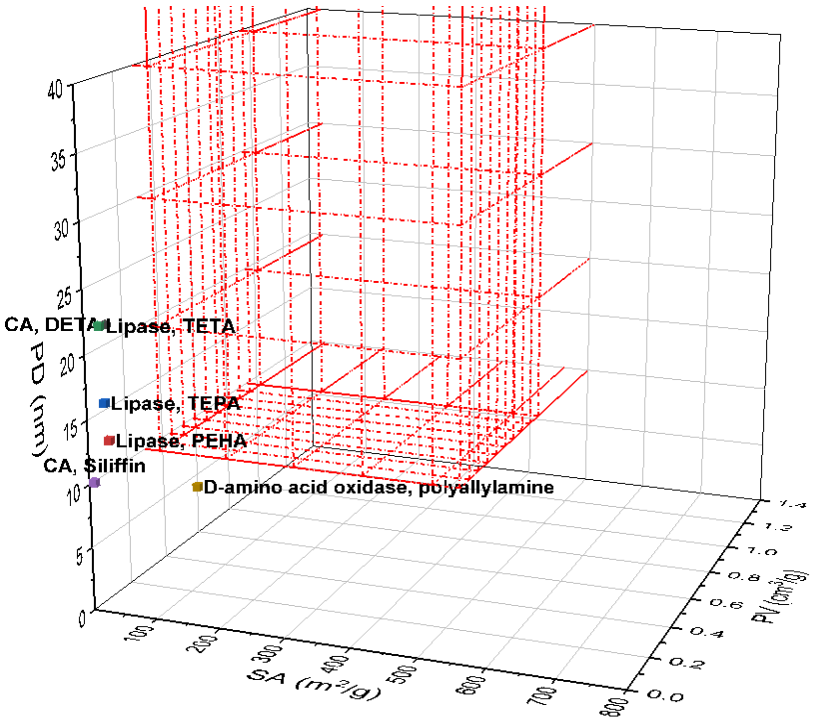

Figure 17. Porosity distribution of different BIS frameworks created using different bioinspired additives, alongside the ideal porosity parameters defined by [168] *and depicted as the red box.*

1.11 Biochar as a Green, Tuneable Enzyme Immobilisation Framework

Gonzalez *et al*. reported in their 2013 study that biochar possesses unique chemical and physical features which may fulfil the requirements of a successful immobilisation framework[256]. In support of this observation, it was concluded by Pandey, Daverey and Arunachalam that biochar could serve as a "stable, inert and economical matrix" for immobilized enzyme systems[150]. One of the reasons for the interest in biochar by researchers is the large SA, often facilitated by pores, which creates a matrix-like structure within the biochar for immobilisation of enzymes (Figure 18)[150,256]. In contrast to other carbon-based materials such as activated carbon and charcoal, biochar has also been reported to have naturally occurring surface functional groups (SFGs) which can be altered depending on the choice of feedstock and hold enzymes in place via adsorption, without the need for additional surface modification treatments[150,153,256,257]. As previously discussed in this chapter, adsorption is considered to be a relatively unintrusive binding mechanism, occurring through van der Waals forces, H-bonds and electrostatic interactions, and has been cited to bind enzymes with a reduced chance of negatively altering their molecular structure[165].

It is important to note however that freshly produced biochar is widely considered to be hydrophobic[258,259]. In contrast, CA is a water-soluble enzyme with a hydrophilic exterior enriched with polar and char amino acids (e.g. lysine, arginine, histidine, aspartate, glutamate,

serine and threonine) that interact readily with water[220,260]. These differences reduce the likelihood of stable adsorption between biochar and CA[185,221]. However, these factors can be overcome with the introduction of carboxylic acid SFGs onto biochar, which increase surface polarity and hydrophilicity[260]. Further, if adsorption is undertaken at neutral pH or slightly basic pH, these carboxylic acid groups impart a negative surface charge which can induce strong electrostatic attraction (ΔG = 12.5 - 25 kJ/mol) with positively charged amino acid residues (e.g. lysine, arginine and histidine) within the CA structure[260,261]. Though weaker than electrostatic interactions (ΔG = 2.0 - 7.5 kJ/mol), carboxylic acids can also provide opportunities for H bonding by acting as H electron donors and acceptors[150,260,261]. Considering this, the presence of carboxylic acids on the surface of biochar may present a means of facilitating bonding between the enzyme and the surface, without altering its structure. Therefore it has been postulated that enzyme immobilisation onto a biochar framework may provide enzyme stability and activity, with minimal cost to its activity[150].

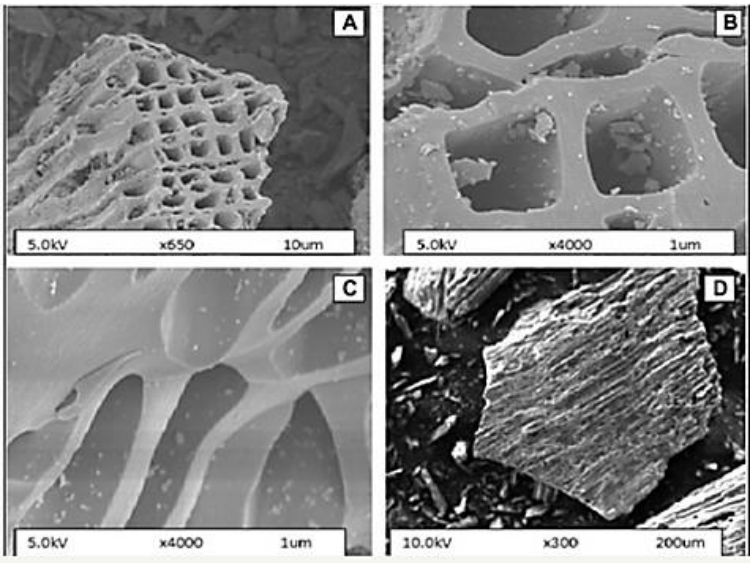

Figure 18. Scanning electron micrograph of biochar derived from pine wood, taken from [262].

In addition to its physio-chemical attributes, biochar's widespread availability and renewable nature, as well as the relative ease in which it can be made also lend it the potential to serve as a comparatively economical and sustainable alternative compared to other immobilisation materials such as conventionally manufactured silicas like SBA-15[150]. It should be noted however that these favourable features of biochar have been cited to be deeply dependent on the type of feedstock and the process conditions, pyrolysis temperature, feedstock, activation treatment, used to create it[150]. Therefore, a careful understanding of the effect of these parameters on resultant biochar porosity is required to select a framework which falls within the optimal porosity range identified for enzyme immobilisation.

1.12 Study Rationale

Careful selection of biochar feedstock and manufacture conditions may result in a sustainable framework with ideal porosity characteristics and surface chemistry for enzyme immobilisation. However, prior to its use, a full understanding of the influence of feedstock, pyrolysis conditions and activation treatments on this porosity is required to select a candidate with ideal porosity for enzyme immobilisation.

In addition to biochar, through the careful selection of specific additives and post-synthesis treatments, could result in a green BIS framework with ideal porosity for CA immobilisation. Informed by the literature, it was decided that immobilisation of CA via both entrapment and adsorption should be investigated, given their ability to immobilise CA without interfering with the enzymes molecular structure. A further justification and rationale for these methods will be discussed in greater detail in Chapter 4.

1.13 Conclusion

There is major concern over the issue of climate change and whilst methods for removing and preventing CO_2 emissions are being rolled out at scale, there are still issues with cost and delays in the transition. This is particularly prevalent for struggling high - CO_2 emitters such as the transport sector and heavy industry. CCC technologies could assist these industries in their transition to low carbon technologies by capturing CO_2 emissions and transforming them into valuable fuels and chemicals such as CH_3OH. Production demand for CH_3OH is currently being met using fossil-fuels, resulting in further CO_2 emissions. Many novel methods of creating sustainable CH_3OH by transforming waste CO_2 are under investigation. The main alternative method for generating CH_3OH is rare-metal catalysis, but this has cost and sustainability concerns.

Enzymatic conversion using dehydrogenases presents an alternative, renewable method. However, the technology is very much in its infancy. Immobilisation of the enzymes are essential for their recovery from the reactor to improve the economics of the process. Immobilisation can also enhance enzyme stability against pH and temperature fluctuations outside of the enzymes optimal range. Studies into immobilisation of dehydrogenase enzymes thus far have used a wide variety of frameworks and significant leaps have been progressively made over years of research. Particularly in the integration of co-factor regeneration systems, and later in the inclusion of CA to speed up CO_2 hydration. As part of reviewing studies for this project, a link was noticed between successful enzyme systems and framework porosity.

This trend was further explored in CA studies, which were far more numerous owing to its own importance as an agent for CO_2 sequestration. Following evaluation of the most successful

CA systems, it was found that the highest-performing systems in terms of efficiency and w/w loading of CA used the silica material SBA-15; with PV and PD characteristics that fell within the ideal range. However, SBA-15 is a high-resource material in its manufacture and produces a significant amount of toxic waste. More recently, a sustainable form of silica with tuneable porosity in the form of BIS has emerged. Most recently, a cutting-edge method [redacted] promises to yield BIS with porosity which falls within the ideal range required for enzyme immobilisation.

Finally, biochar has also been the object of intense investigation for enzyme immobilisation. This is due to its regenerative and economical nature, purported high SA and tuneable porosity through careful selection of feedstock and manufacture conditions. Therefore, a deeper investigation into its applicability for CA immobilisation seemed worthwhile. By developing sustainable frameworks with optimal porosity and evaluating them for enzyme immobilisation and activity, this investigation aims to advance the use of CA immobilisation to enhance CO_2 conversion. Ultimately, it seeks to contribute to enzyme-mediated carbon capture and conversion (CCC) toward the production of valuable fuels and chemicals, such as methanol (CH_3OH).

1.14 Thesis Aims and Hypotheses

The overarching aims of this thesis are:

1. To conduct an in-depth desk-based analysis of the applicability of biochar as an enzyme immobilisation framework based on whether its porosity can be intentionally tuned through choice of feedstock, pyrolysis conditions and activation treatment.
2. To characterise commercial biochar samples informed by the desk-based analysis for porosity, stability and presence of SFGs.
3. To examine whether the activity of CA immobilised onto BIS, [redacted] . achieves activity efficiency comparable to the best performing frameworks discussed in Section 1.9.
4. To compare the activity of CA adsorbed onto BIS against the activity of CA encapsulated during BIS formation.

Hypothesis 1: The extensive SA of biochar makes it a suitable framework for enzyme immobilisation and this SA can be selected for based on feedstock, manufacture conditions and activation treatment.

Biochar has often been reported to be porous and possess a large SA. As such, it has been cited to be a sustainable and potentially effective enzyme immobilisation framework. This has led to 43 studies using it in enzyme immobilisation trials. The extent of SA and the porous nature of biochar have been linked by many studies to the influence of pyrolysis temperature, feedstock and activation treatment. Therefore, for Chapter 3, porosity and manufacture data from 52 biochar studies was collated and the link between manufacture conditions and resultant porosity was explored in-depth to see if any trends between feedstock, pyrolysis temperature, activation treatment and PV, SA or PD could be discerned. Porosity data was also evaluated to see if any biochar candidates fell within the ideal SA, PV and PD parameters for enzyme immobilisation. This work was also supplemented with further data analysis and discussion into the application of N_2 gas adsorption for biochar analysis.

This hypothesis is explored in Chapter 3

Hypothesis 2: Selection of biochar informed by trends cited in the literature between feedstock, manufacture conditions and activation treatment and SA, PV and PD outcomes will produce a material with porosity features which will be suitable for immobilisation. This biochar will also be chemically stable and possess SFGs favourable for CA immobilisation.

It is claimed in the literature that the properties of biochar are dependent on pyrolysis temperature, activation treatment and feedstock. Therefore, three commercial biochars were selected based on their feedstock origins and manufacture conditions. Their porosity characteristics were then analysed using N_2 gas adsorption and mercury intrusion porosimetry (MIP). These porosity outcomes were informed by earlier findings from Chapter 3 and their suitability as an enzyme framework evaluated according to the ideal porosity zone identified in Chapter 1. Additional analyses in the form of FT-IR and CHNS and O analysis were also undertaken to see if favourable biochar SFGs were present and whether biochar was chemically stable enough to withstand an aqueous reaction system. In the case of FT-IR, in addition to possible enzyme binding sites, the presence and absence of certain SFGs also gave some indication of chemical stability. For CHNS and O, total C, C:O ratio and H:C ratio was each evaluated against published guidelines for biochar chemical stability. Results from the porosity analyses, FT-IR and CHNS and O were all informed by the chemical changes which occur in biochar, such as a reduction in total O and aliphatic groups and increases in total C and aromatic groups, depending on the pyrolysis temperature and lignocellulosic composition of the feedstock.

This hypothesis is explored in Chapter 3.

Hypothesis 3: CA and BSA loading success is influenced by temperature during adsorption and, by reactant concentration during entrapment.

Two immobilisation routes for CA on BIS were tested: temperature-dependent adsorption onto BIS post-synthesis and Syloid 244 and reactant concentration-dependent entrapment during BIS synthesis. An increase in adsorption temperature has been linked to an increase in enzyme immobilisation onto the framework, this is attributed to an increase in the number of potential interactions between the enzyme and BIS SFGs in which bonds such as van der Waals forces and hydrogen bonds can occur. Increasing the concentration of template molecules and silicate precursor in the reaction will lead to greater amounts of silica matrix forming per mL of reaction solution, giving greater opportunity for CA entrapment during particle aggregation. Bovine serum albumin (BSA) was also used as a model protein during entrapment to see if uptake varied between protein types. Outcomes from both hypotheses will be reported as enzyme loading success (%) and in w/w loading in terms of mg of CA per mg of framework.

This hypothesis is explored in Chapter 4.

Hypothesis 4: Protein immobilisation during BIS synthesis is influenced by protein concentration and pH at time of addition.

This hypothesis was tested using BSA as a model protein, with outcomes described similarly to CA as enzyme loading success (%) and in w/w loading in terms of mg of CA per mg of framework. BIS polymerisation is triggered when the pH of the basic reaction solution drops >10 due to the change in charge in the solution. As the pH continues to fall, dimer species join to form trimer, tetramer and oligomer molecules and eventually colloids which aggregate together to form the final matrix at pH 7. Addition of protein before this process begins may increase enzyme loading success by greater entrapment of the enzyme as oligomers come together and trap enzymes within their matrices. However, charges on the outer surface of the protein may interfere with aggregation, leading to poor immobilisation and non-optimal porosity. There is also the risk of enzyme denaturation when they are exposed to pH beyond their optimal range. The impact of pH addition point on protein loading was also tested at three different enzyme concentrations.

This hypothesis is explored in Chapter 4.

Hypothesis 5: CA and BSA entrapped in BIS with 'ideal' porosity features facilitates good CA and BSA loading, leads to activity close or equivalent to that of the free enzyme and is comparable or better than other leading frameworks.

The synthesis of BIS with optimal porosity should result in a material with PDs large enough for enzymes to pass through and occupy the inner SA of the particle, resulting in high loading due to greater access to the available SA. PVs should also be spacious enough to accommodate multiple enzyme units. Post-synthesis elution of the framework further removes the additives used during synthesis, resulting in even greater porosity. In response, enzyme activity should increase due to reduced mass transfer limitations leading to greater contact with the substrate and better diffusion of products from the matrix.

This hypothesis is explored in Chapter 4

2 Chapter 2: Materials and Methods

2.1 Chemical Reagents

Biochar pyrolysed at 700 - 800°C in the gasification system at the Translational Energy Research Centre (TERC) in Sheffield in the United Kingdom was obtained. The feedstock was wood pellets derived from an unknown mixed feedstock. The second biochar was sourced from WoodTek Ltd (WT) in Welshpool in the United Kingdom. It was derived from high lignin feedstock consisting of willow, alder, hazel, hawthorn, and chestnut materials and pyrolysed at 700 – 800 °C. The final biochar was hydrothermal char (HTC) obtained from Coal Products Limited (CPL) Industries and consisted of an unknown wood feedstock. It was pyrolysed at temperatures 170 – 300 °C under pressure using steam.

All deionised water used for these experiments was 18 m Ω. *p* - nitrophenol acetate (*p* - NPA) (≥99.0%) was used as a dissolution in ethanol, p - nitrophenol (*p* - NP) (≥99%) and used as a dissolution in pH 7 phosphate buffered solution (PBS) at 10 - 500 mM concentrations (>99%), both were obtained from Sigma Aldrich. CA from bovine erythrocytes ≥3, 500 and ≥2, 000 U / mg lyophilised powder (≥95%) were obtained from Sigma Aldrich and used in DIW or PBS, sodium phosphate dibasic heptahydrate (98 – 102%) and sodium phosphate monobasic monohydrate (≥98%) were obtained from Sigma Aldrich and used to create PBS solution. 37% hydrochloric acid was obtained from J. T. Baker and diluted to 0.1, 0.5, 1 and 2 M solutions accordingly. Trizma® base (≥99.9%) was obtained from Sigma Aldrich and used with DIW to create Tris buffer. Technical grade PEHA was obtained from Sigma Aldrich and diluted with DIW to a 1 M concentration solution. Anhydrous sodium metasilicate was obtained from Sigma – Aldrich and dissolved in DIW to create a 1 M solution. [redacted]

Bovine serum albumin (BSA) (≥96%) was obtained from Sigma Aldrich and dissolved in DIW at various concentrations. Syloid 244® was obtained from W. R. Grace Ltd (USA) and used as received.

2.2 Biochar Characterisation

2.2.1 Porosity Analyses

2.2.1.1 Sample Preparation

Sample homogeneity for biochar was ensured according to a reference protocol from[258]. Following that protocol, portions of the samples were taken and dried at 40 °C overnight. The first set of dried, uncrushed sample was stored in an airtight container with desiccant and used for porosity analyses using gas adsorption and mercury intrusion porosimetry analysis.

2.2.1.2 N_2 Gas Adsorption

Gas adsorption was selected for biochar characterisation because it is a well-established method for characterising the microporous and mesoporous fraction of solid carbon materials[263]. It works by adhering gas molecules to the surface of a material under pressure[264]. The pressure ranges can be as low as ~0.00001 to ~760 torr, and are adjusted based on what information is required from the material[264]. As the pressure is escalated, the pores begin to fill, beginning with small pores and filling progressively larger ones at the material becomes saturated[264]. This uptake of gas into the material forms an isotherm curve, which is expressed as pressure and the amount of gas adsorbed[264]. As gas is desorbed from the material, the two isotherms will often not coincide, forming a gap between adsorption and the desorption curve called a hysteresis[263]. Mathematical models such as Barrett Joyner and Helenda (BJH) , t-plot and Brunauer, Emmett and Teller (BET) were then used to explain the isotherm and determine the SA, PV and PD of the material[264].

2.2.1.3 Micromeritics Tristar Porosimetry

Porosity determination of biochar was initially carried out using a Tristar II Plus analyser from Micromeritics, USA according to a protocol by[265]. In the case of TERC biochar, N_2 gas adsorption revealed a high concentration of pores at ~2.5 nm which suddenly fell away <2.5 nm (Figure 1).

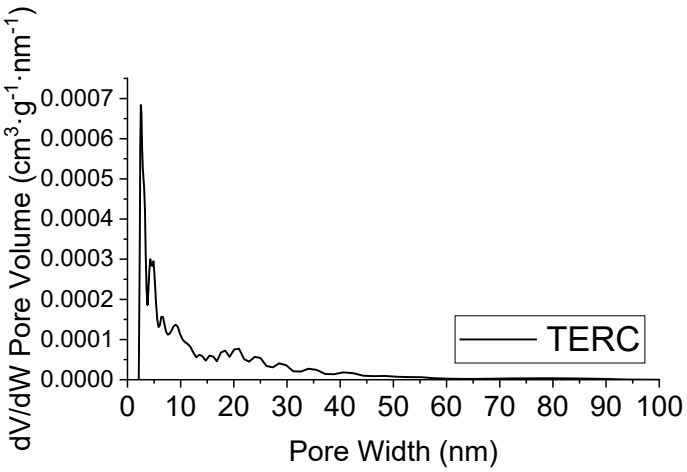

Figure 1. Pore size distribution for TERC and biochar from N_2 gas adsorption using a Micromeritics Tri-Star analyser.

Informed by Figure 1 and findings from Chapter 3, a high degree of microporosity in the TERC biochar was suspected. Therefore, all three samples were subsequently analysed using a 3 - Flex analyser (Micromeritics, USA) which has a superior capability to accurately measure adsorption at low partial pressures, where micropore filling takes place[266]. The same methodology from [265] was followed, with each biochar sample being degassed for two hours at 100°C. Adsorption of N_2 was then performed at 77K. At the end of the analysis time, only one of the biochar samples had a complete isotherm. This was suspected to be due to a high quantity of micropores in the material, which warrant longer degassing periods to completely remove any adsorbed H_2O. The degassing time was therefore increased from two hours to overnight (~12 hours). Results from both Tri-star and 3-Flex samples were analysed using the Micromeritics' MicoActive (version 4.06) data analysis software. For Tri-Star data, SA was calculated using the BET isotherm, and mesopores (>2.5 nm) were assessed using the BJH model. For 3-Flex data, BET was used for SA, BJH for mesoporous samples like HTC, and the t-plot model for microporous samples like TERC.

2.2.1.4 Mercury Intrusion Porosimetry

Macropores can constitute up to 95% of a biochar's total porosity[258] and gas adsorption is limited to pores of ~0.3 to 100 nm[267]. Therefore, Mercury Intrusion Porosimetry (MIP) was selected to characterise the macroporous faction of biochar, owing to its ability to accurately characterise porosity at a wide measurement range from 0.003 – 600 µm[268] (Figure 2). Unlike gas adsorption, mercury does not wet the surface of the material and thus must be forced into pores at considerable pressure[267]. The intrusion and extrusion of mercury occurs over several cycles, with isotherms generated from intrusion at lower pressures corresponding to

macropore filling and emptying. Conversely, lower pressures correspond to mesopores filling and emptying. In this way, MIP can measure pore sizes over a wide range of distributions[269].

Biochar samples were analysed with a Micromeritics Pore Sizer 9600 (Micromeritics, USA). A penetrometer with a 5 cm^3 bulb volume and 1.13 cm^3 capillary volume was used. Both the penetrometer and sample were evacuated prior to the measurement to reach 25 mmHg vacuum pressure prior to filling with Hg. The measurements consisted of two measurement cycles, one intrusion and one extrusion. Intrusion and extrusion were conducted in the high-pressure measurement range - from 7 kPa up to 414 MPa. Data was generated during the intrusion cycle after 345 kPa. The extrusion cycle was conducted from 413.7 MPa down to atmospheric pressure. This difference in pressure was then used to calculate a corresponding pore size, assuming a surface tension of 0.485 N/m and a contact angle of 130°. Data was analysed using the Micromeritics' MicoActive (version 4.06) data analysis software.

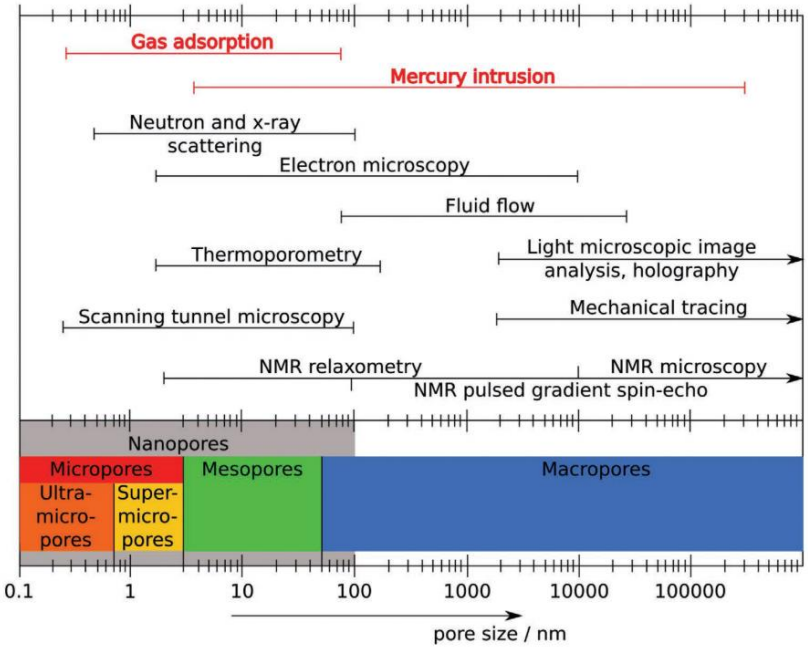

Figure 2. Pore size measurement range capabilities for various methodologies, taken from [269].

2.2.2 Ash Determination, CHNS and O and ATR-FTIR

2.2.2.1.1 Biochar Sample Preparation

The second set of samples was ground using a pestle and mortar followed by further homogenisation according to the protocol by[258] before being divided into sample pots for CHNS & O, ash determination and FT-IR analysis.

2.2.2.1.2 Ash Determination

Ash content is influenced by the composition of organic matter to inorganic matter in the feedstock[258] and was carried out as part of CHNS and O analysis according to a protocol by [258]. Briefly, prior to ash determination, biochar was dried at 105°C. Then biochar was sieved before being placed in a crucible. The biochar was then weighed, placed in a furnace (Thermo Scientific Heratherm™ OGS60) and programmed to heat from ambient temperature to 750°C at a rate of 5°C per minute and then held at 750°C under air for 6h before cooling to 105°C. Samples were then removed, covered and allowed to cool to ambient temperature before being weighed[258]. Ash weight was determined according to E. 2.1 below.

$$(2.1)\ Ash\% = \frac{weight_{\ residue\ after\ 750°C}}{weight_{105°C\ dried}}\ x\ 100$$

2.2.2.1.3 C, H, N, S and O Analysis

Elemental analysis was carried out in order to determine the C content of the biochars and the C:O and H:C ratio all of which can provide information relating to biochars chemical stability[270,271]. CHNS analysis works by introducing a precisely weighed sample to a furnace >1000 °C under a constant stream of high-purity helium[258]. Oxygen is then suddenly introduced resulting in near-instantaneous combustion of the sample[258]. The resulting gases are then passed through a quartz column with various metal catalysts to ensure complete oxidation of elements such as S, C and H to CO_2, SO_2 and H_2O[258]. The gas is then passed through a reduction column to remove unreacted O and reduce nitrogen species to N_2. Gas separation then occurs via a chromatographic column, with each species picked up by a signal from a detector[258].

CHNS and O analysis was performed using 1.8 – 2.2 mg of sample in an Elementar Vario Micro Cube (Elementar Analysensysteme GmbH). Samples were carried out in triplicate. The instrument used sulphanilamide and acetanilide for calibration and sulphanilamide as the correction factor. Samples underwent combustion in a pure oxygen environment at 1150 °C which then increased to 1800 °C owing to the exothermic reaction. Helium was used as the carrier gas. Once the C,H,N,S proportions were obtained, the O% was determined according to [272] as the residual value from the total C, H, N, S and ash in the sample subtracted from 100%[272]. H:C and O:C ratios were calculated at the % amount of H divided by the % amount of C and the % amount of O divided by the % amount of C respectively.

2.2.2.1.4 FT-IR Analysis

Attenuated total reflectance Fourier transform infrared spectroscopy (ATR FT-IR) was used as a semi-quantitative analysis of biochar formation and comparison of SFGs on the biochar surface. ATR FT-IR subjects a chemical substance to infrared radiation, which is absorbed at specific adsorption bands, leading to vibrations between their bonds which are specific to that

functional group[273]. These vibrations are detected as light signals by a detector and translated into units of absorbance, with the wavenumber spectrum (cm^{-1}) on the x-axis[258]. Biochar commonly absorbs radiation between the 4000 - 2700 cm^{-1} region and the 1800 - 1000 cm^{-1} region[258,273]. Strong adsorption tends to occur with polar groups such as carboxylic acids, which occur >1,680 cm^{-1} (owing to the *v*(C=O) mode) and of particular interest to this study[273].

ATR FT-IR was performed on each sample using a 'single bounce' Perkin Elmer Spectrum 2 instrument. The sampling protocol began by cleaning the sample stage using dichloromethane, followed by a background scan. Sample homogeneity was then ensured by inverting the sample several times before transferring it to the sampling stage and applying pressure to yield a 70% transmittance for the strongest spectral bands. The scan range was set to between 400 to 4000 cm^{-1}, 16 scans were performed in total and background subtraction was included. Resolution and temperature were set at 4 cm^{-1} and 20 °C respectively. The peak picking threshold was 0.8%. Spectral analysis was then performed, followed by baseline correction and application of an algorithm with 2% threshold for picking prominent peaks. Baseline correction was performed using OriginPro's 2024b baseline-correction tool with a "user defined" mode and "Adjacent-Averaging" smoothing. The tool was used initially to find anchor points automatically and then additional points were manually added where needed. A straight baseline was selected, which was set to connect by interpolation.

2.3 BIS Synthesis and Protein Entrapment

[redacted]

[redacted]

Once the reaction was complete, the solution was then centrifuged for 5 minutes at 5000 rpm in a centrifuge with a rotor size of 18 cm to separate the BIS-protein complexes from the solution. The remaining supernatant containing unbound silica oligomers, colloids, amines and sometimes unbound protein was then separated from the pellet. In the case of protein immobilisation, this supernatant was kept for quantification of unbound protein using UV-Vis spectroscopy. A portion of control solution without protein was also kept for use as a background blank.

The silica pellet was then washed with DIW, and the centrifugation process was repeated twice. In the case of protein immobilisation, these supernatants and their controls were also kept for unbound protein quantification. Once washed, the solid residue was then dried in an oven at 40°C overnight in the case of no-enzyme BIS. For CA entrapment, falcon tubes were filled with desiccation crystals, separated from the BIS by filter paper, and placed in the fridge. Equal removal of H_2O was confirmed via a comparison assay between the two drying methods (Figure 3).

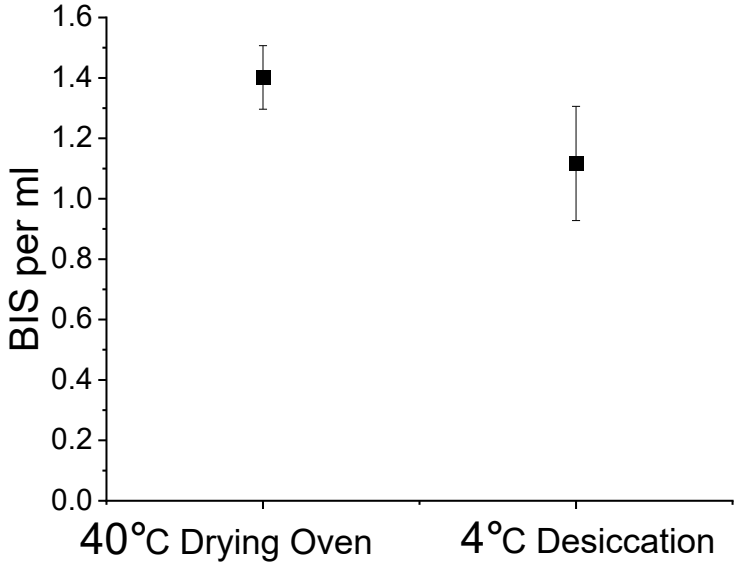

Figure 3. Impact of drying method on BIS yield. Expressed per mL of reaction solution. Error bars are the standard deviation between experimental replicates, where N = 3 and n = 3.

2.3.1 Quantifying Protein Entrapment

UV-Vis spectroscopy was used for the detection of unbound protein leftover in the reaction solution. Modern UV-Vis spectrophotometers such as the ones used for this experiment consist of a light source, monochromator, sample holder, detector, and signal processor. The light source illuminates a sample from a light range between 190 (UV) to 900 nm (visible wavelength)[275]. In some molecules and atoms, the photons from this light source cause electrons to be transferred from a lower energy level to a higher energy level[275]. This leads to the creation of a narrow band of absorbance for a particular wavelength which is specific to certain molecules. The instrument then measures the absorbance at each wavelength. The quantification is based on the Beer-Lambert Law. Which operates on the principle that absorbance (A) is proportional to molecule concentration (c), the sample path length (l) and the molar absorptivity (ε) of the molecule. This is expressed as $A = \varepsilon lc$[275]. If wavelength and absorbance at a particular concentration for that instrument is known, they can be identified and quantified[275].

UV-Vis was used to detect unbound BSA and CA in the supernatant and rinsing solution. All UV-Vis analyses were carried out using two different ThermoFisher Genesys 150 spectrophotometers. Initially, this was attempted using the Bradford protein quantification technique according to a protocol by[274], with experimental replicates (N) and sample replicates (n) performed in triplicate (Figure 4). However, this failed to produce a calibration curve with precise enough equations of a straight line (Figure 4).

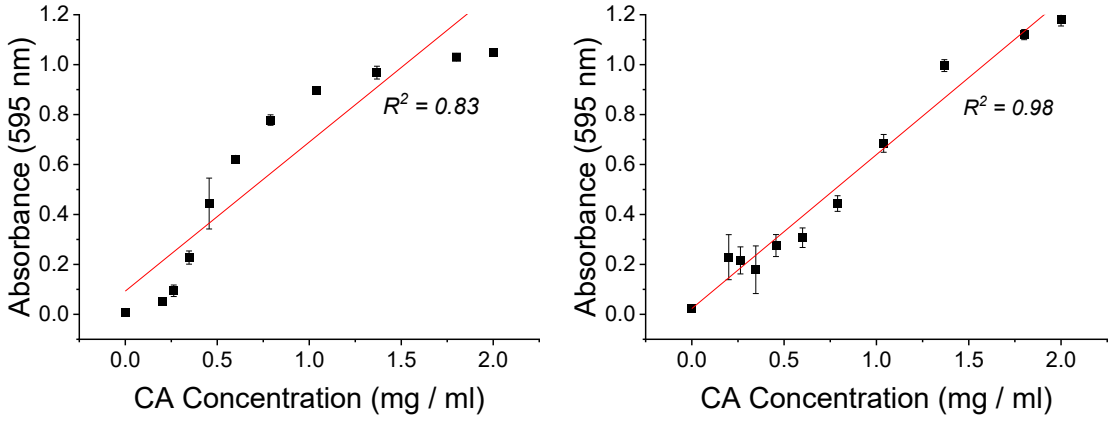

Figure 4. First and second attempt at a CA calibration curve using Bradford reagent. Error bars represent sample standard deviation, where N = 3 and n = 3.

According to a protocol by[276], CA could be detected in solution based on its own capacity for UV absorbance. This is owing to the presence of the amino acid tryptophan within its structure[277], which absorbs light at the 279 nm wavelength[275]. This was also found to be the

case for BSA[278]. Therefore, full-wavelength scans were performed to investigate if the presence of CA and BSA protein could be detected in solution without Bradford reagent (Figure 5).

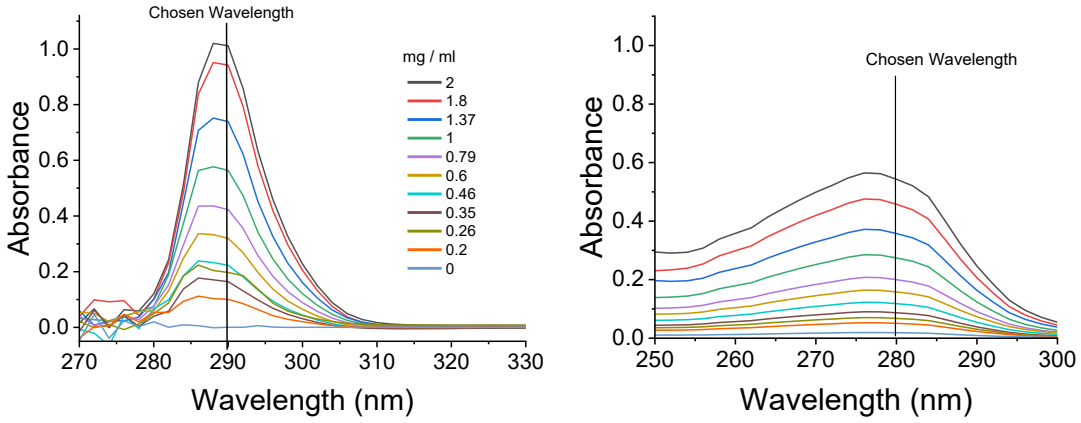

Figure 5. Full wavelength scans for 0 - 2 mg/mL CA (left) and BSA (right). Samples were diluted 1:1 with DIW prior to analysis. Selected wavelengths were 290 nm and 280 nm for CA and BSA respectively.

These wavelengths were then used to generate calibration curves (Figure 6), with equations of a straight line for a known amount of protein in solution which would be used for quantification of CA and BSA in the supernatant throughout the experiments (Table 1). Two different spectrophotometers located in E55 and C10 laboratories were used throughout these analyses. Variations in design, age, instrumental noise, cell positioning and surrounding environment conditions such as temperature can lead to differences in absorbance between instruments[279]. Therefore, standard curves were generated using both instruments (Figure 6). These curves were then used to calculate protein concentrations throughout the subsequent experiments.

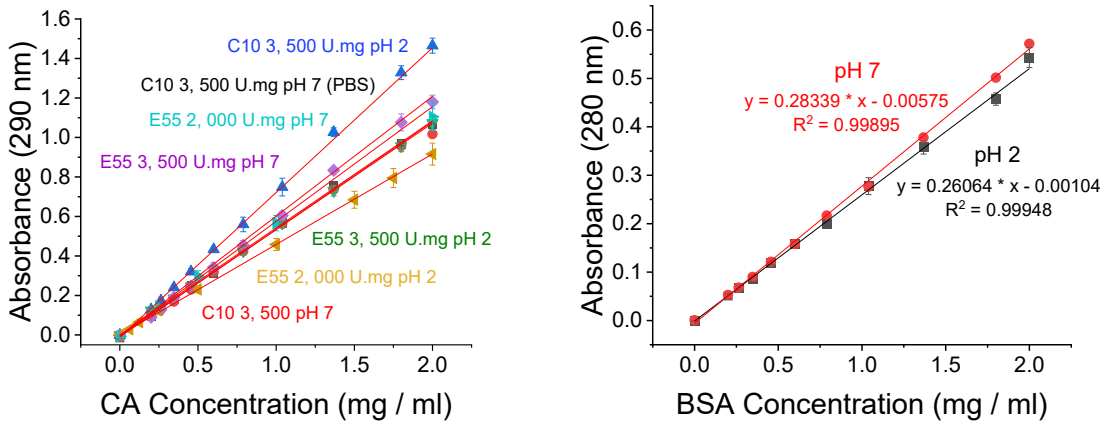

Figure 6. Calibration curves used for CA (top) and BSA (bottom) throughout experiments. CA quantification was performed on two different instruments "C10" and "E55". BSA quantification was only performed using the E55 instrument. Error bars represent the standard deviation, with N = 3 and n = 3.

Table 1: Calibration curve IDs for the different CA reagents, instruments and solutions used for CA quantification, along with the R^2 value and equation of the line.

Calibration Curve ID	Equation	R^2
C10 3, 500 U.mg pH2	y = 0.73278x - 0.01161	0.998
E55 3, 500 U.mg pH 7	y = 0.60634x - 0.00485	0.997
E55 3, 500 U.mg pH 2	y = 0.54212x - 3.2726E-4	0.999
E55 2, 000 U.mg pH 7	y = 0.58093x - 0.00606	0.998
C10 3, 500 U.mg pH 7 (PBS)	y = 0.5444x - 0.00935	0.999
E55 2, 000 U.mg pH 2	y = 0.4581x + 1.47598E-4	0.999
C10 3, 500 pH 7	y = 0.53978x - 0.00691	0.998

BIS samples were centrifuged quickly (using an optimised centrifugation time to separate BIS containing entrapped BSA or CA from unbound BSA or CA in the supernatant. This centrifugation time was optimised using a brief trial using reactant solution containing no protein (Figures 7 and 8). In Figure 7, some absorbance occurs without centrifugation in the supernatant solution at pH 7, this may be from residual unbound silica oligomers, colloids and amines. However, after 1 minute of centrifugation, the absorbance of these molecules and particles is reduced and equivalent to that of DIW. Meanwhile, CA remained suspended in solution at both pH 7 and 2, as indicated by the lack of change in absorbance. Therefore, it was determined that the remaining reactants could be effectively removed from the solution following centrifugation at 10, 000 for 1 minute (Figure 7). The same centrifugation procedure was then confirmed for BSA for 2 minutes (Figure 8).

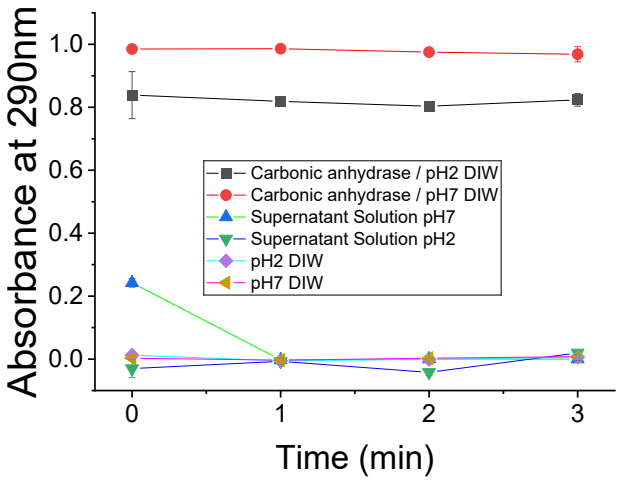

Figure 7. Testing CA separation via centrifugation at 10, 000 rpm using ~2mg/mL CA DIW solution at pH7 and pH 2 and BIS reaction supernatant. Error bars represent the standard deviation of experimental samples, where N = 3 and n = 3.

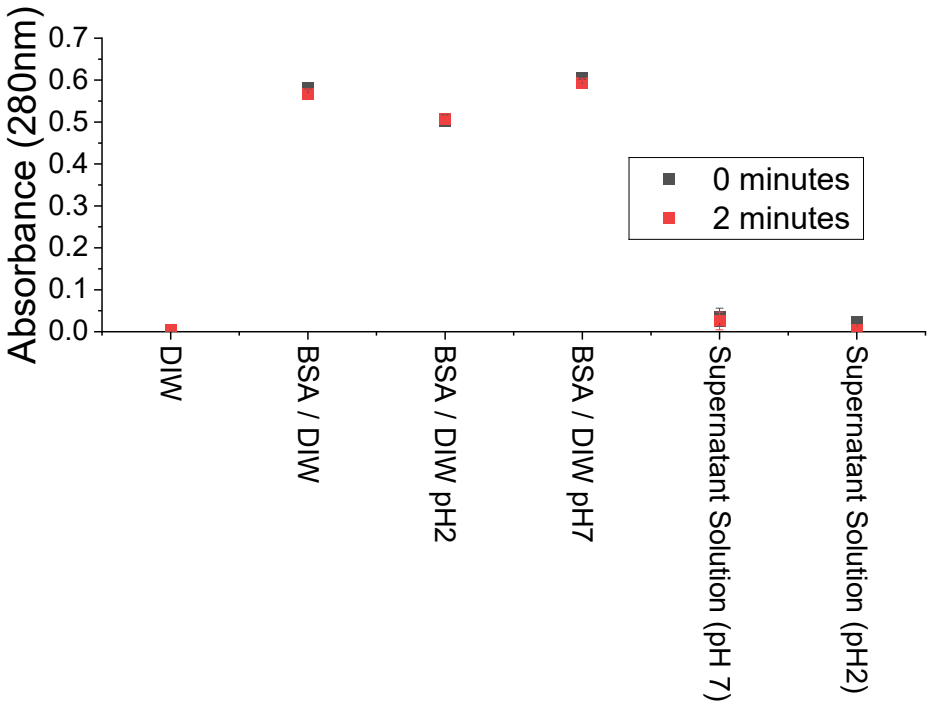

Figure 8. Confirming BSA separation via centrifugation at 10, 000 rpm after 2 minutes using ~2 mg/mL BSA solution in DIW at pH7 and pH 2 and BIS reaction supernatant. Error bars represent the standard deviation of experimental samples, where N = 3 and n = 3.

2.3.1.1.1 Measurements of Protein Immobilisation

Protein immobilisation for CA or BSA was determined using the equation of the line generated from calibration curves in Figure 5. This was used to determine the concentration of protein in solution. This was then multiplied by the reaction volume, which was repeated for subsequent rinsing stages. The amount of immobilised protein on the BIS was then calculated as E. 2.2 shows below.

$$(2.2)\ Initial\ Protein\ (mg) - \ Unbound\ Protein\ (mg) = Immobilised\ Protein\ (mg)$$

Loading success was then calculated as E. 2.3 describes.

$$(2.3)\ Loading\ success\ (\%) = \frac{Immobilised\ Protein\ (mg)}{Initial\ Protein\ (mg)}\ x\ 100$$

The total yield of BIS in mg was then calculated (E. 2.4):

$$(2.4)\ BIS\ and\ protein\ weight\ (mg) - \ Immobilised\ Protein\ (mg) = BIS\ yeild\ (mg)$$

This value was then used to determine the w/w loading of protein to support (E. 2.5):

$$(2.5)\ \frac{Immobilised\ Protein\ (mg)}{BIS\ Yield\ (mg)} = weight\ protein\ (mg)\ per\ weight\ BIS\ (mg)$$

The BIS yield per mL of reaction solution was calculated as below (E. 2.6).

$$(2.6)\ \frac{BIS\ Yield\ (mg)}{Reaction\ Volume\ (ml)} = mg\ BIS\ per\ ml\ of\ Reaction\ Fluid$$

2.3.2 Porosity Analyses

N_2 gas adsorption was performed at 77 K using a Tristar instrument (Micromeritics). Samples were degassed at 120 °C for 4 hours prior to analysis. Isotherms were analysed using MicroActive software (Micromeritics). SA was calculated using BET models and PD and PV size distributions were obtained from BJH models.

2.3.3 Statistical Analyses

To determine if there were statistically significant differences between entrapment experiments and between reactant concentrations for CA and BSA, a one-way analysis of variance (ANOVA) was used in Origin 2024b Software alongside a Tukey test to identify values responsible for significance and a Brown-Forsythe test to test if the variances were normally distributed. Significance was reported at p <0.05.

2.4 CA Immobilisation by Adsorption

The adsorption of CA was carried out by dissolving CA into 6 mL of 0.1 pH 7.5 PBS solution to obtain a final concentration of 2 mg/mL. To this, 100 mg of Gen 2, Gen 3 or Syloid 244 silica was added. These were then placed in a water bath at 37 °C, placed in the fridge at 4 °C or left in a water bath at room temperature (21 °C) for 24 hours. Experiments for each temperature were carried out in replicates of three. The interference of Gen 2 and Gen BIS silica had been discounted during entrapment reactant separation trials. However, the potential for interference of Syloid 244 had not. Therefore, another centrifugation analysis was performed, and separation via centrifugation was reached after 3 minutes (Figure 9).

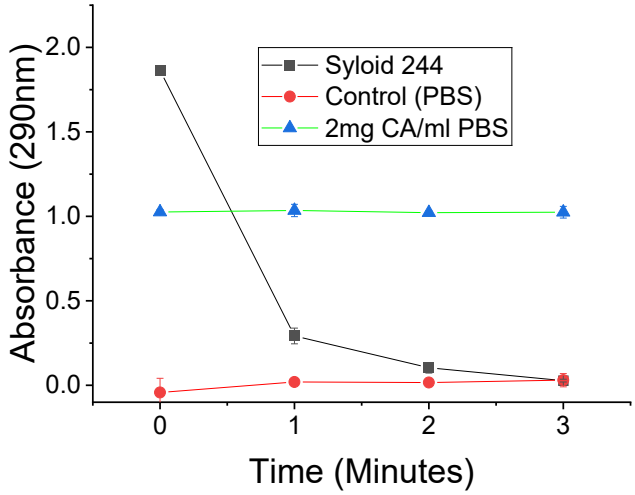

Figure 9. Testing CA separation from Syloid 244 via centrifugation at 10, 000 rpm using ~2mg/mL CA solution in 0.1 M PBS at pH 7.5. Error bars represent the standard deviation of experimental samples, where N = 3 and n = 3.

All silica was then separated from the supernatant using this method and the supernatant was tested using UV-Vis spectroscopy at 290 nm. Protein quantification was then performed using a CA and PBS specific calibration curve (Figure 9). CA loading, total BIS, and w/w loading was calculated according to equations 2.2 to 2.6.

2.4.1 Statistical Analysis

To determine if there were statistically significant differences between two independent variables (silica type and adsorption temperature) and whether temperature causes CA to behave differently across materials, a two-way analysis of variance (ANOVA) was used in Origin 2024b. For these experiments N = 3 and n = 3. Significance was reported at $p < 0.05$.

2.5 Assays for Free and Immobilised Carbonic Anhydrase

2.5.1 *p*-nitrophenyl acetate hydrolysis

CA can catalyse the cleavage of p-NPA to p-NP and acetate acid (Figure 10). This results in a colour change from colourless (p-NPA) to pale yellow and then yellow at >pH 7 (p-NP), which can be detected using UV-vis spectroscopy and therefore can be used as a proxy measurement of CA activity. It was selected because it is a simple and highly - time sensitive assay, thus allowing for more direct observation of the impact of free and immobilised CA activity[280].

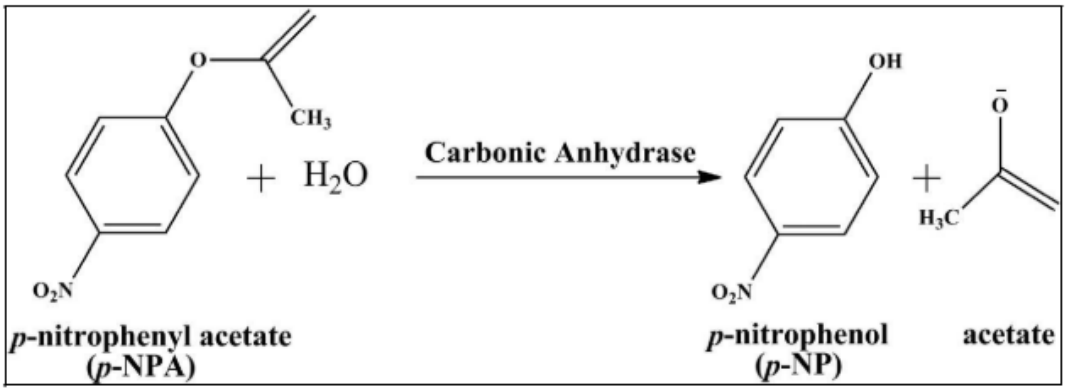

Figure 10. The hydrolysis of p-NPA to p-NP and acetate, catalysed by CA. Taken from [281].

Figure 11 shows the wavelength scans performed on both spectrophotometers used during experiments to identify the wavelength at which p-NP was best detected. Experiments began using the C10 instrument and the highest peak was at 405 nm; this was used alongside the 324 nm peak to create a calibration curve. The 324 nm peak showed less sensitivity at higher concentrations of p-NP in the calibration curve (Figure 12). Therefore, the 405 nm wavelength was selected for all experiments performed on this instrument. In later experiments, a more convenient instrument became available. Wavelength scans revealed a slightly higher sensitivity at 322 nm. However, when tested for CA activity it was found that range detection of p-NP was far narrower. Therefore, the higher peak (398 nm) was also selected in the E55 spectrophotometer in later experiments (Figure 11). Calibration curves for these instruments are displayed in Figure 12. All calibration curves were created via serial dilution using 0.1M pH 7.5 PBS solution as the solvent.

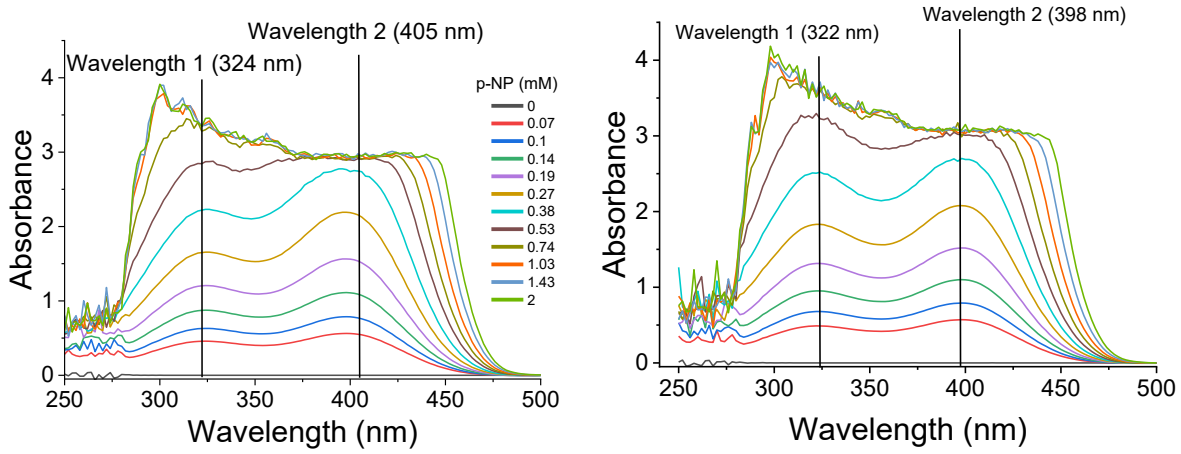

Figure 11. Full wavelength scans for 0 - 2 mM p-NP for C10 (left) and E55 (right) spectrophotometers with assigned optimal wavelengths in 0.1M pH7 PBS.

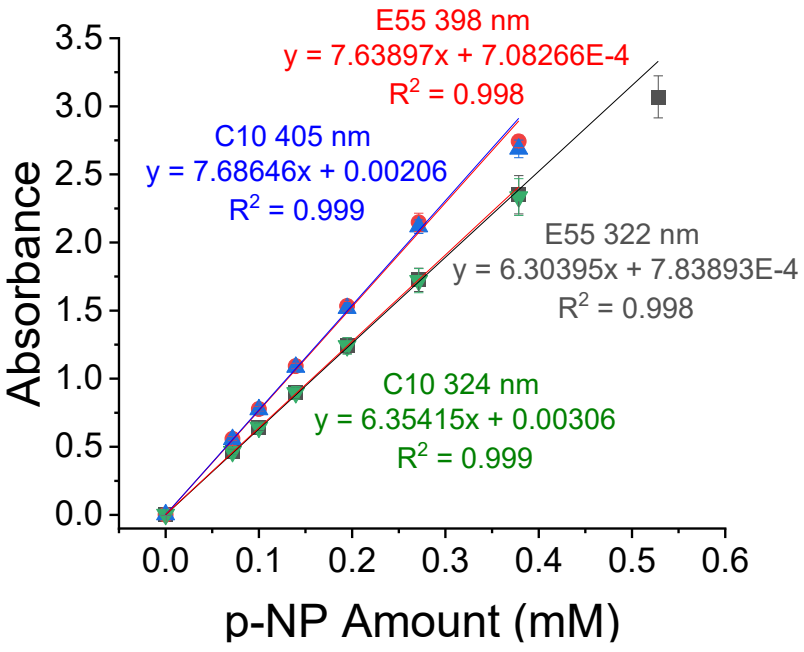

Figure 12. Calibration curve for p-NP dissolved in 0.1M PBS at pH 7.5.

Free and immobilised CA were tested according to the protocol by [276], with some adjustments. The first adjustment was that the rate of p-NPA hydrolysis for immobilised CA was tested only using a 50 mM dissolved in ethanol. In accordance with the protocol, this was added in a 30 µl volume to 3 mL of pH 7.5 0.1 M PBS solution containing 15 µl of 1 mg/mL free CA or immobilised CA. In the case of immobilised CA, an amount of BIS with immobilised CA equivalent to 1 mg was suspended in pH 7.5 0.1 M PBS and a 15 µl volume of this solution was then added to the reaction solution. It should be noted that in later experiments, the CA reagent used for immobilisation analyses needed to be changed from 3500 to 2000 U / mg. This would have made cross-comparisons between the first and latter experiments difficult, therefore the amount of CA added to each reaction was adjusted to give the equivalent units of 3500 U. Furthermore, the rate of free CA was tested in every batch, which still enabled comparisons between the free and immobilised system for each experiment.

The reaction was initiated with the addition of p-NPA reagent. The breakdown of p-NPA to p-NP can occur in the absence of CA, but at a lower rate. A parallel experiment was therefore run in the absence of CA to determine the reaction rate in its absence; this rate was then subtracted from the rate of hydrolysis from the CA experiments. Unlike [276], experiments were able to be performed using self-stirring thermostatically controlled heating module inserted into the spectrophotometer (Peltier Thermostatted single cell holder for ThermoFisher Genesys 150). This reduced human error from the sampling process and allowed for more frequent sampling intervals to capture a faster rate of the reaction. Therefore, experiments

were able to be performed at CA optimum temperature (37 °C) instead of 25 °C as described by Forsyth and Patwardhan[276]. Absorbance data was then collected and processed according to Forsyth and Patwardhan to find the rate of the reaction (V0), with the difference that Michaelis-Menten analyses for Vmax and Km were not produced[276].

To determine whether rate variation between samples was due to experimental variation or the influence of the immobilisation material, a free CA analysis was performed 15 times using 15 different 50 mM p-NPA and CA solutions. This was then analysed using a One Sample t - test to determine if any of the rates varied significantly from the sample mean.

2.5.2 $CaCO_3$ Formation for CA Sequestration

Whilst *p* – NPA hydrolysis can give some indication of enzyme reaction kinetics, it was important to measure the actual capacity for free and immobilised CA to catalyse CO_2 sequestration. This can be performed using the principle of $CaCO_3$ mineralisation. When dissolved in a buffer at pH 10, CA can catalyse the interconversion of CO_2 to HCO_3^- (E. 2.7).

$$(2.7)\ CO_2 + H_2O \underset{CA}{\leftrightarrow} H^+ + HCO_3^-$$

As the pH of the solution increases, the bicarbonate ions deprotonate to form CO_3^{2-} ions, which in the presence of calcium will react to form $CaCO_3$ (E. 2.8)

$$(2.8)\ Ca^{2+} + CO_3^{2-} \rightarrow CaCO_3$$

When used alongside a control containing no CA, the formation of $CaCO_3$ can serve as a proxy measurement of CAs ability to sequester CO_2. The protocol for this experiment was performed exactly according to [276].

2.6 Leaching Examination of Immobilised CA

In order to determine the amount of enzyme loss from the framework, examination of was carried out according to a protocol by[276], with some adjustments. A mass of BIS containing immobilised enzyme was added to 0.1 M pH 7.5 PBS solution to create a final concentration of 1 mg CA / mL. This was then placed in a shaking incubator for 24 hours, with samples taken at 0, 8 and 24 hour time points. Absorbance was measured at 290 nm using UV - Vis spectroscopy and the concentration of CA was quantified based on the calibration curve in Figure 12. Total leaching of the enzyme was then expressed as mg of free CA per mL solution.

3 Chapter 3: Exploring Biochar for Enzyme Immobilisation

This chapter builds on the discussion in Chapter 1 by examining how biochar manufacture conditions influence porosity characteristics relevant to enzyme immobilisation. The stability and porous structure of biochar (commonly described in terms of SA, PD and PV have made it an attractive candidate for this application. However, clear guidance on how to reliably produce biochars with suitable properties remains limited. This uncertainty largely arises from the strong interdependence between porosity and factors such as feedstock type, pyrolysis temperature, and activation treatment.

To address this, Chapter 3 first presents a meta-analysis of published biochar studies that used N_2 gas adsorption to characterise porosity. Data relating to SA, PD, and PV were collated alongside reported manufacture conditions, allowing trends and correlations to be explored where sufficient information was available. In total, 56 studies were reviewed. Of these, 15 reported all three porosity parameters, while a further 28 reported at least two, enabling partial comparisons across feedstocks and processing conditions. Gaps in reporting, particularly around feedstock specification, pyrolysis temperature, and activation protocols, limited the inclusion of some studies in specific analyses.

Based on insights from the literature review, three biochar candidates were then selected for experimental investigation. These materials were chosen to reflect contrasting feedstock origins and manufacture conditions. Their porosity was characterised using both N_2 gas adsorption and mercury intrusion porosimetry (MIP). Additional characterisation, including CHNS and O analysis to assess chemical stability, and ATR-FTIR to confirm biochar formation and compare functional features, was also undertaken.

The chapter concludes by evaluating the suitability of both literature-reported and experimentally produced biochars for use as enzyme immobilisation frameworks. Although many porosity trends aligned with established theoretical expectations, notable deviations were observed. Interpreting these discrepancies proved difficult due to confounding factors such as methodological variability and incomplete reporting. Overall, none of the biochars examined met the porosity requirements of an ideal enzyme support. The final section therefore outlines recommendations for improved experimental design and reporting in biochar engineering studies, with the aim of enabling more robust comparisons to aid the future development of biochar–enzyme systems.

3.1 Introduction

In recent years, CA has been recognized as a potential aid to enzymatic upgrading of CO_2 into valuable fuels as chemicals[152]. The progression of research into enzymatic conversion of CO_2 could develop into a less energy-intensive alternative[152] to inorganic heterogeneous catalysts which avoids the use of rare-metal catalysts, which have sustainability concerns[106]. Compared to inorganic catalysis, CA reactions are also able to take place under relatively mild conditions[152,282]. However, CA is also required to sustain high stability and activity over multiple cycles, often under adverse temperatures and pH and in the presence of solvents[165]. CA also needs to operate efficiently and cost-effectively in high-throughput industrial applications[149,153]. Whilst many enzymes are extremely economical as a single-use reagent[283,284], CA is relatively costly[219] and could create unfeasibly high operational costs if is not able to resilient, reused or recovered in meaningful amounts[154,283,285]. As discussed in Chapter 1, efforts towards overcoming these challenges have been diverse, widespread and well documented in many in-depth reviews[160,185,201–210,193,211–218,194–200] but can be classified into two main themes:

1. Protein engineering, in which CA is altered through techniques such as site-directed mutagenesis and directed evolution[222,286].
2. Immobilisation, with or without chemical modification of the enzyme and / or support[185,219,220].

Of these two themes, immobilisation has the potential to address all of the limitations cited with the use of CA in industrial processes: it can have a stabilizing effect on enzymes[153], enhance their activity[169] and lower process costs by enabling re-use and recovery[157,287]. A dynamic range of substances have been explored for their use as enzyme immobilisation frameworks, ranging from natural polymers, synthetic polymers, carbon structures, minerals and synthetic materials[165,288]. Enzymes have also been immobilised to other proteins in the form of cross-linked enzyme crystals (CLECs) and to each other via crosslinked subunits to form crosslinked enzyme aggregates (CLEAs)[14]. Many beneficial features of these different materials have been reported, such as a large SA available for catalysis in addition to better tolerance to adverse temperatures and pH[293] as a result of a shielding effect[207].

Despite the diverse range of enzyme immobilization frameworks that have been reported over the past 50 years[284], only a few have reached commercial scale[285]. Researchers often cite issues with engineering immobilised enzyme systems, namely that they are expensive, complicated and time consuming to produce[285,294]. Many frameworks are also chemically inert, requiring functionalisation to make them compatible for enzyme immobilisation[169]. As discussed in Section 1.9, amines have been reported as some of the most successful functionalisation molecules in terms of CA immobilisation. In some cases modification of the

enzyme molecule is also required to compliment the functionalisation[156,286]. A common modifier is glutaraldehyde, which interacts with primary amino groups within the enzyme protein structure or groups such as thiols, phenols and imidazoles[295]. This results in a Schiff base interaction in which a primary amine within the protein reacts via a condensation reaction with an aldehyde group in the glutaraldehyde molecule, leading to covalent binding between the enzyme and glutaraldehyde[295]. An additional aldehyde within the glutaraldehyde is then able to interact with an amine which has functionalised the framework surface. In addition to taking advantage of the SA and porosity of a previously unsuitable framework, studies have reported enhanced activity as a result of binding[295]. However, modifications can also lead to loss of enzyme activity due to alteration of an enzyme structure, which can affect the active site[156,285]. To overcome these limitations, an ideal material should possess the following features:

- Possess a large SA to improve immobilisation efficiency, PDs that enzymes can permeate, and large PVs for enzymes to function[168].
- The surface allows enzyme binding without denaturation[288].
- Is chemically, thermally, and mechanically stable[260,288].
- Protects the enzyme during use[296].
- Sustains efficient catalysis for multiple cycles without leaching or degradation[297].
- Is easy to generate and cost is effective[293].

3.2 Biochar as an Immobilisation Framework

Biochar is formed in an anoxic or low stoichiometric oxygen environment as a consequence of the thermochemical conversion (pyrolysis) of organic material using temperatures >300 °C[298–301]. The result is a lightweight material with high refractory stability[272]. Depending on the pyrolysis temperature, residence time and heating rate, energy-rich liquid (bio-oil) and gas (bio-syngas) (CO, CO_2, H_2 and C_1-C_2) can also be produced[300,301]. Aside from enzyme immobilisation, more established applications for biochar are as a soil amendment[302,303] and for pollutant removal[304].

In recent years, researchers have explored biochar as a potential enzyme immobilisation framework (Table 1 Appendices). This is due to its stability, regenerative nature and economical production[150]. Researchers also hope to utilise biochar features such as SFGs and its porosity to better accommodate enzymes and maximise their activity[150]. However, selecting an appropriate biochar for enzyme immobilisation is nuanced and complex. This is because biochar features are highly dependent on various pyrolysis conditions, feedstock choices and activation treatments (Figure 1)[150].

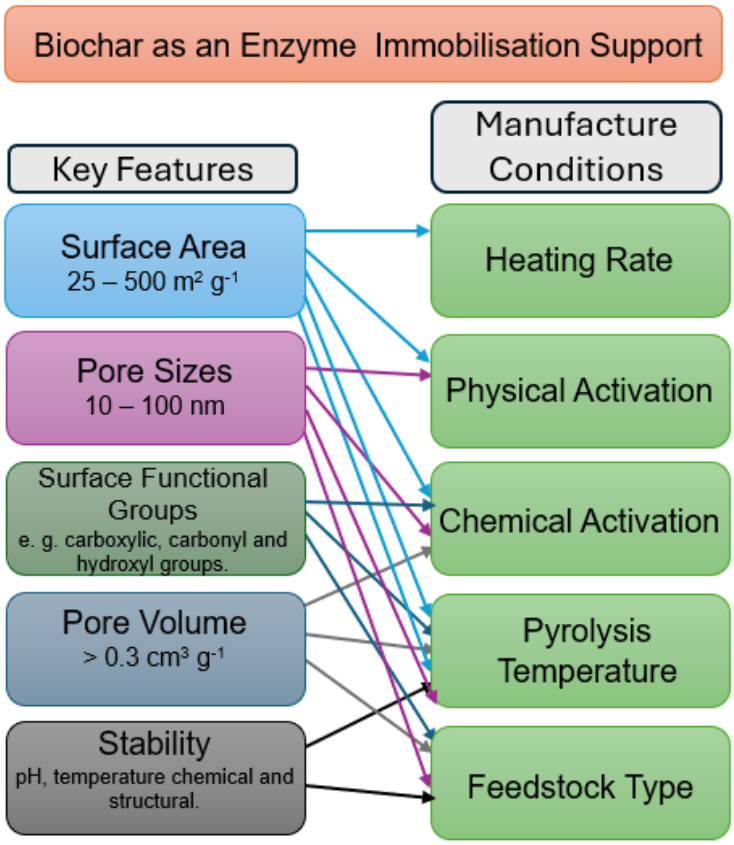

Figure 1. Key requirements of an enzyme immobilisation framework and the manufacture conditions which influence these requirements in biochar. Taken and adapted from [150].

The multi-parameter nature of biochar manufacture conditions makes drawing insights into its selection difficult. Therefore this report takes an inverse approach by focusing on porosity because it is foundational to enzyme immobilisation[256,305]. Biochar PDs serve as the gateway for enzymes to access and take advantage of the inner SA of the biochar particle[168]. This depends, however, on whether the PD is large enough to allow enzymes into them (Figure 2). It has been found that protein loading is lower in materials with average PDs <10 nm[168]. Once inside, the capacity provided by the PV must be large enough to accommodate enzymes and any movements associated with their activity[306] (Figure 2). A minimum total pore volume of 0.3 cm^3 g^{-1} has been linked to successful enzyme immobilisation[168]. The SA must also be present in sufficient quantities to facilitate good enzyme loading and therefore high activity efficiency[168]. The ideal SA range has been identified as 25 - 500 m^2 g^{-1} [168]. It is hoped that evaluating biochar samples solely on these factors will better focus the search for an appropriate candidate. If one exists, other essential criteria such as beneficial enzyme-surface interactions via SFGs, chemical stability within the reaction system and environmental impact can then be considered.

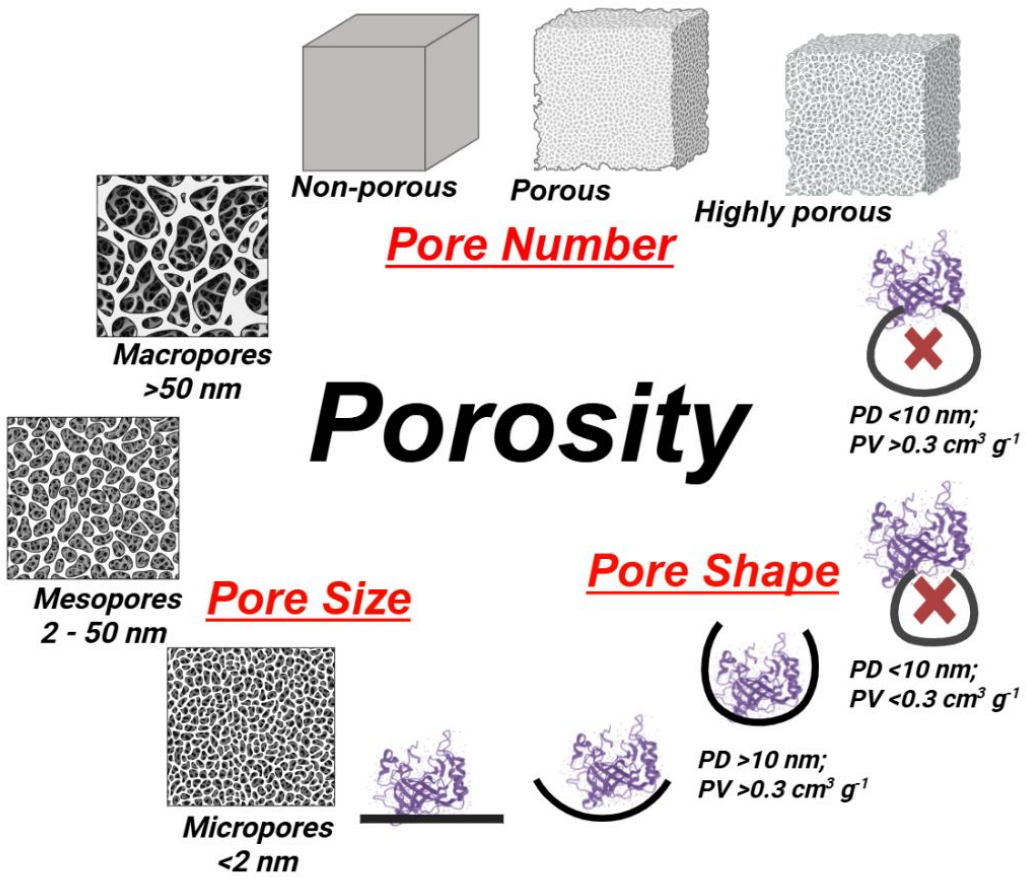

Figure 2. Qualities of an immobilisation material which contribute to material porosity and subsequent enzyme immobilisation. Created using Biorender.

The following sections analyse the relationship between biochar processing conditions, feedstock properties, and activation treatments on porosity using N_2 gas adsorption data gathered from enzyme – biochar immobilisation and wider biochar characterisation studies. The outcomes of this porosity data will then be used to determine biochar's suitability as an immobilisation framework using the optimal range, in terms of PD, PV, and SA, identified in Chapter 1. Porosity analyses of biochars selected from the literature, based on information deduced from the literature on which feedstock origins and manufacture conditions should give rise to a framework with ideal porosity. This porosity of these samples will then be analysed using N_2 adsorption and MIP, in addition stability assessments using CHNS and O analyses and FT-IR analyses will also be conducted. Finally, the impact of N_2 adsorption methods on the reporting of biochar porosity will be discussed.

3.3 Engineering Biochar via Feedstock and Processing Conditions Selection for Enzyme Immobilisation

The following section focuses on identifying any trends found in the data between causal factors such as feedstock choice and pyrolysis conditions and their effect on PD, PV, or PD. These features will then be considered individually for their suitability for enzyme immobilisation. It is hoped these summaries may help to inform researchers for future attempts in engineering a biochar with suitable porosity features for enzyme immobilisation. Of the 56 studies which conducted N_2 gas adsorption, data from 43 studies was able to be extracted. In many cases, data was only provided for two of the three criteria. This has been applied in different ways in Figures 3 - 6 to provide the richest-possible detail relating to the impact of feedstock and processing conditions on biochar SA, PD and PV. Ultimately, 15 studies provided adequate processing details and data for all three criteria. These outcomes are depicted in Figure 6 alongside the ideal PD, PV and PD parameters as outlined by Bayne *et al.* for comparison[166].

3.4 The Influence of Biochar Production on PD

3.4.1 Influence of Pyrolysis Temperature

Pyrolysis is cited as a critical process for pore formation in biochar and is comprised of two discrete stages known as the primary and secondary phases[150,307]. During primary pyrolysis, the feedstock is cleaved and devolatilised into its main constituents and (depending on the conditions and feedstock) forms carboxyl, carbonyl and hydroxyl groups[307]. In secondary pyrolysis, the feedstock converts into char as a result of the cracking and repolymerization of heavy compounds[150,307]. According to Gray *et al*., the pyrolysis process leads to the development of porosity, with micropores comprising the predominant fraction[308]. Further, higher pyrolysis temperatures lead to an increase in the formation of micropores[308]. To investigate this pattern, PDs and pyrolysis temperatures from eleven studies which investigated different feedstocks were compared (Figure 3). Contrary to Gray *et al.,* biochar with average PDs in the micropore range were not concentrated at higher pyrolysis temperatures, suggesting that engineering the average PDs of biochar is influenced by more than pyrolysis temperature alone (Figure 3).

3.4.2 Influence of Feedstock

In addition to pyrolysis, feedstock type has also been cited to influence PDs[309,310]. During pyrolysis, the three natural polymers of biomass: cellulose, hemicellulose and lignin undergo cross-linking, depolymerisation and fragmentation. Cellulose and hemicellulose thermally

decomposes between 200 - 350°C, leading to a rapid release of volatile gases and the creation of porosity[309]. Therefore, the greater the proportion of cellulose and hemicellulose in a feedstock, the greater the degree of pore formation. Lignin degradation is slower and occurs between 400 - 1200°C[311]. Lignin comprises the larger and more dense cellular framework and the extent of its degradation determines the extent of macropore formation[310].

When the influence of feedstock is accounted for in Figure 3, there are instances where the resulting PDs are consistent with how different types and quantities of plant tissues respond to pyrolysis temperature. For instance, in the case of rubber wood sawdust, average mesopore diameter rose in accordance with increasing temperature from 7 nm at 300 °C to 16 nm at 700 °C (Figure 3). This outcome is consistent with the proportion of hemicellulose and cellulose (~60 – 70%) and high content of lignin (~20%) reported for this feedstock [312,313] (Table 1). High proportions of lignin in the feedstock leads to greater framework degradation as temperatures escalate beyond 400 °C, leading to the formation of macropores and an increase in average PD.

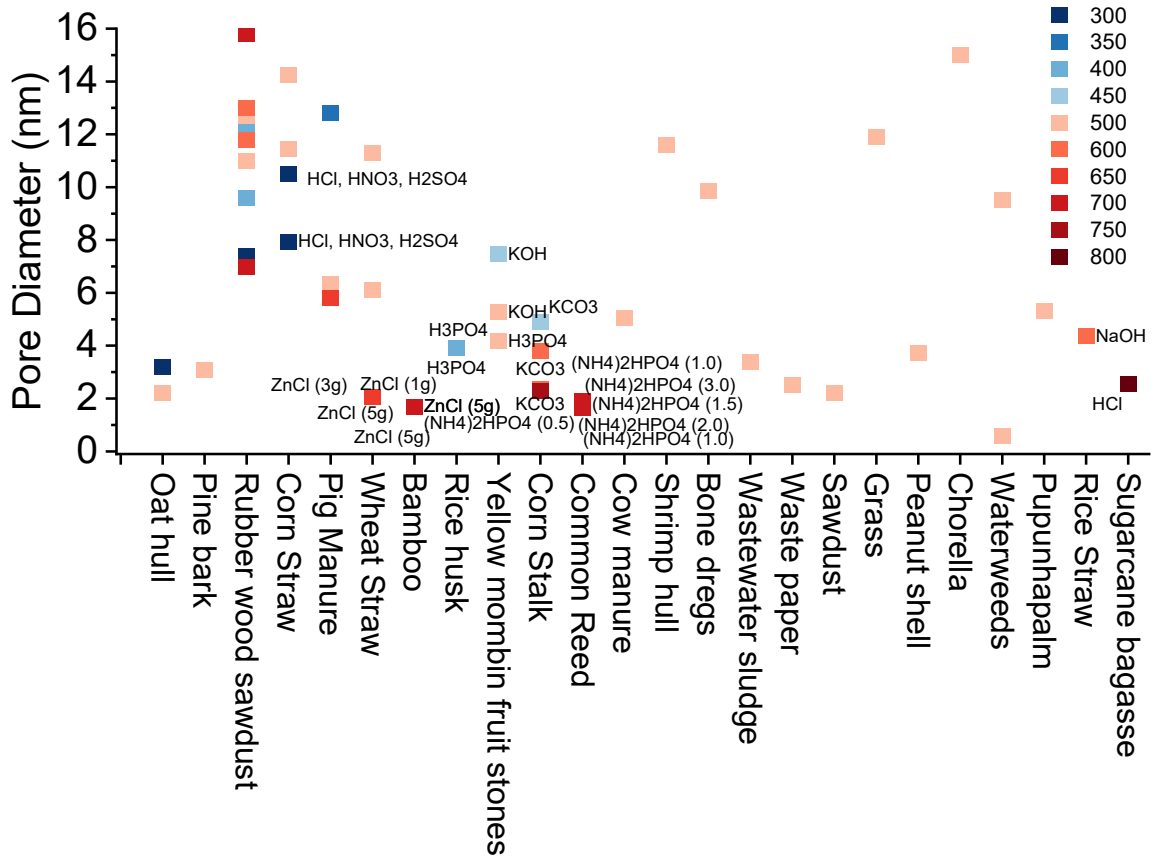

Figure 3: Biochar PD with respect to pyrolysis temperature, feedstock and activation treatment. Data was collated from multiple studies which reported these manufacture conditions and PD.

Conversely, wheat straw possessed similar proportions of hemicellulose and cellulose (~60%) and lignin (~25%) compared to rubber wood sawdust (Table 1). However, average PD instead decreased from 11.1 to 2 nm over a similar temperature range of 350 to 650 °C (Figure 3)[313–315]. This study suggests significant micropore formation occurred beyond 350 °C, contradicting the literature which states that the majority of micropore formation should occur between 200 - 350 °C due to hemicellulose and cellulose decomposition[309]. Another study which investigated bamboo reported no change in PD, despite having a similar pyrolysis temperature (700 °C) and lignocellulosic content to rubber wood sawdust[313,316] (Table 1). Highly variable PDs (0.5 and 9.5 nm) were also reported for the same waterweed feedstock, all of which were pyrolysed at 500 °C[314].

Table 1. Lignocellulosic compositions of feedstocks analysed as part of this study.

Feedstock	**Hemicellulose %**	**Cellulose %**	**Lignin %**
Sugarcane bagasse[317]	20 - 32	32 - 45	17 - 32
Rice straw[318]	12 - 32	28 - 45	5 - 24
Pupunhapalm[319]	25	41.2	7.70
Chlorella[320]	26	46	15
Peanut shell[321]	15.6	36.3	25
Wastepaper[322]	25 - 35	40 - 45	1 - 20
Cow manure[323]	21.3	20.4	11.4
Common reed[324]	20.1	51.2	12.34
Corn stalk[322]	20.4	36.8	17.3
Yellow mombin fruit stones[325]	8.2	14.8	9.4
Rice husk[318]	12 - 32	28 - 45	5 - 24
Bamboo[316]	23.9	47.2	23.8
Wheat straw[315]	25.2	35.5	25.1
Pig manure[326]	22.1 - 26.6	7 - 12.7	3.8 - 8.7
Rubber wood sawdust[313]	25 - 30	40 - 44	20 - 22
Pine bark[327]	15	25	45
Oat hull[328]	35	23	25

3.4.3 Influence of Activation Treatment

According to the literature, PDs in biochar have been further increased following pyrolysis through physical and chemical activation[329]. This is a process in which volatile compounds which have re-condensed back onto the char following pyrolysis are removed, increasing the

size of biochar pores or unblocking them[329]. No cases were identified in this study in which chemical activation increased average PDs. However, the absence of controls for non-activated samples in some studies limited comparisons, allowing only for the assessment of activation effects of biochars produced at different pyrolysis temperatures[325,330] (Figure 3). In studies which did use a control, a reduction in average PD was observed (Figure 3). Corn stalk biochar pyrolysed at 600 °C and activated using potassium carbonate (KCO_3) reported a PD reduction from ~4 to ~2 nm compared to the non-activated control (Figure 3)[331]. KCO_3 treatment was used on chars pyrolysed at other temperatures, however no control values were reported thus limiting further comparisons[331] (Figure 3). Another study which used corn-straw biochar produced at 300 and 500 °C reported ~10 to ~8 nm and ~14 to ~11 nm reduction in PDs following activation using a formulation of HCl, HNO_3 and H_2SO_4[332]. An explanation for this could be that activation unblocked smaller pores, causing a reduction in average PD. In addition, margins of error were not included for values in either study, giving rise to the potential that differences in PD may be due to sample variations.

3.5 The Influence of Biochar Production on SA

3.5.1 Influence of Pyrolysis Temperature and Feedstock

According to the literature, SA formation is governed by pyrolysis temperature through the determination of the extent of cellulose, hemicellulose, and lignin decomposition in feedstocks. For example, at pyrolysis temperatures of ~350 °C, all cellulose and hemicellulose within a feedstock should have degraded, leaving behind more mesopores and micropores compared to a pyrolysis temperature of 200 °C. The extent of this pore formation has been cited to contribute to final SA[150]. At temperatures >400 °C lignin present within the feedstock will degrade, leading to the potential for macropore formation as lignin structures which separated pores degrade to form larger pores which reduces SA[258]. Feedstock is therefore another factor behind SA formation. Hemicellulose and cellulose proportions influence the extent of micro and mesopore formation, which contributes to SA development[309]. Lignin proportions influence macropore development and the degree to which SA development may be reversed[258].

To inspect this relationship, N_2 adsorption data from biochar studies which reported PD and SA, were compiled (Figure 4). The low SA range of 0 - 25 $m^2\ g^{-1}$ contained all samples (n = 8) pyrolysed at temperatures ≤350 °C (Figure 4). At this SA range, materials have been classified as non-porous by the literature[267]. This contradicts the notion that temperatures up to 350 °C would have an increased SA due to micropore and mesopore formation from cellulose and hemicellulose degradation.

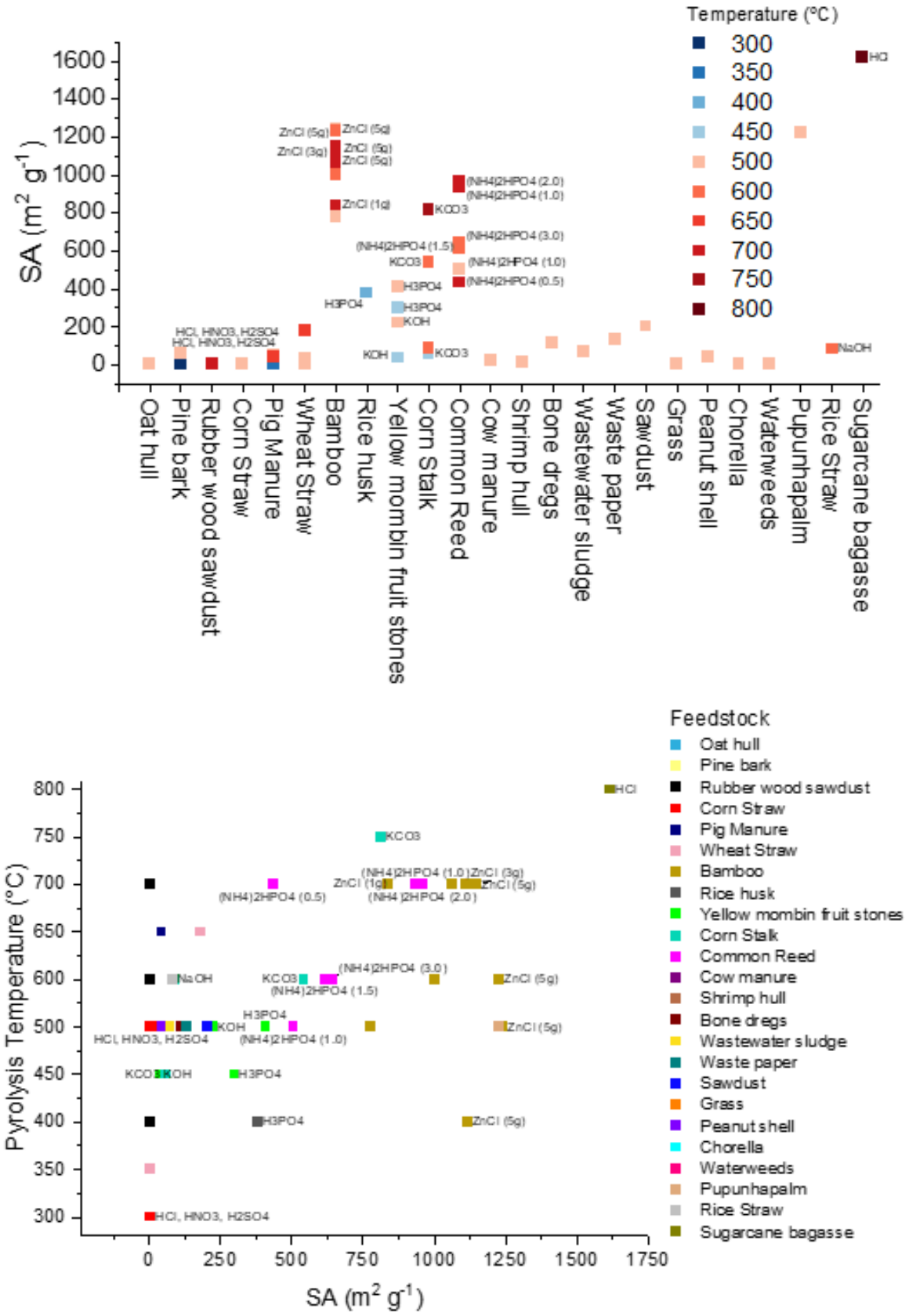

Figure 4. A) Biochar SA vs. feedstock with label colour representing pyrolysis temperature and labels denoting activation treatment. B) Biochar SA vs. pyrolysis temperature with label colour representing feedstock type and labels denoting activation treatment.

Biochars within the 0 - 25 m^2 g^{-1} range were from a diverse range of feedstocks, suggesting little relationship between the proportions of hemicellulose and cellulose with SA development (Figure 4). This range also contained biochars pyrolysed at >400 °C, which is the point according to the literature at which lignin degradation can occur[258]. This perhaps explains why 24 out of 25 of PDs within this SA range were mesoporous (Figure 4), as lignin degradation could have caused greater amounts of macropore formation, which cannot be detected using N_2 adsorption methods, leading to reduced SA and an increase in average PDs[333].

3.5.2 Influence of Activation treatment

As discussed in Section 5.1.3, studies have indicated a positive relationship between the use of activation treatment and the removal of condensed volatile compounds, which can lead to the unclogging of smaller pores and therefore an increase in SA[308,333]. For example, corn straw biochar activated using HCl, HNO_3 and H_2SO_4 and pyrolysed at 300 °C and 500 °C increased SA from ~1.8 to 5 m^2 g^{-1} and 5 to 9 m^2 g^{-1} respectively (~170% and ~70%) relative to inactivated controls[332] (Figure 4). This SA increase coincided with a reduction in average PDs, from 10.5 to 7.95 nm and 14 to 11.5 nm for 300 and 500 °C pyrolysed biochars, respectively[332] (Figure 4). In another instance, the SA of corn-stalk biochar pyrolysed at 600 °C was also increased from ~87 to 542 m^2 g^{-1} (~530%) following potassium carbonate (K_2CO_3) activation treatment, while average PDs reduced from 3.79 to 2.38 nm[331] (Figure 4). In addition, the reduced degree of SA development for biochar produced at higher temperatures is consistent with the concept that higher pyrolysis temperatures during biochar manufacture prevents the recondensation of volatile compounds[168], leaving less available for removal via activation treatment. This mechanism may explain why there was up to a 115% increase in SA for specific biochars when pyrolysed at higher temperatures (450 – 700 °C) despite no change occurring in average PDs (Figure 3). Notably, when these biochars were subjected to increasing concentrations of activation agent, further gains in SA reduced dramatically (<2%), suggesting that the low amounts of condensed volatile compounds present were able to be removed sufficiently using lower concentrations of activation agent.

3.6 The Influence of Biochar Production on Pore Volume

3.6.1 Influence of Pyrolysis Temperature and Feedstock

Volatile compound release during feedstock pyrolysis is concentrated between temperatures of 300 - 500 °C and according to the literature a large increase in biochar PV also occurs within this range[333]. Beyond 500 °C, volatile release diminishes, along with its impact on PV[334,335]. As previously discussed in Section 5.2.1, lignin is a large, dense, and complex polymer[333]. Depending on pyrolysis temperature and lignin content, lignin degradation may not completely occur; resulting in a network of preserved lignin-structures which once served

as vascular and support tissues for the feedstock[333]. Greater pyrolysis temperatures lead to greater degradation of this lignin network, resulting in larger PVs as shared lignin walls between voids collapse[310,333]. Studies have reported greater SAs and porosity in feedstocks with greater lignin content[333,336–338].

When PVs and pyrolysis temperatures from six reports were examined for this study, a similar pattern was found. Temperatures between 300 - 500 °C were linked to a 30, 82, 250, 33, 213 and 100% increases in PV in feedstocks derived from corn straw, wheat straw, pine bark, oat hull, pig manure and rubber wood feedstocks, respectively (Figure 5)[256,312,314,331]. In the case of two studies which also pyrolysed samples of rubber wood sawdust and pig manure feedstock >500 °C, the extent of PV growth decreased in line with the end of the volatile release phase[312,314] (Figure 5). However, in the case of wheat straw biochar PV increased from 0.093 to 0.808 $cm^3\ g^{-1}$ (768%) when samples were pyrolysed at 650 °C compared to 500 °C[314] (Figure 5). Therefore, whilst PV development mostly behaved in accordance with the literature, it is not guaranteed. This continuation in PV development suggests that the presence of lignin may continue to influence PVs beyond the volatile compound release phase[314,339] (Figure 5). Notably, samples of corn straw, pine bark and oat hull were not pyrolysed beyond 500 °C, so the impact of higher pyrolysis temperature on PV formation was unable to be observed. This may also explain why Zhao *et al.* observed low porosity of <0.150 $cm^3\ g^{-1}$ for diverse lignocellulosic feedstocks such as cow manure, pig manure, wastepaper, sawdust, grass, wheat straw, peanut shell, and waterweeds pyrolysed at 500 °C; lower pyrolysis temperatures (<500 °C) may have caused less lignin degradation, indicated by the resultant low PVs[314] (Figure 5). Finally, when pine bark feedstock with greater lignin content (~37%) was pyrolysed at 300 and 500 °C, PVs increased by from 0.093 to 0.808 (250%) between temperatures, evidencing a link between high lignin content and greater PV (Figure 5)[256].

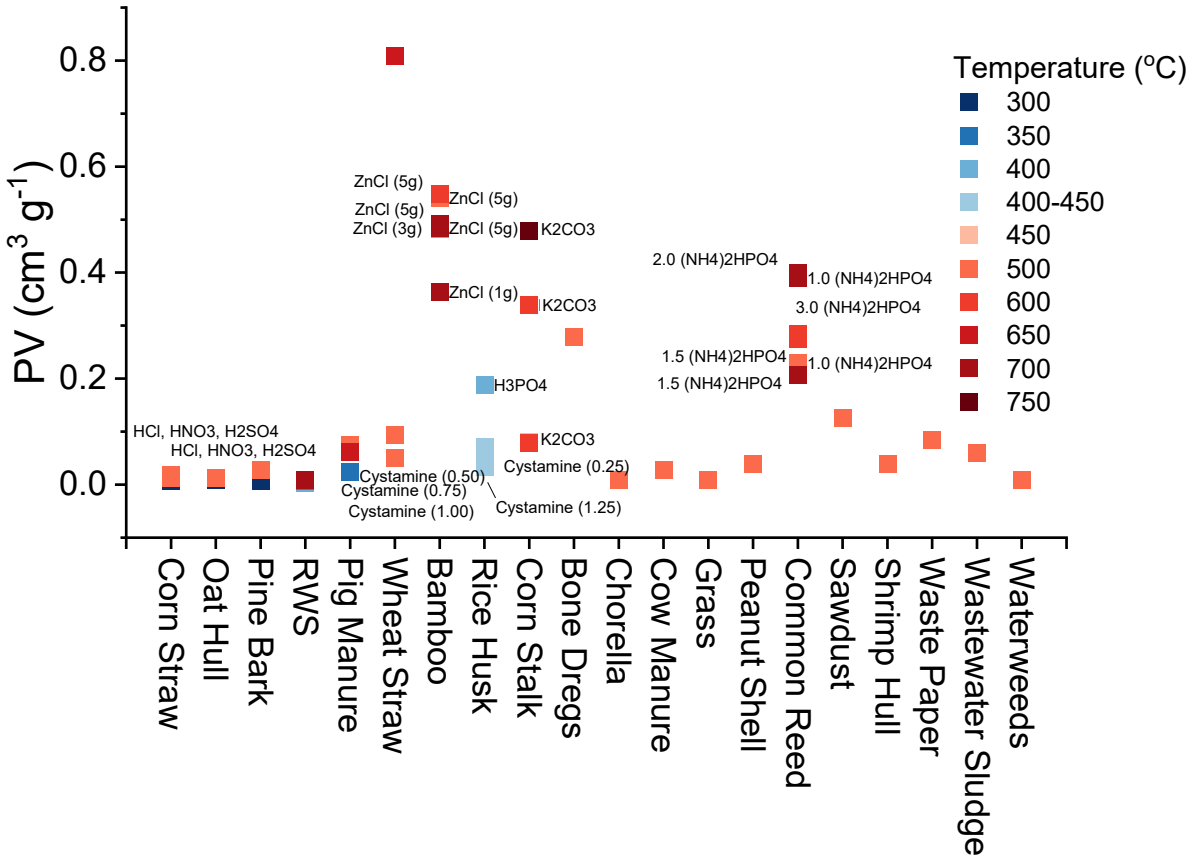

Figure 5: The distribution of biochar samples as a function of PV according to pyrolysis temperature and activation treatment.

3.6.2 Influence of Activation Treatment

Chemical and physical activation treatment (Section 3.5.2) following biochar synthesis has also been purported to increase PV in biochar. In the case of bamboo biochar pyrolysed at 700 °C, PVs increased from 0.35 to 0.5 $cm^3\ g^{-1}$ (42%) in response to increased concentrations of $ZnCl_2$ activation agent from 1 to 3 g (Figure 5)[340]. Beyond 3 g no further increase in PV size was observed (Figure 5)[340]. Common reed biochar was pyrolysed at 500, 600, and 700 °C and then activated with various concentrations of diammonium hydrogen phosphate $(NH_4)_2HPO_4$ (Figure 5)[330]. PVs increased from 0.225 to 0.275 and then to 0.4 $cm^3\ g^{-1}$ (22 and 45%) but unlike $ZnCl_2$ this correlated more with increasing pyrolysis temperatures instead of increasing $(NH_4)_2HPO_4$ concentration (Figure 5)[330,340]. In the case of both $ZnCl_2$ and $(NH_4)_2HPO_4$ activation, these differing outcomes for PV enlargement may be explained by a single mechanism: that higher pyrolysis temperatures lead to increased prevention of volatile compound recondensation. In the case of $ZnCl_2$, biochars produced at higher pyrolysis temperatures had fewer volatile compounds for removal by $ZnCl_2$, which were adequately removed using lower $ZnCl_2$ concentrations (<3 g)[340]. For $(NH_4)_2HPO_4$, higher pyrolysis temperatures completely prevented volatile compound recondensation, rendering the application of increasing concentrations of $(NH_4)_2HPO_4$ ineffective[330]. In the case of both $ZnCl_2$

and $(NH_4)_2HPO_4$ activation control values for non-activated samples and margins for error were omitted, making it impossible to attribute PV growth solely to activation treatment, pyrolysis temperature or sample variation.

In a study which included controls, corn straw biochar pyrolysed at 300 and 500°C was chemically activated using HCl, HNO_3 and H_2SO_4; PVs increased from 0.00064 to 0.014 $cm^3\ g^{-1}$ (2087%) and from 0.013 to 0.018 $cm^3\ g^{-1}$ (38%) compared to the control[332] (Figure 5). In another study, corn stalks pyrolysed at 450, 600, and 750 °C showed significant increases in PV from 0.081 to 0.339 and then 0.478 $cm^3\ g^{-1}$ (318 and 41%) following K_2CO_3 activation (Figure 5). In this case a single control value was provided for 600 °C biochar, which was able to show that K_2CO_3 treatment led to an increase from 0.079 to 0.339 (250%) in PV compared with 600 °C untreated samples[332] (Figure 5). Since margins of error were also absent for both studies, it is possible smaller differences in PV may be due to sample variation. However, the inclusion of control values for these studies along with those of bamboo and common reed enables some important observations. Firstly, that activation treatments can be highly effective for increasing PVs for biochars produced at low temperatures. Such information is useful if biochar is produced as a waste-product from low temperature pyrolysis and requires modification of PVs for re-purposing as an enzyme framework. Secondly that if biochar is to be manufactured solely for the purpose of enzyme immobilisation, evidence suggests that using activation treatments for higher temperature biochars largely results in lower gains in PV, which may be explained by lower amounts of volatile compound re-condensation. This is particularly evidenced by comparison of PVs obtained for corn straw at 300 and 500 °C, which suggests that similar volumes (+/- 0.001) can be attained without chemical activation by instead increasing pyrolysis temperature during synthesis[332].

3.7 Section Summary: Linking Biochar Porosity to Enzyme Immobilisation

Pores are responsible for biochar's internal SA and can serve as a matrix-like structure for enzymes to occupy[150,256]. As outlined in Chapter 1, a study by Bayne *et al.,* analysed data from 182 immobilised enzyme studies[166]. It was found that protein loading was lower in materials with average PDs <10 nm - this has been cited to be due to the enzyme's diameter surpassing the diameter of most pores in the material, thus restricting enzyme access. If some enzymes can enter, their number may be restricted due to limited PDs and capacity (Figure 2)[168]. Additionally, PDs >100 nm reduced enzyme loading due to a "concomitant reduction in surface area"[168]. The optimum PD range for enzyme immobilisation was in the mesoporous range, between 10 - 100 nm (Figure 6). This was determined based on the observation that enzyme loading was unaffected by the PD of the material[168].

If enzymes can enter the pores of biochar, sufficient space within the pore in relation to the size and movement range of the enzyme is also required[260] (Figure 2). To put this into context, CA has a size of 5 x 4 x 4 nm but requires an operational space of 3 - 9 times its molecular diameter[306]. This corresponds to 8 x 10^{-20} cm^3 for the physical bulk of a single enzyme and a requirement of up to 7.2 x 10^{-19} cm^3 for its operational space. An effective enzyme matrix should be able to accommodate the bulk and catalytic activity of multiple enzyme units. When these requirements are considered per gram of material, Bayne *et al.* concluded that a minimum total pore volume of 0.3 cm^3 g^{-1} is required for successful enzyme immobilisation[168] (Figure 6).

As with other immobilisation frameworks, SA is cited as an integral feature to the success of biochar-supported enzyme catalysis. SAs for biochars can range between 2 and 1200 m^2 g^{-1} (Figure 4). It has been shown that a greater SA is conducive to greater adsorption capacity of chemical compounds[259,341]. However, this logic cannot necessarily be applied to enzymes because they are often large molecules with greater potential for their molecular diameter to surpass the PD of the material[168]. This can restrict access to portions of the framework and limit loading. According to the study by Bayne *et al.* enzyme loading increased as SA rose from 25 up to 500 m^2 g^{-1} [168]. However, beyond 500m^2 g^{-1} enzyme loading plateaued which corresponded with a reduction in pore size and a thus a restriction of enzyme access to many pores and the surface area within them[168] (Figure 6).

Of the 65 different feedstocks assessed from 43 studies, 16 (24%) possessed PDs sufficient for enzyme immobilisation (>10 nm). Some studies reported PDs consistent with the relationship described in the literature between lignocellulosic degradation and pyrolysis temperature. However, an equal number of examples demonstrated that this relationship is not a predictable way of selecting for a material with minimum PDs to suit enzyme immobilisation. It should be acknowledged that this sample size was small, owing to few studies reporting consistent data. Consistency with regards to biochar manufacture conditions and PD data reporting would help to define these relationships further. In addition, providing the proportions of cellulose, hemicellulose and lignin in feedstocks would also help to gauge the influence of plant tissue type on PD outcomes.

Regarding SA, the 0 - 25 m^2 g^{-1} range contained all biochar samples with mesopores suitable for enzyme immobilisation (>10 nm). According to Bayne *et al.*, this SA is inadequate as pores wide enough for enzyme access would not have sufficient SA to create an extensive catalytic surface[168], whereas, biochar enzyme loading would be optimised within the 25 - 500 m^2 g^{-1} range (Figure 6).

Despite the increases in pore volume achieved in some studies, 19 out of 21 feedstocks did not possess PVs large enough (>0.3 cm^3 g^{-1}) for enzyme immobilisation, suggesting neither pyrolysis temperature nor feedstock were effective for achieving useable PVs for enzymes (Figure 6). The exception was wheat straw biochar, which obtained a PV of ~0.8 cm^3 g^{-1} when pyrolysed at 650 °C[314] (Figure 5). Two studies – bamboo and corn stalk - produced activated biochars with PVs large enough (>0.3 cm^3 g^{-1}) for enzyme immobilisation. Unfortunately, none of the chars possessed adequate PVs which met the substantiated threshold (>10 nm) required for enzyme access into the inner SA of the biochar framework[168] (Figure 6).

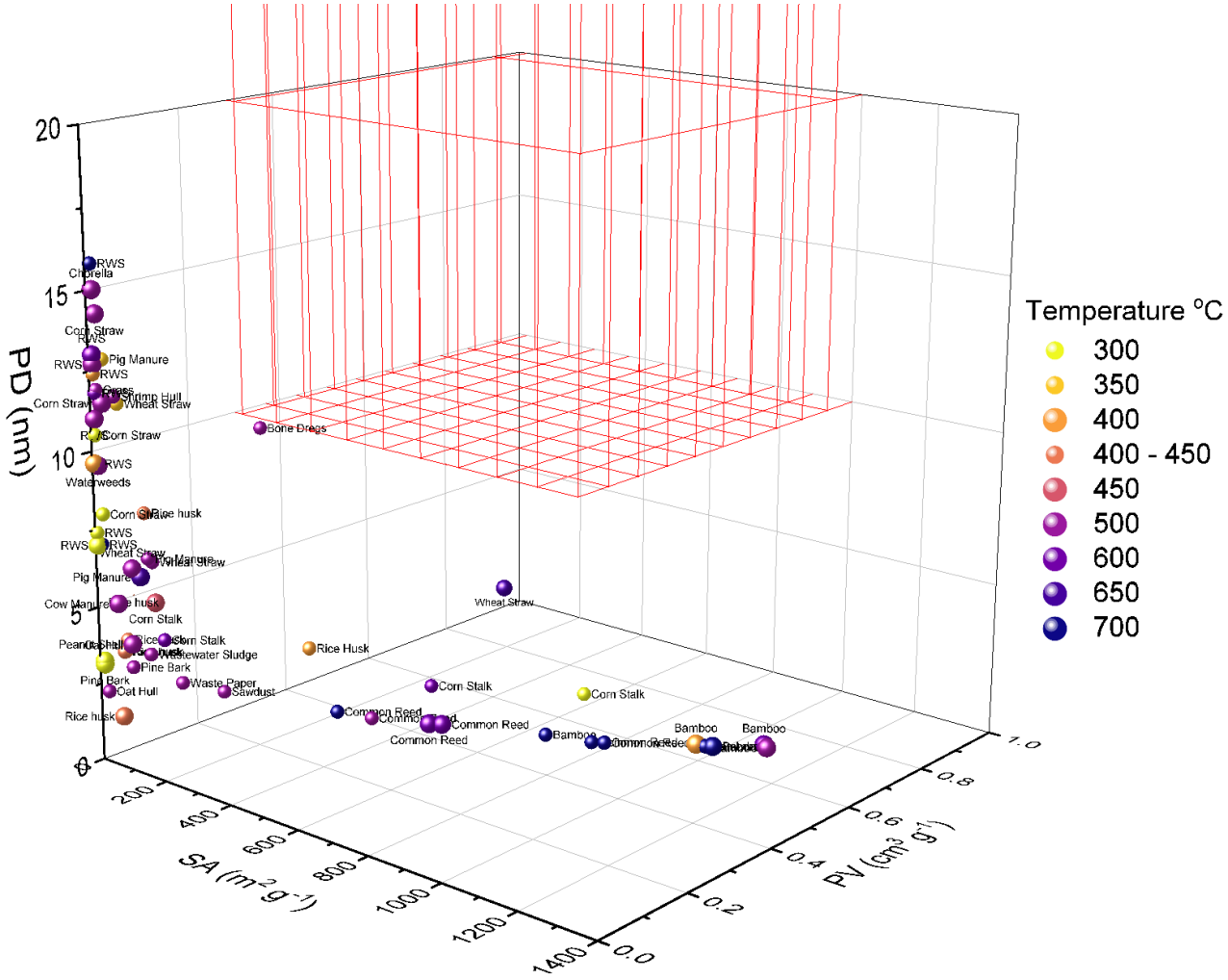

Figure 6. PD (y), SA (x) and PV (z) values for biochars from various feedstocks. The red zone denotes the lower region of the ideal PD, PV and SA parameters for enzyme immobilisation discussed in Section 1.7 outlined by [166].

3.8 Biochar Characterisation

3.8.1 Section Overview

In this section an assessment of three biochar candidates was conducted to determine porosity, SFGs and chemical stability to inform suitability as a support material for enzyme immobilisation. Biochar selection was informed by trends between feedstock type and manufacture conditions and resulting porosity from previous sections in this chapter. MIP and N_2 gas adsorption using Micromeritcs 3-Flex and Tri-Star equipment was used to characterise biochar porosity. It was hoped these characterisation techniques could provide a complete picture of biochar porosity for biochar pores ranging from 0.1 up to 500 nm. Chemical composition and stability of the biochars were further determined using CHNS elemental analysis. O composition was determined by deduction of these values in addition to ash composition. Results from C, H, N, S and O analysis for TERC, WT and HTC biochars all exhibited suitable chemical stability characteristics required for an enzyme reaction system.

Semi-quantitative analyses of biochar SFGs were conducted using ATR FT-IR spectrometry. Carboxylic SFGs - which are favoured for enzyme immobilisation - were identified on TERC biochar, however this was in a single replicate and in low amounts. WT and HTC biochars possessed carboxylate anions, which hold potential for upgrading into carboxylic acid SFGs following further treatment. However, significant issues with ATR FT-IR analysis were also identified. Firstly the potential presence of sorbed water in HTC samples indicating improper handling or drying and secondly low signal transmittance and a high degree of noise for TERC samples, reducing confidence in these results.

3.8.2 Selection of Biochars for Porosity Characterisation

As part of its role in facilitating BECCS research, the TERC has installed a gasification system. Virgin or waste-derived wood pellets are gasified at temperatures, with TERC biochar produced as a bi-product of this reaction[168]. Flue gas is then captured via integration with an amine capture plant, to achieve BECCS. The other two biochars used were those described in section 2.1 and Table 2, WT and HTC.

Table 2. A comparison of the biochars analysed in this chapter, their feedstock and processing conditions and other beneficial credentials.

Biochar	**Feedstock and Processing Conditions**	**Other Credentials**
TERC	High lignin content from wood pellets and pyrolysis temperatures 700 – 800 °C.	Carbon savings from using a bi-product of bio-oil and bio-gas production

WT	High lignin content from willow, alder, hazel, hawthorn, and chestnut feedstocks. Pyrolysis temperatures 700 – 800 °C.	Sustainably harvested UK feedstock near pyrolysis plant, thus low transport carbon footprint[266].
HTC	High lignin feedstock. Pyrolysis temperatures 170 – 300 °C, under pressure using steam[271].	Low specific energy input and thus lower carbon manufacturing footprint[5]. Commonly possess favourable SFGs such as carboxylic acids[270,342]

3.8.3 Results and Discussion

3.8.3.1 Porosity Analyses

According to MIP results, TERC biochar had the highest SA (75 m^2 g^{-1}) and one of the smallest PDs (200 nm) (Figure 7). WT contained the next highest SA (30 m^2 g^{-1}) and intermediate PDs (300 nm) (Figure 7). Finally, HTC possessed the smallest SA (21 m^2 g^{-1}) and the largest average PDs (500 nm) (Figure 7). It should be noted however due to the cost of analysis, the availability of only single batches of biochar samples and limited equipment availability only single sample repeats of each biochar were subjected to MIP testing. This limitation was partially addressed by ensuring large samples of each biochar were mixed, dried and ground to ensure sample homogeneity, however further testing with greater sample replicates would help to increase the reliability of these results. In the case of TERC and WT, the macroporous aspects of biochars may serve as a suitable site for enzyme immobilisation. However, SAs are towards the lower end of the ideal range (25 - 500 m^2 g^{-1}) therefore any catalytic surface created may have comparably low enzyme loading and subsequent system efficiency compared to other commercially established frameworks such as Syloid 244[2] or MCF - 335[168].

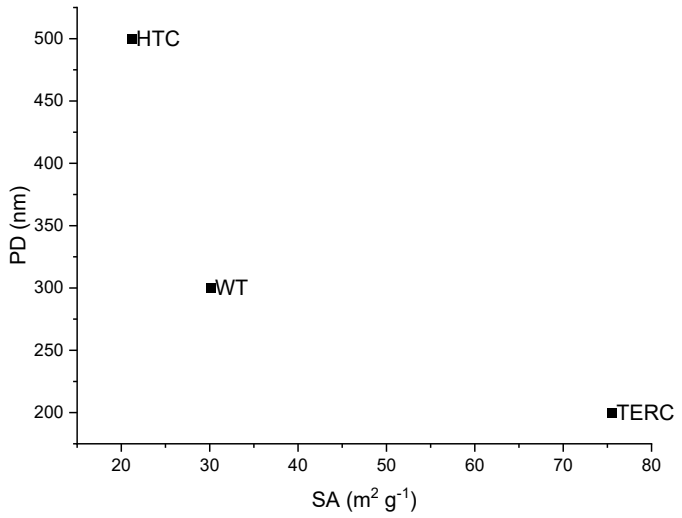

Figure 7. MIP values for PD and SA for HTC, WT, and TERC, where (N = 1 and n = 1).

MIP analysis was unable to provide data for PV, making it impossible to know if biochar PVs are suitable for accommodating multiple enzyme units as well as any spatial movement required for substrate interaction[168]. Finally, MIP may not be able to probe the mesoporous and microporous aspects of biochar, therefore these PDs may not have been accurately accounted for. If pores <10 nm are present in significant quantities, there is a danger of enzymes becoming lodged in biochar pore openings, potentially leading to loss of activity[168].

To quantify PDs in the lower ranges of the biochars and any additional SA associated, N_2 gas adsorption analysis suitable for microporous and nanoporous aspects of biochar was conducted. N_2 gas adsorption also provided values for average pore volumes. According to the results in Figure 8, TERC biochar had the largest PVs and SAs of all the biochar samples, with SAs of 793 and 975 m^2 g^{-1} and PVs of 0.31 and 0.4 cm^3 g^{-1} for 3-Flex and Tristar instruments respectively. Data revealed PD readings of 5.6 and 3.8 nm for 3-Flex and Tristar instruments, which are not large enough to be considered suitable for enzyme immobilisation[168] (Figure 8). In addition, whilst SAs up to 1000 m^2 g^{-1} are not deleterious to enzyme immobilisation, SAs >500 m^2 g^{-1} are not considered ideal since enzyme immobilisation has been found to plateau beyond this point[1]. Readings for both 3-Flex and Tristar analyses for SA of HTC biochar were 12 m^2 g^{-1}, with PVs of 0.02 and 0.08 cm^3 g^{-1} respectively, which did not meet the minimum criteria for enzyme immobilisation (Figure 8). Despite multiple attempts, it was not possible to characterise WT biochar using 3-Flex analysis. Based on data from TriStar analysis, WT had suitable SA (70 m^2 g^{-1}), but did not have sufficient PVs (0.03 cm^3 g^{-1}) or PDs (3.2 nm) for enzyme immobilisation (Figure 8). Contrary to what was expected, greater SA and PV readings for TERC biochar and greater PD (25 nm) for HTC biochar were observed by the Tristar analyser. This may be explained by the superior accuracy of 3-Flex, which is able to analyse PDs down to 0.3 nm^3 leading to measurement variations.

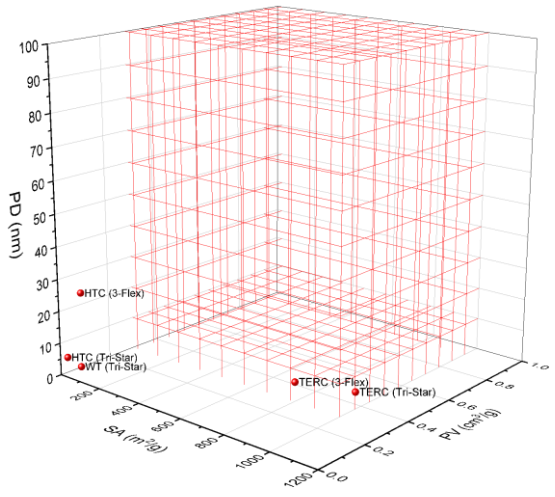

Figure 8. The relationship between SA, PD and PV for HTC, TERC and WT samples measured using N_2 gas adsorption on 3-Flex and Tri-star instruments.

3.8.4 Chemical Stability

The results from C, H, N, S and O analysis are presented in Figure 9. C in biochar has been cited to be highly stable and intrinsically chemically recalcitrant[271,343]. Therefore, the total fraction of C present in a biochar can provide a rudimentary indication of a biochar frameworks resilience to degradation in aqueous reaction systems[342]. TERC biochar had the greatest carbon content (89%), followed by WT (63%) and then HTC (49%) (Figure 9).

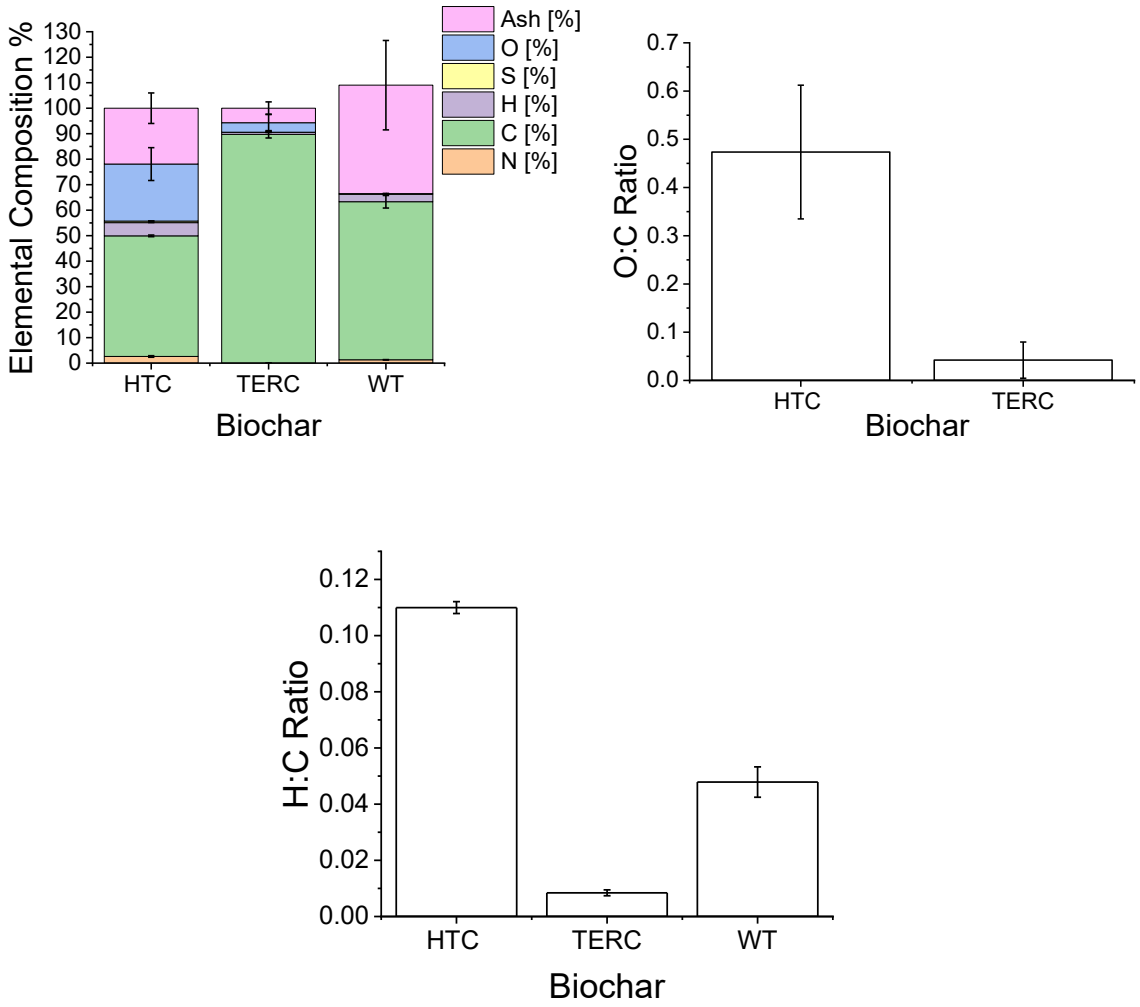

Figure 9. (Left)C, H, N, S and O content, (right) the O:C ratio and the H:C ratio (below) for TERC, HTC and WT biochars. Error bars represent the standard deviation of experimental samples, where N = 3 and n = 3.

Greater pyrolysis temperatures have often been linked to greater biochar stability due to an overall increase in the proportions of C[270]. TERC and WT biochars were both created at similarly high pyrolysis temperatures (700 – 800 °C) and had the highest (TERC) and second highest (WT) proportions of C. These outcomes were therefore consistent with the literature.

In addition to C, higher pyrolysis temperatures have also been linked to reductions in total O content[270]. This pattern was consistent with TERC biochar, which had the lowest proportion of O (3%) out of the three candidates (Figure 9). Lower O proportions are favourable because O - associated SFGs have been linked with increased reactivity of biochar constituents with the surrounding environment[270]. The O content for WT was zero, this was suspected to be due to the high ash content reported for WT, which is known to cause inaccuracies in O calculation[272]. O results were therefore omitted from consideration.

A more precise indicator for biochar stability is the molar ratio of O to C (O:C)[270,271]. According to Spokas *et al.*, "the O:C ratio is related to the number and composition of substituted functional groups"[270]. The less oxygen-containing functional groups attached to hydrocarbon chains or rings, the less reactive that biochar will be to chemical compounds in the surrounding environment[270]. Lower O:C ratios are also associated with a higher incidence of fused aromatic rings[344,345], which are highly stable molecules due to their molecular geometry[345,346] and so are also less likely to react with molecules in the surrounding environment. Lower O:C ratios can indicate low polarity, which is linked to increased hydrophobicity and therefore decreased water solubility, which is important for a biochar framework operating in an aqueous medium[344]. Based on these principles, O:C ratios can therefore serve as an indicator for biochar stability against chemical degradation[270]. As a rule, a molar O:C ratio <0.2 indicates a minimum half-life of 1000 years in terms of biochar stability in the environment. A molar ratio between 0.2 – 0.6 indicates a half-life of 100 - 1000 years and a ratio >0.6 indicates a half-life <100 years[270]. According to Figure 9, HTC biochar was the least stable, with a O:C ratio of 0.4 and therefore a half-life of 100 - 1000 years. TERC was the most chemically stable, with an O:C ratio of 0.04 and therefore would be the biochar most resistant to chemical weathering an enzymatic reaction system.

H:C ratio can also be used as an indicator of stability and aromaticity[345]. H:C ratio is preferred as a stability measure by academic organisations such as the International Biochar Initiative (IBI)[272]. This is because H content in biochar is determined experimentally whereas O is content is calculated by subtracting all other values for C, H, N, S and ash from 100, and has led to inaccuracies in data reporting for biochars with high-ash content[272]. Decreasing H:C ratio correlates to increasing incidence of aromatic ring structures, which are another indicator of C stability in biochars[272]. In the H:C framework, a lower ratio of H to C equates to greater % of C within biochar[271]. A H:C ratio of ≤0.4 is equivalent to 70% of carbon within the biochar being highly stable and likely to remain so for 100 years[271]. HTC, TERC and WT all surpassed this stability threshold, with values of 0.1, 0.008 and 0.047 respectively (Figure 9).

3.8.5 Surface Chemistry Analyses Using FT-IR

FT-IR spectra for HTC, WT and TERC biochars are shown in Figure 10. The HTC samples contained bands within the range 4000 - 2700 cm^{-1} and 1650 - 1610 cm^{-1} and the absorbance can likely be attributed to v(OH) from sorbed water and hydrogen-bonded biochar O-H groups and H – O – H bending for water respectively[258]. This indicates that the samples may not have been adequately handled or dried prior to analysis. With regards to SFGs for enzyme immobilisation, HTC contained bands between the 1280 - 1200 cm^{-1} and 1740 - 1650 regions, which are associated with C-OH stretches and v C=O bonds from carboxylic acids[258]. WT and HTC also had adsorption in the 1000 - 1140 cm^{-1} region, which is associated with v(Si-O) from clay minerals which is often linked to ash deposits and the 1590 - 1520 cm^{-1} region, which could indicate the presence of v(COO–) carboxylate anions (a negatively charged form of carboxylic acid)[258]. The presence of carboxylate anions is encouraging, since its treatment with a strong acid such as HCl, H_2SO_4 and HNO_3 or gas such as CO_2 could protonate this carboxylate anion, leading to the formation of carboxylic acid[347] SFGs desired for enzyme immobilisation. The evidence of carboxylic acids and carboxylate anions is encouraging for enzyme immobilisation; however, it is worth noting that potential contamination with water may call the validity of these results into question.

In the case of HTC aliphatic structures were also observed between 2920 and 2848 cm^{-1} as asymmetric and symmetric stretching vibrations between C – H atoms[348]. In the case of HTC this was expected since aliphatic structures are normally present for low temperature (170 - 300 °C) biochars[258,349]. Aliphatic structures arise is due to the avoidance of the temperature point at which thermal cracking is induced, which initiates the release of volatile organic matter and a proliferation of chemically stable aromatic structures[349] such as benzene rings[335] and graphitic sheets[350]. These structures also arise “by condensation after dehydrogenation of carbohydrates”[349], Which removes hydroxyl groups (-OH), hydrogen (-H) atoms and H_2O molecules from aliphatic structures and enables the formation of conjugated double bonds, leading to ring formation. Therefore, as the incidence of chemically stable aromatic rings increases, aliphatic group incidence decreases[349]. Their presence in HTC could indicate a lower degree of chemical stability.

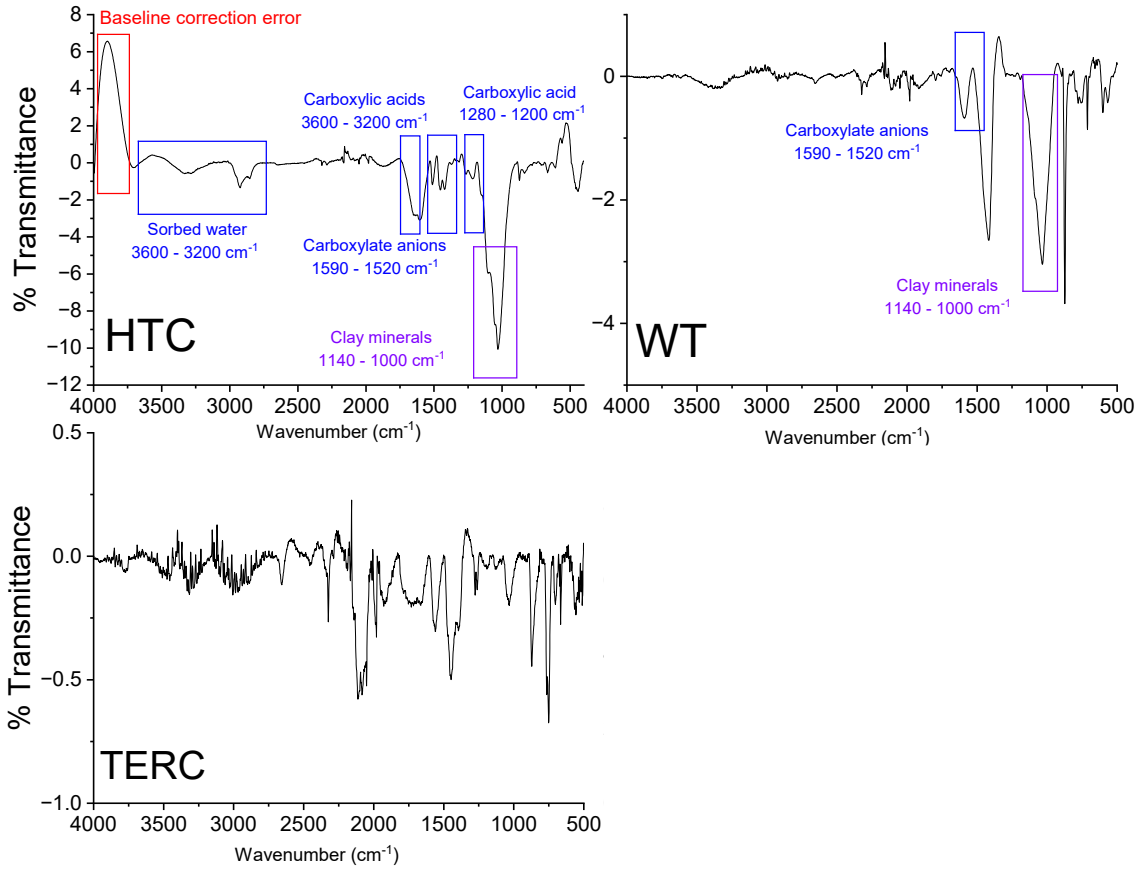

Figure 10. IR Spectrum of TERC, HTC and WT biochars.

TERC biochar transmittance was significantly lower and featured a significant amount of noise compared with HTC and WT samples (Figure 10). This could be due to the carbonaceous nature of TERC biochar, which has been found to limit FT-IR analysis due to enhanced optical absorption[258]. It could be the result of contamination of the ATR crystal or diamond from the environment (air-borne dust particles), or inadequate cleaning between runs or from laboratory reagents. Another cause could be not enough sample or not enough IR interactions. As such, it is difficult to draw any reliable inferences from TERC data. Carboxylic acid groups, which are favoured for enzyme immobilisation, were observed on the surface of the TERC biochar, however, this only occurred in one of the replicates and not in large amounts (Figure 10 and Table 2).

3.9 Section Summary

A summary of results outcomes for biochar analyses performed in this chapter is presented in Table 3. In conclusion, none of the biochars tested met the porosity requirements outlined by Bayne *et al.* for an ideal enzyme immobilisation framework (Table 3)[168]. MIP results for WT and TERC samples both met the minimum SA and PD requirements, however PVs were not provided (Table 3). This would mean that enzymes may have a suitably extensive SA to occupy and PDs large enough to access the SA but have potentially inadequate PVs, which are a vital

aspect of successful enzyme-substrate interactions. HTC biochar did not possess adequate SA according to MIP analysis (Table 3).

MIP porosimetry is limited to mesopores >4 nm, leaving a large potentially large portion of porosity data unquantified. Therefore PDs, PVs and SA for mesopore regions 2 - 100 nm were analysed using a Micromeritics Tristar N_2 gas adsorption instrument. TERC biochar had sufficient SA and PV for enzyme immobilisation but did not have sufficient PDs for enzyme access into the inner SA. WT had sufficient SA, but not sufficient PV or PDs and HTC did not meet any porosity criteria (Figure 2; Table 3). The meso and microporous fraction (0.3 - 15 nm) was characterised using a Micromeritics N_2 gas adsorption 3-Flex instrument. TERC biochar far surpassed the minimum SA requirements and PV requirements but did not meet the minimum PD threshold (Table 3). HTC only met minimum PD requirements and microporous analysis of WT samples failed after two attempts. In summary, whilst MIP data may indicate that a portion of TERC and WT biochar may be suitable for enzyme immobilisation, N_2 gas adsorption results reveal a significant portion which may be inaccessible to enzymes or impede enzyme activity (Table 3).

The high stability of TERC biochar - as indicated by low O:C and H:C ratios and absence of aliphatic groups - may make it a structurally viable candidate for enzyme immobilisation. Whilst carboxylic acids groups and carboxylate anions may be present for WT and HTC biochars, characterisation of SFGs was insufficient and all biochars would benefit from repeated ATR - FTIR analysis or diffuse reflectance FTIR[258]. Diffuse reflectance FTIR may be particularly useful for biochar analysis because it aligns with biochars physical and chemical properties. Biochar is an opaque, highly porous, and irregular material that can scatter infrared radiation, limiting the representativeness of SFGs detected via ATR-FTIR. Diffuse reflectance FTIR instead exploits this scattering behaviour by allowing infrared light to penetrate and interact with a larger volume of sample, resulting in spectra that are more representative of the biochar sample bulk chemistry than just the outer surface[351]. Biochar samples for diffuse reflectance FTIR are diluted in KBr solution, which has a wide spectral range with no peaks in the middle infrared region, whilst preserving the biochar structure[351]. If SFGs were favourable following these analyses, other findings have described studies which have attempted to enlarge biochar PDs through activation techniques. Such techniques may increase the PD of TERC biochar sufficiently for enzyme immobilisation. However, outcomes for activation treatments have been mixed and can often be counterintuitive due to the removal of volatile compounds which leads to the unblocking of smaller pores. Activation treatments have also been shown to be ineffective for chars produced at high temperatures, which often prevents volatile compound recondensation.

Table 3. Summary table of results for TERC, HTC and WT biochars. Text is coloured to indicate suitability for enzyme immobilisation. For porosity measurements, red indicates unsuitable and green indicates suitable. For CHNS and O, red is worst-rated, yellow is intermediate and green is best-rated. For FT-IR green indicates suitable and yellow indicates suitable with modification and additional testing.

Biochar Sample	MIP	N_2 Gas Adsorption (Tri-star)	N_2 Gas Adsorption (3-Flex)	C, H, N, S and O	FT-IR
TERC	SA = 75 m^2 g^{-1} PDs = 200 nm PV values absent.	SA = 975 m^2 g^{-1} PV = 0.4 cm^3 g^{-1} PD = 3.8 nm	SA = 793 m^2 g^{-1} PV = 0.31 cm^3 g^{-1} PD = 5.6 nm	C % = 89% O:C = 0.04 H:C = 0.008	Results failed.
HTC	SA = 21 m^2 g^{-1} PDs = >500 nm. PV values absent.	SA = 12 m^2 g^{-1} PV = 0.08 cm^3 g^{-1} PD = 5 nm	SA = 12 m^2 g^{-1} PV = 0.02 cm^3 g^{-1} PD = 25 nm	C % = 49% O:C = 0.4 H:C = 0.1	Aliphatic groups = lower chemical stability. Carboxylic acid groups and carboxylate anions - could be changed to carboxylic acid groups.
WT	SA = 30 m^2 g^{-1} PD = 300 nm. PV values absent.	SA = 70 m^2 g^{-1} PV = 0.03 cm^3 g^{-1} PD = 3.2 nm	Results failed	C % = 63% O:C = Result failed H:C = 0.047	Carboxylate anions - could be changed to carboxylic acid groups. No aliphatic groups = chemically stable.

3.10 Impact of Gas Adsorption and Results Processing Methodology on Biochar Surface Area and Porosity Reporting

3.10.1 Choice of Adsorbate

The choice of adsorptive gas can be highly important for obtaining accurate measurements of the SA, PD, and PV of biochar. This is because certain molecules can be restricted from accessing all spaces within a material if the diameter of the molecule is too wide to fit through a materials pores and passages[263]. This can lead to inaccurate measurement of SA and PVs due to selective filling instead of even mono or multi-layer coverage[263,352,353]. If options of adsorbate are limited, these restrictions can be overcome in certain instances by varying adsorptive gas pressure during analysis and through careful selection of temperature[263]. According to IUPAC guidance, the distribution of pore sizes for carbon materials such as

biochar can lie in the microporous to mesoporous range[263]. Therefore, an adsorptive gas with a molecular diameter small enough to access micropores would be most appropriate for biochar analysis. In this regard, CO_2 has been considered a more favourable choice of adsorbate for biochar since its molecular diameter of 0.33 nm[354] is smaller compared with the molecular diameter of N_2 of 0.364 nm[355] and argon 0.363 nm[356]. This has been confirmed in practice: a study compared the performance of CO_2 and N_2 adsorption in carbons and found pores with PDs of 0.7 nm could be filled using CO_2 and as a result, PD distribution was more accurate compared to N_2 adsorption[357].

Polarity of the adsorptive gas molecules and adsorbent surface chemistry also affects the orientation at which common adsorptive gas molecules, such as N_2 and CO_2, interact with the surface of the adsorbent. The properties of biochar can range from polar to non-polar depending on pyrolysis temperature[258,358]. Both N_2 and CO_2 possess quadruple moments which may interact selectively with polar sites on the surface, leading to variations in pore filling pressure and inaccurate surface area and porosity measurements[263,358,359]. Therefore, the choice of adsorptive gas, its pressures and temperature should also be informed by the expected porosity and surface chemistry of the biochar[263]. Further helpful in-depth technical information relating to the appropriate application of gas adsorption analyses for material characterisation have been extensively covered by Silvestre-Albero *et al*., 2012, Brewer *et al*., 2014, Ambroz *et al*., 2018, Kim, Yoon and Bae., 2016; Bae, Yazaydn and Snurr, 2010 and, Hassan *et al*., 2020[352,353,358,360–362].

In reviewing studies for this report, we found only one study used CO_2 and N_2[363] as the adsorptive gases, while 36 used N_2 and six did not report the adsorptive gas[259,341,364–366]. In addition only two studies[367,368] provided the pressures used and only eight provided the temperature of N_2[305,329,367,369–372]. Ultimately, the choice of gas used for these studies and the omission of methodology details for gas adsorption analyses could reduce confidence and the accuracy of porosity reported in many studies.

3.10.2 Porosity and Isotherm Analysis

The correct computational modelling method is essential for calculating accurate SA, PD and PV in biochar samples. Of the 56 studies reviewed in this report, only 12 studies elaborated on the type of computational modelling used. The methods used were non-localised and localised density functional theory [329,341,371,373], Barrett-Joyner-Halender (BJH)[325,331,374,375], the t-plot method[331,372] and BET[331,371]. In some cases, the procedure was inappropriate for biochar. For example, the non-localised density functional theory model is only accurate for microporous materials and “assumes a smooth and homogenous carbon surface”[263], which could be inappropriate for biochar as its surface structure can range from heterogeneous to

homogenous depending on pyrolysis temperature[358]. In other cases, a single model was used for determining multiple aspects of porosity. This approach could lead to errors since most computational models only provide information relating to a certain aspect of porosity. For instance BJH is only used for obtaining information relating to PDs in meso- and macro-pores[376] and t-plot models are used for assessing micropore volume and external SA. In relation to this study, two cases were found in which BET was used for analysing PD and PV but should only be used for obtaining information relating to SA[263,376].

3.10.3 Section Summary

To accurately measure biochar porosity, deeper consideration must be given to the choice of adsorptive gas as well as its pressure and temperature. Whilst many studies have undertaken biochar analysis using N_2 gas adsorption, there is potential that N_2 may not be able to completely penetrate microporous materials, and CO_2 has been explored as an alternative given is smaller molecular diameter. However, neither N_2 nor CO_2 may be appropriate given the often-polar nature of biochar, which could lead to uneven adsorption and inaccurate measurements. Overall, methodological details such as adsorptive gas type, pressure and temperature were inconsistently reported in the studies reviewed. In addition, results in the form of isotherms and hysteresis were often omitted, removing an opportunity for researchers to compare biochar material properties with what is expected in the general literature and decide whether the choice of computational method for analysing data was appropriate. Finally, in certain cases the misuse or overgeneralisation of computational models may have led to inaccuracies in porosity measurements. In summation, the cumulative impact of these factors could reduce overall confidence in the strength of the dataset obtained for this study, which may compromise conclusions drawn pertaining to whether the porosity of biochar is suitable as an enzyme support.

3.11 Chapter 3 Summary

In this chapter, published data from studies which undertook gas adsorption analyses to determine characterise biochar porosity were reviewed. Data relating to manufacture conditions and material properties was collected and evaluated to discern the effect of pyrolysis temperature, feedstock, and activation treatment on porosity characteristics. No biochar candidate met the minimum PD, PV and SA requirements for an effective enzyme immobilisation framework. In some cases, wide enough PDs and sufficiently extensive SAs were present. These features might have allowed enzymes to penetrate the inner biochar matrix and form an effective catalytic surface, but candidates did not possess PVs large enough for enzymes to operate. These outcomes contradict the prevailing justification for the

transformation of lignocellulosic feedstock into biochar for its application as an enzyme immobilisation framework.

The data also indicates that whilst in many cases porosity features of biochar developed according to the prevailing literature, there are many instances where they did not. Inspection of these instances to understand these deviations were often curtailed by a lack of inclusion of controls for data and a lack of consistency in sample treatments. This analysis was further hindered by incomplete or inappropriate methodologies for gas adsorption and computational modelling. These factors have reduced confidence that a trend could exist between selecting an appropriate feedstock and its pyrolysis conditions and the development of material with critical quality attributes within the correct range for enzyme immobilisation.

Future investigations into biochars use as an immobilisation framework may be aided by a Quality by Design framework, which takes a more intentional and systematic approach towards engineering bioinspired solutions. A recommended resource for Quality by Design is “Introduction to Quality by Design (QbD): From Theory to Practice”[377]. To put the Quality by Design approach into the context of biochar engineering for enzyme immobilisation, it would begin by understanding biochar as a material for enzyme immobilisation[377]. This would be followed by understanding the process requirements for developing a biochar material with these desired characteristics. Achieving these characteristics in practise would be achieved by employing design solutions to reduce the potential of producing a biochar with porosity characteristics which are undesirable for enzyme immobilisation[377].

To begin along this pathway, sufficient and consistent information relating to biochar manufacture conditions and porosity must be available to researchers. This can be achieved through extensive and systematic campaigns into biochar manufacture using greater diversities of feedstocks created using standardised process conditions. If post-synthesis treatments such as activation are used, a non-activated control should always be included for direct comparison. Lignocellulosic analyses of each feedstock would also be a useful addition, so that lignocellulosic content can be directly compared with pyrolysis and subsequent porosity outcomes. This approach could increase researcher confidence in identifying critical process parameters for adapting biochar porosity for enzyme immobilisation.

Results from the laboratory analyses indicated that whilst high chemical stability was evidenced in samples such the TERC biochar. Ultimately, none of the biochars tested met the porosity requirements outlined by Bayne *et al*.[168]. Therefore, based on findings from this chapter, biochar was abandoned as a potential framework for enzyme immobilisation and investigations were re-focused on the application of highly ordered mesoporous bioinspired silica.

4 Chapter 4: Investigating the Immobilisation of Bovine Serum Albumin (BSA) and CA on Novel BIS.

4.1 Introduction

4.1.1 Overview

This chapter begins by discussing the impact of additive selection on BIS porosity followed by an overview of the impact of conditions temperature, pH and protein concentration on enzyme adsorption. Based on these outcomes, each section will then justify the conditions used for CA adsorption for these analyses. Entrapment of proteins into BIS will then be discussed, followed by a summary of the methods. Finally, the section will discuss the risks and benefits associated with both of immobilisation techniques and present an overview of the intended work for this chapter.

The next section will begin by examining the results of both CA and BSA enzyme entrapment trials. Following these discussions, porosity data from N_2 gas adsorption analyses from synthesis [redacted] with and without entrapped enzyme is then presented and the suitability for enzyme immobilisation and the impact of the enzyme on BIS formation is discussed. Temperature dependent adsorption of CA is then investigated onto [redacted] BIS and commercially available Syloid 244 silica. The degree of immobilisation onto each material is reported as immobilisation success (%) and protein loading (mg CA/mg BIS). Free and immobilised CA activity is then assessed using both p-NPA hydrolysis and CO_2 mineralisation to $CaCO_3$, with the outcomes for these studies being reported as rates (V_0) and, CO_2 sequestration (mg) and CO_2 yield (%). The presence of CA for CO_2 mineralisation is confirmed using XRF analysis and both the adsorbed and encapsulated enzyme retention was characterised via a leaching assessment. Results from the pH dependent immobilisation by entrapment of BSA at pH addition points from 7 - 11, are then presented and described. An assay involving exposure of CA to pH conditions (7 - 11) for one minute is also performed to judge the prospective impact on CA activity on addition at pH >8.

Finally, this chapter concludes with a discussion of the findings from this research, which materials show promise for future investigations and how they may fit into the landscape of CA applications for carbon capture. It finishes with future questions and directions for this material.

4.1.2 The Impact of Additive Choice on BIS Porosity

Section 1.9.3. discussed the role of conventional silica materials and the intrinsic role of template molecules in the manufacture of many commercially available mesoporous silicas. In the case of SBA-15 for instance, template molecules guide assembly of silica monomers around them resulting in a spherical micelle, with the template molecule in the centre and silica monomers surrounding it[236,237]. When precipitation is finished and the surfactant is removed via calcination, the result is a highly ordered mesoporous structure[237]. Some of the most successful forms of framework for CA immobilisation have been achieved using SBA-15 silica, functionalised using silver, gold or amines to enhance the adsorption potential of CA onto the framework[219]. CA has also been successfully covalently bonded to SBA-15 using the amine octa(aminophenyl)-silsesquioxane (OAPS)[378]. SBA-15 has also acted as a successful framework for CA cross-linked enzyme aggregates (CLEAs)[227]. Unfortunately, the manufacture of these conventional silicas such as SBA-15 is not considered to be sustainable[379,380].

BIS could be an alternative sustainable framework for immobilisation, which achieves its porosity differently to conventional silicas. During aggregation of primary particles (10 - 30 nm) to form secondary particles (200 - 400 nm), additives act as a bridge between these primary particles, with the gap roughly equating to the length of the additive molecule[255]. Primary particles are not the same size, which unlike SBA-15 results in a disordered material as gaps between particles occur during their aggregation. In the case of PEHA, the final material is pre-functionalised due to the presence of PEHA, microporous (PD = 2 nm), and has a low SA (~15 m^2 g^{-1}) and PV (~0.01 cm^3 g^{-1})[255] (Figure 1). Materials which are made in this way [redacted] are termed Gen 1 BIS. Following Gen 1 BIS synthesis it has been found that removing the PEHA via a post-synthesis elution using HCl has further increased microporosity and SA by up to 300 m^2 g^{-1} and resulted in a pure, non-functionalised material[255] (Figure 1).

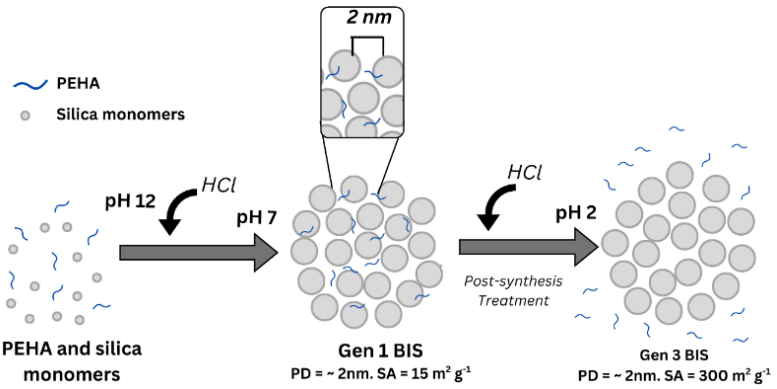

Figure 1. BIS synthesis begins with PEHA and $NaSiO_3$ forming primary silica particles as pH decreases. PEHA guides aggregation between particles, and an optional post-synthesis elution step removes the additive.

4.1.3 BIS Synthesis and Enzyme Immobilisation

Many previous studies have harnessed the mechanism of Gen 1 BIS formation to entrap enzymes during particle aggregation. One notable study used PEHA and amine additives such as tetraethylenepentamine, triethylenetetramine and diethylenetriamine to synthesise BIS for lipase entrapment[381]. This study reported PVs of 0.04 - 0.06 $cm^3\ g^{-1}$ and SAs of 12 - 15.6 $m^2\ g^{-1}$ with PDs in the mesoporous range (13 - 22 nm) regardless of the additive[381]. Despite these porosity characteristics being too low, in terms of SA and PV, for enzyme immobilisation according to criteria outlined by Bayne *et al.*, high activity and low enzyme leaching was reported for all four materials[168,381]. Additionally, a w/w loading between 0.15 - 0.25 mg lipase per mg BIS was achieved across the four materials[381]. Despite efforts to increase immobilisation by increasing the total concentration of lipase in the reaction solution, the authors concluded that there was a maximum loading capacity where total immobilised enzyme did not increase further[381].

In another more direct example, immobilisation of CA was investigated using Gen 1 BIS entrapment with the amine additive diethylenetriamine. This resulted in the formation of a material with low SA (17 $m^2\ g^{-1}$) and PV (0.06 $cm^3\ g^{-1}$) but high PD (22 nm)[212]. Despite the low SA and PV, CA still displayed a high CO_2 sequestration activity of 86%, which was getting close to the higher 90% activity seen in free CA enzyme[276]. Similarly to lipase immobilisation, the authors also reported low leaching and a w/w loading of 0.23 mg CA per mg BIS. Interestingly, N_2 gas adsorption measures were performed with and without CA entrapment, finding that that the addition of CA did not appear to have any adverse effect on porosity.

4.1.4 Improving Immobilisation [redacted]

Recently, a highly novel [redacted] method of BIS production has been developed [redacted] . to generate a mesoporous framework. [redacted] .

N_2 adsorption analyses without CA have reported porosity values for this new material of ~16 nm for PDs, SAs of 365 $m^2\ g^{-1}$ and PVs of 0.79 $cm^3\ g^{-1}$, which are well within the desired porosity for an enzyme immobilisation framework. The synthesis of this material [redacted] .

is referred to as Gen 2 BIS. Like [redacted]BIS, porosity can be enhanced further [redacted] . to create a pure, non-functionalised material (Figure 2)[255]. Materials which have had additives removed in this way are termed Generation 3 (Gen 3) BIS (Figures 1 and 2).

[redacted]

Figure 2. *[redacted]*

Based on the porosity outcomes of this material it was determined that further exploration of enzyme immobilisation on [redacted] Gen 2 and 3 materials was worthwhile. Due to the high novelty of these materials and the fact that they were developed within the Green Nanomaterials Research Group at the University of Sheffield in the UK, their application for the immobilisation of CA is unreported in the literature.

4.1.5 Research Questions

Based on the information in Section 4.2, the following chapter focuses on investigating whether the entrapment of CA into Gen 2 BIS leads to an improvement in CA activity. Activity could increase with entrapment due to several factors. Firstly, confinement of the CA molecule within the matrix, instead of binding the CA to the framework, may decrease the risk of CA denaturation and subsequent loss of activity. Secondly, the improved SA, PD and PV could: increase total loading of CA, improve activity by providing additional space for the enzyme to interact with the substrate, and enhance mass transfer of the substrates through the framework. Chapter 4 will also explore the use [redacted] to create CA entrapped Gen 3 BIS. The removal of additives should increase BIS porosity factors even further through potentially improving mass transfer and increasing CA operational space, both of which could improve CA activity. Alternatively, the effect of HCl during elution could lead to loss of CA activity from protein denaturation due to pH exposure far below its optimal range.

Finally, the Gen 2 and 3 BIS will be tested to determine if they are able to retain the CA enzyme effectively within the framework.

Adsorbed CA onto mesoporous silica has had some success in the literature. Therefore Chapter 4 also aimed to test whether Gen 2 and 3 BIS, which offer optimal porosities and are both sustainable, could successfully support CA adsorption relative to the non-sustainable Syloid 244 framework. Two things will be tested, firstly whether Gen 2 and 3 porosities facilitate CA adsorption and whether its loading is comparable to Syloid 244, and other CA frameworks found in the literature. Secondly, Gen 2 and 3 BIS will be compared to investigate whether the additives [redacted] affect CA adsorption, stability and activity. Chapter 4 will conclude with comparing how Gen 2 and 3 entrapped and adsorbed frameworks to identify the best candidate for CA immobilisation.

4.2 Experimental Strategy

4.2.1 Adsorption

In addition to the research questions posed in Section 4.1.5 and informed by the literature review carried out in Chapter 3. Further experimental parameters will also be investigated.

4.2.1.1 Impact of pH, Temperature and Protein Concentration

The adsorption was conducted at pH 7.5, as this is close to the reported optimum pH for CA activity and is expected to support preservation of its catalytic function[383]. The isoelectric point for CA from bovine erythrocytes is approximately 5.4[382]. At this pH, which is above the isoelectric point of CA, the enzyme is anticipated to possess a net negative charge[383]. This charge state may facilitate electrostatic interactions with the positively charged functional groups of PEHA and L-arginine, potentially promoting favourable adsorption while maintaining enzymatic activity (Figure 3)[255,384].

[redacted]

Figure 3. Adsorption of CA [redacted] (Gen 2) and [redacted] (Gen 3) BIS.

Higher adsorption temperatures have been linked to increasing amounts of enzyme adsorption on mesoporous materials[385]. Whilst the adsorption process is exothermic and

hence it should decrease with increasing temperature; higher temperatures help to overcome initial molecular interactions between an enzyme and the framework, allowing them to move deeper into the pores and access the full SA available[385]. Enzyme movement by breaking surface interactions is endothermic and therefore requires greater thermal energy to occur, leading to an increase in adsorption with increasing temperature[385]. However, temperatures beyond CAs optimal range may lead to denaturation and loss of activity. The first temperature selected was 4 °C since a low temperature can help to preserve the protein, the second was 21 °C and the third was 37 °C, which is the enzymes optimal operational temperature, beyond which there is a risk of enzyme denaturation.

Protein concentrations can significantly impact the enzyme loading success of a framework and the expectation is that an adsorption isotherm for loading should be developed to identify optimum enzyme loading concentrations[385]. However, this approach would require multiple trials, and the cost and unpredictability of CA sourcing made these unfeasible. Previously, the concentration of CA and the model protein BSA in mg/mL of reaction volume has been optimised for BIS[276,386]. Both studies recommended 2 mg/mL of reactant volume as the ideal concentration for maximum immobilisation. It should be noted that this was for an encapsulation procedure for BIS frameworks with different porosities, however it was determined that this concentration could serve as a baseline from which researchers could base future investigations if Gen 2 or 3 BIS shows promise.

4.2.2 Entrapment [Jenny's redactions start here]

The entrapment of CA occurs as BIS particles aggregate (Figure 4). Therefore, increasing the concentrations of additives and silicate should lead to greater amounts of BIS yield and potentially greater opportunity for CA uptake, therefore the impact of increasing silicate and additive concentrations (30, 50 and 100 mM) was tested. While higher reactant concentrations could lead to more CA immobilisation, the amount of CA immobilised per mg BIS (w/w) may not increase due increased yields of BIS. It may however improve overall loading success (%) and reduce enzyme waste.

[redacted]

Figure 4. Encapsulation of CA into Gen 2 BIS

[redacted] …

As part of this investigation into CA entrapment, experiments were interspersed with BSA entrapment assessments as a trouble-shooting measure, the outcomes of all these trials were also subject to statistical analysis.

4.2.2.1 Impact of the pH Point of Protein Addition and the Effect of Protein Concentration on Immobilisation and BIS Synthesis.

According to a published protocol for protein immobilisation in BIS, an optimal protein concentration of 2 mg/mL has been documented for enzyme encapsulation[386]. However, the enhanced porosity of Gen 2 BIS may accommodate a greater enzyme loading. Therefore, an analysis using BSA was included to determine the effect of increasing protein concentration on immobilisation success and BIS formation. In the literature the timing of protein addition during BIS synthesis has varied. Some research papers suggest adding proteins at neutral conditions[276,381] while others recommend adding them under more alkali conditions (around pH 10)[386]. Because of these differences, the protein concentration study was expanded to examine the impact of pH on BSA immobilisation and BIS synthesis. In parallel, the CA catalytic activity was evaluated using p-NPA hydrolysis following exposure to solutions ranging between pH 7 - 10.

4.2.3 Section Summary

It is hoped that the topics discussed in this section have helped to justify the approach towards immobilising CA and testing its activity. Temperature - dependent adsorption of CA onto silica materials will be explored using Gen 2 and 3 BIS and Syloid 244 substrates, using a PBS solution adjusted to pH 7.5 to preserve optimal CA activity (Figure 5). Entrapment of CA into Gen 2 BIS will be performed using a range of reactant concentrations (30, 50 and 100 mM) (Figure 5). Following entrapment, half of the samples were [redacted] resulting in Gen 3 BIS containing entrapped CA (Figure 5). As part of this investigation into CA entrapment, experiments were interspersed with BSA entrapment assessments as a trouble-shooting measure, the outcomes of all these trials were subject to statistical analysis and a referral guide for these experiments is listed in Table 1 in the experimental section. Protein immobilisation is reported in two ways, as loading success (%) and as the mg protein to mg BIS weight per weight ratio (w/w) (Figure 4). CA activity is then tested using *p* - NPA hydrolysis and CO_2 mineralisation via $CaCO_3$ formation. Activity assessments are then followed with a leaching analysis. At the end of this chapter, BSA is also used as a model protein to determine whether adjustments in total protein concentration or the pH at which protein is added can increase protein loading into the framework.

[redacted]

Figure 5. Chapter 4 Experimental Overview

4.3 Results

4.3.1 BIS Formation in the Absence of Protein

The amount of BIS formed in the absence of protein (mg/mL reaction solution) can provide insights into the consistency of background BIS formation across Gen 2 and Gen 3 entrapment reactions and indicate whether variations in CA immobilisation were due to differences in the amount of BIS formed per mL (Table 1). For Gen 2 BIS, the yield in terms of mg per mL was not significant across experiments (p >0.05), indicating that no variation occurred in the amount of BIS formed in the absence of protein (Table 1).

For Gen 3 BIS synthesis, statistically significant differences in BIS formation (p <0.05) were observed across all three experiments (E2, E3, and E6) (Table 1). However, rather than reflecting insufficient BIS formation, these differences are more likely attributable to reduced BIS recovery in these experiments. The reasons behind low recovery are twofold. Firstly, due to limited CA availability, reaction volumes were decreased, resulting in lower total BIS yields. Yields were further diminished during the [redacted] .

. These lower yields made it harder to recover and accurately weigh the amount of Gen 3 BIS formed from the synthesis.

Table 1. BIS formation at 30 mM in the absence of protein for Gen 2 and 3 BIS over experimental campaigns. Values with (±) represent standard deviation between experimental replicates.

BIS type	Experiment Number	mg BIS/mL	Equal Variance
Gen 2	E2	1.09 (± 0.16)	Yes
	E3	0.96 (± 0.13)	Yes
	E5	1.25 (± 0.20)	Yes
	E6	1.11 (± 0.16)	Yes
Gen 3	E2	0.7267 (± 0.0321) *	Yes

	E3	0.3917 (± 0.09) *	Yes
	E6	0.7433 (± 0.21) *	Yes

** Indicates the value which caused significance (p <0.05) according to the Tukey test output.*

4.3.2 BSA Entrapment on Gen 2 and Gen 3 BIS.

No significant variation occurred for BSA entrapment across experimental trials for both Gen 2 and 3 BIS during synthesis (p >0.05) (Table 2). However, loading success was far greater in Gen 2 (25 - 33.5%) compared with Gen 3 (0.1 - 4%) which suggests that BSA was removed from the framework [redacted] (Table 2). The use of [redacted] from BIS frameworks, whilst retaining entrapped BSA, has previously been recommended for low SA Gen 1[386]. Therefore, the high amount of BSA removal observed for Gen 3 BIS contrasts significantly with current expectations of how BSA should respond to [redacted]. Gaining a true understanding of the mechanisms which lead to this difference in BSA retention is beyond the scope of this project. However, a difference in BSA retention between Gen 1 and 2 BIS may have been the enhanced porosity of Gen 2 BIS, facilitated by the [redacted] Gen 2 BIS synthesis. The larger PVs and PDs between these particles may have allowed BSA to leave the framework through these spaces [redacted] during Gen 3 BIS creation.

Despite the reduction in BSA loading observed for Gen 3 BIS, w/w loading of Gen 2 BIS was consistently high across experiments, between 0.9 – 1.2 mg protein per mg of BIS (Table 2). Previous studies which have immobilised protein on Gen 1 BIS using various additives have reported values of 0.15 – 0.25 mg enzyme per mg BIS[212,246,386], therefore these results are consistent with prevailing literature. In the wider context of enzyme immobilisation, w/w loading of enzymes onto a carrier are more typically around 0.02 mg/mg carrier, which is insufficient when scaled to industrial applications[226]. Therefore, loading of BSA for this Gen 2 BIS far surpasses this threshold and thus offers a promising increase on the potential w/w loading of protein which can be achieved. However, it should be noted that whilst the differences between these values was not significant, there was between 34 to 64% variation between experimental replicates across experiments E1, 4 and 5 for Gen 2 (Table 2). This indicates that while high protein loading can be reached, there is scope for further investigations into reducing w/w loading variability.

Another important observation for Gen 2 BIS is that whilst there was no significant difference in the mg of BIS formed per mL across experiments, the average amounts of BIS were notably lower (0.53 - 0.68 mg BIS/mL) compared to the BIS formation per mL during control

experiments (0.96 - 1.11 mg BIS/mL). Therefore, whilst high BSA immobilisation looks to be achievable in Gen 2 BIS, it also appears to come at the cost of total BIS yield.

Table 2. Statistical analyses for BSA-immobilisation consistency (mg BIS/mL; mg BSA/mg BIS and immobilisation efficiency (%)) between experimental days onto Gen 2 and 3 BIS at 30 mM reactant concentration. Values with (±) represent standard deviation between experimental replicates.

BIS type	Experiment Ref.	Loading Success (%)	mg BSA/mg BIS	mg BIS/mL	Equal Variance
Gen 2	E1	25.52 (± 10.09)	1.17 (± 0.76)	0.53 (± 0.27)	Yes
	E4	28.70 (± 3.52)	0.93 (± 0.44)	0.69 (± 0.3)	Yes
	E5	33.53 (± 3.81)	1.05 (± 0.34)	0.68 (± 0.16)	Yes
Gen 3	E1	4.08 (± 7.83)	0.11 (± 0.24)	0.74 (± 0.42)	Yes
	E4	0.11 (± 7.81)	0 (*)	0.60 (± 0.66)	Yes
	E5	2.82 (± 2.81)	0.04 (± 0.01)	0.87 (± 0.25)	Yes

** Indicates the value which caused significance ($p < 0.05$) according to the Tukey test output. (*) Indicates average negative value and so was adjusted to zero prior to significance testing.*

In an experiment where the impact of reactant concentration (30, 50 and 100 mM) on Gen 2 BIS formation and BSA entrapment was investigated, it was found that BIS formation per mL increased significantly with increasing reactant concentrations (Table 3). Significance occurred between 30 - 50 mM (p = 0.002) and then increased further between 50 - 100 mM (p = <0.0001).This is in line with what was expected since higher concentrations of additive and silica precursors should lead to higher amounts of primary particle aggregation to from BIS Gen 2[243]. Greater precursor and additive concentrations can also lead to higher chances of collision with other particles and thus faster aggregation rates[243]. Therefore, as reactant concentrations increase, BSA may have less time to become trapped between primary particles during aggregation. However, despite this narrower window for entrapment, it was found that BSA loading success (%) increased with increasing reactant concentration (Table 3). A significant increase of 22% (p = 0.03) and 38% (p = 0.002) in BSA loading success was seen between 30 to 50 mM and 50 to 100 mM reactant concentrations respectively. These increases were not significantly (p >0.05) reflected however in the w/w loading of BSA to BIS per mg (Table 3). This indicates that whilst greater amounts of BSA become entrapped because of increased precursor and additive concentrations, resulting in less BSA wastage in the reaction solution, this is reflected in reduced w/w loading in the final BIS product.

As expected, a highly significant increase in BIS formation per mL occurred with increasing reactant concentrations for Gen 3 BIS (p <0.0004) (Table 3). However, unlike Gen 2 BIS, this increase did not lead to a significant increase in BSA loading success (p >0.05) or w/w loading (p >0.05). This outcome is consistent with experimental outcomes thus far, in that despite higher reactant concentrations leading to increased amounts of BSA immobilisation, the w/w loading of BSA per mg of BIS reduced due to increasing overall BIS formation. As outlined in Section 4.3.2, it appears that these lower amounts of BSA are then removed from the framework [redacted] to produce Gen 3 BIS.

Table 3. Statistical Analyses for BSA-immobilisation consistency (E1) (mg BIS/mL; mg BSA/mg BIS and immobilisation efficiency (%)) between reactant concentrations onto Gen 2 and Gen 3 BIS. Values with (±) represent standard deviation between experimental replicates.

BIS Type	Reactant Concentration	Loading Success (%)	mg BSA/mg BIS	mg BIS/mL	Equal Variance
Gen 2	30 mM	25.52 (± 10.09) *	1.17 (± 0.76)	0.53 (± 0.27) *	Yes
	50 mM	47.93 (± 7.15) *	0.40 (± 0.09)	2.21 (± 0.15) *	Yes
	100 mM	85.37 (± 5.71) *	0.30 (± 0.04)	5.47 (± 0.48) *	Yes
Gen 3	30 mM	4.08 (± 7.83)	0.11 (± 0.24)	0.74 (± 0.42) *	Yes
	50 mM	0.03 (± 0.98)	0 (#)	2.84 (± 0.29) *	Yes
	100 mM	12.26 (± 8.05)	0.03 (± 0.02)	5.94 (± 0.17) *	Yes

** Indicates the value which caused significance according to the Tukey test output. (#) Indicates average negative value and so was adjusted to zero prior to significance testing.*

4.3.3 CA Entrapment in Gen 2 and Gen 3 BIS.

4.3.2.1 Experimental Variation During 30 mM Reactions

For CA loading onto Gen 2, both loading efficiency (%) and w/w loading exhibited a decrease from E3 to E6 (Table 4, Figure 6). Whilst these reductions were not statistically significant (p >0.05), it is worth noting that this decline occurred alongside a statistically significant 34% reduction (p = 0.003) in the total mg of BIS formed per mL in E6 relative to E3 (Table 4). Similarly to the trend found with BSA (Section 4.3.2), in which increased reactant concentrations led to greater immobilisation efficiency CA loading at 30 mM may therefore also be sensitive to the quantity of available BIS matrix formed in solution, where reduced BIS formation constrained overall loading capacity.

In the case of Gen 2 30 mM BIS formation in the absence of protein, there appeared to be no difference in the amount of BIS formation per mL between the no protein and CA - entrapment trials across either E3 or E6 experiments. Therefore, while some variation in CA loading may be occurring between experiments, unlike BSA it appears to be unlikely that the presence of CA is interfering with the formation of BIS during the reaction (Table 4).

Despite variations in w/w loading between experiments, Gen 2 BIS from E3 and E6 had w/w loadings of ~0.29 and 0.16 respectively. This is consistent with the values for previous BIS studies which immobilised enzyme on Gen 1 BIS and reported w/w loading values of 0.15 - 0.25 mg enzyme per mg BIS[212,246,386]. E3 and E6 samples both surpassed the minimum w/w enzyme loading of 0.02 mg enzyme per mg carrier, making it suitable for potential industrial applications[226].

Table 4. Difference Between CA Entrapment Experiments for Gen 2 and Gen 3 BIS at 30mM and 50mM Reactant Concentrations. Values with (±) represent standard deviation between experimental replicates.

	Exp. Ref.	Loading Success (%)	mg CA/mg BIS	mg BIS/mL	Equal Variances
Gen 2 30 mM	E3	19.38 (± 5.29)	0.29 (± 0.10)	1.20 (± 0.09) *	yes
	E6	11.86 (± 3.02)	0.16 (± 0.04)	0.79 (± 0.11) *	yes
Gen 3 30 mM	E3	14.71 (± 2.67) *	0.34 (± 0.13) *	0.74 (± 0.23)	yes
	E6	0 * (#)	0* (#)	0.89 (± 0.22)	yes
Gen 2 50 mM	E3	23.01 (± 5.68)	0.15 (± 0.03)	2.72 (± 0.06)	yes
	E6	15.09 (± 5.62)	0.07 (± 0.03)	2.42 (± 0.38)	yes
Gen 3 50 mM	E3	22.89 (± 4.55)	0.22 (± 0.04)	1.72 (± 0.2)	yes
	E6	2.31 (± 15.9)	0.03 (± 0.11)	1.93 (± 0.55)	yes

** Indicates the value which caused significance (p <0.05) according to the Tukey test output. (#) Indicates average negative value and so was adjusted to zero prior to significance testing.*

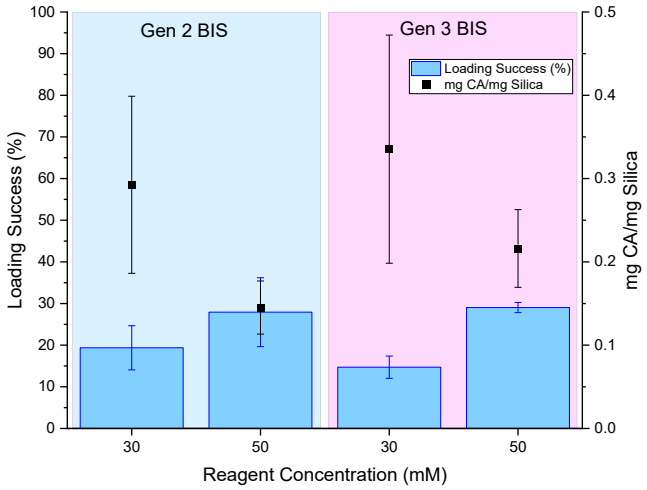

Figure 6. E3 results: loading success in response to reactant concentration for entrapment of CA in Gen 2 and Gen 3 BIS. Error bars represent the standard deviation of experimental samples, where N = 3 and n = 3.

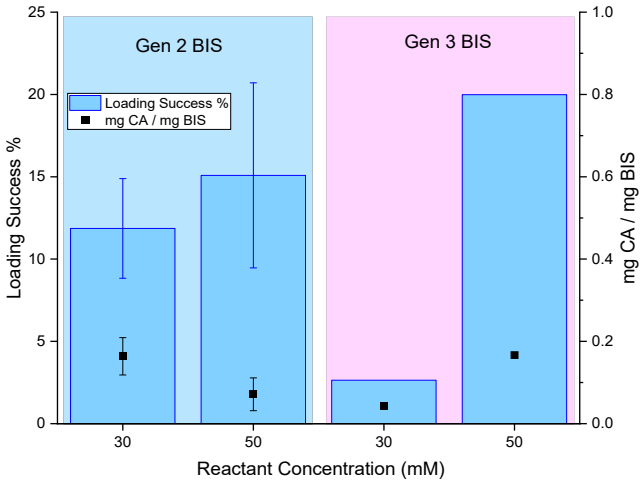

Figure 7. E6 results. Loading success in response to reactant concentration for entrapment of CA in Gen 2 and for a single sample in Gen 3 BIS. Error bars represent the standard deviation of experimental samples, where N = 3 and n = 3.

In contrast to Gen 2 BIS, CA loading onto Gen 3 BIS at 30 mM reactant concentrations decreased significantly between E3 and E6, from ~14 to ~0% ($p \leq 0.005$) (Table 5, Figure 7). This decline was paralleled by a significant reduction ($p \leq 0.005$) in the w/w ratio of CA to BIS, decreasing from 0.34 to ~0 (Table 4, Figure 7). Importantly, BIS formation per mL for Gen 3 did not significantly decrease between these experiments. In reactions conducted without CA, BIS formation remained stable between E3 and E6, ranging from 0.39 to 0.74 mg/mL ($p = 0.79$) (Table 1). The absence of a significant change in BIS formation, both in the CA - containing reactions and in parallel control experiments, indicates that reduced BIS formation per mL does not account for the marked decrease in CA loading.

Instead, consistent with observations for BSA, it is plausible that [redacted] However, the effect of [redacted] appears to differ between BSA and CA. For BSA, [redacted] consistently reduced immobilisation efficiency from 25 - 33% to 4 - 2%. In contrast, the effect on CA was variable between experiments. In E3, [redacted] had no significant impact on CA loading, with reductions in loading percentage remaining within the variability observed across experimental replicates. Conversely, in E6, CA loading decreased from 11 to ~0% in several samples, with a single replicate reporting ~2% loading efficiency, as shown in Figure 7 (without error bars). This variability is also reflected in w/w loading values. Gen 3 BIS produced in E3 achieved an average w/w loading of 0.34 mg CA per mg BIS. This exceeds values of 0.15 - 0.25 mg previously reported for Gen 1[212,246,386] as well as the minimum 0.02 mg enzyme loading for industrial applications[226]. However, this loading did not appear to be reproducible. In E6, w/w loading decreased to ~0 mg CA per mg BIS, indicating substantial variability in loading outcomes under identical reaction conditions (Figure 7; Table 4). E6 findings indicate

a need for further troubleshooting to understand the cause of this variation so that CA loading can be achieved consistently before Gen 3 BIS loading with CA can be utilised in industrial settings.

4.3.2.2 Experimental Variation During 50 mM Reactions

Similarly to the 30 mM reactant concentration outcomes the 50 mM Gen 2 BIS also showed a reduction in loading success (%) and w/w amounts of CA between E3 and 6, which declined from 23 to 15% and from 0.15 to 0.07 mg CA to mg BIS respectively. However, these changes were not statistically significant (p = 0.2) (Table 4) and therefore any variation in w/w loading of CA was less cause for attention for the 50 mM reactant concentrations compared with 30 mM experiments (Table 4).

For Gen 3 there was no statistically significant difference in enzyme binding between E3 and 6 in terms of CA loading success (%) and w/w amounts (p >0.05) (Table 4, Figures 6 and 7). However, this lack of statistical significance may be attributable to the large standard deviations found in E6 for loading success (± 15.9%) and w/w loading (± 0.11). When comparing the actual values between E3 and 6, a mean difference of 20% is seen for loading success (%) and 0.19 in w/w loading. Given that many of the most successful CA reaction frameworks on SBA-15 have w/w loading of 0.3 mg CA/mg support, the variation in w/w loading in these samples is therefore considerable[387]. When these samples are compared to Gen 2 BIS created at 50 mM reactant concentrations, the variation for Gen 2 BIS samples was smaller. This indicates that whilst the process of [redacted] for CA frameworks may not lead to the complete removal of CA as was the case with 30 mM, the amount of CA that is left in the framework can vary significantly between experiments.

4.3.2.3 Experimental Variation and Reaction Concentrations for Gen 2 BIS

Unlike BSA, no significant difference for E3 and 6 was observed between increasing reactant concentrations from 30 to 50 mM and increased CA loading success (%) (Table 5, Figures 6 and 7). This lack of increase in CA immobilisation in accordance with BIS formation resulted in no significant difference in w/w CA loading for E3 and E6 (p >0.05) (Table 5, Figures 6,7). This was despite the yield of BIS in mg per mL significantly increasing in accordance with reactant concentration across both experiments, for E3 (p = 0.00012) and E6 respectively (p = 0.002) (Table 5). This suggests that unlike BSA, CA is unable to take advantage of the increased opportunities for entrapment offered by the greater concentration of particles aggregating in the solution[243].

Table 5. Statistical analyses for reactant-concentration dependent entrapment of CA for Gen 2 BIS. Values with (±) represent standard deviation between experimental replicates.

Exp. Ref.	Reactant Conc.	Loading Success (%)	mg CA/mg BIS	mg BIS/mL	Equal Variance
E3 (22.1.25)	30 mM	19.38 (± 5.29)	0.29 (± 0.1)	1.20 (± 0.09) *	Yes
	50 mM	23.01 (± 5.68)	0.15 (± 0.03)	2.72 (± 0.06) *	Yes
E6 (10.3.25)	30 mM	11.85 (± 3.02)	0.16 (± 0.04)	0.79 (± 0.11) *	Yes
	50 mM	15.08 (± 5.62)	0.07 (± 0.03)	2.42 (± 0.38) *	Yes

** Indicates the value which caused significance ($p < 0.05$) according to the Tukey test output.*

Similarly to Gen 2 BIS, the concentration of Gen 3 BIS per mL of reactant solution significantly increased with increasing reactant concentrations (30 and 50 mM) for each experiment (p = 0.03) (Table 6) but had no significant impact on CA immobilisation. For E3, [redacted] appeared to have no significant impact on CA loading for BIS created at 30 and 50 mM reactant concentrations. However, for E6, [redacted] led to the complete removal of CA for certain experimental replicates at 30 mM concentrations. For 50 mM, all replicates contained some CA within the framework, but it was significantly reduced to ~2%, with a w/w loading of 0.03 mg CA per mg of BIS which is considered to be too small an amount for industrial applications[226]. This variability was similar to what was observed in BSA entrapment.

Table 6. Statistical analyses for reactant-concentration dependent entrapment for Gen 3 BIS. Values with (±) represent standard deviation between experimental replicates.

Exp. Ref.	Reactant Conc.	Loading Success (%)	mg CA/mg BIS	mg BIS/mL	Equal Variance
E3 (22.1.25)	30 mM	14.71 (± 2.67)	0.34 (± 0.13)	0.74 (± 0.23) *	Yes
	50 mM	22.89 (± 4.55)	0.22 (± 0.04)	1.72 (± 0.2) *	Yes
E6 (10.3.25)	30 mM	0 (*)	0 (*)	0.89 (± 0.22) *	Yes
	50 mM	2.31 (± 15.98)	0.03 (± 0.11)	1.92 (± 0.55) *	Yes

** Indicates the value which caused significance according to the Tukey test output. (*) Indicates average negative value and so was adjusted to zero prior to significance testing.*

4.3.2.4 Section Summary

Based on the outcomes described in this section, it appears that protein entrapment in Gen 2 and 3 BIS can lead to different outcomes in terms of loading success (%), w/w loading and BIS formation per mL depending on the type of protein.

In the case of BSA, loading success in Gen 2 BIS was higher compared to CA, remained consistent across trials and increased with increasing reactant concentrations. Another interesting note is that BSA appeared to reduce BIS formation in mg per mL. When it came to post-synthesis treatment to create Gen 3 BIS, elution consistently resulted in a significant removal of BSA from the BIS across experiments.

For CA, the amount of loading for Gen 2 also remained consistent across experiments for both 30 and 50mM reactant concentrations. However, unlike BSA, CA loading success % and w/w loading did not increase with increasing reactant concentrations. Furthermore, the impact of [redacted]appeared to have a far more variable effect on w/w loading and loading success % compared to BSA.

4.3.3 Porosity Results for BIS without CA Immobilisation

Results for Gen 2 and Gen 3 BIS without CA are depicted in Figure 8, along with the porosity values and standard deviations in addition to the known porosity of Syloid 244 as described by Kostelanská *et al*. 2022[388] (Table 7). Figure 8 demonstrates that the use of [redacted] for generating mesoporous Gen 2 and 3 BIS results in porosity within the ideal zone for enzyme adsorption and has comparable porosity to commercially available Syloid 244 in terms of PD and PV (Figure 8). The impact of [redacted] also produced some key differences between Gen 2 and 3 BIS. Gen 2 BIS had significantly lower SA (119.2 $m^2 g^{-1}$) compared to Gen 3 BIS (358 $m^2 g^{-1}$) (Figure 8 and Table 7). This increase is consistent with other outcomes for Gen 1 BIS, [redacted] has been found to significantly increase porosity in Gen 1 BIS created using additives such as PEHA from ~30 $m^2 g^{-1}$ up to 300 $m^2 g^{-1}$ [255].

Table 7. Porosity values for Gen 2 and 3 BIS and Syloid 244 with standard deviations represented in brackets.

Silica Type	SA ($m^2 g^{-1}$)	PD (nm)	PV ($cm^3 g^{-1}$)
Gen 2 30mM	119 (± 21)	25 (± 1.6)	0.82 (± 0.23)
Gen 3 30mM	358 (± 134.7)	15 (± 3.8)	0.73 (± 0.16)
Syloid 244[388]	189	17	0.8

A notable observation is that Gen 2 had significantly less variation in SA (± 21 m^2 g^{-1}) between replicates compared with Gen 3 (± 134 m^2 g^{-1}) (Table 8). There is yet no published information in the literature regarding the variation that can occur following additive removal of BIS using [redacted], so it is difficult to know what variation can be expected. Gen 2 had larger average PDs (25.8 nm) compared to Gen 3 (15.6 nm), but unlike SA both materials showed only small PD variation between replicates (Table 7). Both materials also possessed similar PVs of 0.82 cm^3 g^{-1} and 0.73 cm^3 g^{-1} for Gen 2 and Gen 3 respectively with only small replicate variation (Table 7). These outcomes demonstrate the potential of [redacted] for creating a pre-functionalised mesoporous material. If functionalisation is less of a concern and greater SA is desired, the use of [redacted] also appears to be an effective means of creating further porosity within the material to enhance SA.

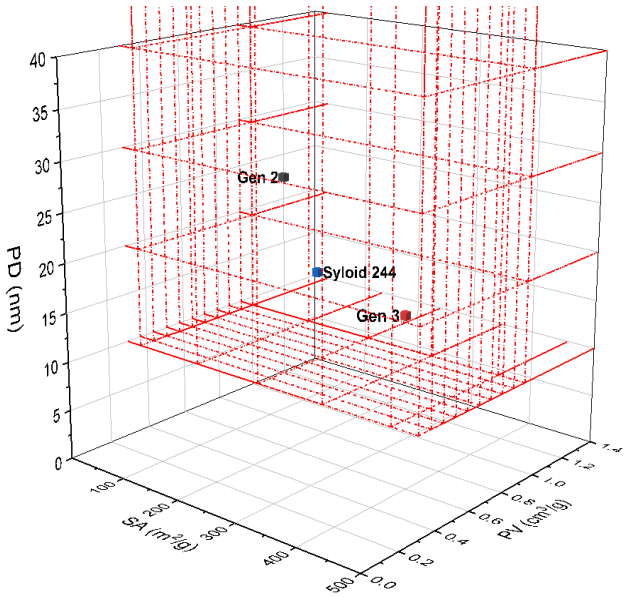

Figure 8. Porosity results for Gen 2 and Gen 3 BIS in the absence of protein taken from N_2 gas adsorption analyses along with the porosity values of Syloid 244 taken from [388].

4.3.4 Porosity Results for CA Entrapped in Gen 2 and 3 BIS

When looking at the porosity for Gen 2 and 3 BIS at 30, 50 and 100 mM reactant concentrations, neither CA immobilisation or reactant concentration appeared to significantly impact PD, PV and SA compared to the control no-protein samples synthesised at 30 mM (Table 8). Most importantly, both Gen 2 and 3 porosities remained in the ideal zone for enzyme immobilisation (Figure 9). However, suitable PVs >0.3 cm^3 g^{-1} and SAs 50 - 500 m^2 g^{-1} for Gen 2 should provide space for greater enzyme interaction with the substrate and reduce internal mass transfer limitations[168]. Enhancement of porosity further via [redacted] to create Gen 3 should lead to even greater operational space and less mass transfer resistance[168].

Table 8. Porosity values for Gen 2 and 3 BIS, with standard deviations represented in brackets.

Silica Type	Reactant Concentration (mM)	SA ($m^2 g^{-1}$)	PD (nm)	PV ($cm^3 g^{-1}$)
Gen 2	**30**	125 (± 65)	25 (± 0.4)	0.76 (± 0.49)
	50	291 (± 83)	20 (± 2)	1.61 (± 0.5)
	100	165 (± 16)	17 (± 2)	0.84 (± 0.06)
Gen 3	**30**	348 (± 198)	18 (± 1)	0.87 (± 0.06)
	50	403 (± 158)	15 (± 3)	0.9 (± 0.38)
	100	484 (± 38)	13 (± 6)	0.78 (± 0.1)

PDs should not be as integral for enzyme entrapment, since it should occur during the aggregation of BIS primary particles without the need for enzymes to enter the matrix via pore entrances. However, CA and BSA have molecular diameters of 5 x 4 and 14 x 4 nm respectively[306,389]. Therefore, PDs of ~22 nm for Gen 2 BIS and ~10 nm for Gen 3 BIS may be large enough in some samples for BSA or CA to leave the framework following entrapment in response to [redacted]. This may explain why variable BSA and CA loading was observed between experiments for Gen 3 BIS, where differences in PD threshold between experiments determined whether CA or BSA exited BIS via PDs during [redacted].

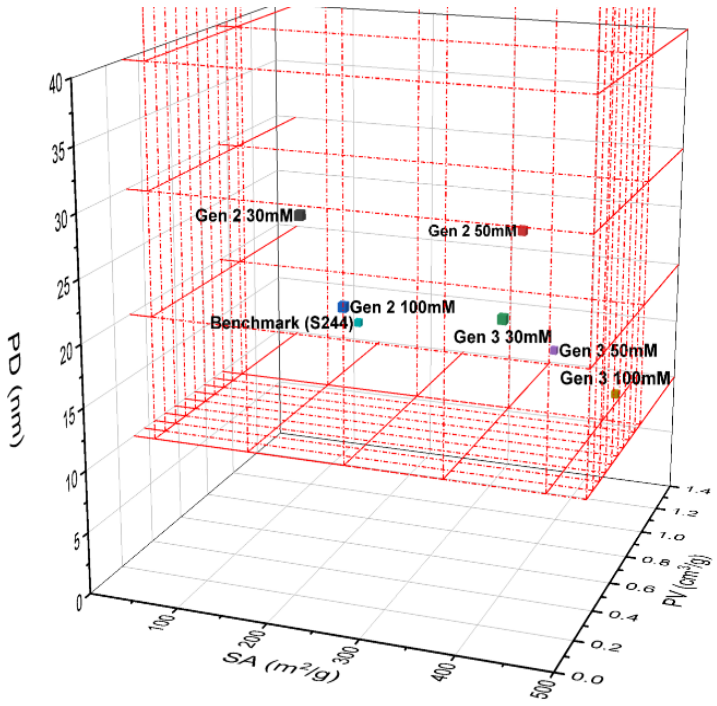

Figure 9. Porosity results for Gen 2 and Gen 3 BIS in the presence of CA taken from N_2 Gas Adsorption analyses along with the porosity values of Syloid 244 taken from Kostelanská et al.*, 2022.*

Whilst optimal porosity appears to have been maintained following CA entrapment, there were where instances greater variations in material porosity were observed compared to the no-protein control. For instance, SA for Gen 2 BIS created at 30 mM had greater variation (± 65 m^2 g^{-1}) compared to Gen 2 BIS which did not contain immobilised CA (± 21 m^2 g^{-1}). This increase in variation may indicate that the presence of CA had some impact on total SA of the material. However, this variation may also be due to experimental variation and given the novelty of this material it is difficult to know which is the case without further material synthesis and rigorous porosity measurements. In a study which explored enzyme immobilisation on Gen 1 BIS using diethylenetriamine as an additive and included analysis of the material containing entrapped enzyme, ~3 m^2 g^{-1} of SA variation between the two BIS materials was observed[212]. However, this material had very low SA and PV by nature and thus using its porosity as a comparison may not be useful for a material like Gen 2 BIS with greater porosity.

When looking at the impact of increasing reactant concentration on Gen 2 BIS porosity, there appeared to be no trend between increasing reactant concentration and increasing SA. Instead, SAs began initially at 125 m^2 g^{-1} for 30 mM reactant concentrations and increase to 291 m^2 g^{-1} at 50 mM and then decreased to 165 m^2 g^{-1} at 100 mM reactant concentrations. This outcome is unexpected since according to the literature, larger SAs have been associated with increased ratios of silica and additives[231]. Gen 3 BIS SAs increased from 348 to 403 to 484 m^2 g^{-1} for 30, 50 and 100 mM reactant concentrations, respectively. However, much larger variations in SA were found within certain concentrations, for instance SA for 30 and 50 mM varied by ~198 and 158 m^2 g^{-1} (Table 9). Predictable material consistency in terms of porosity and particularly SA of a material is essential for a material to be manufactured and applied at scale[390]. Therefore, whilst SA increased with increasing concentrations in accordance with the literature, the high variability obtained between different experiments may be a limitation worth addressing if it is to be applied in industry.

4.3.4.1 Section Summary

Ultimately, the use of [redacted] to synthesise a sustainable alternative to SBA-15 with comparable porosity features was successful. Gen 2 and 3 BIS both have porosity features which fall within the ideal criteria for CA immobilisation; however, they also introduce greater variation in certain porosity measures. Contrary to what was seen with BSA CA entrapment during BIS synthesis did not appear to significantly impact the porosity metrics. It is hoped the creation of these two materials with suitable PVs (>0.3 cm^3 g^{-1}) and SAs (50 - 500 m^2 g^{-1}) could offer a greater CA activity. Any increases to activity using the Gen 2 and 3 BIS may be the result of increases to the internal mass transfer, and greater space within the pores to allow the enzyme to undergo any necessary conformational changes.

Whilst PDs may not be as essential to enzyme entrapment, variations in PDs which surpass molecular dimensions of CA and BSA may permit proteins to escape from the framework during [redacted] to create Gen 3. Further research could explore reducing PD variability and PDs during BIS synthesis for entrapment to below the critical size threshold for protein escape.

In terms of the application of Gen 2 and 3 BIS for CA adsorption, it is hoped the wide PDs will enable CA to have greater access to the extensive inner SA of the BIS particles. In the case of the Gen 3 BIS, the enhanced SA may also lead to a greater total immobilisation of CA, without it being at risk of denaturing during [redacted]. To test these theories the capability of Gen 2 and 3 as an adsorption material will be assessed against commercially available Syloid 244.

4.3.5 Adsorption of CA onto Gen 2, Gen 3 and Syloid 244 Silicas

Results from Figure 10 indicate that the highest immobilisation success (70 - 90%) and w/w loading (~0.1 mg CA/mg silica) of CA was achieved for Syloid 244. The second highest immobilisation success was observed for Gen 3 BIS (33 - 45%), with a w/w loading of ~0.05 mg CA/mg silica. In contrast, CA adsorbed onto Gen 2 BIS exhibited the lowest immobilisation success (1 - 15%) and w/w loading (~0.01 mg CA/mg silica) (Figure 10).

Statistical analysis confirmed that silica type had a highly significant effect on both immobilisation success and w/w loading (p <0.0001) whereas adsorption temperature did not (p = 0.23322). Furthermore, no significant interaction was observed between silica type and adsorption temperature for either response variable, indicating that the effect of material on CA adsorption was independent of temperature across the range investigated. These findings support the observation that temperature exerted minimal influence on enzyme loading performance.

Based on the porosity values shown in Figure 9, it appears that the functionalising presence of [redacted] did not confer any benefit to CA immobilisation. Instead, the significantly greater immobilisation success observed for Gen 3 BIS suggests that [redacted] may have enhanced CA adsorption. Although CA possesses a net negative charge above its isoelectric point (5.4)[382], the protein contains amino acid residues that carry both positive and negative charges[282]. For example, arginine residues are positively charged, whereas glutamic acid residues are negatively charged[282]. Because the distribution and accessibility of these charges were not explicitly controlled for, electrostatic repulsion may have occurred between the functionalising groups on the Gen 2 BIS surface

and charged residues within the CA molecule[282]. This may be one explanation for the reduced binding observed for Gen 2 BIS.

Increased Gen 3 BIS SA may have significantly contributed to enhanced adsorption capacity. Thus, it cannot be conclusively stated that [redacted] directly reduced adsorption; rather, the improved CA loading may be attributable to the greater accessible SA available in Gen 3 BIS. Whilst enhanced porosity may have contributed to differences between BIS materials, porosity alone does not fully explain the observed trends. Syloid 244 did not possess the highest SA nor the largest PD, yet it significantly outperformed both Gen 2 and Gen 3 BIS in terms of CA loading efficiency. This strongly suggests that surface chemistry plays a dominant role in governing CA adsorption behaviour. The statistical confirmation that silica type was the only significant factor further supports the conclusion that intrinsic material properties, rather than adsorption temperature, are the primary determinants of immobilisation performance under the conditions studied.

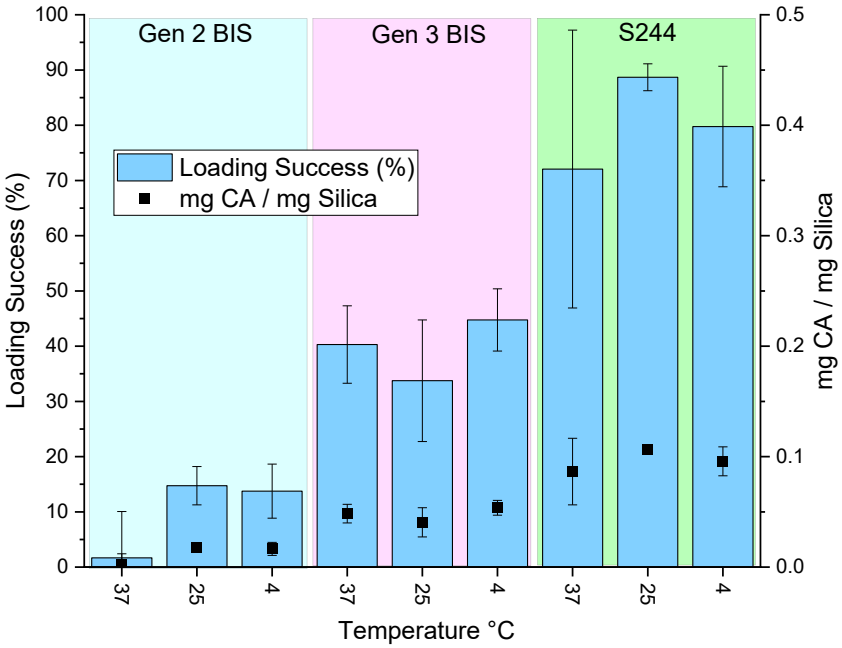

Figure 10. Loading success for temperature dependent CA adsorption onto Gen 2 and 3 BIS and Syloid 244. Error bars represent the standard deviation of experimental samples, where N = 3 and n = 3.

4.3.5.1 Section Summary

The silica materials tested during these adsorption trials demonstrated significant differences in enzyme immobilisation performance: Syloid 244 achieved the highest success, followed by Gen 3 then 2 BIS. Temperature had no significant impact on CA loading, regardless of the framework. Contrary to the research hypothesis, Gen 2 functionalisation with [redacted]

[redacted] did not lead to increased loading success (%) or w/w loading. Instead, Gen 3 exhibited superior loading over Gen 2 BIS, suggesting that functionalisation with [redacted] may have potentially negatively impacted CA binding, although increased SA for Gen 3 BIS complicates this interpretation. The exceptional performance of Syloid 244, despite not having optimal porosity parameters, indicates other factors beyond ideal porosity are also important to consider for successful CA immobilisation.

4.3.6 CA Activity Testing

4.3.6.1 Testing Entrapped CA Activity via the Rate of P-NPA Hydrolysis to P-NP

Figures 11 and 12 depict the catalytic activity of CA immobilised for each successive entrapment experiment under various reagent concentrations. To assess experimental variation in CA p-NPA hydrolysis, standard deviations from 15 free CA experiments were analysed. The results showed no significant differences between experiments. Therefore, any variation within the range of the error bars for free CA (Figure 11) was considered not statistically significant.

Surprisingly while free CA exhibited activity for hydrolysis of p-NPA, entrapped CA within both Gen 2 and 3 BIS exhibited no detectable hydrolytic activity (~0 mM / sec) (Figure 11). The lack of any detectable hydrolytic activity was predicted to be the result of storing samples at 4°C until testing. Following these results, it was decided that following desiccation, samples should instead be stored in a freezer at -20°C.

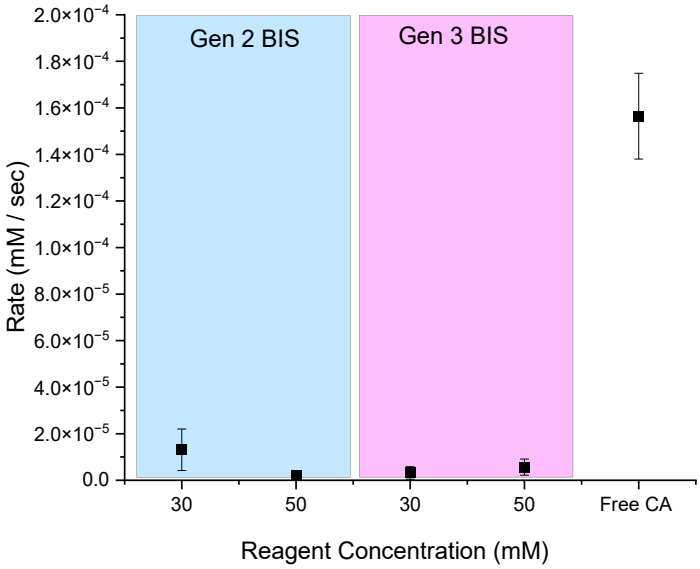

Figure 11. Entrapped CA activity for Gen 2 and Gen 3 BIS for E3. Error bars represent the standard deviation of experimental samples, where N = 3 and n = 3.

E6 demonstrated significantly improved activity relative to the E3 experiment (Figure 12). Most notably, Gen 3 BIS created at 30 mM displayed activity which was equivalent to that of free CA and even exceeded the free CA activity of other studies for that substrate concentration[212]. However, due to the total removal of CA following [redacted]for two replicates, the activity of only one sample for this silica type was able to be tested. This was also the case for the Gen 3 50 mM concentration. It is difficult to know if this outcome is representative of the material, but if it is it suggests that the additional porosity created from the [redacted] led to an improvement in CA activity (Figure 12). The 30 and 50 mM reactant concentration Gen 2 BIS, also still had significantly higher activity at that substrate concentration relative to free CA from other experiments[212]. As expected, the no-protein BIS controls produced no detectable p-NPA hydrolysis indicating that the rate of p-NPA degradation to p-NP was attributable to CA alone (Figure 12).

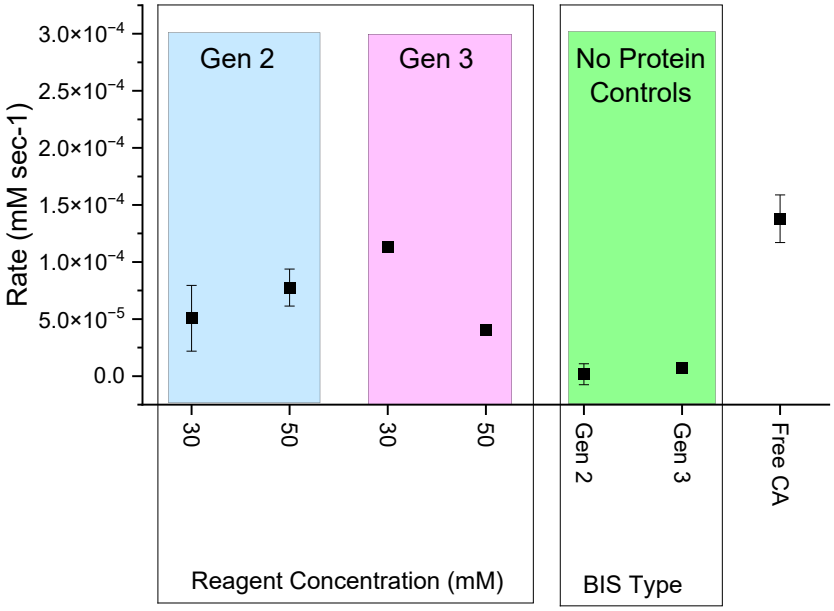

Figure 12. Entrapped CA activity for Gen 2 and Gen 3 BIS from E6. Error bars represent the standard deviation of experimental samples, where N = 3 and n = 3 except for Gen 3 where N = 1 and n = 3.

4.3.6.2 Testing Adsorbed CA Activity via the Rate of P-NPA Hydrolysis to P-NP

In the case of adsorbed samples, none of the rates for p-NPA hydrolysis were comparable to that of free CA, while interestingly there was very little variation in activity seen between replicates regardless of the BIS framework (Figure 13). A potential explanation for the low variability could be that all three materials possessed frameworks with PDs and PVs which enabled good mass transfer of substrates and products to and from CA[168]. This could give rise to similar rates of enzyme activity, regardless of mg CA/mg BIS loading for each framework. Furthermore, adsorption temperature appeared to have no bearing on the subsequent rate of enzyme activity. (Figure 14).

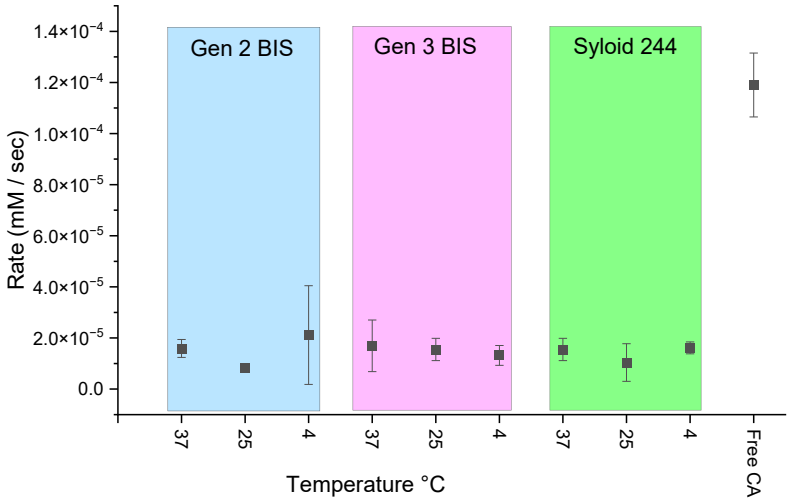

Figure 13. Adsorbed CA activity for Gen 2 and Gen 3 BIS and Syloid 244 samples. Error bars represent the standard deviation of experimental samples, where N = 3 and n = 3.

4.3.7 Comparing BIS / CA Frameworks to the Literature

When considering the w/w loading of CA adsorbed onto Syloid 244, Gen 2 or Gen 3 BIS or entrapped in Gen 2 and 3 BIS from E6 against the w/w loading for the most successful CA frameworks; it can be seen from Figure 14B that none of the frameworks had comparable w/w loading in terms of mg CA/mg of support. The SBA-15 frameworks therefore still appear to be the best frameworks in terms of w/w loading of CA (Figure 14B).

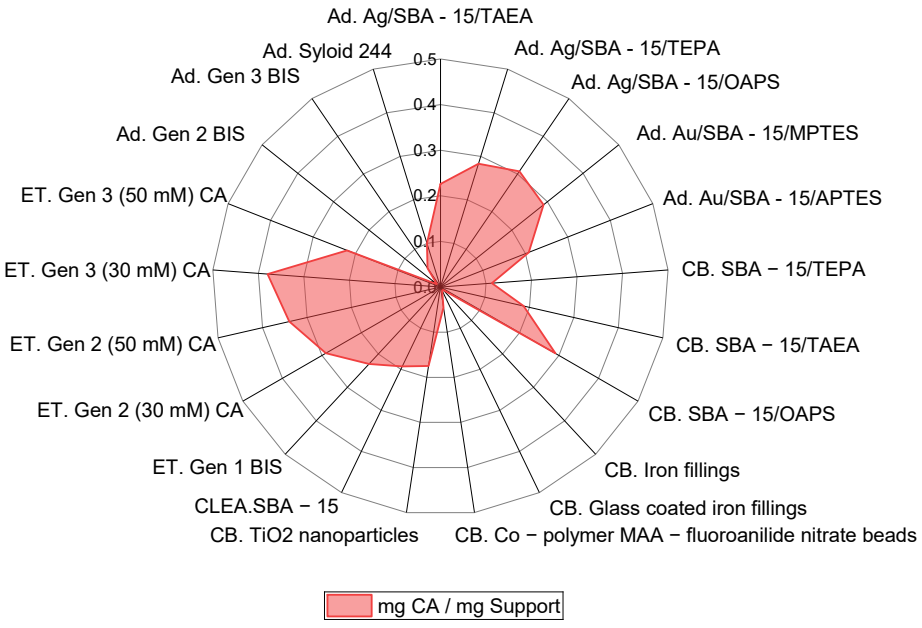

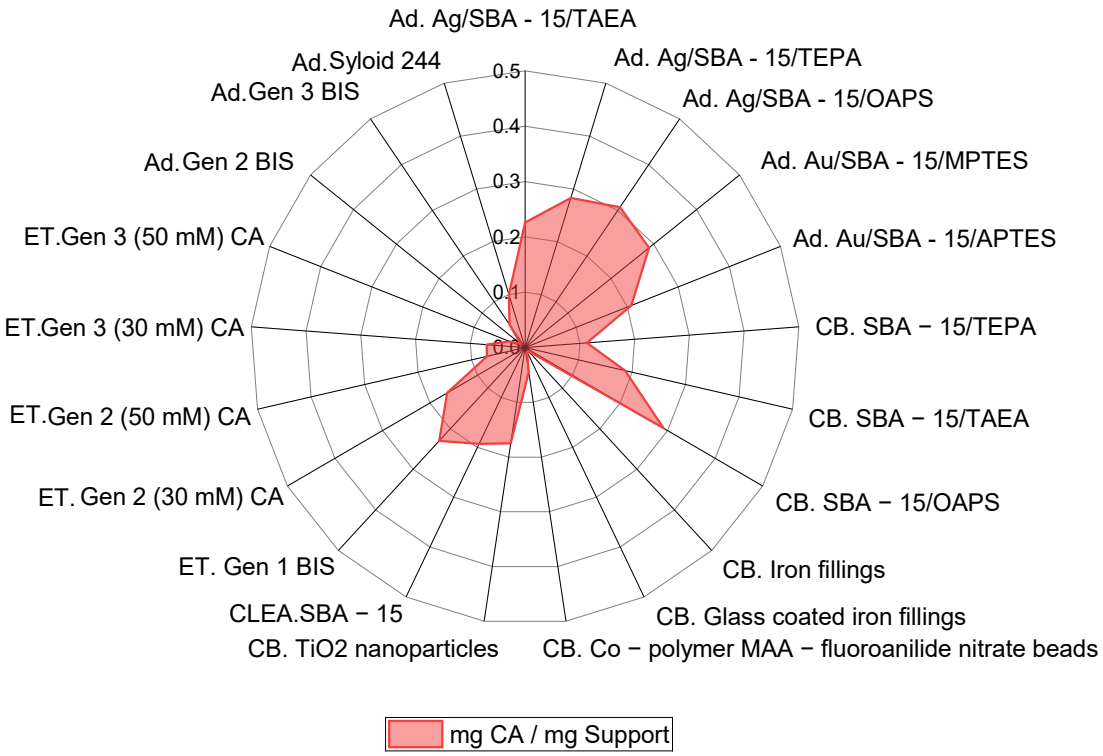

Figure 14. A) A comparison of the w/w loading of CA (mg) to support (mg) for E3 samples and B) E6 samples within this chapter alongside the most successful immobilised CA studies identified by [219].

However, it should be noted that these values were taken from E6, which had lower CA loading success compared to E3. When the w/w immobilisation is considered for entrapment values for E3, w/w loading of CA onto Gen 3 BIS (30 mM) and Gen 2 BIS (50 mM) surpasses the w/w loading of CA on the most successful SBA-15 studies (Figure 14A). This indicates that if immobilisation can be increased in E6 samples by 5 - 10% and the correct drying and preservation technique is applied, a sustainable CA BIS framework with w /w loading which is competitive with SBA-15 may be possible.

The highest performing (95 - 99%) materials depicted in Figure 15 are covalently bonded SBA-15 / TAEA, SBA–15/OAPS, iron filings, glass-coated filings, co-polymer beads, TiO_2 nanoparticles, and CLEA / SBA-15 (Figure 15). These systems have established a high-performance benchmark for immobilisation strategies. In comparison, entrapped CA within Gen 2 and 3 BIS achieved activity efficiencies between 30 - 80%. CA adsorbed onto Syloid 244, Gen 2 and Gen 3 BIS had lower activity efficiencies of ~8% (Figure 15). All values from materials generated in this Chapter therefore fall below values reported in the wider literature.

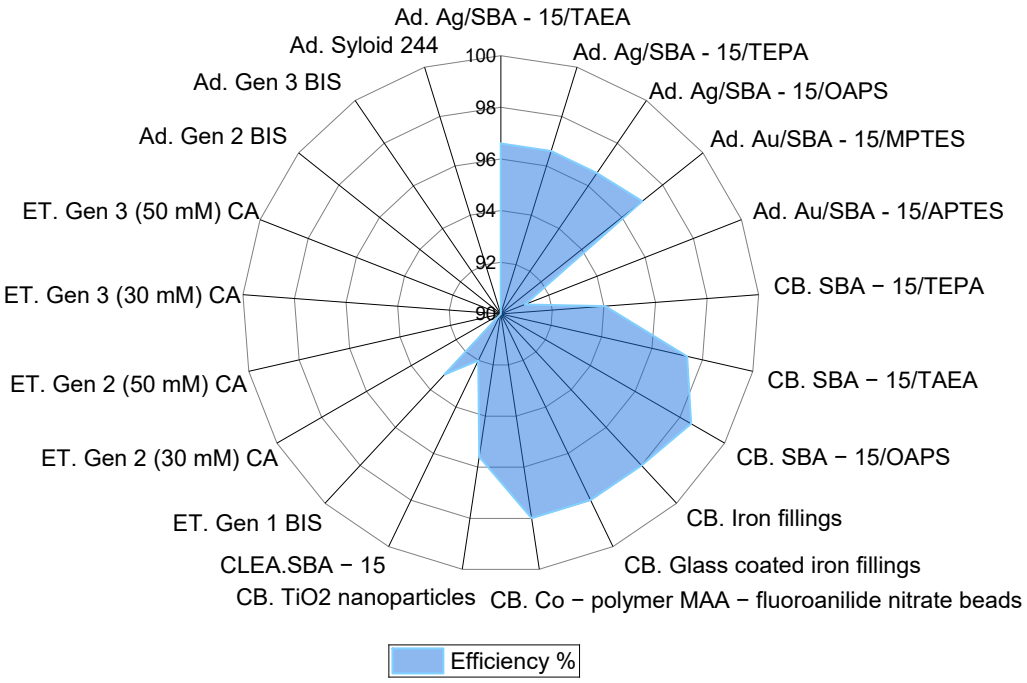

Figure 15: the activity efficiency of CA for (E6) samples within this chapter and the most successful immobilised CA studies identified by [219].

4.3.7.1 CA Loading vs. CA Activity

As evidenced by Figure 14 and 15, covalently bonded and CLEA systems (specifically, SBA-15 / TAEA, SBA–15/OAPS, iron filings, glass-coated filings, co-polymer beads, TiO_2 nanoparticles, and SBA-15 crosslinked enzyme aggregates) consistently demonstrated near-complete activity retention (95–99%) across a broad loading range (0.0085–0.291 mg CA per mg support). This indicates that surface immobilisation in these systems preserved native enzyme conformation and maintained substrate accessibility, without enzyme crowding or diffusion limitations[168,260].

Amongst the entrapment (ET) systems, Gen 1 BIS achieves a strong balance between w/w loading (0.23 mg CA/mg BIS) and activity efficiency (93.2%) and came close to the activity efficiency of covalently bonded systems. This suggests that its internal architecture effectively supports enzyme confinement without significantly restricting catalytic function. Gen 1 BIS for this study was reported to have a SA of 17 m^2 g^{-1}[276]. A value as low as this indicates little to no internal SA and is non-porous. Therefore, it could be that CA was entrapped in pores on

the outer surface of the BIS particle and benefitted from higher substrate access and greater diffusional freedom for substrate and product molecules[168].

In contrast, whilst Gen 2 BIS showed enzyme loading comparable to the highest performing systems for both experiments E3 and E6 (0.07 - 0.29), E6 samples indicated poor activity efficiency (36.7 - 56.3%). Since enzymes are entrapped, its structure should have been preserved. This leaves reasons such as limited substrate accessibility, enzyme crowding or diffusion limitations for its reduced performance[168,260] and thus suggests that achieving material porosity within the ranges defined by Bayne *et al.* did not incur a benefit to enzyme activity[168].

The Gen 3 tested from E6 demonstrated one of the lowest w/w loading capacities (0.0 – 0.03 mg CA/mg BIS), despite such low loading the samples which did contain CA demonstrated relatively strong activity retention (81.8%). This may be due to the increased porosity observed for Gen 3 BIS which occurred because of the [redacted] Enhanced porosity may have increased substrate accessibility and reduced diffusional constraints and enzyme crowding effects within the framework, resulting in greater CA activity[168,260]. This suggests that in the case of CA entrapment within BIS, greater porosity than that defined by Bayne *et al*. might be required for CA enzyme activity[168]. However, these conclusions were drawn from a reduced sample set since not all experimental replicates contained CA, so further testing would be required to strengthen this conclusion.

Despite varying success in w/w CA loading (0.01 - 0.1), adsorption onto Gen 2 or 3 BIS or Syloid 244 exhibited uniformly low activity efficiency (~8%), indicating a substantial disruption to CA activity across all supports. Since CA w/w loading onto silica supports varied so greatly between types, it is unlikely that the cause in uniform reduction was due to enzyme overcrowding, differences in support SA, PV or PD or the presence of additives and SFGs within the framework. The uniformity of CA activity loss may indicate that the cause is due to a shared trait between all three BIS types and that physical adsorption alone is insufficient to preserve enzymatic function.

4.3.8 Sequestration Potential of Free, Adsorbed and Entrapped CA

4.3.8.1 Entrapped CA

To determine the CO_2 sequestration activity of entrapped CA, the CA catalysis of CO_2 conversion to HCO_3^- was tested. Following the catalysis to HCO_3^- deprotonation of HCO_3^- occurs to form CO_3^- under higher pHs, which can then react with Ca^{2+} to form $CaCO_3$[182]. In this way, $CaCO_3$ can act as a proxy measurement for CA activity. CO_2 sequestration analyses for

entrapped samples were performed using samples from E6. Results from Gen 2 and 3 created at 30 and 50 mM reactant concentrations were evaluated to determine whether an effect on CA activity could be seen between the different materials. In the case of Gen 2 BIS, the difference in w/w loading of mg CA/mg BIS may incur a difference in activity due to more available space within the framework for CA to operate and reduced mass transfer resistance[168,306]. Observing Gen 3 activity would allow the observation of CA [redacted] which should enhance framework porosity and increase these beneficial factors further[168,255,306].

Results from Figure 16 show that Gen 2 and 3 BIS from both 30 and 50 mM reactant concentrations did not appear to be different for either elevated CO_2 sequestration activity (mg CO_2 sequestered) and % yield of CO_2 relative to the no-protein controls. However, it is important to note that only a single replicate was available in the case of the Gen 3 materials meaning the outcome may not be representative.

Ultimately, none of the activities from the entrapped samples were equivalent to the CO_2 sequestration or % yield of free CA, which was significantly higher than all other samples (Figure 16). In the case of % yield, free CA sequestered >110% of CO_2 present in the solution. This surplus in CO_2 yield gives some indication of the potential error associated with this analysis (Figure 16). In the case of Gen 2 30 and 50 mM concentrations, certain replicates reached values of 80 - 90%, which is close (~10%) to that of the free enzyme. However, when considered in terms of activity efficiency and compared to other studies in Figure 15, the activity of CA on Gen 2 and Gen 3 at 30 mM is ~66%, which is far lower than the best performing frameworks and within the same value region as no protein controls. It should be noted however that in the case of Gen 3 this experiment was only performed once due to limited material.

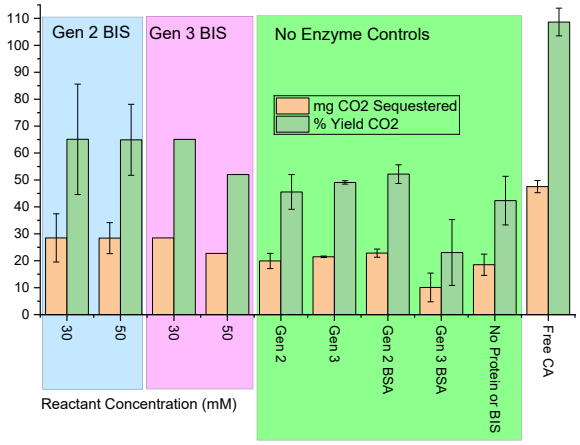

Figure 16. Entrapped CA activity towards CO_2 sequestration for Gen 2 and Gen 3 BIS from the final experiment. Error bars represent the standard deviation of experimental samples, where N = 3 and n = 3.

4.3.8.2 Adsorbed CA

Due to time constraints and informed by a lack of difference in immobilisation and p-NPA hydrolysis activity, the decision was made to assess CO_2 sequestration at a single temperature (25 °C) range for adsorbed samples (Figure 17). The values and error variation for the free CA enzyme in terms of mg CO_2 sequestered and % yield of CO_2 was significantly higher than the rest of the values, except for Syloid 244 which had sample variation within the same value range as the free enzyme. However, the sample variation observed for Syloid 244 was large, indicating that this similarity may not be statistically meaningful. When compared to Gen 2 and 3 BIS, Syloid 244 had significantly better activity in terms of mg CO_2 sequestered and % yield of CO_2 for CA activity. The reason as to why this might be is unclear, Syloid 244 did not have distinctly different PDs, SA, and PVs to Gen 2 and 3 BIS. However, it was observed that Syloid 244 dispersed well during in the reaction solution, potentially due to its low density and hydrophilic nature[391]. This may have allowed the immobilised CA more opportunities to interact with the CO_2 substrate and convert it to HCO_3^-.

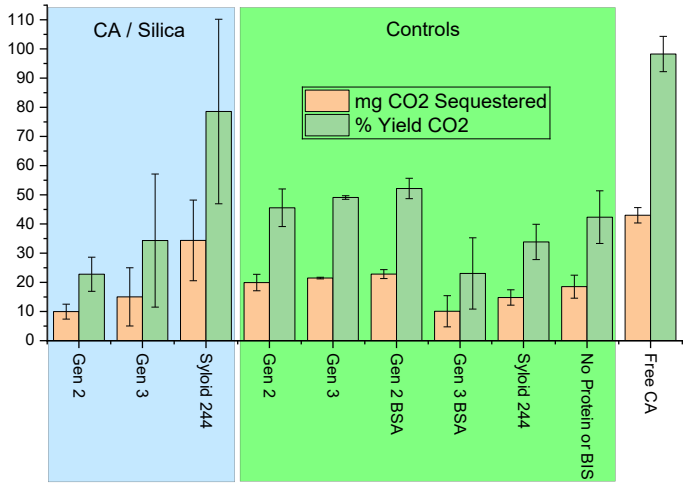

Figure 17. Adsorbed CA activity towards CO_2 sequestration for Gen 2 and Gen 3 BIS from the final experiment. Error bars represent the standard deviation of experimental samples, where N = 3 and n = 3.

4.3.9 Section Summary

Statistical analyses of free CA showed no significant differences in experimental variation after 15 runs. Therefore, any variation between replicates within the range of the error bars produced was considered to not be significant. Ultimately, all activity analysis produced no variation beyond that expected from experimental variation (p <0.05).

In the case of Gen 2 and 3 BIS entrapped CA systems tested from E3, Gen 2 and 3 BIS exhibited no detectable hydrolytic activity (~0 mM / sec). Based on these outcomes, adjustments were made to the storage protocol for samples.

E6 demonstrated significantly improved activity, indicating that improving the sample storage protocol had a significant effect on CA activity within the Gen 2 and 3 BIS systems. The most notable outcome was Gen 3 BIS created at 30 mM, which had an activity efficiency of ~81% and surpassed the activity in terms of rate of conversion (V_0) of p-NPA to p-NP of free CA analyses conducted for other studies. However, this analysis could only be performed for a single replicate and so this limits the inferences which can be drawn from this conclusion. Meanwhile, adsorbed samples consistently produced low V_0 for conversion of p-NPA to p-NP, with absorption temperature and silica type having no significant impact on V_0.

When the systems created for this chapter were compared to the most successful studies in the literature, Gen 2 BIS exhibited competitive w/w loading across E3 and E6 experiments. However, this was not the case for activity efficiency which was far below the most successful studies to date. Gen 3 BIS w/w CA loading did not compare to leading studies but activity in samples which were able to be tested was far higher than Gen 2 and closer to the best performing studies. By comparison, adsorbed CA onto Gen 2, Gen 3 and Syloid 244 exhibited widely varying success in terms of w/w loading that was within the ranges of some of the best performing frameworks. But CA activity efficiency was far below the best performing frameworks and did not appear to vary, suggesting that there was a uniform cause for such low activity across all frameworks.

The ability of CA to increase the hydration of CO_2 into solution was also tested via formation of calcium carbonate using E6 samples. Ultimately, none of the activities from the entrapped samples were equivalent to the CO_2 sequestration or % yield of free CA. Activity efficiency values were lower than the best performing frameworks and equivalent to no protein controls. However, in the case of Gen 3 only single experimental replicates were able to be tested due to limited replicates and sample volume. When adsorbed CA samples were tested for CA activity, Syloid 244 displayed results with sample variation which was within the same region as that of free CA, a potential explanation for this might be its enhanced dispersal in the reaction solution compared to Gen 2 and 3 BIS.

In addition to CA performance, it is important to consider enzyme retention during reaction, to ensure CA is not lost from the framework during the reaction.

4.3.10 Leaching Analysis

The risk of CA leaching from the framework of Gen 2 and 3 BIS has not yet been explored and so the effectiveness of BIS for retaining enzymes is not yet known. Considering this, the enhanced porosity of Gen 2, Gen 3 and Syloid 244 frameworks may present a particular risk of leaching for adsorbed samples. Whilst larger PVs and PDs may allow enzymes to enter the framework of the support material; there is equally a risk of them easily leaving again if only

weak associations are holding the enzymes on the support which can then be overcome by pH, ionic strength or temperature changes in the surrounding environment[254]. In the case of entrapment, low leaching has consistently been reported on Gen 1 BIS frameworks using various additives[212,246–248]. However, in many of these cases enzymes were entrapped between particles which were more tightly clustered (PV <0.1 cm^3 g^{-1}), giving rise to the low SAs (<25 m^2 g^{-1})[212,246]. This tight clustering may hold enzymes within the framework more effectively compared with a more mesoporous framework, with a larger SA open to greater mass transfer of molecules passing through and larger PDs for CA to potentially exit from[168]. Therefore, a test to quantify the potential effect of leaching seems worthwhile

Adsorbed CA materials demonstrated the least amount of leaching over a 24-hour period, with no significant loss of CA from Syloid 244, Gen 2 or Gen 3 samples (Figure 17). This is the first outcome for leaching of adsorbed enzyme on Gen 2 BIS and it is encouraging, since it was anticipated that a more mesoporous framework with PDs >10 nm may give rise to greater opportunities for a dissociated enzyme to leach away. Instead, it appears that the adsorption which occurred between the functionalising molecules within Gen 2 BIS or its surface and the surface of Gen 3 BIS or Syloid 244 was secure enough to resist enzyme dissociation[282]. This result contrasts with findings from leaching analyses of SBA-15, which found that enzymes leach from the framework when immobilised directly on the surface[392]. To overcome this issue for CA, studies which achieved high w/w loading and low leaching have instead employed various gold and silver nanoparticles on the surface of SBA-15 in addition to functionalising amines to ensure secure CA adsorption[228,387]. When it comes to applying adsorbed enzymes at scale, industries are drawn to simple, straightforward methods of enzyme immobilisation[158]. Therefore, an option for high CA loading success on Syloid 244 without modification may be a useful option for researchers.

In contrast to adsorbed samples, significant leaching did occur for CA samples with the highest loss occurring in Gen 2 (50 mM), which lost ~30 - 70% of entrapped CA from its framework over a 24 hour period (Figure 17). This was followed by Gen 3 (50 mM) and Gen 2 (30 mM), which lost ~40% and 20% of total entrapped CA (Figure 17). In comparison to BIS enzyme literature, which has reported negligible enzyme leaching[212,246–248], this loss of enzyme from the framework represents a significant deviation from previous findings. A key difference between this study and previous studies is the difference in porosity, which will have greater mass transfer of molecules running through and wider PDs for enzymes to exit from. This may explain the difference seen between this result and previous study results. An alternative explanation is that prior to the analysis entrapped BIS samples were crushed and passed through a sieve. This was with the aim of breaking up the silica pellet to standardise the

adsorption and entrapment materials. It may be that this crushing led to the shearing of CA from within the BIS into the analysis solution.

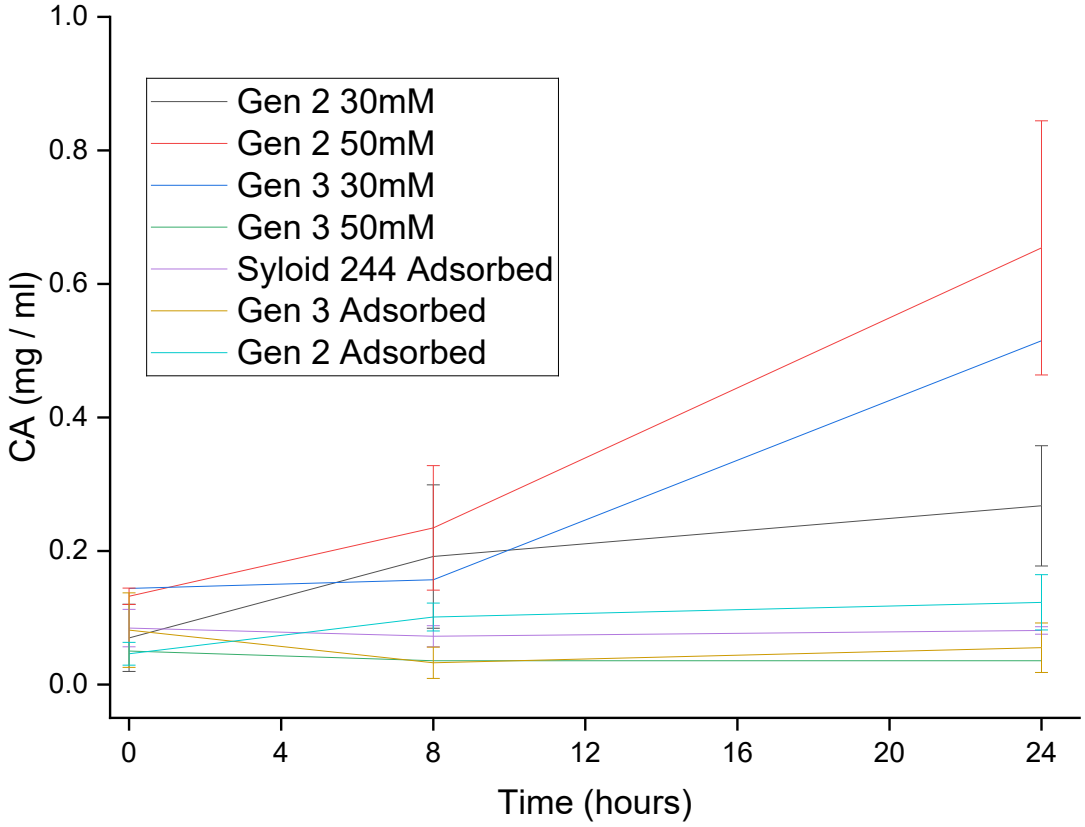

Figure 17. Leaching analysis for 1 mg CA/mg framework per mL of PBS for CA from entrapped and adsorbed samples across a 24-hour period. Error bars represent the standard deviation of experimental samples, where N = 3 and n = 3.

4.3.11 Exploring Increasing Protein Immobilisation onto BIS

As part of their research into enzyme entrapment within BIS, two studies have previously conducted optimisation analyses to determine what was the optimal concentration of protein in the solution to facilitate maximum enzyme entrapment. The first study investigated lipase immobilisation and found that a final mg/mL concentration of 2.5 achieved ~100% immobilisation efficiency for a range of different additives[246]. In this case, immobilisation efficiency was referred to as:

$$immobilisation\ efficiency = \frac{mg\ protein\ immobilised}{total\ mg\ of\ protein\ added}\ x\ 100$$

For the purposes of this report, enzyme immobilisation efficiency has instead been referred to as loading success % to avoid confusion between terminology. Interestingly, the authors concluded that in relation to these Gen 1 BIS materials, there appeared to be a w/w loading limit of 0.25 mg per mg of BIS support[246]. In a second report which investigated CA

immobilisation onto BIS formed using diethylenetriamine as the additive, a different mass of 2 mg/mL in the reaction solution was cited to achieve ~100% immobilisation efficiency[212]. Similarly, the author reported ~100% protein loading with a w/w protein concentration of 0.23 mg/mg BIS[212]. These reports have provided some detail regarding the maximum amount of protein that can be added to a solution for 100% immobilisation efficiency[212,246]. However, these protein amounts were used alongside additives to create BIS with low SAs <50 m^2 g^{-1} and PVs <0.1 cm^3 g^{-1} [212,246]. Larger SA, PDs and PVs have been linked to increased amounts of enzyme immobilisation[168]. Therefore, the advent of Gen 2 silica with a larger SA (119 m^2 g^{-1}), PD (25 nm) and PV (0.82 cm^3 g^{-1}) of mesoporous framework with larger SA and PVs could lead to increased opportunities for enzyme entrapment during BIS synthesis. Therefore, a new exploration into the effect of increasing protein on mesoporous Gen 2 BIS seemed worthwhile. This investigation uses BSA as a model protein with the aim of applying the principles of enzyme immobilization to enzymes like CA.

In addition to the effect of BSA concentration, there also appears to be some differences in approach with regards to the pH point at which the BSA should be added during silica formation. Some studies have recommended circumneutral conditions (pH ~7)[276,381], whereas others have recommended adding the protein directly after the reaction has been initiated (pH ~10)[386].

In the case of Gen 2 BIS specifically, addition of the protein [redacted] at the earliest possible moment that [redacted] begin to aggregate together[231]. Therefore, there may be the greatest opportunity for BSA to become entrapped during BIS synthesis, leading to a potential increase in loading. However, applying this protocol to enzymes such as CA may lead to denaturation due their exposure beyond optimal pH (>7.5). Since Gen 2 BIS synthesis is a novel method, it is also not known whether earlier addition of protein in a Gen 2 system will in fact lead to greater amounts of enzyme immobilisation. It is also not known whether the potential loss of enzyme activity will be worth any additional enzyme loading achieved from higher pH addition.

Therefore, in addition to investigating the impact of protein concentration, it was determined that the impact of the pH at which BSA is added would also be investigated. If BSA does significantly increase from addition at a high pH, it would be helpful to anticipate what effect this might have on CA activity. Therefore, exposure of CA to increasing pH concentrations would also be performed to determine what effect exposure to non-optimal pH will have on CA activity and whether addition at a higher pH would be worth a reduction in CA activity.

4.3.11.1 Influence of Exposure to pH 7 to 10 on CA Activity

To gauge the impact of exposure of CA to non-optimal alkali conditions, an analysis was carried out in which CA was exposed for 1 minute to various pH concentrations between 7 to 10. It can be seen from Figure 18 that a reduction in CA activity was seen at pHs ≥9, with a reduction of ~1.25 x 10^{-5} p-NP activity following exposure at both pH 10 and 11 for 1 minute.

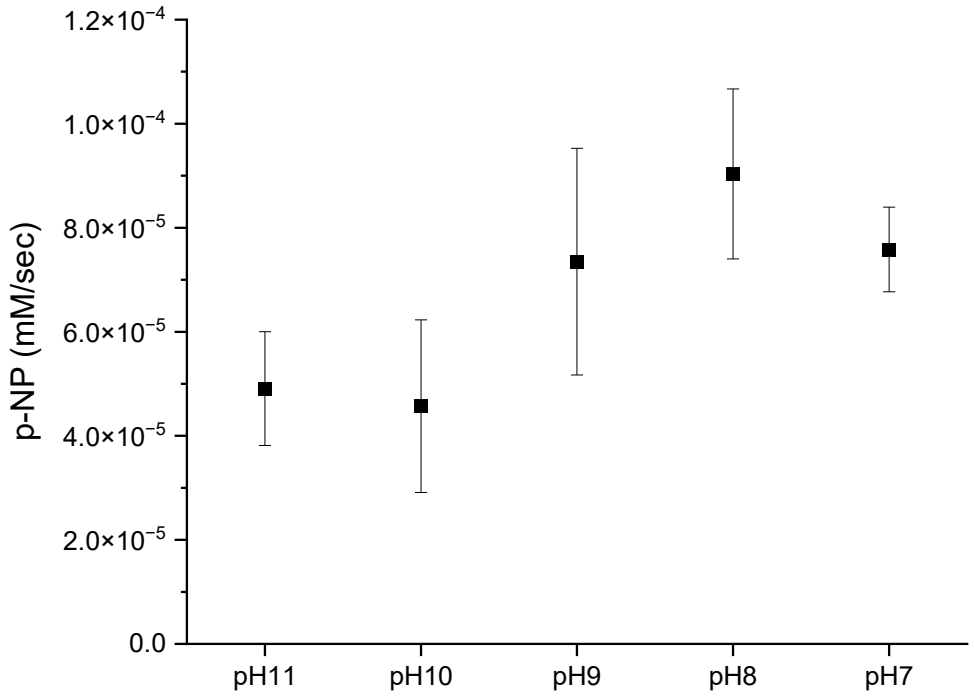

Figure 18. Influence of pH exposure for one minute using 2000 U / mg free CA. Error bars represent the standard deviation of experimental samples, where N = 3 and n = 3.

4.3.11.2 Influence of Protein Concentration and pH Addition Point on BSA Immobilisation

Results from Figure 19 indicate that for a BSA concentration of 2 mg/mL in the reaction fluid, pH of BSA addition had a small effect on immobilisation, with an immobilisation success of 35% compared to 20 - 30% success for lower pH addition points Figure 18. This culminated however in no significant difference in the mg BSA immobilised per mg of BIS across the different pH points Figure 19. For Gen 3, the impact of [redacted]appeared to completely remove any entrapped BSA from the framework, resulting in an immobilisation success % and w/w amount of BSA to BIS of ~0, regardless of pH addition time.

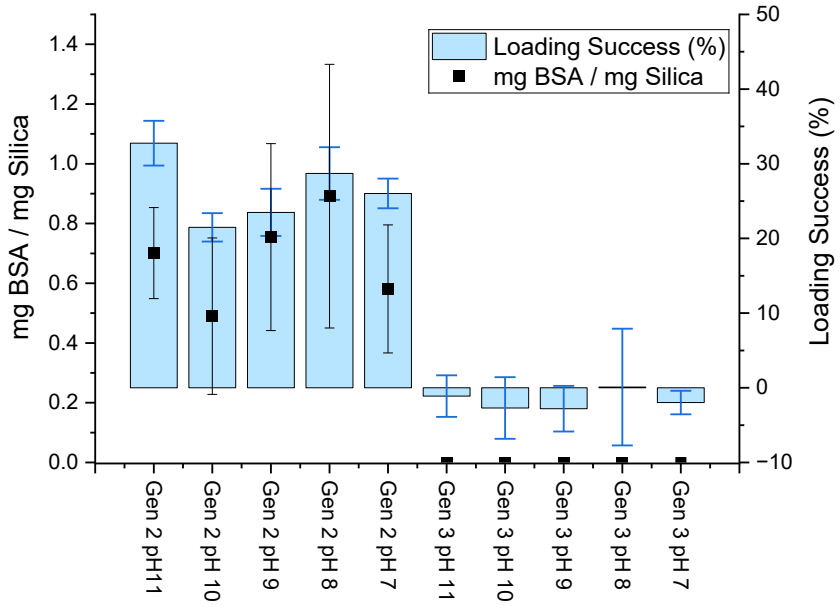

Figure 19. Influence of pH on 2 mg per mL BSA loading success and w/w for Gen 2 and 3 BIS. Error bars represent the standard deviation of experimental samples, where N = 3 and n = 3.

In contrast to Figure 19, Figure 20 shows a clear pH dependence for BSA immobilisation following a 20% increase in BSA final concentration (2.4 mg/mL). This is particularly prevalent for Gen 2 BIS, which has a loading success rate between 55 – 95%, corresponding with increasing for pH values from 7 – 11 (Figure 20). Whilst there appeared to be very little difference in loading success between pH 9 and pH 10, both of which had loading success scores of ~65%, a significant step up in loading then occurred at pH 11 (Figure 20). This suggests that adding the protein prior to the reaction initiation may be the most effective means of immobilisation. However, addition of CA at pH 11 would incur a cost to activity as demonstrated in Figure 18. Despite the high loading success for Gen 2, the actual BSA to BIS ratio was non-detectable across all Gen 2 samples (Figure 20). This was due to the amount of immobilised BSA surpassing the total yield of BIS, resulting in a negative value which is discussed further at the end of this section.

Gen 3 showed a consistently lower loading success (10 - 15%) compared with Gen 2 BIS. However, all samples returned far higher BSA to silica ratios compared to Gen 2, particularly pH 11, which had an immobilisation ratio of 3.0 (Figure 20). This implies that while the loading success may be lower, overall binding capacity was higher. Particularly at pH 11, though no difference in BSA to BIS ratio occurred at lower pH values (Figure 20). Furthermore, the error bars for Gen 3 measurements at pH 9 and 7 indicate considerable variability between experimental replicates at each pH (Figure 20).

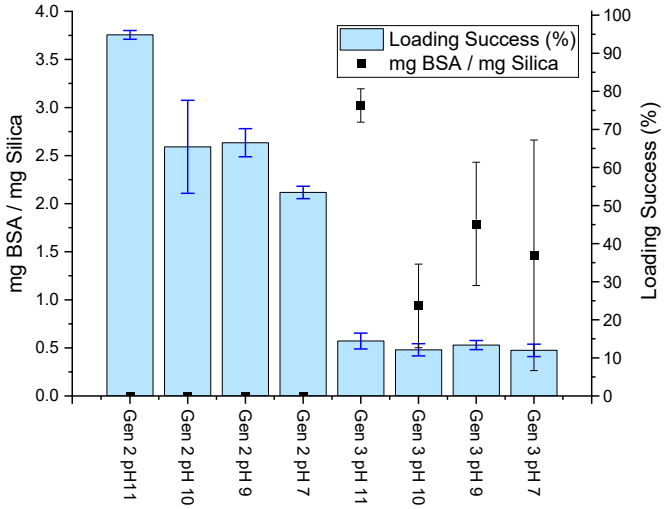

Figure 20. Influence of pH on 2.4 mg per mL BSA loading success and w/w for Gen 2 and 3 BIS. Error bars represent the standard deviation of experimental samples, where N = 3 and n = 3.

Figure 21 depicts the pH - dependent immobilisation of BSA onto Gen 2 and Gen 3 at final concentrations of 4 mg/mL in the reaction solution. Compared with 2.4 mg/mL, loading success for Gen 2 BIS was significantly lower across all pH additions (Figures 20 and 21). Whereas in Figure 20, loading success was more distinct and ranged from 95 - 55% for pH 11 down to 7 accordingly. BSA loading on Gen 2 BIS also appears to reduce more gradually from 35 - 25% between pH 11 to 7 (Figure 21). Gen 3 BIS continues this gradual reduction in immobilisation success, with a maximum value of ~30% leading down to ~15% at pH 7 (Figure 21). Whilst some immobilisation success occurred, this was not reflected in the w/w amounts of BSA to BIS, which consistently remained at zero (Figure 21).

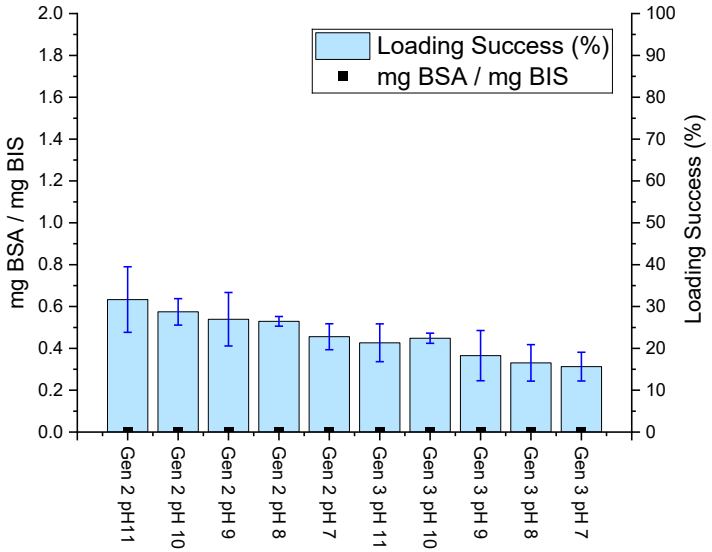

Figure 21. Influence of pH on 4 mg per mL BSA loading success and w/w for Gen 2 and 3 BIS. Error bars represent the standard deviation of experimental samples, where N = 3 and n = 3.

Based on the inconsistent or absent results for w/w amounts of BSA to BIS across experiments, another analysis was performed to visually inspect the BIS material following immobilisation. What was noticed upon inspection was that two different layers of material were forming inside the falcon tube following centrifugation (Figure 22). The first was a BIS-like material and the second which lay above was a gel-like material (Figure 22). This resuspended into the reaction medium with little agitation and was easily tipped away following disposal of the supernatant. It was therefore concluded that the increased concentrations of BSA was interfering with BIS formation and forming an inferior material, which was then being lost during disposal of the supernatant following centrifugation (Figure 22).

Figure 22. Three examples of gel formation above the BIS silica pellet from BSA protein experiments, where the red brackets indicate the gel layer.

4.4 Chapter 4 Summary

This chapter set out to determine what effect CA immobilisation within a framework with ideal porosity for enzyme immobilisation would have on enzyme immobilisation and activity. It aimed to do this using a recently developed and highly novel framework made [redacted] called Gen 2 BIS. [redacted] of Gen 2 BIS to [redacted] resulted in the creation of a different type of framework with greater SA. This was called Gen 3 BIS.

Results from porosity analyses demonstrated that a Gen 2 framework was able to be synthesised with porosity values which were fell within the ideal criteria for enzyme immobilisation which was defined in the literature review. The Gen 3 framework possessed similar ideal SA, PVs and PDs but had significantly enhanced SA due to [redacted]

4.4.1 Adsorption Outcomes

These materials with optimal porosities were then used alongside a commercially available silica called Syloid 244 to see if adsorption of CA would be comparable. Another question was whether the functionalising capability of [redacted], which remained in Gen 2 BIS,

also would lead to increased CA adsorption and enzyme activity. Ultimately, Syloid 244 outperformed Gen 2 and 3 BIS in terms of CA loading success and w/w loading onto the framework. Further Gen 3 BIS outperformed Gen 2, suggesting that the functionalising features of Gen 2 BIS did not lead to enhanced CA binding. However, the increased binding seen in Gen 3 BIS, which had a greater SA, may indicate that increased SA between Gen 2 and 3 BIS may have been a factor behind the higher CA binding. No difference was found in the rates of CA activity in terms of p-NPA hydrolysis, suggesting that despite differences in loading all enzymes had the same activity once they were within the framework. However, this activity was not comparable to the free enzyme, suggesting that the enhanced porosity available in the framework did not improve enzyme activity.

With regards to CO_2 sequestration, the Gen 2 and 3 BIS samples had CO_2 sequestration capabilities which were less than or equal to that of the no-enzyme controls, suggesting that they were not suitable materials for CO_2 sequestration. Contrastingly, Syloid 244 displayed activity which was comparable to that of the free enzyme however the large variation in sample replicates should be considered. A potential explanation for this may be the lower density and hydrophilicity of Syloid 244, which may have allowed it to be better dispersed during reaction mixing. All three silica types exhibited very little leaching over 24 hours.

4.4.2 Entrapment Outcomes

The second type of CA immobilisation was via entrapment during BIS synthesis to create a Gen 2 BIS with CA immobilised within it. A Gen 3 CA material could then be created by [redacted]

Results from the CA entrapment trials revealed that w/w loading and loading success for Gen 2 BIS was consistent across experiments for both 30 and 50 mM reactant concentrations. However, CA immobilisation did not increase with increasing reactant concentrations. [redacted] CA Gen 3 BIS resulted in highly variable w/w loading and loading success between different experiments at both 30 and 50 mM reactant concentrations. When the porosity of Gen 2 with encapsulated BIS was examined, it could be seen that CA encapsulation had no significant impact on Gen 2 or Gen 3 porosity, and both remained within the ideal zone for enzyme immobilisation. The rate of CA activity in terms of p-NPA hydrolysis was tested for samples from two separate experiments. The first experiment produced rates of ~0 for CA activity. However, after refining the storage method for BIS the second experiment produced rates of CA activity for a single sample which was comparable to the activity of the free enzyme. This sample came from Gen 3 BIS created at 30 mM concentration, but unfortunately due to the impact of[redacted] only one sample was available for testing. Gen 2 BIS created at 30 and 50 mM concentrations also displayed activity which matched that of the

free activity from previous studies. Therefore, it could be that the enhanced porosity of these samples did in fact lead to greater CA activity, particularly in the Gen 3 BIS created at 30 mM. When the w/w loading and loading success was compared to the most successful immobilised CA frameworks however, none of the samples were high enough. But, when the w/w loading of previous CA samples was compared to the most successful studies, the w/w values exceeded those of the most successful studies. This suggests that if CA encapsulation can be slightly increased and loading stabilised across experiments, a CA BIS framework with good loading could be achieved.

In terms of CO_2 sequestration, unlike the p-NPA analysis none of the candidates had activity equivalent to that of free CA in solution. However, some of the Gen 2 30 and 50 mM replicates did come close. Combined with the activity demonstrated in the p-NPA analysis and the potential for greater w/w loading seen in earlier experiments, these candidates may be worth further investigation to see if their activity can be enhanced. Significant leaching was observed across all entrapped CA samples for both Gen 2 and 3 BIS; however, it is strongly suspected that this outcome would be worth re-testing to make sure there was no methodological mistake.

5 Chapter 5: Conclusion.

5.1 Thesis Summary and Research Motivation

The combustion of fossil fuels has increased CO_2 in the Earth's atmosphere to 428.01 parts per million (ppm) globally as of March 2025, the highest concentration in the last 800,000 years[1]. The iron and steel and cement sectors respectively account for 7 - 9% and 7% of global CO_2 emissions and face challenges with decarbonisation due to the inherent CO_2 emissions associated with their manufacturing processes[2].

Carbon capture, utilisation and storage (CCUS) technologies are one response to these hard-to-abate emissions, and the conversion of CO_2 to methanol (CH_3OH) has been identified as particularly promising. CH_3OH is a versatile feedstock for thousands of specialised chemicals and is the second most effective chemical, after urea, for sequestering anthropogenic CO_2 emissions[3,4]. Global CH_3OH production currently stands at approximately 98 Mt per year and is predominantly produced using coal (35%) and gas (65%) feedstocks, with only 0.2 Mt produced renewably[5,6]. Demand for CH_3OH is expected to rise by 50% by 2030 and double by 2050 and producing it from waste CO_2 could prevent emissions of >211 Mt CO_2 per year[5,7–9][10]. The most developed route for CO_2 to CH_3OH conversion is hydrogenation via Fischer-Tropsch synthesis[11]. The most commercially advanced example, the George Olah Plant in Iceland, produces 4,000 tonnes of methanol annually[12]. However, significant challenges remain including low reaction efficiency, the need for expensive rare metal catalysts, poor CH_3OH selectivity, and catalyst disintegration[13–16].

Enzymatic conversion of CO_2 to CH_3OH has been proposed as a greener alternative and exploits the ability of enzymes to reduce reaction activation energy, increase substrate selectivity and avoids the use of expensive and unsustainable rare-metal catalysts[17,18]. Research began with Obert and Dave in 1999, using a cascade of formate dehydrogenase, formaldehyde dehydrogenase, and alcohol dehydrogenase[19,20]. CA was later identified as a valuable addition at the beginning of this cascade, aiding hydration of CO_2 by catalysing its interconversion with bicarbonate (HCO_3^-) at a rate of 10^4 to 10^6 reactions per second[21–23]. CA inclusion has been reported to improve the reaction rate of CO_2 to formate, since in its hydrated form the reaction free energy for conversion to formate is much lower ($\Delta rG° = -165.39$ kcal / mol at 25°C)[19]. However, the use of free enzymes creates unfeasibly high operational costs due to their high initial cost and low recovery[24]. Immobilisation of enzymes by attaching them to a support has been cited to lower process costs by enabling their recovery and reuse[25,26]. This study therefore chose to focus on exploring the immobilisation of CA.

5.2 Theoretical Background

5.2.1 Enzyme Immobilisation Methods

Enzyme immobilisation methods fall into two broad categories. Chemical methods include covalent bonding and cross-linking[27]. Covalent bonding is favoured by industry but requires modification of the enzyme's structure, which can interfere with its conformation[28]. Cross-linking links enzymes to other enzymes or supports to form aggregates but is difficult to reproduce and can involve unfavourable interactions[27].

Physical immobilisation occurs by adsorption via van der Waals forces, hydrogen bonds, and ionic bonds, generally carrying a reduced risk of structural alteration[29,30]. However, enzyme leaching from the framework remains a significant drawback, particularly for industrial applications requiring recovery and recycling[29,31]. Entrapment within a polymer matrix assembled around the enzyme also suffers from leaching due to the relatively small size of enzymes.

5.2.2 Performance Criteria for Immobilisation Frameworks

A SA between 25 and 500 $m^2\ g^{-1}$ has recently been identified to be optimal for an immobilisation framework, with greater protein loading linked to SAs towards the higher end of this range[32]. PDs must be large enough to allow enzyme access into the inner SA, and PVs must allow efficient enzyme–substrate interactions[32]. A meta-analysis by Bayne *et al*. identified that SAs of 25 - 500 $m^2\ g^{-1}$, PDs between 10 -100 nm, and PVs >0.3 $cm^3\ g^{-1}$ are key parameters for a successful immobilisation framework[32]. Mesoporous materials with highly ordered pore structures have also been observed to be effective owing to more even molecular diffusion[32]. In relation to CA, SBA-15 silicas displayed good activity efficiency and higher w/w loading[33], though conventional ordered mesoporous silica manufacture is currently energy and resource intensive[34].

5.2.3 Candidate Framework Materials

Bioinspired silica (BIS) has emerged as a more sustainable method to produce silicas and are characterised by comparatively mild synthesis at pH 6 - 7 and <40 °C[34–36]. However, the predominant forms of BIS are generally reported to have low PVs and SAs which fall outside the ideal porosity range for enzyme immobilisation. A novel [redacted] method developed by the Green Nanomaterials Research Group at the University of Sheffield has produced Generation 2 (Gen 2) BIS with SA PDs and PVs within the optimal range. [redacted] Generation 3 (Gen 3) BIS.

Biochar, produced by pyrolysis of biomass feedstocks, was also investigated as an immobilisation material due to its purported large SA, chemical stability and naturally occurring

SFGs that can enable enzyme binding via adsorption[18]. However, freshly produced biochar is widely considered hydrophobic[37,38], in contrast to CA, which is a water-soluble enzyme with a hydrophilic exterior[39,40]. The presence or introduction of certain SFGs such as carboxylic acids can overcome this, imparting a negative surface charge that can induce electrostatic attraction with positively charged residues within the CA structure[40]. However, the physical and chemical properties of biochar are cited to be deeply dependent on feedstock, pyrolysis temperature, and activation treatment[18].

The overarching aims of this study:

1. To conduct an in-depth desk-based analysis of the applicability of biochar as an enzyme immobilisation framework based on whether its porosity can be intentionally tuned.
2. To characterise commercial biochar samples for porosity, stability, and presence of SFGs.
3. To examine whether the activity of CA immobilised onto BIS achieves activity efficiency comparable to the best performing frameworks in the literature.
4. To compare the activity of CA adsorbed onto BIS against the activity of CA encapsulated during BIS formation.

5.3 Biochar as an Immobilisation Framework

5.3.1 Meta-Analysis of Biochar Porosity

Similarly to other immobilisation frameworks, biochar SA is considered to be an important factor in the effectiveness of biochar enzyme systems[18]. This study found that biochar SAs can range greatly from 2 to 1200 $m^2 g^{-1}$. While greater SA has been associated with increased adsorption capacity for chemical compounds, this relationship does not translate directly to enzymes, as the molecular diameters of enzymes may exceed the PDs of biochar, restricting their access to portions of the framework SA[32]. Bayne *et al*. reported that enzyme loading increased with SA up to 500 $m^2 g^{-1}$, beyond which loading plateaued, coinciding with a reduction in pore size that limited enzyme access to the internal SA[32].

Of 65 feedstocks evaluated across 43 studies, only 16 (24%) exhibited PDs exceeding the 10 nm threshold defined by Bayne *et al*. as the minimum required for enzyme immobilisation. All biochar samples with suitable mesopore diameters (>10 nm) fell within the 0 - 25 $m^2 g^{-1}$ SA range, which Bayne *et al*. considered insufficient to support an extensive catalytic surface. Regarding PV, 90% of feedstocks failed to meet the minimum threshold of 0.3 $cm^3 g^{-1}$, suggesting that neither pyrolysis temperature nor feedstock type reliably produced adequate PVs. The wheat straw, bamboo, and corn stalk biochars represent the 10% that did. Nonetheless, they failed to satisfy the minimum PD requirement, meaning enzymes would be

unable to access the internal SA. **Therefore, no biochar candidates were identified as suitable frameworks, and hypothesis one was rejected: biochar was deemed unsuitable for enzyme immobilisation, with porosity features not reliably selectable based on feedstock, manufacture conditions, or activation treatment.**

This metanalysis also identified methodological issues with porosity analysis and reporting. For instance, the use of N_2 for gas adsorption has been considered an insufficient adsorbate for accurately characterising microporosity. In addition, inconsistencies in gas adsorption methods and computational modelling further limited confidence in the data, and the absence of controls precluded direct comparisons in some studies.

Future work would benefit from greater methodological standardisation in biochar porosity characterisation, including careful consideration of adsorptive gas choice, since neither N_2 nor CO_2 may be fully appropriate for microporous, polar biochars. Consistent reporting of pressure and temperature conditions, alongside inclusion of isotherms and hysteresis data, would allow more meaningful cross study comparison and better informed selection of computational models. Together, addressing these issues would improve confidence in porosity datasets and strengthen conclusions regarding the suitability of biochar as an enzyme support material.

5.3.2 Laboratory Characterisation of Selected Biochars

Laboratory N_2 gas adsorption and MIP analyses confirmed that none of the selected biochars met the ideal porosity criteria outlined by Bayne *et al*. for enzyme immobilisation. **The first part of hypothesis two was therefore rejected: selection of biochar informed by literature trends between feedstock, manufacture conditions, activation treatment, and SA, PV and PD outcomes did not produce a material with porosity features suitable for CA immobilisation.** However, CHNS and O elemental analysis showed that higher pyrolysis temperature biochars (TERC, WT) had lower H:C and O:C ratios, consistent with greater chemical stability. ATR FT-IR spectra also detected SFGs on WT biochar in the form of carboxylate anion bands (1590 -1520 cm^{-1}), which can be modified to carboxylic acid groups suitable for enzyme binding. **The second part of hypothesis two was therefore accepted: certain biochars were chemically stable and possessed SFGs favourable for CA immobilisation. However, given that no biochar met the necessary porosity requirements, biochar was not progressed to enzyme loading experiments.**

5.4 Bioinspired Silica as an Immobilisation Framework

5.4.1 BIS Porosity Characterisation

N_2 gas adsorption analysis confirmed that Gen 2 and Gen 3 BIS synthesised without CA or BSA both fell within the ideal porosity zone defined by Bayne *et al*. Gen 2 BIS exhibited a

mean SA, PD and PV of 119 $m^2 g^{-1}$, 25 nm, and 0.82 $cm^3 g^{-1}$ respectively. Gen 3 BIS, produced by [redacted], exhibited a substantially enhanced mean SA of 358 $m^2 g^{-1}$, with mean PD and PV of 15 nm and 0.73 $cm^3 g^{-1}$ respectively. These outcomes are consistent with the SA increases observed in previous studies for Gen 1 BIS[41]. For both generations, neither CA loading nor reactant concentration impacted PD, PV, or SA relative to no protein controls, with all materials remaining within the ideal porosity zone.

Gen 2 BIS is therefore a reproducible, green framework within the ideal porosity ranges for enzyme immobilisation. [redacted] Gen 3 BIS can enhance porosity further and [redacted] However, CA has a molecular diameter of approximately 5 × 4 nm and BSA approximately 14 × 4 nm[42,43]. Therefore, PDs of approximately 22 nm for Gen 2 and 10 nm for Gen 3 BIS, mean PDs may be large enough for CA or BSA to exit the framework following entrapment or adsorption. This may explain the variable protein retention observed for Gen 3 BIS between experiments. Leaching may also have occur during rinsing and centrifugation following immobilisation via entrapment or adsorption.

5.4.2 BSA Entrapment

BSA entrapment in Gen 2 BIS was reproducible across experiments, with consistent loading successes of 25 - 33.5% and w/w loading of 0.9 - 1.2 mg BSA per mg BIS, substantially exceeding the ~0.02 mg/mg threshold for ideal w/w loading onto a carrier. However, studies investigating CA immobilisation into Gen 1 BIS reported significantly lower overall porosity (SA 14 $m^2 g^{-1}$, PD 19 nm, PV 0.037 $cm^3 g^{-1}$) yet achieved comparable loading, indicating that **hypothesis 5 cannot be accepted: BSA entrapped in Gen 2 BIS with ideal porosity did not facilitate improved loading compared to a BIS with non-ideal porosity.**

[redacted] Gen 3 BIS consistently resulted in near-complete removal of BSA, with loading success of 0.1 - 4.1% and w/w loading of 0 - 0.11 mg BSA per mg BIS. This contrasts with published findings for Gen 1 BIS, in which protein retention was maintained [redacted], and may reflect the larger PVs and PDs of Gen 2 BIS allowing BSA to exit the framework [redacted] through interparticle spaces. **Hypothesis 5 is therefore also rejected for Gen 3 BIS.**

In the case of Gen 2, increasing reactant concentrations (30, 50, and 100 mM) led to increased BIS formation per mL, matched by increases in BSA loading success of 22% between 30 and 50 mM and 38% between 50 and 100 mM. Whilst not reflected in w/w loading, this indicates that higher reactant concentrations could reduce protein wastage, partly confirming **hypothesis 3: that BSA loading success is influenced by reactant concentration during entrapment.**

5.4.3 CA Entrapment

Similarly to BSA, CA entrapment in Gen 2 BIS was consistent across experiments, with loading successes of 11 - 19.38% and w/w loadings of 0.16 - 0.29 mg CA per mg BIS at 30 mM reactant concentrations. Unlike BSA, CA immobilisation did not increase with increasing reactant concentrations; for instance, at 50 mM, loading success remained between 15.1 - 23.0%, with w/w loadings of 0.07 - 0.15 mg CA per mg BIS. **Hypothesis 3 is therefore rejected for Gen 2 BIS on CA: loading success is not influenced by reactant concentration during entrapment, and concentration-dependent uptake into Gen 2 BIS can vary depending on protein type.**

CA w/w loading of 0.16 - 0.29 mg per mg BIS compared well with Gen 1 BIS studies (0.15 - 0.25 mg/mg)[45] and surpassed the industrial minimum threshold of 0.02 mg enzyme per mg carrier[46]. However, given that Gen 1 BIS had significantly lower porosity (SA 14 $m^2 g^{-1}$, PD 19 nm, PV 0.037 $cm^3 g^{-1}$)[45] it appears that the enhanced SA and PVs of Gen 2 did not equate to greater CA entrapment. **Hypothesis 5 for Gen 2 BIS is therefore rejected.**

CA entrapment in Gen 3 BIS varied considerably between experiments, ranging between 0 - 14.7% loading success and 0 - 0.34 mg CA per mg BIS, with similar variability at 50 mM. This likely reflects the larger PVs and PDs of Gen 2 BIS allowing CA to exit the framework [redacted] **Whilst improved loading compared to Gen 1 BIS was possible in some instances, it was not consistent, and hypothesis 5 for Gen 3 BIS is therefore also rejected.**

When compared against the most successful CA immobilisation frameworks in the literature (Ag/SBA-15/TEPA, Ag/SBA-15/OAPS, Au/SBA-15/MPTES and SBA-15/OAPS)[47,48], results varied between experiments. In some cases, Gen 2 and Gen 3 BIS w/w loading surpassed the best performing studies, but this was not reproducible across experiments. An important recommendation for future work is therefore to reduce variability in immobilisation outcomes.

5.4.4 CA Adsorption

Temperature dependent adsorption experiments demonstrated that silica type had a highly significant effect on both immobilisation success and w/w loading (p <0.0001), whereas adsorption temperature did not (p = 0.233), with no significant interaction between silica type and temperature observed. **Hypothesis 3 is therefore rejected: CA loading success is not influenced by temperature during adsorption.**

Syloid 244 achieved the highest immobilisation success (70 - 90%) and w/w loading (~0.1 mg CA per mg silica), followed by Gen 3 BIS (33 - 45%, ~0.05 mg CA per mg silica), with Gen 2 BIS exhibiting the lowest immobilisation success (1 – 15%) and w/w loading (~0.01 mg CA per mg silica). These values fall far below the best frameworks in the literature, and **hypothesis 5 is therefore rejected: BIS with ideal porosity features does not facilitate good CA adsorption loading.**

The presence of [redacted] in Gen 2 BIS did not confer any benefit to CA adsorption; indeed, the significantly greater immobilisation success of Gen 3 BIS suggested that their absence may have enhanced adsorption. The superior performance of Syloid 244, despite not possessing distinctly different PDs, SAs, or PVs from the BIS materials, indicates that a different aspect of silica surface chemistry may govern CA adsorption.

5.4.5 CA Activity

Samples derived from E6 Gen 2 BIS at both 30 and 50 mM exhibited significantly higher activity than free CA from other experiments. Gen 3 BIS at 30 mM also achieved activity equivalent to, or exceeding, that of free CA reported in comparable studies. A key limitation was the complete loss of CA [redacted] in two Gen 3 30 mM replicates, meaning conclusions for those samples are based on a single data point. If representative, this may imply **that the additional porosity generated [redacted] contributed to improved CA activity, and part of hypothesis 5 may tentatively be accepted.** However, further generation of Gen 3 BIS with consistent CA retention would be needed to substantiate this.

Entrapped CA within Gen 2 and Gen 3 BIS from E6 achieved activity efficiencies of 30 - 80%, and Gen 3 30 mM achieved 81.8%. By comparison, Gen 1 BIS previously achieved 93.2% activity efficiency[45], and the highest-performing immobilised CA systems (covalently bonded SBA-15/TAEA, SBA-15/OAPS, iron filings, glass-coated filings, co-polymer beads, TiO_2 nanoparticles, and CLEA/SBA-15) have reported activity efficiencies of 95 - 99%. **Hypothesis 5 is therefore rejected: CA entrapped in BIS with ideal porosity features did not achieve activity comparable to the free enzyme or to leading frameworks.**

For adsorbed CA, no p-NPA hydrolysis activity was comparable to free CA, with activity efficiency of around 8% across all replicates regardless of silica type. Whilst silica type significantly influenced w/w loading, it had no apparent impact on catalytic function, suggesting a conserved feature amongst Gen 2, Gen 3, and Syloid 244 that negatively impacts CA activity. **Despite all three materials possessing porosities within the ideal zone defined by Bayne *et al*., this conferred no benefit to CA activity. Hypothesis 5 is therefore also rejected for adsorbed CA.**

5.4.6 CO_2 Sequestration

Despite demonstrating catalytic activity during p-NPA hydrolysis assays, CO_2 mineralisation assays for entrapped CA in Gen 2 and Gen 3 BIS displayed sequestration activity equivalent to no-CA controls. Whilst certain Gen 2 30 and 50 mM replicates reached 80 - 90% of free CA sequestration yield, overall activity efficiency was approximately 66%, within the value region of no-CA controls. By comparison, free CA sequestered all available CO_2 in solution, suggesting that entrapment within Gen 2 and Gen 3 BIS impeded CA access to CO_2 substrate.

Similarly, Gen 2 and Gen 3 BIS-adsorbed CA activity was equivalent to no-enzyme controls. CA adsorbed onto Syloid 244 showed sample variation within the same range as the free enzyme, though with large variation between replicates. This was attributed to the low density and hydrophilic nature of Syloid 244, which may have allowed greater CA interaction with dissolved CO_2 substrate.

Due to time and material limitations, this analysis was performed only once, with only a single Gen 3 replicate available for the CO_2 sequestration assay. **Further refinement with full sample replicates would therefore be needed before hypothesis 5 can be accepted or rejected with confidence.**

5.4.7 Leaching

Adsorbed CA on Gen 2 BIS, Gen 3 BIS, and Syloid 244 demonstrated no loss of CA over a 24 hour incubation period, contrasting with findings from SBA-15 leaching analyses in which enzymes have been reported to leach from the framework when immobilised directly on the surface.

Significant leaching was observed from entrapped samples. The highest loss occurred in Gen 2 BIS at 50 mM (30 - 70% over 24 hours), with Gen 3 BIS at 50 mM and Gen 2 BIS at 30 mM losing 40 and 20% respectively. This deviates substantially from the negligible leaching reported in previous Gen 1 BIS entrapment studies. Two possible explanations were identified: the larger PVs and PDs of Gen 2 and Gen 3 BIS may facilitate greater mass transfer of dissociated enzyme out of the framework compared with more tightly clustered Gen 1 particles (PV ≤ 0.1 $cm^3\ g^{-1}$)[49]. Alternatively, entrapped BIS samples were crushed and sieved prior to analysis, which may have released CA into solution. A repeat analysis without sample crushing is recommended to rule out this cause before drawing firm conclusions.

5.4.8 Optimisation of Protein Addition Conditions

A separate assay exposing free CA to pH 7 - 11 for one minute revealed a reduction in CA activity at pH ≥9, indicating that any gains in CA loading from earlier addition must be weighed against potential loss of activity due to non-optimal pH exposure.

Due to limited reagent availability, BSA was selected as a model protein to investigate whether increasing protein concentration or adding CA at an earlier reaction time point improves immobilisation. BSA concentrations of 2, 2.4, and 4 mg/mL and pH points between 7 - 11 were tested for both Gen 2 and Gen 3 BIS.

At 2 mg/mL, pH at the point of addition had little effect on protein loading, with immobilisation success ranging from 25% at pH 7 - 8 to a maximum of 35% at pH 11. Elution consistently removed BSA completely from Gen 3 BIS. **Hypothesis 4 is therefore rejected at this concentration: the pH at the time of addition did not influence BSA entrapment at a protein concentration of 2 mg/mL.**

At 2.4 mg/mL, a clear pH dependence emerged for Gen 2 BIS, with loading success increasing from 55% at pH 7 to 95% at pH 11. Gen 3 BIS loading remained at 10% regardless of pH, indicating that [redacted] removes protein to a consistent level regardless of original loading. Despite high Gen 2 loading success, w/w ratios were non-detectable as immobilised BSA surpassed total BIS yield. **Hypothesis 4 is therefore partially accepted for Gen 2 BIS only at this concentration.**

At 4 mg/mL, BSA loading remained consistently between 25 - 30% for Gen 2 and 15 - 20% for Gen 3 regardless of pH addition point, and w/w loading remained indiscernible. Visual inspection confirmed that at elevated BSA concentrations (2.4 and 4 mg/mL), a gel-like material formed above the BIS pellet which re-suspended easily and was discarded during rinsing. This indicates that these concentrations interfered with proper BIS formation, distorting results through reduced final BIS yield.

5.5 Conclusion

This study investigated the feasibility of using biochar and BIS as sustainable porous immobilisation frameworks for CA, with the aim of advancing the enzymatic conversion of CO_2 to CH_3OH and overcoming the prohibitive cost of free enzyme systems that currently undermines the commercial viability of biocatalytic CO_2 reduction.

The meta-analysis of biochar porosity yielded a clear finding: across feedstocks drawn from 43 published studies, no biochar candidate simultaneously satisfied the SA, PD, and PV criteria defined by Bayne *et al*., a conclusion corroborated by laboratory characterisation of selected commercial biochars. Although certain high-temperature pyrolysis biochars (notably WT) demonstrated chemical stability and SFGs favourable for CA binding, hypothesis one was rejected: biochar does not constitute a reliable or tuneable immobilisation framework for CA, and porosity cannot be intentionally selected for through choice of feedstock, manufacture conditions, or activation treatment.

Investigation of Gen 2 and Gen 3 BIS produced mixed outcomes. Both generations exhibited porosity within the ideal zone defined by Bayne *et al*., and CA and BSA were reproducibly entrapped within Gen 2 BIS at w/w loadings consistent with leading studies and exceeding the industrial minimum threshold. However, enhanced porosity did not translate into improved CA loading relative to lower-porosity Gen 1 BIS, and [redacted] to produce Gen 3 BIS consistently resulted in near-complete protein loss in BSA experiments and variable CA entrapment outcomes, this has been postulated to be as a result of larger PDs facilitating protein exit during additive removal.

Activity efficiency for entrapped CA reached up to 81.8% in Gen 3 BIS, though based on limited replicates, and fell short of the 95 - 99% efficiencies reported for leading frameworks such as SBA-15 / TAEA, SBA–15/OAPS, iron filings, glass-coated filings, co-polymer beads, TiO_2 nanoparticles, and CLEA / SBA-15. CO_2 sequestration assays suggested that entrapment within BIS impeded CO_2 substrate access to CA, limiting sequestration to levels comparable with enzyme-free controls.

Adsorption experiments indicated that silica type, rather than temperature, governs CA loading, with Syloid 244 outperforming both BIS generations. However, CA activity efficiency following adsorption was unifor mly low (~8% across all silica types, suggesting a conserved and undefined surface feature may be suppressing catalytic function irrespective of loading success.

These findings make a meaningful contribution to the field. They highlight methodological inconsistencies within biochar literature and the need for standardisation, and challenge previous assumptions about the direct relationship between framework porosity and enzyme loading and performance. For adsorption, factors beyond porosity appear to influence CA loading and activity and warrant further investigation. The comparatively mild and sustainable manufacture of Gen 2 and Gen 3 BIS may outweigh the additional activity efficiency of conventional frameworks such as SBA-15 in terms of environmental impact, and pursuing covalent bonding or functionalisation strategies on these materials may represents a promising future research direction.

5.5.1 Research Recommendations

- **Standardise biochar porosity characterisation:** Future research should adopt consistent gas adsorption protocols, including careful selection of adsorbate gases, and standardised reporting of SA, PV, PD, manufacture conditions, feedstock controls, isotherms, and hysteresis data to improve comparability and clarify biochar's suitability as an enzyme support.

- **Investigate CA activity suppression during adsorption:** The unifor mly low activity efficiency (~8%) across all silica types despite markedly different loading outcomes suggests a undefined conserved inhibitory feature. Future work could characterise the surface chemistry of Gen 2 BIS, Gen 3 BIS, and Syloid 244 in greater detail to inform surface modifications that preserve CA conformation and catalytic function.
- **Reduce variability in BIS entrapment and validate CO_2 sequestration assays:** Future studies should optimise entrapment protocols to reduce variation and establish consistent w/w loading values, which would clarify whether the enhanced porosity of Gen 3 BIS reliably improves CA activity efficiency and [redacted] is a beneficial or counterproductive step.
- **Evaluate the full enzymatic cascade using BIS-immobilised CA:** Future work should assess whether BIS-immobilised CA retains sufficient activity to support cascade reactions with formate dehydrogenase, formaldehyde dehydrogenase, and alcohol dehydrogenase, and explore co-immobilisation strategies to enhance multi-enzyme proximity and overall conversion efficiency.

References

1. Ghiat I, Al-Ansari T. A review of carbon capture and utilisation as a CO2 abatement opportunity within the EWF nexus. *J CO2 Util*. 2021;45:101432. doi:10.1016/j.jcou.2020.101432

2. Tal H. *Global Sustainable Development Report 2019: The Future Is Now – Science for Achieving Sustainable Development*.; 2019.

3. Lindsey R. Climate Change: Atmospheric Carbon Dioxide. NOAA Climate.gov. 2020. Accessed April 1, 2025. www.climate.gov/news-features/understanding-climate/climate-change-atmospheric-carbon-dioxide

4. Global Monitoring Laboratory: Trends in CO2, CH4, N2O, SF6. NOAA Climate.gov. doi:https://gmL.noaa.gov/ccgg/trends/mLo.htmL

5. Ehhalt D, Prather M. Atmospheric Chemistry and Greenhouse Gases. Climate Change 2001: The Scientific Basis. 2001. Accessed April 25, 2026. www.ipcc.ch/site/assets/uploads/2018/03/TAR-04.pdf

6. EPA. Overview of Greenhouse Gases. United States Environmental Protection Agency. 2021. Accessed February 9, 2025. www.epa.gov/ghgemissions/overview-greenhouse-gases

7. Masson-Delmotte, V., P. Zhai, H.-O. Pörtner, D. Roberts, J. Skea, P.R. Shukla, A. Pirani, W. Moufouma-Okia, C. Péan, R. Pidcock, S. Connors, J.B.R. Matthews, Y. Chen, X. Zhou, M.I. Gomis, E. Lonnoy, T. Maycock, M. Tignor, and T. WaterfieldMasson-Delmotte, and TW. *Global Warming of 1.5°C. An IPCC Special Report on the Impacts of Global Warming of 1.5°C above Pre-Industrial Levels and Related Global Greenhouse Gas Emission Pathways, in the Context of Strengthening the Global Response to the Threat of Climate Change,*.; 2019.

8. *Industrial Decarbonisation Strategy*.; 2021. www.assets.publishing.service.gov.uk/government/uploads/system/uploads/attachment_data/file/970229/Industrial_Decarbonisation_Strategy_March_2021.pdf

9. *Energy Technology Perspectives: Catalysing Energy Technology Transformations*.; 2017. www.iea.org/reports/energy-technology-perspectives-2017

10. Meng KC, Rode A. The social cost of lobbying over climate policy. *Nat Clim Chang*. 2019;9(6):472-476. doi:10.1038/s41558-019-0489-6

11. Davis SJ. Net-zero emissions energy systems. *Sci Mag*. Published online 2018:9793. doi:10.1126/science.aas9793

12. COP27: UN report shows pathways to carbon-neutrality in “energy intensive” steel, chemicals and cement industries. UNECE. 2025. Accessed April 1, 2025. www.unece.org/media/press/372890

13. Sarandrea L, Gabriele Vola. Evaluating and predicting process behaviour in a double shaft regenerative kiln. In: *LimeCon*. Vol 2016. ; 2016:1-2.

14. *Mind the Gap: How Carbon Dioxide Removals Must Complement Deep Decarbonisation to Keep 1.5°C Alive*.; 2022.

15. *In Emissions Gap Report 2023: Broken Record – Temperatures Hit New Highs, yet World Fails to Cut Emissions (Again)*.; 2023.

16. Smith SM, Geden O, Gidden MJ, et al. *A Global, Independent Scientific Assessment of Carbon Dioxide Removal 2024 - 2nd Edition*.; 2024. doi:10.17605/OSF.IO/F85QJ

17. Fuss S, Lamb WF, Callaghan MW, et al. Negative emissions - Part 2: Costs, potentials and side effects. *Environ Res Lett*. 2018;13(6). doi:10.1088/1748-9326/aabf9f

18. Ozkan M, Nayak SP, Ruiz AD, Jiang W. Current status and pillars of direct air capture technologies. *iScience*. 2022;25(4):103990. doi:10.1016/j.isci.2022.103990

19. Lamb WF, Gasser T, Roman-Cuesta RM, et al. The carbon dioxide removal gap. *Nat Clim Chang*. 2024;14(6):644-651. doi:10.1038/s41558-024-01984-6

20. Terlouw T, Bauer C, Rosa L, Mazzotti M. Life cycle assessment of carbon dioxide removal technologies: A critical review. *Energy Environ Sci*. 2021;14(4):1701-1721. doi:10.1039/d0ee03757e

21. *Energy Technology Perspectives 2020: Special Report on Carbon Capture Utilisation and Storage*.; 2020. doi:10.1787/208b66f4-en

22. Steel. IEA. 2025. Accessed April 1, 2025. www.iea.org/energy-system/industry/steel

23. Tracking Report: Cement. IEA. 2022. Accessed October 30, 2022. www.iea.org/reports/cement

24. UK Government. Carbon Capture, Usage and Storage: A Vision to Establish a Competitive Market. Department for Energy Security and Net Zero.

25. Cuéllar-Franca RM, Azapagic A. Carbon capture, storage and utilisation technologies: A critical analysis and comparison of their life cycle environmental impacts. *J CO2 Util*. 2015;9:82-102. doi:10.1016/j.jcou.2014.12.001

26. Akram M, Milkowski K, Gibbins J, Pourkashanian M. Comparative energy and environmental performance of 40% and 30% monoethanolamine at PACT pilot plant. *Int J Greenh Gas Control*. 2020;95:102946. doi:10.1016/j.ijggc.2019.102946

27. Yamada H. Amine-based capture of CO2 for utilization and storage. *Polym J*. 2021;(53):93-102. doi:10.1038/s41428-020-00400-y

28. Neerup R, Rasmussen VE, Vinjarapu SHB, et al. Solvent degradation and emissions from a CO2 capture pilot at a waste-to-energy plant. *J Environ Chem Eng*. 2023;11(6). doi:10.1016/j.jece.2023.111411

29. Chang M hui, Chen W cheng, Huang C ming, et al. Design and Experimental Testing of a 1 . 9MW th Calcium Looping Pilot Plant. 2014;63:2100-2108. doi:10.1016/j.egypro.2014.11.226

30. Shuzhuang S, Hongman S, Williams PT, Wu C. Recent advances in integrated CO2 capture and utilization: A review. *Sustain Energy Fuels*. Published online 2013:1-3. doi:10.1039/D1SE00797A

31. Zhang S, Shen Y, Wang L, Chen J, Lu Y. Phase change solvents for post-combustion CO2 capture: Principle, advances, and challenges. *Appl Energy*. 2019;239:876-897. doi:10.1016/j.apenergy.2019.01.242

32. Gao W, Liang S, Wang R, et al. Industrial carbon dioxide capture and utilization: State of the art and future challenges. *Chem Soc Rev*. 2020;49(23):8584-8686. doi:10.1039/d0cs00025f

33. Chandra M, Waheed A, Singh RK. Characterization of functionally active immobilized carbonic anhydrase purified from sheep blood lysates. *Process Biochem*. 2013;48(2):231-241. doi:10.1016/j.procbio.2012.12.010

34. Ã NAO, Cockerill TT. Life cycle GHG assessment of fossil fuel power plants with carbon capture and storage. *Energy Policy*. 2008;36:367-380. doi:10.1016/j.enpol.2007.09.026

35. Viebahn P, Nitsch J, Fischedick M, Esken A, Supersberger N, Zuberbu U. Comparison of carbon capture and storage with renewable energy technologies regarding structural , economic , and ecological aspects in Germany. *Int J Greenh Gas Control*. Published online 2007:121-133. doi:10.1016/S1750-5836(07)00024-2

36. Zheng L. *Oxy-Fuel Combustion for Power Generation and Carbon Dioxide (CO2) Capture*. Woodhead Publishing Series in Energy: Number 17; 2011.

37. Borgert KJ, Rubin ES. Oxyfuel combustion: technical and economic considerations for the development of carbon capture from pulverized coal power plants. *Energy Procedia*. 2013;37:1291-1300. doi:10.1016/j.egypro.2013.06.004

38. Pröll T, Hofbauer H. Chemical Looping Combustion and Reforming. In: *Proceedings of the 9th European Conference on Industrial Furnaces and Boilers*. ; 2011:26-29.

39. Najera M, Solunke R, Gardner T, Veser G. Chemical Engineering Research and Design Carbon capture and utilization via chemical looping dry reforming. *Chem Eng Res Des*. 2011;89(9):1533-1543. doi:10.1016/j.cherd.2010.12.017

40. IEA and United Nations Industrial Development Organization. *Technology Roadmap: Carbon Capture and Storage in Industrial Applications*.; 2012. www.iea.org/reports/roadmap-carbon-capture-and-storage-in-industrial-applications

41. Smith E, Morris J, Kheshgi H, Teletzke G, Herzog H, Paltsev S. The cost of CO2 transport and storage in global integrated assessment modeling. *Int J Greenh Gas Control*. 2021;109:103367. doi:10.1016/j.ijggc.2021.103367

42. Page B, Turan G, Zapantis A, et al. Global Status of CCS: 2020. *Glob CCS Inst*. Published online 2020. www.globalccsinstitute.com/resources/global-status-report/

43. Lal B, Sudhakar S. Recent developments and challenges ahead in carbon capture and sequestration technologies. *SN Appl Sci*. 2019;1(8):1-20. doi:10.1007/s42452-019-0909-2

44. Mcgrail BP, Schaef HT, Ho AM, Chien Y ju, Dooley JJ, Davidson CL. Potential for carbon dioxide sequestration in flood basalts. *J Geogr Res*. 2006;111:1-13. doi:10.1029/2005JB004169

45. Gislason S, Sigurdardottir H, Aradottir E, Oelkers E. A brief history of CarbFix : Challenges and victories of the project's pilot phase. *Energy Procedia*. 2018;146:103-114. doi:10.1016/j.egypro.2018.07.014

46. Bui M, Adjiman CS, Anthony EJ, et al. Carbon capture and storage (CCS): the way forward. *Energy Environ Sci*. 2018;(11):1062-1176. doi:10.1039/c7ee02342a

47. Fakher S, Imqam A. Application of carbon dioxide injection in shale oil reservoirs for increasing oil recovery and carbon dioxide storage. *Fuel*. 2020;265:116944. doi:10.1016/j.fuel.2019.116944

48. Li L, Zhao N, Wei W, Sun Y. A review of research progress on CO 2 capture, storage, and utilization in Chinese Academy of Sciences. *Fuel*. 2013;108:112-130.

doi:10.1016/j.fuel.2011.08.022

49. Metz B, Davidson O, de Coninck H, Loos M, Meyer L. *IPCC Special Report on Carbon Dioxide Capture and Storage. Prepared by Working Group III of the Intergovernmental Panel on Climate Change*.; 2005.

50. IEA. *Technology Roadmap: Low-Carbon Transition in the Cement Industry*.; 2018. www.iea.org/reports/technology-roadmap-low-carbon-transition-in-the-cement-industry

51. Singh B, Strømman AH, Hertwich EG. International Journal of Greenhouse Gas Control Comparative life cycle environmental assessment of CCS technologies. *Int J Greenh Gas Control*. 2011;5(4):911-921. doi:10.1016/j.ijggc.2011.03.012

52. Pehnt M, Henkel J. Life cycle assessment of carbon dioxide capture and storage from lignite power plants. 2009;3:49-66. doi:10.1016/j.ijggc.2008.07.001

53. Mcling TL, Neupane G. The use of environmental tracers to characterize a leaky CO2 CCS natural analogue site, Soda Springs, Idaho, USA. *Greenh Gases Sci Technol*. 2019;74(2020):50-74. doi:10.1002/ghg.1949

54. Zheng L, Apps JA, Zhang Y, Xu T, Birkholzer JT. Reactive Transport Simulations to Study Groundwater Quality Changes in Response to CO2 Leakage from Deep Geological Storage. *Energy Procedia*. 2009;1(1):1887-1894. doi:10.1016/j.egypro.2009.01.246

55. Kharaka YK, Thordsen JJ, Kakouros E, Ambats G, Herkelrath WN. Changes in the chemistry of shallow groundwater related to the 2008 injection of CO2 at the ZERT field site, Bozeman, Montana. *Environ Earth Sci*. 2010;60:273-284. doi:10.1007/s12665-009-0401-1

56. Siirila ER, Navarre-sitchler AK, Maxwell RM, Mccray JE. Advances in Water Resources A quantitative methodology to assess the risks to human health from CO2 leakage into groundwater. *Adv Water Resour*. 2012;36:146-164. doi:10.1016/j.advwatres.2010.11.005

57. Assayag N, Matter J, Ader M, Goldberg D, Agrinier P. Water-rock interactions during a CO2 injection field-test: Implications on host rock dissolution and alteration effects. *Chem Geol*. 2009;265(1-2):227-235. doi:10.1016/j.chemgeo.2009.02.007

58. Apps JA, Zhang Y, Zheng L, Xu T, Birkholzer JT. Energy Procedia Identification of thermodynamic controls defining the concentrations of hazardous elements in potable ground waters and the potential impact of increasing carbon dioxide partial pressure. *Energy Procedia*. 2009;1(1):1917-1924. doi:10.1016/j.egypro.2009.01.250

59. Wang S, Jaffe PR. Dissolution of a mineral phase in potable aquifers due to CO2 releases from deep formations; effect of dissolution kinetics. *Energy Convers Manag*. 2004;45:2833-2848. doi:10.1016/j.enconman.2004.01.002

60. Hardarson BS, Franzson H, Gislason SR, Alfredsson AH. CO2 sequestration in basaltic rock at the Hellisheidi site in SW Iceland: stratigraphy and chemical composition of the rocks at the injection site. *Mineral Mag*. 2008;72:1-5. doi:10.1180/minmag.2008.072.1.1

61. Zheng L, Apps JA, Spycher N, et al. Geochemical modeling of changes in shallow groundwater chemistry observed during the MSU-ZERT CO2 injection experiment. *Int J Greenh Gas Control*. 2012;7:202-217. doi:10.1016/j.ijggc.2011.10.003

62. Mikkelsen M, Jørgensen M, Krebs FC. The teraton challenge. A review of fixation and transformation of carbon dioxide. *Energy Environ Sci*. 2010;3:43-81.

doi:10.1039/b912904a

63. Wang H, Liu Y, Laaksonen A, et al. Carbon recycling – An immense resource and key to a smart climate engineering: A survey of technologies, cost and impurity impact. *Renew Sustain Energy Rev*. 2020;131:110010. doi:10.1016/j.rser.2020.110010

64. Baskaya FS, Zhao X, Flickinger MC, Wang P. Thermodynamic feasibility of enzymatic reduction of carbon dioxide to methanol. *Appl Biochem Biotechnol*. 2010;162(2):391-398. doi:10.1007/s12010-009-8758-x

65. Sakakura T, Choi J chul, Yasuda H. Transformation of Carbon Dioxide. *Chem Rev*. 2007;107:2365–2387. doi:doi.org/10.1021/cr068357u

66. Otto A, Grube T, Stolten D. Environmental Science Closing the loop: captured CO2 as a feedstock in the chemical industry. *Energy Environ Sci*. 2015;8:3283-3297. doi:10.1039/c5ee02591e

67. Chauvy R, Meunier N, Thomas D, Weireld G De. Selecting emerging CO 2 utilization products for short- to mid-term deployment. *Appl Energy*. 2019;236(November 2018):662-680. doi:10.1016/j.apenergy.2018.11.096

68. Tian S, Yan F, Zhang Z, Jiang J. Calcium-looping reforming of methane realizes in situ CO 2 utilization with improved energy efficiency. *Sci Adv*. 2019;5(April):5077. doi:10.1126/sciadv.aav5077

69. Xu D, Wang Y, Ding M, Hong X, Liu G, Tsang SCE. Advances in higher alcohol synthesis from CO2 hydrogenation. *Cell Press*. 2021;7(4):849-881. doi:10.1016/j.chempr.2020.10.019

70. Artz J, Mu TE, Thenert K, et al. Sustainable Conversion of Carbon Dioxide: An Integrated Review of Catalysis and Life Cycle Assessment. *Chem Rev*. 2018;118:434-504. doi:10.1021/acs.chemrev.7b00435

71. Orgilés-calpena E, Arán-aís F, Torró-palau AM, Montiel-parreño E, Orgilés-barceló C. Synthesis of polyurethanes from CO2-based polyols: A challenge for sustainable adhesives. *Int J Adhes Adhes*. 2016;67:63-68. doi:10.1016/j.ijadhadh.2015.12.027

72. Aresta M, Dibenedetto A, Quaranta E. State of the art and perspectives in catalytic processes for CO2 conversion into chemicals and fuels: The distinctive contribution of chemical catalysis and biotechnology. *J Catal*. 2016;343:2-45. doi:10.1016/j.jcat.2016.04.003

73. Langanke J, Wolf A. Carbon dioxide (CO2) as sustainable feedstock for polyurethane production. *Green Chem*. Published online 2014. doi:10.1039/C3GC41788C

74. Al-mamoori A, Krishnamurthy A, Rownaghi AA, Rezaei F. Carbon Capture and Utilization Update. *Energy Technol*. 2017;5:834-849. doi:10.1002/ente.201600747

75. Abanades JC, Herzog HJ, Rubin ES, Mazzotti M. Environmental Science On the climate change mitigation potential of CO2 conversion to fuels. *Energy Environ Sci*. 2017;10:2491-2499. doi:10.1039/c7ee02819a

76. Gulzar A, Gulzar A, Bismillah M, He F, Gai S, Yang P. Carbon dioxide utilization : A paradigm shift with CO 2 economy. *Chem Eng J Adv*. 2020;3(August):100013. doi:10.1016/j.ceja.2020.100013

77. Meylan FD, Moreau V, Erkman S. CO2 utilization in the perspective of industrial ecology, an overview. *J CO2 Util*. 2015;12:101-108. doi:10.1016/j.jcou.2015.05.003

78. Alper E, Orhan OY. CO2 utilization: Developments in conversion processes. *Petroleum*. 2017;3(1):109-126. doi:10.1016/j.petlm.2016.11.003

79. Koytsoumpa EI, Bergins C, Kakaras E. The CO2 economy: Review of CO2 capture and reuse technologies. *J Supercrit Fluids*. 2018;132(July 2017):3-16. doi:10.1016/j.supflu.2017.07.029

80. Norhasyima RS, Mahlia TMI. Advances in CO_2 utilization technology: A patent landscape review. *J CO2 Util*. 2018;26:323-335. doi:10.1016/j.jcou.2018.05.022

81. Frederick J, Tapia D, Lee J yuan, Ooi REH, Foo DCY, Tan RR. A review of optimization and decision-making models for the planning of CO2 capture , utilization and storage (CCUS) systems. *Sustain Prod Consum*. 2017;13:1-15. doi:10.1016/j.spc.2017.10.001

82. Dindi A, Quang DV, Vega LF, Nashef E. Applications of fly ash for CO2 capture, utilization, and storage. *J CO2 Util*. 2019;29:82-102. doi:10.1016/j.jcou.2018.11.011

83. UN Economic Commission. *The Evolving Chemicals Economy: Status and Trends Relevant for Sustainability*.; 2018. https://www.unep.org/topics/chemicals-and-pollution-action/chemicals-management/global-chemicals-outlook

84. Zhang Z, Pan S yuan, Li H, et al. Recent advances in carbon dioxide utilization. *Renew Sustain Energy Rev*. 2020;125:109799. doi:10.1016/j.rser.2020.109799

85. International Renewable Energy Agency. *Innovation Outlook: Renewable Methanol*.; 2021. www.irena.org/publications/2021/Jan/Innovation-Outlook-Renewable-Methanol

86. Luk HT, Mondelli C, Ferre DC, Stewartband JA, Pérez-Ramırez J. Status and prospects in higher alcohols synthesis from syngas. Published online 2017. doi:10.1039/c6cs00324a

87. (IEA) IEA. Tracking Report: Chemicals. International Energy Agency (IEA). 2020. https://www.iea.org/reports/chemicals

88. Abdelaziz OY, Hosny WM, Gadalla MA, Ashour FH, Ashour IA, Hulteberg CP. Novel process technologies for conversion of carbon dioxide from industrial flue gas streams into methanol. *J CO2 Util*. 2017;21:52-63. doi:10.1016/j.jcou.2017.06.018

89. Pan X, Fan Z, Chen WEI, Ding Y, Luo H, Bao X. Enhanced ethanol production inside carbon-nanotube reactors containing catalytic particles. Published online 2007:507-511. doi:10.1038/nmat1916

90. Centi G, Perathoner S. Opportunities and prospects in the chemical recycling of carbon dioxide to fuels. *Catal Today*. 2009;148:191-205. doi:10.1016/j.cattod.2009.07.075

91. Arcoumanis C, Bae C, Crookes R, Kinoshita E. The potential of dimethyl ether (DME) as an alternative fuel for compression-ignition engines: A review. *Fuel*. 2008;87:1014-1030. doi:10.1016/j.fuel.2007.06.007

92. Olah GA, Goeppert A, Prakash GKS. Beyond Oil and Gas: The Methanol Economy. *Angew Chemie - Int Ed*. 2005;44(18):2636-2639. doi:doi.org/10.1002/anie.200462121

93. Aresta M, Dibenedetto A, Angelini A. Catalysis for the Valorization of Exhaust Carbon: from CO2 to Chemicals, Materials, and Fuels. Technological Use of CO2. *Chem Rev*. 2014;(114):1709-1742. doi:dx.doi.org/10.1021/cr4002758

94. Liu B jin, Torimoto T, Yoneyama H. Photocatalytic reduction of carbon dioxide in the presence of nitrate using TiO2 nanocrystal photocatalyst embedded in SiO2 matrices. *J Photochem Photobiol*. 1998;115:227-230. doi:1010-6030/98/

95. Ikeue K, Yamashita H, Anpo M. Photocatalytic Reduction of CO2 with H2O on Ti-Zeolite Photocatalysts: Effect of the Hydrophobic and Hydrophilic Properties. *J Phys Chem B*. 2001;105:8350-8355. doi:10.1021/jp010885g

96. Tseng I hsiang, Wu JCS, Chou H ying. Effects of sol-gel procedures on the photocatalysis of Cu/TiO2 in CO2 photoreduction. *J Catal*. 2004;221:432-440. doi:10.1016/j.jcat.2003.09.002

97. Ku Y, Lee W hui, Wang W yu. Photocatalytic reduction of carbonate in aqueous solution by UV/TiO 2 process. *J Mol Catal*. 2004;212:191-196. doi:10.1016/j.molcata.2003.10.047

98. Yamashita H, Fujii Y, Ichihashi Y, Gou S, Ikeue K. Selective formation of CH3OH in the photocatalytic reduction of CO2 with H2O on titanium oxides highly dispersed within zeolites and mesoporous molecular sieves. *Catal Today*. 1998;45:221-227.

99. Li H, Lei Y, Huang Y, Fang Y, Xu Y. Photocatalytic reduction of carbon dioxide to methanol by Cu2O/SiC nanocrystallite under visible light irradiation. *J Nat Gas Chem*. 2011;20(2):145-150. doi:10.1016/S1003-9953(10)60166-1

100. Liu S, Zhao Z, Wang Z. Photocatalytic reduction of carbon dioxide using sol-gel derived titania-supported CoPc catalysts. *Photochem Photobiol Sci*. 2007;6:695-700. doi:10.1039/b613098d

101. Reli M, Šihor M, Kočí K, Praus P, Kozák O, Obalová L. Influence of Reaction Medium on CO2 Photocatalytic Reduction Yeilds Over ZnS-MMT. *Geosci Eng*. 2012;(1):34-42.

102. Sato T, Usui S, Tsuchiya Y, D YK. Invention of outdoor closed type photobioreactor for microalgae. *Energy Convers Manag*. 2006;47:791-799. doi:10.1016/j.enconman.2005.06.010

103. Show PL, Tang MSY, Nagarajan D, Ling TC, Ooi C wei. A Holistic Approach to Managing Microalgae for Biofuel Applications. *Int J Mol Sci*. 2017;18(215). doi:10.3390/ijms18010215

104. Luu MT, Milani D, Abbas A. Analysis of CO2 utilization for methanol synthesis integrated with enhanced gas recovery. *J Clean Prod*. 2016;112:3540-3554. doi:10.1016/j.jclepro.2015.10.119

105. Ere J, Ateka A, Paula P. A comparative thermodynamic study on the CO2 conversion in the synthesis of methanol and of DME. *Energy*. 2017;120:796-804. doi:10.1016/j.energy.2016.11.129

106. Hunt A, Farmer T, Clark J. *Element Recovery and Sustainability*. (Hunt A, ed.). The Royal Society of Chemistry; 2013. doi:doi.org/10.1039/9781849737340

107. Chng LM, Lee KT, Chan DCJ. Evaluation on Microalgae Biomass for Bioethanol Production. *29th Symp Malaysian Chem Eng*. Published online 2016. doi:10.1088/1757-899X/206/1/012018

108. Rajarapu SP, Scharf ME. Saccharification of Agricultural Lignocellulose Feedstocks and Protein-Level Responses by a Termite Gut-Microbe Bioreactor. *Front Energy Res*. 2017;5. doi:10.3389/fenrg.2017.00005

109. Zhong J, Yang X, Wu Z, Liang B, Huang Y, Zhang T. State of the art and perspectives in heterogeneous catalysis of CO2 hydrogenation to methanol. *Chem Soc Rev*. 2020;49(5). doi:10.1039/c9cs00614a

110. Lu-xiang Z, Yong-chun Z, Shao-yun C. Effect of promoter TiO2 on the performance of

CuO – ZnO – Al2O3 catalyst for CO2 catalytic hydrogenation to methanol. *J Fuel Chem Technol*. 2011;39(12):912-917. doi:10.1016/S1872-5813(12)60002-4

111. Huang C, Chen S, Fei X, Liu D, Zhang Y. Catalytic Hydrogenation of CO2 to Methanol: Study of Synergistic Effect on Adsorption Properties of CO2 and H2 in CuO/ZnO/ZrO2 System. Published online 2015:1846-1861. doi:10.3390/catal5041846

112. Liaw BJ, Chen YZ. Liquid-phase synthesis of methanol from CO2/H2 over ultrafine CuB catalysts. *Appl Catal*. 2001;206:245-256.

113. Collins E, Chiavassa DL, Bonivardi AL, Baltana MA. Hydrogen spillover in Ga2O3-Pd/SiO2 catalysts for methanol synthesis from CO2/H2. *Catal Letters*. 2005;103(September):83-88. doi:10.1007/s10562-005-6507-5

114. Liu J, Shi J, He D, et al. Surface active structure of ultra-fine Cu/ZrO2 catalysts used for the CO2 + H2 to methanol reaction. *Appl Catal A Gen*. 2001;218:113-119.

115. An X, Li J, Zuo Y, Zhang Q, Wang D, Wang J. A Cu/Zn/Al/Zr Fibrous Catalyst that is an Improved CO2 Hydrogenation to Methanol Catalyst. *Catal Letters*. 2007;118:264-269. doi:10.1007/s10562-007-9182-x

116. Raudaskoski R, Niemela MV. The effect of ageing time on co-precipitated Cu/ZnO/ZrO2 catalysts used in methanol synthesis from CO2 and H2. *Top Catal*. 2007;45:57-60. doi:10.1007/s11244-007-0240-9

117. Guo X, Mao D, Wang S, Wu G, Lu G. Combustion synthesis of CuO – ZnO – ZrO2 catalysts for the hydrogenation of carbon dioxide to methanol. *Catal Commun*. 2009;10(13):1661-1664. doi:10.1016/j.catcom.2009.05.004

118. Arena F, Italiano G, Barbera K, et al. Applied Catalysis A: General Solid-state interactions, adsorption sites and functionality of Cu-ZnO/ZrO2 catalysts in the CO2 hydrogenation to CH3OH. *Appl Catal A Gen*. 2008;350:16-23. doi:10.1016/j.apcata.2008.07.028

119. Arena F, Italiano G, Barbera K, Bonura G, Spadaro L, Frusteri F. Basic evidences for methanol-synthesis catalyst design. *Catal Today*. 2009;143(2009):80-85. doi:10.1016/j.cattod.2008.11.022

120. Guo X, Mao D, Lu G, Wang S, Wu G. Glycine – nitrate combustion synthesis of CuO – ZnO – ZrO2 catalysts for methanol synthesis from CO2 hydrogenation. *J Catal*. 2010;271(2):178-185. doi:10.1016/j.jcat.2010.01.009

121. Jung KT, Bell AT. Effects of zirconia phase on the synthesis of methanol over zirconia-supported copper. *Catal Letters*. 2002;80(3). doi:1011-372X/02/0500-0063/0

122. Arena F, Barbera K, Italiano G, Bonura G, Spadaro L, Frusteri F. Synthesis , characterization and activity pattern of Cu – ZnO / ZrO 2 catalysts in the hydrogenation of carbon dioxide to methanol. 2007;249:185-194. doi:10.1016/j.jcat.2007.04.003

123. Saito M, Murata K. Development of high performance Cu / ZnO-based catalysts for methanol synthesis and the water-gas shift reaction. 2004;8(4):285-294.

124. Behrens M, Studt F, Kasatkin I, et al. The Active Site of MethanolSynthesis over Cu/ZnO/Al2O3Industrial Catalysts. *www.sciencemag.org*. 2012;759(May):893-898.

125. Bansode A, Urakawa A. Towards full one-pass conversion of carbon dioxide to methanol and methanol-derived products. *J Catal*. 2014;309:66-70. doi:10.1016/j.jcat.2013.09.005

126. Cai W, Ramirez P, Piscina D, Toyir J, Homs N. CO 2 hydrogenation to methanol over CuZnGa catalysts prepared using microwave-assisted methods. *Catal Today*. 2015;242:193-199. doi:10.1016/j.cattod.2014.06.012

127. Fiordaliso EM, Sharafutdinov I, Carvalho HWP, et al. Intermetallic GaPd 2 Nanoparticles on SiO 2 for Low-Pressure CO 2 Hydrogenation to Methanol : Catalytic Performance and In Situ Characterization. *Am Chem Soc*. Published online 2015. doi:10.1021/acscatal.5b01271

128. Ralston WT, An K, Brooks C, et al. High-performance hybrid oxide catalyst of manganese and cobalt for low-pressure methanol synthesis. *Nat Commun*. Published online 2015:1-5. doi:10.1038/ncomms7538

129. Yang X, Kattel S, Senanayake SD, et al. Low Pressure CO 2 Hydrogenation to Methanol over Gold Nanoparticles Activated on a CeO. *Am Chem Soc*. Published online 2015:2-5. doi:10.1021/jacs.5b06150

130. Martin O, Martín AJ, Mondelli C, et al. Indium Oxide as a Superior Catalyst for Methanol Synthesis by CO 2 Hydrogenation. Published online 2016:6261-6265. doi:10.1002/anie.201600943

131. Porosoff MD, Yan B, Chen JG. Environmental Science CO , methanol and hydrocarbons : challenges and opportunities. Published online 2016:62-73. doi:10.1039/c5ee02657a

132. Chen R, Zhao X, Jiao J, Li Y, Wei M. Surface-Modified Biochar with Polydentate Binding Sites for the Removal of Cadmium. *Int J Mol Sci*. Published online 2019:1775. doi:10.3390/ijms20071775

133. Wang J, Li G, Li Z, et al. A highly selective and stable ZnO-ZrO 2 solid solution catalyst for CO 2 hydrogenation to methanol. 2017;(October):1-11.

134. Liu X mei, Lu GQ, Yan Z feng, Beltramini J. Recent Advances in Catalysts for Methanol Synthesis via Hydrogenation of CO and CO 2. Published online 2003:6518-6530.

135. Hong Z shan, Cao Y, Deng J fa, Fan K nian. CO 2 hydrogenation to methanol over Cu / ZnO / Al 2 O 3 catalysts prepared by a novel gel-network-coprecipitation method. 2002;82(1):2-9.

136. Nitta Y, Fujimatsu T, Okamoto Y, Imanaka T. Effect of starting salt on catalytic behaviour of Cu-ZrO 2 catalysts in methanol synthesis from carbon dioxide. *Catal Letters*. 1992;17:157-165.

137. Słoczynski J, Grabowski R, Olszewski P, et al. Effect of metal oxide additives on the activity and stability of Cu / ZnO / ZrO 2 catalysts in the synthesis of methanol from CO 2 and H 2. 2006;310:127-137. doi:10.1016/j.apcata.2006.05.035

138. Słoczynski J, Grabowski R, Kozłowska A, et al. Effect of Mg and Mn oxide additions on structural and adsorptive properties of Cu / ZnO / ZrO 2 catalysts for the methanol synthesis from CO 2. *Elsevier*. 2003;249:129-138. doi:10.1016/S0926-860X(03)00191-1

139. Słoczynski J, Grabowski R, Kozłowska A, et al. Catalytic activity of the M/(3ZnO Á ZrO2) system (M = Cu , Ag , Au) in the hydrogenation of CO2 to methanol. *Appl Catal*. 2004;278:11-23. doi:10.1016/j.apcata.2004.09.014

140. Köppel RA, Stöcker C, Baiker A. Copper- and Silver – Zirconia Aerogels: Preparation, Structural Properties and Catalytic Behavior in Methanol Synthesis from Carbon Dioxide. *J Catal*. 1998;179:515-527. doi:10.1006/jcat.1998.2252

141. Carnes CL, Klabunde KJ. The catalytic methanol synthesis over nanoparticle metal oxide catalysts. *J Mol Catal A Chem*. 2003;194:227-236. doi:10.1016/S1381-1169(02)00525-3

142. Choi Y, Futagami K, Fujitani T, Nakamura J. The role of ZnO in Cu/ZnO methanol synthesis catalysts - morphology effect or active site model? *Appl Catal A Gen*. 2001;208:163-167. doi:10.1016/S0926-860X(00)00712-2

143. Wang L cun, Liu Y mei, Chen M, et al. Production of hydrogen by steam reforming of methanol over Cu/ZnO catalysts prepared via a practical soft reactive grinding route based on dry oxalate-precursor synthesis. *J Catal*. 2007;246:193-204. doi:10.1016/j.jcat.2006.12.006

144. Avgouropoulos G, Ioannides T. Selective CO oxidation over CuO-CeO2 catalysts prepared via the urea - nitrate combustion method. *Appl Catal A Gen*. 2003;244:155-167.

145. Yazhi YIN, Bing HU, Guoliang LIU, Xiaohai Z, Xinlin H. ZnO @ ZIF-8 Core-Shell Structure as Host for Highly Selective and Stable Pd / ZnO Catalysts for Hydrogenation of CO2 to Methanol. *Acta Physico-Chimica Sin*. 2019;35(3):327-336. doi:10.3866/PKU.WHXB201803212

146. Zhang F hua, Liu C, Li W, Tian G long, Xie J hua, Zhou Q lin. An Efficient Ruthenium Catalyst Bearing Tetradentate Ligand for Hydrogenations of Carbon Dioxide †. Published online 2018:1000-1002. doi:10.1002/cjoc.201800278

147. Chen Y, Choi S, Thompson LT. Low-Temperature CO2 Hydrogenation to Liquid Products via a Heterogeneous Cascade Catalytic System. *ACS Catal*. 2015;5:1717-1725. doi:10.1021/cs501656x

148. Yanfang LIU, Bing HU, Yazhi YIN, Guoliang LIU, Xinlin H. One-Pot Surfactant-Free Synthesis of Transition Metal / ZnO Nanocomposites for Catalytic Hydrogenation of CO2 to Methanol. *Acta Physico-Chimica Sin*. 2019;35(2):223-229. doi:10.3866/PKU.WHXB201802263

149. Marpani F, Pinelo M, Meyer AS. Enzymatic conversion of CO2 to CH3OH via reverse dehydrogenase cascade biocatalysis: Quantitative comparison of efficiencies of immobilized enzyme systems. *Biochem Eng J*. 2017;127:217-228. doi:10.1016/j.bej.2017.08.011

150. Pandey D, Daverey A, Arunachalam K. Biochar: Production, Properties and Emerging Role as a Support for Enzyme Immobilization. *J Clean Prod*. 2020;255. doi:10.1016/j.jclepro.2020.120267

151. Obert R, Dave BC. Enzymatic conversion of carbon dioxide to methanol: Enhanced methanol production in silica sol-gel matrices. *J Am Chem Soc*. 1999;121(51):12192-12193. doi:10.1021/ja991899r

152. Shi J, Jiang Y, Jiang Z, et al. Enzymatic conversion of carbon dioxide. *Chem Soc Rev*. 2015;44(17):5981-6000. doi:10.1039/c5cs00182j

153. Zhang Y, Ge J, Liu Z. Enhanced Activity of Immobilized or Chemically Modified Enzymes. *ACS Catal*. 2015;5:4503-4513. doi:10.1021/acscatal.5b00996

154. Sheldon RA, Brady D. The limits to biocatalysis: Pushing the envelope. *Chem Commun*. 2018;54(48):6088-6104. doi:10.1039/c8cc02463d

155. Bornscheuer UT, Huisman GW, Kazlauskas RJ, Lutz S, Moore JC, Robins K. Engineering the third wave of biocatalysis. *Nature*. 2012;485(7397):185-194.

doi:10.1038/nature11117

156. Rodrigues RC, Ortiz C, Berenguer-Murcia Á, Torres R, Fernández-Lafuente R. Modifying enzyme activity and selectivity by immobilization. *Chem Soc Rev*. 2013;42(15):6290-6307. doi:10.1039/c2cs35231a

157. Chapman J, Ismail AE, Dinu CZ. Industrial applications of enzymes: Recent advances, techniques, and outlooks. *Catalysts*. 2018;8(6). doi:10.3390/catal8060238

158. Basso A, Serban S. Industrial applications of immobilized enzymes - A review. *Mol Catal*. 2019;479:2468-8231. doi:10.1016/j.mcat.2019.110607

159. Anastas, P. T.; Warner JC. 12 Principles of Green Chemistry. ACS. 1998. https://www.acs.org/green-chemistry-sustainability/principles/12-principles-of-green-chemistry.htmL

160. Hosseinkhani S, Nemat-gorgani M. Partial unfolding of carbonic anhydrase provides a method for its immobilization on hydrophobic adsorbents and protects it against irreversible thermoinactivation. 2003;33:179-184. doi:10.1016/S0141-0229(03)00097-8

161. Cowan DA, Fernandez-Lafuente R. Enhancing the functional properties of thermophilic enzymes by chemical modification and immobilization. *Enzyme Microb Technol*. 2011;49(4):326-346. doi:10.1016/j.enzmictec.2011.06.023

162. Imam HT, Marr PC, Marr AC. Enzyme entrapment, biocatalyst immobilization without covalent attachment. *Green Chem*. 2021;23(14):4980-5005. doi:10.1039/d1gc01852c

163. Iyer P V., Ananthanarayan L. Enzyme stability and stabilization - Aqueous and non - aqueous environment. *Process Biochem*. 2008;43(10):1019-1032. doi:10.1016/j.procbio.2008.06.004

164. Franssen MCR, Steunenberg P, Scott EL, Zuilhof H, Sanders JPM. Immobilised enzymes in biorenewables production. *Chem Soc Rev*. 2013;42(15):6491-6533. doi:10.1039/c3cs00004d

165. Jesionowski T, Zdarta J, Krajewska B. Enzyme immobilization by adsorption: a review. *Springer Sci*. 2014;(20):801-821. doi:10.1007/s10450-014-9623-y

166. Sharma S, Berne BJ, Kumar SK. Thermal and Structural Stability of Adsorbed Proteins. *Biophysj*. 2010;99(4):1157-1165. doi:10.1016/j.bpj.2010.05.030

167. Sheldon RA, van Pelt S. Enzyme immobilisation in biocatalysis: Why, what and how. *Chem Soc Rev*. 2013;42(15):6223-6235. doi:10.1039/c3cs60075k

168. Bayne L, Ulijn R V., Halling PJ. Effect of pore size on the performance of immobilised enzymes. *Chem Soc Rev*. 2013;42(23):9000-9010. doi:10.1039/c3cs60270b

169. Zdarta J, Meyer AS, Jesionowski T, Pinelo M. A general overview of support materials for enzyme immobilization: Characteristics, properties, practical utility. *Catalysts*. 2018;8(2). doi:10.3390/catal8020092

170. Mateo C, Palomo JM, Fernandez-Lorente G, Guisan JM, Fernandez-Lafuente R. Improvement of enzyme activity, stability and selectivity via immobilization techniques. *Enzyme Microb Technol*. 2007;40(6):1451-1463. doi:10.1016/j.enzmictec.2007.01.018

171. Verma P, Kuwahara Y, Mori K, Raja R, Yamashita H. *Functionalized Mesoporous SBA-15 Silica: Recent Trends and Catalytic Applications*. Royal Society of Chemistry; 2020. doi:10.1039/d0nr00732c

172. Obert R, Dave BC. Enzymatic conversion of carbon dioxide to methanol: Enhanced methanol production in silica sol-gel matrices. *J Am Chem Soc*. 1999;121(51):12192-12193. doi:10.1021/ja991899r

173. Jiang Z, Wu H, Xu S, Huang S. *Enzymatic Conversion of Carbon Dioxide to Methanol by Dehydrogenases Encapsulated in Sol-Gel Matrix*. Utilization of Greenhouse Gases; 2003. doi:10.1021/bk-2003-0852.ch014

174. Xu S wei, Lu Y, Li J, Jiang Z yi, Wu H. Efficient Conversion of CO 2 to Methanol Catalyzed by Three Dehydrogenases Co-encapsulated in an Alginate - Silica (ALG - SiO 2) Hybrid Gel. Published online 2006:4567-4573.

175. Jiang Y, Sun Q, Zhang L, Jiang Z. Capsules-in-bead scaffold: A rational architecture for spatially separated multienzyme cascade system. *J Mater Chem*. 2009;19(47):9068-9074. doi:10.1039/b914268a

176. Sun Q, Jiang Y, Jiang Z, Zhang L, Sun X, Li J. Green and Efficient Conversion of CO 2 to Methanol by Biomimetic Coimmobilization of Three Dehydrogenases in Protamine-Templated Titania. *Ind Eng Chem Res*. 2009;48:4210-4215. doi:10.1021/ie801931j

177. Cazelles R, Drone J, Fajula F, Ersen O, Moldovan S, Galarneau A. Reduction of CO2 to methanol by a polyenzymatic system encapsulated in phospholipids–silica nanocapsules. *R Soc Chem Cent Natl la Rech Sci*. Published online 2013:3721-3730. doi:10.1039/c3nj00688c

178. Wang X, Li Z, Shi J, Wu H, Jiang Z, Zhang W. Bioinspired Approach to Multienzyme Cascade System Construction for Efficient Carbon Dioxide Reduction. *ACS Catal*. 2014;(4):962-972. doi:10.1021/cs401096c

179. Ji X, Su Z, Wang P, Ma G, Zhang S. Tethering of nicotinamide adenine dinucleotide inside hollow nanofibers for high-yield synthesis of methanol from carbon dioxide catalyzed by coencapsulated multienzymes. *ACS Nano*. 2015;9(4):4600-4610. doi:10.1021/acsnano.5b01278

180. El-Zahab B, Donnelly D, Ping W. Particle-Tethered NADH for Production of Methanol From CO2 Catalyzed by Coimmobilized Enzymes. *Biotechnol Bioeng*. Published online 2007:508-514. doi:DOI 10.1002/bit.21584

181. Peretz S, Anghel DF, Vasilescu E, Florea-Spiroiu M, Stoian C, Zgherea G. Synthesis, characterization and adsorption properties of alginate porous beads. *Polym Bull*. 2015;72(12):3169-3182. doi:10.1007/s00289-015-1459-4

182. Markandan K, Sankaran R, Tiong YW, et al. A Review on the Progress in Chemo-Enzymatic Processes for CO2 Conversion and Upcycling. *Catalysts*. 2023;13:611. doi:doi.org/10.3390/ catal13030611

183. Favre N, Christ ML, Pierre AC. Enzymatic Biocatalytic capture of CO 2 with carbonic anhydrase and its transformation to solid carbonate. *J Mol Catal B*. 2009;60:163-170. doi:10.1016/j.molcatb.2009.04.018

184. Smith KS, Ferry JG. Prokaryotic carbonic anhydrases. *Microbiol Rev*. 2000;24:335-366. doi:10.1111/j.1574-6976.2000.tb00546.x

185. Ren S, Jiang S, Yan X, Chen R, Cui H. Challenges and Opportunities: Porous Supports in Carbonic Anhydrase Immobilization. *J CO2 Util*. 2020;42(100):101305. doi:10.1016/j.jcou.2020.101305

186. Wang Y, Li M, Zhao Z, Liu W. Effect of carbonic anhydrase on enzymatic conversion of CO2 to formic acid and optimization of reaction conditions. *J Mol Catal B Enzym*. 2015;116:89-94. doi:10.1016/j.molcatb.2015.03.014

187. Liao Q, Liu W, Meng Z. Strategies for overcoming the limitations of enzymatic carbon dioxide reduction. *Biotechnol Adv*. 2022;60(July):108024. doi:10.1016/j.biotechadv.2022.108024

188. Mao M, Zhai T, Meng L, Meng Z, Liu W. Controllable preparation of mesoporous silica and its application in enzyme-catalyzed CO2 reduction. *Chem Eng J*. 2022;437(P2):135479. doi:10.1016/j.cej.2022.135479

189. Gao S, Mohammad M, Yang HC, et al. Janus Reactors with Highly Efficient Enzymatic CO2 Nanocascade at Air-Liquid Interface. *ACS Appl Mater Interfaces*. 2017;9(49):42806-42815. doi:10.1021/acsami.7b14465

190. Statista. Monthly methanol spot prices worldwide from January 2020 to July 2024, by region. 2024. https://www.statista.com/statistics/1323381/monthly-methanol-spot-prices-worldwide-by-region/

191. Hocquet D, Muller A, Bertrand X. What happens in hospitals does not stay in hospitals: antibiotic-resistant bacteria in hospital wastewater systems. *J Hosp Infect*. Published online 2016. doi:10.1016/j.jhin.2016.01.010

192. Chafik A, El K, Essamadi A, Yildirim S. Efficient sequestration of carbon dioxide into calcium carbonate using a novel carbonic anhydrase purified from liver of camel (Camelus dromedarius). 2020;42(July).

193. Effendi W, Chiu C yaw, Chang Y kaung, Ng I son. Crosslinked on novel nanofibers with thermophilic carbonic anhydrase for carbon dioxide sequestration. *Int J Biol Macromol*. 2020;152:930-938. doi:10.1016/j.ijbiomac.2019.11.234

194. Perfetto R, Prete S Del, Vullo D, et al. Production and covalent immobilisation of the recombinant bacterial carbonic anhydrase (SspCA) onto magnetic nanoparticles. *J Enzyme Inhib Med Chem*. 2017;6366(May). doi:10.1080/14756366.2017.1316719

195. Cowan DA, Fernandez-lafuente R. Enzyme and Microbial Technology Enhancing the functional properties of thermophilic enzymes by chemical modification and immobilization. *Enzyme Microb Technol*. 2011;49(4):326-346. doi:10.1016/j.enzmictec.2011.06.023

196. Wanjari S, Prabhu C, Yadav R, Satyanarayana T, Labhsetwar N, Rayalu S. Immobilization of carbonic anhydrase on chitosan beads for enhanced carbonation reaction. *Process Biochem*. 2011;46(4):1010-1018. doi:10.1016/j.procbio.2011.01.023

197. Lim HK, Kim DR, Hwang IT. Sequestration of CO2 into CaCO3 using Carbonic Anhydrase Immobilization on Functionalized Aluminum Oxide. *Appl Biochem Microbiol*. 2019;55(4):375-379. doi:10.1134/S0003683819040112

198. Vinoba M, Bhagiyalakshmi M, Jeong SK, Yoon YII, Nam SC. Capture and Sequestration of CO2 by Human Carbonic Anhydrase Covalently Immobilized onto Amine-Functionalized SBA-15. 2011;(Ic):20209-20216.

199. Bhattacharya S, Schiavone M, Chakrabarti S, Bhattacharya SK. CO2 hydration by immobilized carbonic anhydrase. 2003;117:111-117.

200. Sun J, Wang C, Wang Y, Ji S, Liu W. Immobilization of carbonic anhydrase on

polyethylenimine/dopamine codeposited membranes. 2019;47784:1-9. doi:10.1002/app.47784

201. Merle G, Fradette S, Madore E, Barralet JE. Electropolymerized Carbonic Anhydrase Immobilization for Carbon Dioxide Capture. Published online 2014.

202. Zhang S, Lu Y, Ye X. Catalytic behavior of carbonic anhydrase enzyme immobilized onto nonporous silica nanoparticles for enhancing CO 2 absorption into a carbonate solution. *Int J Greenh Gas Control*. 2013;13:17-25. doi:10.1016/j.ijggc.2012.12.010

203. Hou J, Dong G, Xiao B, Malassigne C, Chen V. Preparation of titania based biocatalytic nanoparticles and membranes for CO2 conversion. *J Mater Chem A*. Published online 2015:3332-3342. doi:10.1039/c4ta05760k

204. Hussein A, Al-dhrub A, Sahin S, Ozmen I, Tunca E, Bulbul M. Immobilization and characterization of human carbonic anhydrase I on amine functionalized magnetic nanoparticles. *Process Biochem*. 2017;57(December 2016):95-104. doi:10.1016/j.procbio.2017.03.025

205. Jun S hyun, Yang J, Jeon H, et al. Stabilized and Immobilized Carbonic Anhydrase on Electrospun Nanofibers for Enzymatic CO2 Conversion and Utilization in Expedited Microalgal Growth. Published online 2020. doi:10.1021/acs.est.9b05284

206. Li J, Zhou X, Zhang L, Di H, Wu H, Yang L. Investigation on the Immobilization of Carbonic Anhydrase and the Catalytic Absorption of Carbon Dioxide. *Energy and Fuels*. Published online 2017. doi:10.1021/acs.energyfuels.6b02652

207. Han Y, Yu S, Liu L, et al. Silk fibroin-based hydrogels as a protective matrix for stabilization of enzymes against pH denaturation. *Mol Catal*. 2018;457(April):24-32. doi:10.1016/j.mcat.2018.07.009

208. Yadav RR, Mudliar SN, Shekh AY, et al. Immobilization of carbonic anhydrase in alginate and its influence on transformation of CO2 to calcite. *Process Biochem*. 2012;47(4):585-590. doi:10.1016/j.procbio.2011.12.017

209. Sukumaran MO V, Sankar S. Immobilization and characterization of carbonic anhydrase purified from E . coli MO1 and its influence on CO2 sequestration. Published online 2013:1813-1820. doi:10.1007/s11274-013-1343-z

210. Zhu Y, Li W, Sun G, Tang Q, Bian H. Enzymatic properties of immobilized carbonic anhydrase and the biocatalyst for promoting CO2 capture in vertical reactor. *Int J Greenh Gas Control*. 2016;49:290-296. doi:10.1016/j.ijggc.2016.03.016

211. Zhang Y tao, Zhi T tian, Zhang L, Huang H, Chen H lin. Immobilization of carbonic anhydrase by embedding and covalent coupling into nanocomposite hydrogel containing hydrotalcite. *Polymer (Guildf)*. 2009;50(24):5693-5700. doi:10.1016/j.polymer.2009.09.067

212. Forsyth C, Yip TWS, Patwardhan S V. CO2 sequestration by enzyme immobilized onto bioinspired silica. *Chem Commun*. 2013;49(31):3191-3193. doi:10.1039/c2cc38225c

213. Badjic JD, Kostic NM. Effects of Encapsulation in Sol - Gel Silica Glass on Esterase Activity , Conformational Stability , and Unfolding of Bovine Carbonic Anhydrase II. 1999;(14):3671-3679.

214. Shao P, Chen H, Ying Q, Zhang S. Structure – Activity Relationship of Carbonic Anhydrase Enzyme Immobilized on Various Silica-Based Mesoporous Molecular Sieves for CO 2

Absorption into a Potassium Carbonate Solution. Published online 2020. doi:10.1021/acs.energyfuels.9b03860

215. Wanjari S, Prabhu C, Satyanarayana T, Vinu A, Rayalu S. Immobilization of carbonic anhydrase on mesoporous aluminosilicate for carbonation reaction. *Microporous Mesoporous Mater*. 2012;160:151-158. doi:10.1016/j.micromeso.2012.04.005

216. Vinoba M, Bhagiyalakshmi M, Kwan S, Ii Y, Chan S. Immobilization of carbonic anhydrase on spherical SBA-15 for hydration and sequestration of CO 2. *Colloids and Surfaces*. 2012;90:91-96. doi:10.1016/j.colsurfb.2011.10.001

217. Vinoba M, Bhagiyalakshmi M, Kwan S, Ii Y, Chan S. Carbonic anhydrase conjugated to nanosilver immobilized onto mesoporous SBA-15 for sequestration of CO 2. *J Mol Catal*. 2012;75:60-67. doi:10.1016/j.molcatb.2011.11.010

218. Vinoba M, Lim KS, Lee SH, Jeong SK, Alagar M. Immobilization of Human Carbonic Anhydrase on Gold Nanoparticles Assembled onto Amine / Thiol-Functionalized Mesoporous SBA-15 for Biomimetic Sequestration of CO 2. Published online 2011:6227-6234.

219. Molina-Fernández C, Luis P. Immobilization of carbonic anhydrase for CO2capture and its industrial implementation: A review. *J CO2 Util*. 2021;47(December 2020). doi:10.1016/j.jcou.2021.101475

220. Sharma T, Sharma S, Kamyab H, Kumar A. Energizing the CO2 utilization by chemo-enzymatic approaches and potentiality of carbonic anhydrases: A review. *J Clean Prod*. 2020;247:119138. doi:10.1016/j.jclepro.2019.119138

221. Effendi SSW, Ng IS. The prospective and potential of carbonic anhydrase for carbon dioxide sequestration: A critical review. *Process Biochem*. 2019;87(August):55-65. doi:10.1016/j.procbio.2019.08.018

222. Ünlü A, Duman-Özdamar ZE, Çaloğlu B, Binay B. Enzymes for Efficient CO2 Conversion. *Protein J*. 2021;40(4):489-503. doi:10.1007/s10930-021-10007-8

223. Sillu D, Achal V. Carbon dioxide sequestration with carbonic anhydrase nanobiocatalysts: a review. *Environ Chem Lett*. 2024;22(5):2213-2239. doi:10.1007/s10311-024-01755-x

224. Hu Y, Dai L, Liu D, Du W, Wang Y. Progress & prospect of metal-organic frameworks (MOFs) for enzyme immobilization (enzyme/MOFs). *Renew Sustain Energy Rev*. 2018;91(May 2017):793-801. doi:10.1016/j.rser.2018.04.103

225. Patil PD, Kelkar RK, Patil NP, et al. Magnetic nanoflowers: a hybrid platform for enzyme immobilization. *Crit Rev Biotechnol*. 2024;44(5):795-816. doi:10.1080/07388551.2023.2230518

226. Maghraby YR, El-Shabasy RM, Ibrahim AH, Azzazy HMES. Enzyme Immobilization Technologies and Industrial Applications. *ACS Omega*. 2023;8(6):5184-5196. doi:10.1021/acsomega.2c07560

227. Vinoba M, Bhagiyalakshmi M, Jeong SK, Yoon YII, Nam SC. Immobilization of carbonic anhydrase on spherical SBA-15 for hydration and sequestration of CO 2. *Colloids Surfaces B Biointerfaces*. 2012;90(1):91-96. doi:10.1016/j.colsurfb.2011.10.001

228. Vinoba M, Lim KS, Lee SK, Jeong SK, Alagar M. Immobilization of human carbonic anhydrase on gold nanoparticles assembled onto amine/thiol-functionalized

mesoporous SBA-15 for biomimetic sequestration of CO2. *Langmuir*. 2011;27(10):6227-6234. doi:10.1021/la105029h

229. Hartmann M, Kostrov X. Immobilization of enzymes on porous silicas – benefits and challenges. *Chem Soc Rev*. 2013;42(15):6277-6289. doi:10.1039/c3cs60021a

230. Coradin T, Lopez PJ. Biogenic silica patterning: Simple chemistry or subtle biology? *ChemBioChem*. 2003;4(4):251-259. doi:10.1002/cbic.200390044

231. Pilling R, Patwardhan S V. Recent Advances in Enabling Green Manufacture of Functional Nanomaterials: A Case Study of Bioinspired Silica. *ACS Sustain Chem Eng*. 2022;10(37):12048-12064. doi:10.1021/acssuschemeng.2c02204

232. Iler RK. Polymerization of Silica. In: *The Chemistry of Silica: Solubility, Polymerisation, Colloid and Surface Properties and Biochemistry*. John Wiley and Sons; 1979:172-312.

233. Kato M, Sakai-Kato K, Toyo'oka T. Silica sol-gel monolithic materials and their use in a variety of applications. *J Sep Sci*. 2005;28(15):1893-1908. doi:10.1002/jssc.200500225

234. Bergna HE. The Colloid Chemistry of Silica: An Overview. *Soil Sci*. 1994;80(1):86. doi:10.1097/00010694-195507000-00014

235. Pierre AC, Pierre AC. The Sol-Gel Encapsulation of Enzymes. *Biocatal Biotransformation*. 2004;2422(2004). doi:10.1080/10242420412331283314

236. Hoffmann F, Cornelius M, Morell J, Fröba M. Silica-based mesoporous organic-inorganic hybrid materials. *Angew Chemie - Int Ed*. 2006;45(20):3216-3251. doi:10.1002/anie.200503075

237. Zhang R, Hua M, Liu H, Li J. How to design nanoporous silica nanoparticles in regulating drug delivery: Surface modification and porous control. *Mater Sci Eng B*. 2021;263(146):114835. doi:10.1016/j.mseb.2020.114835

238. Malgras V, Ji Q, Kamachi Y, et al. Templated synthesis for nanoarchitectured porous materials. *Bull Chem Soc Jpn*. 2015;88(9):1171-1200. doi:10.1246/bcsj.20150143

239. Patwardhan S V., Manning JRH, Chiacchia M. Bioinspired synthesis as a potential green method for the preparation of nanomaterials: Opportunities and challenges. *Curr Opin Green Sustain Chem*. 2018;12:110-116. doi:10.1016/j.cogsc.2018.08.004

240. Drummond C, McCann R, Patwardhan S V. A feasibility study of the biologically inspired green manufacturing of precipitated silica. *Chem Eng J*. 2014;244:483-492. doi:10.1016/j.cej.2014.01.071

241. Walsh TR, Knecht MR. Biointerface Structural Effects on the Properties and Applications of Bioinspired Peptide-Based Nanomaterials. *Chem Rev*. 2017;117(20):12641-12704. doi:10.1021/acs.chemrev.7b00139

242. Patwardhan S V. Biomimetic and bioinspired silica: Recent developments and applications. *Chem Commun*. 2011;47(27):7567-7582. doi:10.1039/c0cc05648k

243. Patwardhan S V., Clarson SJ, Perry CC. On the role(s) of additives in bioinspired silicification. *Chem Commun*. 2005;(9):1113-1121. doi:10.1039/b416926c

244. Belton DJ, Patwardhan S V., Annenkov V V., Danilovtseva EN, Perry CC. From biosilicification to tailored materials: Optimizing hydrophobic domains and resistance to protonation of polyamines. *Proc Natl Acad Sci U S A*. 2008;105(16):5963-5968. doi:10.1073/pnas.0710809105

245. Manning JRH, Brambila C, Patwardhan S V. Unified mechanistic interpretation of amine-assisted silica synthesis methods to enable design of more complex materials. *Mol Syst Des Eng*. 2021;6(3):170-196. doi:10.1039/d0me00131g

246. Forsyth C, Patwardhan S V. Controlling performance of lipase immobilised on bioinspired silica. *J Mater Chem B*. 2013;1(8):1164-1174. doi:10.1039/c2tb00462c

247. Li L, Jiang Z, Wu H, Feng Y, Li J. Protamine-induced biosilica as efficient enzyme immobilization carrier with high loading and improved stability. *Mater Sci Eng C*. 2009;29(6):2029-2035. doi:10.1016/j.msec.2009.03.020

248. Jo BH, Seo JH, Yang YJ, et al. Bioinspired Silica Nanocomposite with Autoencapsulated Carbonic Anhydrase as a Robust Biocatalyst for CO 2 Sequestration. *ACS Catal*. Published online 2014. doi:dx.doi.org/10.1021/cs5008409

249. Kuan IC, Wu JC, Lee SL, Tsai CW, Chuang CA, Yu CY. Stabilization of d-amino acid oxidase from Rhodosporidium toruloides by encapsulation in polyallylamine-mediated biomimetic silica. *Biochem Eng J*. 2010;49(3):408-413. doi:10.1016/j.bej.2010.02.003

250. Shi J, Jiang Z. An efficient and recyclable enzyme catalytic system constructed through the synergy between biomimetic mineralization and polyamine-salt aggregate assembly. *J Mater Chem B*. 2014;2(28):4435-4441. doi:10.1039/c4tb00440j

251. Naik RR, Tomczak MM, Luckarift HR, Spain JC, Stone MO. Entrapment of enzymes and nanoparticles using biomimetically synthesized silica. *Chem Commun*. 2004;4(15):1684-1685. doi:10.1039/b404586f

252. Rao A, Bankar A, Shinde A, Kumar AR, Gosavi S, Zinjarde S. Phyto-inspired silica nanowires: Characterization and application in lipase immobilization. *ACS Appl Mater Interfaces*. 2012;4(2):871-877. doi:10.1021/am201543e

253. Haase NR, Shian S, Sandhage KH, Kröger N. Biocatalytic nanoscale coatings through biomimetic layer-by-layer mineralization. *Adv Funct Mater*. 2011;21(22):4243-4251. doi:10.1002/adfm.201101202

254. Betancor L, Luckarift HR. Bioinspired enzyme encapsulation for biocatalysis. *Trends Biotechnol*. 2008;26(10):566-572. doi:10.1016/j.tibtech.2008.06.009

255. Manning JRH, Yip TWS, Centi A, Jorge M, Patwardhan S V. An Eco-Friendly , Tunable and Scalable Method for Producing Porous Functional Nanomaterials Designed Using Molecular Interactions. Published online 2017:1683-1691. doi:10.1002/cssc.201700027

256. González ME, Cea M, Sangaletti N, et al. Biochar derived from agricultural and forestry residual biomass: Characterization and potential application for enzymes immobilization. *J Biobased Mater Bioenergy*. 2013;7(6):724-732. doi:10.1166/jbmb.2013.1373

257. Matuoog N, Li K, Yan Y. Thermomyces lanuginosus lipase immobilized on magnetic nanoparticles and its application in the hydrolysis of fish oil. *J Food Biochem*. 2018;42(5). doi:10.1111/jfbc.12549

258. Singh B, Camps-Abestian M, Lehmann J. *Biochar: A Guide to Analytical Methods*. Taylor & Francis; 2017. doi:10.1111/sum.12389

259. Sajjadi B, Zubatiuk T, Leszczynska D, Chen WY. Chemical activation of biochar for energy and Environmental Applications: A Comprehensive Review. *Rev Chem Eng*. 2018;35(7):777-815. doi:doi.org/10.1515/revce-2018-0003

260. Hanefeld U, Magner E. Understanding enzyme immobilisation. Published online 2009:453-468. doi:10.1039/b711564b

261. Bugg TDH. *Introduction to Enzyme and Coenzyme Chemistry*. Wiley; 2012. doi:10.1002/9781118348970

262. Essandoh M, Kunwar B, Pittman CU, Mohan D, MLsna T. Sorptive removal of salicylic acid and ibuprofen from aqueous solutions using pine wood fast pyrolysis biochar. *Chem Eng J*. 2015;265:219-227. doi:10.1016/j.cej.2014.12.006

263. Thommes M, Kaneko K, Neimark A V, et al. Physisorption of gases, with special reference to the evaluation of surface area and pore size distribution (IUPAC Technical Report). *Pure Appl Chem*. 2015;87:1051-1069. doi:10.1515/pac-2014-1117

264. Micromeritics. Gas Adsorption. https://micromeritics.com/gas-adsorption/

265. Leszczynska D. Impact of Biomass Source and Pyrolysis Parameters on Physicochemical Properties of Biochar Manufactured for Innovative Applications. 2020;8(July). doi:10.3389/fenrg.2020.00138

266. Micromeritics. 3Flex: High Performance Gas Adsorption. 2025. https://micromeritics.com/products/3flex/#elementor-toc__heading-anchor-1

267. Schlumberger C, Scherdel C, Kriesten M, et al. Reliable surface area determination of powders and meso/macroporous materials: Small-angle X-ray scattering and gas physisorption. *Microporous Mesoporous Mater*. 2022;329. doi:10.1016/j.micromeso.2021.111554

268. Micromeritics. Mercury Intrusion. 2025. https://micromeritics.com/porosimetry/

269. Schlumberger C, Thommes M. Characterization of Hierarchically Ordered Porous Materials by Physisorption and Mercury Porosimetry—A Tutorial Review. *Adv Mater Interfaces*. 2021;8(4). doi:10.1002/admi.202002181

270. Spokas KA. Review of the stability of biochar in soils: Predictability of O:C molar ratios. *Carbon Manag*. 2010;1(2):289-303. doi:10.4155/cmt.10.32

271. Adhikari S, Moon E, Paz-Ferreiro J, Timms W. Comparative analysis of biochar carbon stability methods and implications for carbon credits. *Sci Total Environ*. 2024;914:0048-9697. doi:10.1016/j.scitotenv.2023.169607

272. Leng L, Huang H, Li H, Li J, Zhou W. Biochar stability assessment methods: A review. *Sci Total Environ*. 2019;647:210-222. doi:10.1016/j.scitotenv.2018.07.402

273. Berthomieu C, Hienerwadel R. Fourier transform infrared (FTIR) spectroscopy. *Photosynth Res*. 2009;101(2-3):157-170. doi:10.1007/s11120-009-9439-x

274. Manning JRH, Routoula E, Patwardhan S V. Preparation of Functional Silica Using a Bioinspired Method. *JOVE J Vis Exp*. 2018;138:1-9. doi:10.3791/57730

275. Agilent. *The Basics of UV-Vis Spectrophotometry*.; 2021.

276. Forsyth C, Yip TWS, Patwardhan S V. Electronic Supporting Information: CO2 sequestration by enzyme immobilized onto bioinspired silica. *Chem Commun*. 2013;49(31):3191-3193. doi:10.1039/c2cc38225c

277. Lindskog S, Nilsson A. The Location of Tryptophanyl Groups in Human and Bovine Carbonic Anhydrases. Ultraviolet Difference Spectra and Chemical Modification.

Biochim Biophys Acta. 1973;295:117-130. doi:10.1016/0005-2795(73)90079-2

278. Wang PY, Yang CT, Chu LK. Differentiating the protein dynamics using fluorescence evolution of tryptophan residue(s): A comparative study of bovine and human serum albumins upon temperature jump. *Chem Phys Lett*. 2021;781(July):138998. doi:10.1016/j.cplett.2021.138998

279. Leito LSEIRAKIKI. Uncertainty sources in UV-Vis spectrophotometric measurement. *Accredit Qual Assur*. 2006;11:246-255. doi:10.1007/s00769-006-0124-x

280. Anderson J, Byrne T, Woelfel KJ, Meany JE, Spyridis GT, Pocker Y. The hydrolysis of p-nitrophenyl acetate: A versatile reaction to study enzyme kinetics. *J Chem Educ*. 1994;71(8):715-718. doi:10.1021/ed071p715

281. Abdullah SN, Hamzah F. Kinetics Of Free Carbonic Anhydrase In Conversion Of P-Nitrophenyl Acetate Into P-Nitrophenol. *Solid State Sci Technol*. 2018;26(2):169-174.

282. Talbert JN, Goddard JM. Enzymes on material surfaces. *Colloids Surfaces B Biointerfaces*. 2012;93:8-19. doi:10.1016/j.colsurfb.2012.01.003

283. Rozzell JD. Commercial Scale Biocatalysis: Myths and realities. *Chim Oggi*. 1998;17(5-6):2243-2261. doi:10.1016/s0968-0896(99)00159-5

284. Přenosil JE, Kut ÖM, Irving J. Dunn, Heinzle E. Biocatalysis, 2. Immobilized Biocatalysts. In: *Ullmann's Encyclopedia of Industrial Chemistry*. ; 2009. doi:10.1002/14356007.a14

285. Di Cosimo R, Mc Auliffe J, Poulose AJ, Bohlmann G. Industrial use of immobilized enzymes. *Chem Soc Rev*. 2013;42(15):6437-6474. doi:10.1039/c3cs35506c

286. Hernandez K, Fernandez-Lafuente R. Control of protein immobilization: Coupling immobilization and site-directed mutagenesis to improve biocatalyst or biosensor performance. *Enzyme Microb Technol*. 2011;48(2):107-122. doi:10.1016/j.enzmictec.2010.10.003

287. Liese A, Hilterhaus L. Evaluation of immobilized enzymes for industrial applications. *Chem Soc Rev*. 2013;42(15):6236-6249. doi:10.1039/c3cs35511j

288. Gray CJ, Weissenborn MJ, Eyers CE, Flitsch SL. Enzymatic reactions on immobilised substrates. *Chem Soc Rev*. 2013;42(15):6378-6405. doi:10.1039/c3cs60018a

289. Fernandez-Lafuente R. Stabilization of multimeric enzymes: Strategies to prevent subunit dissociation. *Enzyme Microb Technol*. 2009;45(6-7):405-418. doi:10.1016/j.enzmictec.2009.08.009

290. Cao L, van Langen L, Sheldon RA. Immobilised enzymes: carrier-bound or carrier-free? *Curr Opin Biotechnol*. 2003;14(4):387-394. doi:10.1016/S0958-1669(03)00096-X

291. Cao L. Immobilised enzymes: Science or art? *Curr Opin Chem Biol*. 2005;9(2):217-226. doi:10.1016/j.cbpa.2005.02.014

292. Cao L, Van Rantwijk F, Sheldon RA. Cross-linked enzyme aggregates: A simple and effective method for the immobilization of penicillin acylase. *Org Lett*. 2000;2(10):1361-1364. doi:10.1021/ol005593x

293. Bilal M, Iqbal HMN. Naturally-derived biopolymers: Potential platforms for enzyme immobilization. *Int J Biol Macromol*. 2019;130:462-482. doi:10.1016/j.ijbiomac.2019.02.152

294. Zdarta J, Meyer AS, Jesionowski T, Pinelo M. Developments in support materials for immobilization of oxidoreductases: A comprehensive review. *Adv Colloid Interface Sci*. 2018;258:1-20. doi:10.1016/j.cis.2018.07.004

295. Santos MPF, Brito MJP, Junior ECS, Bonomo RCF, Veloso CM. Pepsin immobilization on biochar by adsorption and covalent binding, and its application for hydrolysis of bovine casein. *J Chem Technol Biotechnol*. 2019;94(6):1982-1990. doi:10.1002/jctb.5981

296. Bisswanger H. *Practical Enzymology*. Wiley Blackwell; 2011. doi:10.1002/9783527659227

297. Rios NS, Pinheiro BB, Pinheiro MP, Bezerra RM, dos Santos JCS, Barros Gonçalves LR. Biotechnological potential of lipases from Pseudomonas: Sources, properties and applications. *Process Biochem*. 2018;75(September):99-120. doi:10.1016/j.procbio.2018.09.003

298. Kim Y min, Han TU, Hwang B, et al. Pyrolysis kinetics and product properties of softwoods, hardwoods, and the nut shell of softwood. 2016;33(8):2350-2358. doi:10.1007/s11814-016-0142-2

299. Heidari A, Stahl R, Younesi H, Rashidi A, Troeger N, Asghar A. Effect of process conditions on product yield and composition of fast pyrolysis of Eucalyptus grandis in fluidized bed reactor. *J Ind Eng Chem*. 2014;20(4):2594-2602. doi:10.1016/j.jiec.2013.10.046

300. Brown RC, Amonette JE, National N. Review of the pyrolysis platform for coproducing bio-oil and biochar. *Biofuels, Bioprod Bioref*. 2009;(3):547-562. doi:10.1002/bbb.169

301. Cha JS, Park SH, Jung SC, et al. Production and utilization of biochar: A review. *J Ind Eng Chem*. 2016;40:1-15. doi:10.1016/j.jiec.2016.06.002

302. Mohan D, Abhishek K, Sarswat A, Patel M. Biochar production and applications in soil fertility and carbon sequestration – a sustainable solution to crop-residue burning in India. *RSC Adv*. 2018;8:508-520. doi:10.1039/c7ra10353k

303. El-naggar A, El-naggar AH, Shaheen SM, et al. Biochar composition-dependent impacts on soil nutrient release, carbon mineralization, and potential environmental risk : A review. *J Environ Manage*. 2019;241(January):458-467. doi:10.1016/j.jenvman.2019.02.044

304. Regkouzas P, Diamadopoulos E. Chemosphere Adsorption of selected organic micro-pollutants on sewage sludge biochar. *Chemosphere*. 2019;224:840-851. doi:10.1016/j.chemosphere.2019.02.165

305. Ramani K, Karthikeyan S, Boopathy R, Kennedy LJ, Mandal AB, Sekaran G. Surface functionalized mesoporous activated carbon for the immobilization of acidic lipase and their application to hydrolysis of waste cooked oil : Isotherm and kinetic studies. *Process Biochem*. 2012;47(3):435-445. doi:10.1016/j.procbio.2011.11.025

306. Zhang S, Zhang Z, Lu Y, Rostam-Abadi M, Jones A. Activity and stability of immobilized carbonic anhydrase for promoting CO 2 absorption into a carbonate solution for post-combustion CO 2 capture. *Bioresour Technol*. 2011;102(22):10194-10201. doi:10.1016/j.biortech.2011.09.043

307. Tripathi M, Sahu JN, Ganesan P. Effect of process parameters on production of biochar from biomass waste through pyrolysis: A review. *Renew Sustain Energy Rev*. 2016;55:467-481. doi:10.1016/j.rser.2015.10.122

308. Gray M, Johnson MG, Dragila MI, Kleber M. Water uptake in biochars: The roles of porosity and hydrophobicity. *Biomass and Bioenergy*. 2014;61:196-205. doi:10.1016/j.biombioe.2013.12.010

309. Xu G, Sun JN, Shao HB, Chang SX. Biochar had effects on phosphorus sorption and desorption in three soils with differing acidity. *Ecol Eng*. 2014;62:54-60. doi:10.1016/j.ecoleng.2013.10.027

310. Johannes Lehmann SJ. *Biochar for Environmental Management: Science, Technology and Implementation*. Routledge. Earthscan Publications; 2015. doi:10.4324/9780203762264

311. Lv D, Xu M, Liu X, Zhan Z, Li Z, Yao H. Effect of cellulose, lignin, alkali and alkaline earth metallic species on biomass pyrolysis and gasification. *Fuel Process Technol*. 2010;91(8):903-909. doi:10.1016/j.fuproc.2009.09.014

312. Shaaban A, Se S meng, Dimin MF, et al. Influence of heating temperature and holding time on biochars derived from rubber wood sawdust via slow pyrolysis. *J Anal Appl Pyrolysis*. 2014;107:31-39. doi:10.1016/j.jaap.2014.01.021

313. Shaaban A, Se SM, Mitan NMM, Dimin MF. Characterization of biochar derived from rubber wood sawdust through slow pyrolysis on surface porosities and functional groups. In: *Procedia Engineering*. Vol 68. Elsevier Ltd; 2013:365-371. doi:10.1016/j.proeng.2013.12.193

314. Zhao L, Cao X, Mašek O, Zimmerman A. Heterogeneity of biochar properties as a function of feedstock sources and production temperatures. *J Hazard Mater jou*. 2013;257:1-9. doi:10.1016/j.jhazmat.2013.04.015

315. Rodríguez-Sanz A, Fuciños C, Torrado AM, Rúa ML. Extraction of the wheat straw hemicellulose fraction assisted by commercial endo-xylanases. Role of the accessory enzyme activities. *Ind Crops Prod*. 2022;179. doi:10.1016/j.indcrop.2022.114655

316. Bai YY, Xiao LP, Shi ZJ, Sun RC. Structural variation of bamboo lignin before and after ethanol organosolv pretreatment. *Int J Mol Sci*. 2013;14(11):21394-21413. doi:10.3390/ijms141121394

317. Alokika, Anu, Kumar A, Kumar V, Singh B. Cellulosic and hemicellulosic fractions of sugarcane bagasse: Potential, challenges and future perspective. *Int J Biol Macromol*. 2021;169:564-582. doi:10.1016/j.ijbiomac.2020.12.175

318. Ramos M, Laveriano E, San Sebastián L, et al. Rice straw as a valuable source of cellulose and polyphenols: Applications in the food industry. *Trends Food Sci Technol*. 2023;131:14-27. doi:10.1016/j.tifs.2022.11.020

319. Arantes MST, Marques GS, Hanse FA, et al. Composition and potential utilization strategies of by-products from the Brazilian peach palm industry. *Cienc e Agrotecnologia*. 2024;48. doi:10.1590/1413-7054202448006224

320. Arora N, Philippidis GP. Insights into the physiology of Chlorella vulgaris cultivated in sweet sorghum bagasse hydrolysate for sustainable algal biomass and lipid production. *Sci Rep*. 2021;11(1). doi:10.1038/s41598-021-86372-2

321. Bajwa DS, Pourhashem G, Ullah AH, Bajwa SG. A concise review of current lignin production, applications, products and their environment impact. *Ind Crops Prod*. 2019;139. doi:10.1016/j.indcrop.2019.111526

322. Zhang Y, Wang H, Sun X, Wang Y, Liu Z. Separation and Characterization of Biomass Components (Cellulose, Hemicellulose, and Lignin) from Corn Stalk. *BioResources*. 2021;16(4):7205-7219. doi:10.15376/biores.16.4.7205-7219

323. Kumar K, Ding L, Zhao H, Cheng MH. Waste-to-Energy Pipeline through Consolidated Fermentation–Microbial Fuel Cell (MFC) System. *Processes*. 2023;11(8). doi:10.3390/pr11082451

324. Pandiarajan P, Kathiresan M. Physicochemical and mechanical properties of a novel fiber extracted from the stem of common reed plant. *Int J Polym Anal Charact*. 2018;23(5):442-449. doi:10.1080/1023666X.2018.1474327

325. Brito MJP, Veloso CM, Bonomo RCF, Fontan R da CI, Santos LS, Monteiro KA. Activated carbons preparation from yellow mombin fruit stones for lipase immobilization. *Fuel Process Technol*. 2017;156:421-428. doi:10.1016/j.fuproc.2016.10.003

326. Sun K, Jiang L, Ye Q, et al. Chemical and microbiological characterization of pig manures and digestates. *Environ Technol (United Kingdom)*. 2023;44(13):1916-1925. doi:10.1080/09593330.2021.2016993

327. Valentín L, Kluczek-Turpeinen B, Willför S, et al. Scots pine (Pinus sylvestris) bark composition and degradation by fungi: Potential substrate for bioremediation. *Bioresour Technol*. 2010;101(7):2203-2209. doi:10.1016/j.biortech.2009.11.052

328. Schmitz E, Nordberg Karlsson E, Adlercreutz P. Warming weather changes the chemical composition of oat hulls. *Plant Biol*. 2020;22(6):1086-1091. doi:10.1111/plb.13171

329. Pallarés J, González-cencerrado A, Arauzo I. Biomass and Bioenergy Production and characterization of activated carbon from barley straw by physical activation with carbon dioxide and steam. *Biomass and Bioenergy*. 2018;115:64-73. doi:10.1016/j.biombioe.2018.04.015

330. Guo Z, Zhang J, Liu H, Kang Y. Development of a nitrogen-functionalized carbon adsorbent derived from biomass waste by diammonium hydrogen phosphate activation for Cr(VI) removal. *Powder Technol*. 2017;318:459-464. doi:10.1016/j.powtec.2017.06.024

331. Zhu L, Zhao N, Tong L, Lv Y. Structural and adsorption characteristics of potassium carbonate activated biochar. *RSC Adv*. 2018;8(37):21012-21019. doi:10.1039/c8ra03335h

332. Zhou H, Huang X, Jiang L, et al. Improved degradation of petroleum contaminants in hydraulic fracturing flowback and produced water using laccase immobilized on functionalized biochar. *Environ Technol Innov*. 2023;32:103280. doi:10.1016/j.eti.2023.103280

333. Leng L, Xiong Q, Yang L, et al. An overview on engineering the surface area and porosity of biochar. *Sci Total Environ*. 2021;763:144204. doi:10.1016/j.scitotenv.2020.144204

334. Anca-Couce A. Reaction mechanisms and multi-scale modelling of lignocellulosic biomass pyrolysis. *Prog Energy Combust Sci*. 2016;53(2016):41-79. doi:10.1016/j.pecs.2015.10.002

335. Collard FX, Blin J. A review on pyrolysis of biomass constituents: Mechanisms and composition of the products obtained from the conversion of cellulose, hemicelluloses and lignin. *Renew Sustain Energy Rev*. 2014;38:594-608. doi:10.1016/j.rser.2014.06.013

336. Břendová K, Száková J, Lhotka M, Krulikovská T, Punčochář M, Tlustoš P. Biochar physicochemical parameters as a result of feedstock material and pyrolysis temperature: predictable for the fate of biochar in soil? *Environ Geochem Health*. 2017;39(6):1381-1395. doi:10.1007/s10653-017-0004-9

337. Sun Y, Yu IKM, Tsang DCW, et al. Tailored design of graphitic biochar for high-efficiency and chemical-free microwave-assisted removal of refractory organic contaminants. *Chem Eng J*. 2020;398:125505. doi:10.1016/j.cej.2020.125505

338. Tomczyk A, Sokołowska Z, Boguta P. Biochar physicochemical properties: pyrolysis temperature and feedstock kind effects. *Rev Environ Sci Biotechnol*. 2020;19(1):191-215. doi:10.1007/s11157-020-09523-3

339. Sun Y, Cheng J. Hydrolysis of lignocellulosic materials for ethanol production: A review. *Bioresour Technol*. 2002;83(1):1-11. doi:10.1016/S0960-8524(01)00212-7

340. Yang E, Yao C, Liu Y, et al. Bamboo-derived porous biochar for efficient adsorption removal of dibenzothiophene from model fuel. *Fuel*. 2018;211(June 2017):121-129. doi:10.1016/j.fuel.2017.07.099

341. Sajjadi B, Chen WY, Egiebor NO. A comprehensive review on physical activation of biochar for energy and environmental applications. *Rev Chem Eng*. 2019;35(6):735-776. doi:10.1515/revce-2017-0113

342. Del Grosso M, Cutz L, Tiringer U, Tsekos C, Taheri P, de Jong W. Influence of indirectly heated steam-blown gasification process conditions on biochar physico-chemical properties. *Fuel Process Technol*. 2022;235(June). doi:10.1016/j.fuproc.2022.107347

343. Fang Y, Singh B, Singh BP, Krull E. Biochar carbon stability in four contrasting soils. *Eur J Soil Sci*. 2014;65(1):60-71. doi:10.1111/ejss.12094

344. Wijitkosum S, Sriburi T. Aromaticity, polarity, and longevity of biochar derived from disposable bamboo chopsticks waste for environmental application. *Heliyon*. 2023;9(9):e19831. doi:10.1016/j.heliyon.2023.e19831

345. Li Y, Gupta R, Zhang Q, You S. Review of biochar production via crop residue pyrolysis: Development and perspectives. *Bioresour Technol*. 2023;369:0960-8524. doi:10.1016/j.biortech.2022.128423

346. Schleyer P von R. Introduction: Aromaticity. *Chem Rev*. 2001;101(5). doi:10.1021/cr0103221

347. Liu AH, Yu B, He LN. Catalytic conversion of carbon dioxide to carboxylic acid derivatives. *Greenh Gases Sci Technol*. 2012;2(1):9-16. doi:10.1002/ghg

348. Liu Y, He Z, Uchimiya M. Comparison of Biochar Formation from Various Agricultural By-Products Using FTIR Spectroscopy. *Mod Appl Sci*. 2015;9(4):246-253. doi:10.5539/mas.v9n4p246

349. Fang Q, Chen B, Lin Y, Guan Y. Aromatic and hydrophobic surfaces of wood-derived biochar enhance perchlorate adsorption via hydrogen bonding to oxygen-containing organic groups. *Environ Sci Technol*. 2014;48(1):279-288. doi:10.1021/es403711y

350. Mcbeath A V, Wurster CM, Bird MI. Influence of feedstock properties and pyrolysis conditions on biochar carbon stability as determined by hydrogen pyrolysis. *Biomass and Bioenergy*. 2015;73:155-173. doi:10.1016/j.biombioe.2014.12.022

351. Beasley MM, Bartelink EJ, Taylor L, Miller RM. Comparison of transmission FTIR , ATR,

and DRIFT spectra: implications for assessment of bone bioapatite diagenesis. *J Archaeol Sci*. 2014;46:16-22. doi:10.1016/j.jas.2014.03.008

352. Ambroz F, Macdonald TJ, Martis V, Parkin IP. Evaluation of the BET Theory for the Characterization of Meso and Microporous MOFs. *Adv Sci News*. 2018;1800173:1-17. doi:10.1002/smtd.201800173

353. Bae YS, Yazayd'n AÖ, Snurr RQ. Evaluation of the BET method for determining surface areas of MOFs and zeolites that contain Ultra-Micropores. *Langmuir*. 2010;26(8):5475-5483. doi:10.1021/la100449z

354. Nguyen HN, Khuong DA. *New Trends in Pyrolysis Methods: Opportunities, Limitations, and Advantages. In: Ramola, S., Mohan, D., Masek, O., Méndez, A., Tsubota, T. (Eds) Engineered Biochar*. Springer Nature; 2022. doi:doi.org/10.1007/978-981-19-2488-0_7

355. Patil M, Mathad SN, Patil AY, et al. Synthesis and Characterization of Microwave-Assisted Copolymer Membranes of Poly(vinyl alcohol)-g-starch-methacrylate and Their Evaluation for Gas Transport Properties. *Polymers (Basel)*. 2022;14(2). doi:10.3390/polym14020350

356. Vallejos-Burgos F, Coudert FX, Kaneko K. Air separation with graphene mediated by nanowindow-rim concerted motion. *Nat Commun*. 2018;9(1):1-9. doi:10.1038/s41467-018-04224-6

357. D'Amico AD, Jiang Y. *Carbon Dioxide Characterization of Carbons with the TriStar II 3020*. Vol 23. www.micromeritics.com/Repository/Files/Carbon_Dioxide_Characterization_of_Carbons_with_the_TriStar_II_3020_-_Andrew_D._D_Amico_and_Yundi_Jiang.pdf

358. Hassan M, Liu Y, Naidu R, et al. Influences of feedstock sources and pyrolysis temperature on the properties of biochar and functionality as adsorbents : A meta-analysis. *Sci Total Environ*. 2020;744:140714. doi:10.1016/j.scitotenv.2020.140714

359. Guidelines For Selecting The Appropriate Adsorptive. Micromeritics. https://www.micromeritics.com/Repository/Files/Guidelines_for_Selectiong_the_Appropriate_Adsorptive.pdf

360. Silvestre-Albero J, Silvestre-Albero A, Rodríguez-Reinoso F, Thommes M. Physical characterization of activated carbons with narrow microporosity by nitrogen (77.4 K), carbon dioxide (273 K) and argon (87.3 K) adsorption in combination with immersion calorimetry. *Carbon N Y*. 2012;50(9):3128-3133. doi:10.1016/j.carbon.2011.09.005

361. Brewer CE, Chuang VJ, Masiello CA, et al. New approaches to measuring biochar density and porosity. *Biomass and Bioenergy*. 2014;66:176-185. doi:10.1016/j.biombioe.2014.03.059

362. Kim KC, Yoon TU, Bae YS. Applicability of using CO2 adsorption isotherms to determine BET surface areas of microporous materials. *Microporous Mesoporous Mater*. 2016;224:294-301. doi:10.1016/j.micromeso.2016.01.003

363. Kim Y, Ok JI, Vithanage M, Park YK, Lee J, Kwon EE. Modification of biochar properties using CO2. *Chem Eng J*. 2019;372(April):383-389. doi:10.1016/j.cej.2019.04.170

364. Li N, Xia Q, Niu M, Ping Q, Xiao H. Immobilizing Laccase on Different Species Wood Biochar to Remove the Chlorinated Biphenyl in Wastewater. *Sci Rep*. 2018;8(1):1-9. doi:10.1038/s41598-018-32013-0

365. Lonappan L, Liu Y, Rouissi T, Brar SK, Verma M, Surampalli RY. Adsorptive immobilization of agro-industrially produced crude laccase on various micro-biochars and degradation of diclofenac. *Sci Total Environ*. 2018;640-641:1251-1258. doi:10.1016/j.scitotenv.2018.06.005

366. Yoo S, Kelley SS, Tilotta DC, Park S. Structural Characterization of Loblolly Pine Derived Biochar by X-ray Diffraction and Electron Energy Loss Spectroscopy. *Sustain Chem Eng*. Published online 2018. doi:10.1021/acssuschemeng.7b04119

367. Naghdi M, Taheran M, Brar SK, Kermanshahi-pour A, Verma M, Surampalli RY. Immobilized laccase on oxygen functionalized nanobiochars through mineral acids treatment for removal of carbamazepine. *Sci Total Environ*. 2017;584-585:393-401. doi:10.1016/j.scitotenv.2017.01.021

368. Vaughn SF, Kenar JA, Tisserat B, et al. Chemical and physical properties of Paulownia elongata biochar modified with oxidants for horticultural applications. *Ind Crop Prod*. 2017;97:260-267. doi:10.1016/j.indcrop.2016.12.017

369. Lonappan L, Liu Y, Rouissi T, et al. Covalent immobilization of laccase on citric acid functionalized micro-biochars derived from different feedstock and removal of diclofenac. *Chem Eng J*. 2018;351(June):985-994. doi:10.1016/j.cej.2018.06.157

370. Nguyen LN, Hai FI, Dosseto A, Richardson C, Price WE, Nghiem LD. Continuous adsorption and biotransformation of micropollutants by granular activated carbon-bound laccase in a packed-bed enzyme reactor. *Bioresour Technol*. 2016;210:108-116. doi:10.1016/j.biortech.2016.01.014

371. Yakout SM. Effect of porosity and surface chemistry on the adsorption- desorption of uranium (VI) from aqueous solution and groundwater. *J Radioanal Nucl Chem*. 2015;308:555-565. doi:10.1007/s10967-015-4408-7

372. Zhao S xiang, Ta N, Wang X dong. Effect of Temperature on the Structural and Physicochemical Properties of Biochar with Apple Tree Branches as Feedstock Material. *MDPI Energies*. 2017;10:1293. doi:10.3390/en10091293

373. Bardestani R, Kaliaguine S. Steam activation and mild air oxidation of vacuum pyrolysis biochar. *Biomass and Bioenergy*. 2018;108(June 2017):101-112. doi:10.1016/j.biombioe.2017.10.011

374. Franciski MA, Peres EC, Godinho M, et al. Development of CO2 activated biochar from solid wastes of a beer industry and its application for methylene blue adsorption. *Waste Manag*. 2018;78:630-638. doi:10.1016/j.wasman.2018.06.040

375. Jin H, Capareda S, Chang Z, Gao J, Xu Y, Zhang J. Biochar pyrolytically produced from municipal solid wastes for aqueous As(V) removal: Adsorption property and its improvement with KOH activation. *Bioresour Technol*. 2014;169:622-629. doi:10.1016/j.biortech.2014.06.103

376. Micromeritics Instrument Corporation: Gas Adsorption Theory. www.researchgate.net/profile/Prem-Baboo/post/Pore-size-in-CMK-3-carbon/attachment/59d6555779197b80779ac8de/AS%3A525372900425728%401502270068889/download/Gas_Adsorption_Theory_poster.pdf

377. Jain NK, Bajwa N. *Introduction to Quality by Design (QbD): From Theory to Practice*. Springer Singapore; 2024. doi:https://doi.org/10.1007/978-981-99-8034-5

378. Vinoba M, Bhagiyalakshmi M, Jeong SK, Yoon YI, Nam SC. Capture and sequestration of

CO2 by human carbonic anhydrase covalently immobilized onto amine-functionalized SBA-15. *J Phys Chem C*. 2011;115(41):20209-20216. doi:10.1021/jp204661v

379. Patwardhan S, Staniland S. *Green Nanomaterials: From Bioinspired Synthesis to Sustainable Manufacturing of Inorganic Nanomaterials*. IOP; 2020. doi:10.1088/978-0-7503-1221-9

380. Patwardhan S V., Manning JRH, Chiacchia M. Bioinspired synthesis as a potential green method for the preparation of nanomaterials: Opportunities and challenges. *Curr Opin Green Sustain Chem*. 2018;12:110-116. doi:10.1016/j.cogsc.2018.08.004

381. Forsyth C, Patwardhan S V. Controlling performance of lipase immobilised on bioinspired silica. *J Mater Chem B*. Published online 2013:1164-1174. doi:10.1039/c2tb00462c

382. Carbonic Anhydrase from bovine erythrocytes. Sigma Aldrich. 2025. https://www.sigmaaldrich.com/GB/en/product/sigma/c3934

383. Demir Y, Demir N, Nadaroglu H, Bakan E. Purification and Characterization of Carbonic Anhydrase from Bovine Erythrocyte Plasma Membrane. *Prep Biochem Biotechnol*. 2000;30:49-60. doi:10.1080/10826060008544944

384. Bagherpour AR, Kashanian F, Seyyed Ebrahimi SA, Habibi-Rezaei M. L-arginine modified magnetic nanoparticles: Green synthesis and characterization. *Nanotechnology*. 2018;29(7). doi:10.1088/1361-6528/aaa2b5

385. Hudson S, Cooney J, Magner E. Proteins in mesoporous silicates. *Angew Chemie - Int Ed*. 2008;47(45):8582-8594. doi:10.1002/anie.200705238

386. Manning JRH, Routoula E, Patwardhan S V. Preparation of functional silica using a bioinspired method. *J Vis Exp*. 2018;2018(138). doi:10.3791/57730

387. Vinoba M, Bhagiyalakshmi M, Jeong SK, Yoon YI, Nam SC. Carbonic anhydrase conjugated to nanosilver immobilized onto mesoporous SBA-15 for sequestration of CO2. *J Mol Catal B Enzym*. 2012;75:60-67. doi:10.1016/j.molcatb.2011.11.010

388. Klára Kostelanská, Barbora Blahová Prudilová SH, Jan Gajdziok. Comparative Study of Powder Carriers Physical and Structural Properties. *Pharmaceutics*. 2022;14:1-18. doi:10.3390

389. Roach P, Farrar D, Perry CC. Surface Tailoring for Controlled Protein Adsorption: Effect of Topography at the Nanometer Scale and Chemistry. *J Am Chem Soc*. 2006;17:3939-3945. doi:10.1021/ja056278e

390. Dewulf L, Chiacchia M, Yeardley AS, Milton RA, Brown SF, Patwardhan S V. Designing bioinspired green nanosilicas using statistical and machine learning approaches. *Mol Syst Des Eng*. 2021;6(4):293-307. doi:10.1039/d0me00167h

391. Li Z, Jiang X, Liu H, Yao Z, Liu A, Ming L. Evaluation of Hydrophilic and Hydrophobic Silica Particles on the Release Kinetics of Essential Oil Pickering Emulsions. *ACS Omega*. 2022;7(10):8651-8664. doi:10.1021/acsomega.1c06666

392. Phadtare S, Vinod VP, Mukhopadhyay K, et al. Immobilization and Biocatalytic Activity of Fungal Protease on Gold Nanoparticle-Loaded Zeolite Microspheres. *Biotechnol Bioeng*. 2004;85(6):629-637. doi:10.1002/bit.10856

393. Cea M, González ME, Abarzúa M, Navia R. Enzymatic esterification of oleic acid by Candida rugosa lipase immobilized onto biochar. *J Environ Manage*. 2019;242:171-177.

doi:10.1016/j.jenvman.2019.04.013

394. Gascón V, Díaz I, Márquez-Álvarez C, Blanco RM. Mesoporous silicas with tunable morphology for the immobilization of laccase. *Molecules*. 2014;19(6):7057-7071. doi:10.3390/molecules19067057

395. Almeida LC, Barbosa AS, Fricks AT, Freitas LS, Lima ÁS, Soares CMF. Use of conventional or non-conventional treatments of biochar for lipase immobilization. *Process Biochem*. 2017;61:124-129. doi:10.1016/j.procbio.2017.06.020

396. Serra E, Díez E, Díaz I, Blanco RM. A comparative study of periodic mesoporous organosilica and different hydrophobic mesoporous silicas for lipase immobilization. *Microporous Mesoporous Mater*. 2010;132(3):487-493. doi:10.1016/j.micromeso.2010.03.031

397. Giussani L, Fois E, Gianotti E, Tabacchi G, Gamba A, Coluccia S. On the compatibility criteria for protein encapsulation inside mesoporous materials. *ChemPhysChem*. 2010;11(8):1757-1762. doi:10.1002/cphc.200901038

398. Souza Júnior EC, Santos MPF, Sampaio VS, et al. Hydrolysis of casein from different sources by immobilized trypsin on biochar: Effect of immobilization method. *J Chromatogr B Anal Technol Biomed Life Sci*. 2020;1146:122124. doi:10.1016/j.jchromb.2020.122124

399. Sasai Y, Kanno H, Doi N, Yamauchi Y, Kuzuya M, Kondo SI. Synthesis and characterization of highly stabilized polymer-trypsin conjugates with autolysis resistance. *Catalysts*. 2017;7(1). doi:10.3390/catal7010004

400. Taheran M, Naghdi M, Brar SK, Knystautas EJ, Verma M, Surampalli RY. Degradation of chlortetracycline using immobilized laccase on Polyacrylonitrile-biochar composite nanofibrous membrane. *Sci Total Environ*. 2017;605-606:315-321. doi:10.1016/j.scitotenv.2017.06.185

401. Naghdi M, Taheran M, Brar SK, Kermanshahi-pour A, Verma M, Surampalli RY. Pinewood nanobiochar: A unique carrier for the immobilization of crude laccase by covalent bonding. *Int J Biol Macromol*. 2018;115:563-571. doi:10.1016/j.ijbiomac.2018.04.105

402. Imam A, Suman SK, Singh R, Vempatapu BP, Ray A, Kanaujia PK. Application of laccase immobilized rice straw biochar for anthracene degradation. *Environ Pollut*. 2021;268. doi:10.1016/j.envpol.2020.115827

403. Pandey D, Daverey A, Dutta K, Arunachalam K. Bioremoval of toxic malachite green from water through simultaneous decolorization and degradation using laccase immobilized biochar. *Chemosphere*. 2022;297:0045-6535. doi:10.1016/j.chemosphere.2022.134126

404. Fernandez-Sanroman A, Acevedo-García V, Pazos M, Sanromán MA, Rosales E. Removal of sulfamethoxazole and methylparaben using hydrocolloid and fiber industry wastes: Comparison with biochar and laccase-biocomposite. *J Clean Prod*. 2020;271. doi:10.1016/j.jclepro.2020.122436

405. García-delgado C, Eymar E, Camacho-arévalo R, Petruccioli M, Annibale AD. Degradation of tetracyclines and sulfonamides by stevensite- and biochar-immobilized laccase systems and impact on residual antibiotic activity. *J Chem Technol Biotechnol*. 2018;93:3394-3409. doi:10.1002/jctb.5697

406. Mo H, Qiu J, Yang C, Zang L, Sakai E, Chen J. Porous biochar/chitosan composites for high performance cellulase immobilization by glutaraldehyde. *Enzyme Microb Technol*.

2020;138:109561. doi:10.1016/j.enzmictec.2020.109561

407. Bubner P, Dohr J, Plank H, Mayrhofer C, Nidetzky B. Cellulases dig deep: In situ observation of the mesoscopic structural dynamics of enzymatic cellulose degradation. *J Biol Chem*. 2012;287(4):2759-2765. doi:10.1074/jbc.M111.257717

408. He L, Yang Y, Kim J, et al. Multi-layered enzyme coating on highly conductive magnetic biochar nanoparticles for bisphenol A sensing in water. *Chem Eng J*. 2020;384:1385-8947. doi:10.1016/j.cej.2019.123276

409. Varghese PK, Abu-Asab M, Dimitriadis EK, Dolinska MB, Morcos GP, Sergeev Y V. Tyrosinase nanoparticles: Understanding the melanogenesis pathway by isolating the products of tyrosinase enzymatic reaction. *Int J Mol Sci*. 2021;22(2):1-17. doi:10.3390/ijms22020734

410. Al-sareji OJ, Meiczinger M, Somogyi V, et al. Removal of emerging pollutants from water using enzyme-immobilized activated carbon from coconut shell. *J Environ Chem Eng*. 2023;11(3). doi:10.1016/j.jece.2023.109803

411. Hoinacki Da Silva CK, Polidoro AS, Cabrera Ruschel PM, et al. Laccase covalently immobilized on avocado seed biochar: A high-performance biocatalyst for acetaminophen sorption and biotransformation. *J Environ Chem Eng*. 2022;10(3). doi:10.1016/j.jece.2022.107731

412. Al-sareji OJ, Meiczinger M, Salman JM, et al. Ketoprofen and aspirin removal by laccase immobilized on date stones. *Chemosphere*. 2023;311. doi:10.1016/j.chemosphere.2022.137133

413. Wang Z, Ren D, Yu H, Zhang S, Zhang X, Chen W. Preparation optimization and stability comparison study of alkali-modified biochar immobilized laccase under multi-immobilization methods. *Biochem Eng J*. 2022;181. doi:10.1016/j.bej.2022.108401

414. dos Santos PM, Baruque JR, de Souza Lira RK, et al. Corn Cob as a Green Support for Laccase Immobilization—Application on Decolorization of Remazol Brilliant Blue R. *Int J Mol Sci*. 2022;23(16). doi:10.3390/ijms23169363

415. Wang Z, Ren D, Zhang X, Zhang S, Chen W. Adsorption-degradation of malachite green using alkali-modified biochar immobilized laccase under multi-methods. *Adv Powder Technol*. 2022;33(11):103821. doi:10.1016/j.apt.2022.103821

416. Zhang H, Liu T, Zhu Y, et al. Lipases immobilized on the modified polyporous magnetic cellulose support as an efficient and recyclable catalyst for biodiesel production from Yellow horn seed oil. *Renew Energy*. 2020;145:1246-1254. doi:10.1016/j.renene.2019.06.031

417. Zhang Y, Piao M, He L, et al. Immobilization of laccase on magnetically separable biochar for highly efficient removal of bisphenol A in water. *RSC Adv*. 2020;10(8):4795-4804. doi:10.1039/c9ra08800h

418. Lonappan L, Rouissi T, Liu Y, Brar SK, Surampalli RY. Removal of diclofenac using microbiochar fixed-bed column bioreactor. *J Environ Chem Eng*. 2019;7(1). doi:10.1016/j.jece.2019.102894

419. Xu W, Yong Y, Wang Z, Jiang G, Wu J, Liu Z. Concanavalin A Coated Activated Carbon for High Performance Enzymatic Catalysis. *ACS Sustain Chem Eng*. 2017;5(1):90-96. doi:10.1021/acssuschemeng.6b02705

420. Ivanov YD, Ableev AN, Shumov ID, et al. Registration of Functioning of a Single Horseradish Peroxidase Macromolecule with a Solid-State Nanopore. *Int J Mol Sci*. 2023;24(21). doi:10.3390/ijms242115636

421. Chen W, Luo J, Du X, Ding L, Zhang W. Activated carbon-gravity driven biomimetic membrane (AC-GDBM) for organic micro-polluted water treatment. *J Clean Prod*. 2021;317. doi:10.1016/j.jclepro.2021.128224

422. Pounsamy M, Somasundaram S, Palanivel S, Ganesan S. Removal of Fat Components in High TDS Leather Wastewater by Saline-Tolerant Lipase-Assisted Nanoporous-Activated Carbon. *Appl Biochem Biotechnol*. 2019;187:474-492. doi:10.1007/s12010-018- 2833-0

423. Thiyagarajan P, Selvam K, Sudhakar C, Selvankumar T. Enhancement of Adsorption of Magenta Dye by Immobilized Laccase on Functionalized Biosynthesized Activated Carbon Nanotubes. *Water Air Soil Pollut*. 2020;231(7). doi:10.1007/s11270-020-04737-1

424. Garcia LF, Rodrigues Siqueira AC, Lobón GS, et al. Bio-electro oxidation of indigo carmine by using microporous activated carbon fiber felt as anode and bioreactor support. *Chemosphere*. 2017;186:519-526. doi:10.1016/j.chemosphere.2017.08.033

425. Ramírez-Montoya LA, Hernández-Montoya V, Montes-Morán MA, Jáuregui-Rincón J, Cervantes FJ. Decolorization of dyes with different molecular properties using free and immobilized laccases from Trametes versicolor. *J Mol Liq*. 2015;212:30-37. doi:10.1016/j.molliq.2015.08.040

426. Ramírez-Montoya LA, Hernández-Montoya V, Montes-Morán MA, Cervantes FJ. Correlation between mesopore volume of carbon supports and the immobilization of laccase from Trametes versicolor for the decolorization of Acid Orange 7. *J Environ Manage*. 2015;162:206-214. doi:10.1016/j.jenvman.2015.07.035

427. Wang Z, Ren D, Zhao Y, et al. Remediation and improvement of 2,4-dichlorophenol contaminated soil by biochar-immobilized laccase. *Environ Technol (United Kingdom)*. 2021;42(11):1679-1692. doi:10.1080/09593330.2019.1677782

428. Khosla K, Rathour R, Maurya R, et al. Biodiesel production from lipid of carbon dioxide sequestrating bacterium and lipase of psychrotolerant Pseudomonas sp. ISTPL3 immobilized on biochar. *Bioresour Technol*. 2017;245:743-750. doi:10.1016/j.biortech.2017.08.194

429. Hyun J, Hun J, Sup D, Young H, Park C, Wook S. Biodiesel production by lipases co-immobilized on the functionalized activated carbon. *Bioresour Technol Reports*. 2019;7:100248. doi:10.1016/j.biteb.2019.100248

430. Liu Y, Yao L, He L, Liu N, Piao Y. Electrochemical enzyme biosensor bearing biochar nanoparticle as signal enhancer for bisphenol a detection in water. *MDPI Sensors*. 2019;19(7). doi:10.3390/s19071619

Appendices

Table 1: A Summary of Studies Which Have Investigated Enzyme Immobilisation onto Biochar

Biochar Source	***Enzyme Type***	***Enzyme Size (nm)***
Oat Husk[393]	Lipase (from Candida rugosa)	6.9[393]
Pinewood[367]	Laccase	6.1 [394]
Pinewood, pig manure, almond shell[369]	Laccase	6.1 [394]
Pinewood, pig manure, almond shell[365]	Laccase	6.1 [394]
Guava seeds[395]	Lipase	4 [396]
Maple and spruce wood[364]	Laccase	6.1 [394]
Pupunha palm[295]	Pepsin	6.6 [397]
Oat hull and pine bark biochar [256]	Lipase (from Candida rugosa)	6.9[393]
Caja seeds[398]	Trypsin	3.3 [399]
Pine white wood, spruce and fir [400]	Laccase	6.1 [394]
Pinewood, fir and spruce [401]	Laccase	6.1 [394]
Granular activated carbon [370]	Laccase	6.1 [394]
Rice-straw biochar [402]	Laccase	6.1 [394]
Pine needle biochar [403]	Laccase	6.1 [394]
Lemons and limes [404]	Laccase	6.1 [394]
Holm Oak [405]	Laccase from *Myceliophthora thermophila* (MtL) and *Pleurotus eryngii* (PeL)	-
Sugarcane bagasse [406]	Cellulase	18 - 21.5 [407]
Bagasse [408]	Tyrosinase	8.3 [409]
Coconut shell [410]	Laccase	6.1 [394]
Avocado seed [411]	Laccase	6.1 [394]
Date stones [412]	Laccase	6.1 [394]
Pomegranate peels	Laccase	6.1 [394]
Pine needle	Laccase	6.1 [394]
Corn straw [332]	Laccase	6.1 [394]
Rice straw [413]	Laccase	6.1 [394]
Corn cob [414]	Laccase	6.1 [394]
Rice straw biochar [415]	Laccase	6.1 [394]
Not provided [416]	Laccase	6.1 [394]
Not provided [417]	Laccase	6.1 [394]
Pine wood, pig manure [418]	Laccase	6.1 [394]
Not provided [419]	Laccase and horseradish peroxidase	6.1 [394] and 5 [420]
Powdered wood [421]	Laccase	6.1 [394]
Rice husk [422]	Lipase	4 [396]
Prosopis julifora bark [423]	Laccase	6.1 [394]
Recyclable textile fibre [424]	Laccase	6.1 [394]
Pecan shells [425]	Laccase	6.1 [394]
Pecan shell, peach stone, pistachio shell, pine nut shell [426]	Laccase	6.1 [394]
Wheat straw [427]	Laccase	6.1 [394]

Sugarcane bagasse [428]	Lipase	4 [396]
Coconut [429]	Lipase	4 [396]
Bagasse [430]	Tyrosinase	8.3 [409]